ABSTRACT

Title: DETERMINATION OF SULFUR ISOTOPE COMPOSITION IN SULFATE FROM TWO HIGH ELEVATION SNOWPITS BY MULTI-COLLECTOR THERMAL IONIZATION MASS SPECTROMETRY USING A DOUBLE SPIKE

Jacqueline Lorraine Mann, Doctor of Philosophy, 2005

Directed By: Associate Professor, Karen L. Prestegaard, Geology

The variability of stable sulfur isotopes in nature provides a chemical tool for tracing the various sources of sulfur and a useful tool for understanding the sulfur cycle. It is also well established that snow and ice preserve a record of the sources, sinks, and processing of sulfur that reflect changes in this cycle through time. Our ability to sample this record is however limited by the total sample concentration and the analytical requirements for isotopic analysis. A high-resolution double spike technique using multi-collector thermal ionization mass spectrometry was developed for stable sulfur isotope composition measurements of small concentration sulfate samples (ppb level).

The capability of this new technique was demonstrated by measuring internationally recognized standards of known isotopic composition and by measuring snowpit samples with low sulfate concentrations collected from the Inilchek Glacier, Kyrgyzstan and Summit, Greenland. The elemental and high resolution sulfur isotope data for the snowpit samples were used to calculate the

relative seasonal contributions of anthropogenic and natural sulfur sources to sulfate at these high-elevation Northern Hemisphere sites.

The isotope composition results for the standards demonstrate the double spike technique to be competitive in accuracy and precision with the traditional methods but the sample requirement is smaller. The average uncertainties on the individual isotope composition measurements for the Inilchek and Summit samples were approximately ± 0.10 ‰ (2σ) and ± 1.5‰ (2σ), respectively. The larger uncertainties for the Greenland samples resulted from increased blank and the smaller sample size used for analysis. Decreasing the blank concentrations by an order of magnitude show that a factor of two to three improvement in the uncertainties on small sample sizes is attainable with the double spike technique.

The sulfur isotope values in the Inilchek snowpit demonstrate no seasonality; while the values observed in the Greenland snowpit exhibit strong seasonality, where the values are ^{34}S-depleted in the winter months and are ^{34}S-enriched in the summer months. Mass balance calculations indicate that anthropogenic sources are the main contributor (75 %) to sulfate during most of the year for both locations.

DETERMINATION OF SULFUR ISOTOPE COMPOSITION IN SULFATE FROM TWO HIGH ELEVATION SNOWPITS BY MULTI-COLLECTOR THERMAL IONIZATION MASS SPECTROMETRY USING A DOUBLE SPIKE

By

Jacqueline Lorraine Mann

Dissertation submitted to the Faculty of the Graduate School of the
University of Maryland, College Park, in partial fulfillment
of the requirements for the degree of
Doctor of Philosophy
2005

Dedication

To Dr. John Thomas for the inspiration,

Dr. Michael O'Connell for helping me define it,

and my parents for all the rest.

Acknowledgements

It would not have been possible for me to complete this dissertation without the help of many people. I would specifically like to thank my advisor, Dr. Karen Prestegaard, for her support and guidance through my years at Maryland; Dr. A. J. Kaufman for keeping me on my toes and being an excellent editor; Dr. James Farquhar not only for his energy and interest but also for his feedback on this project and supporting me when I most needed it; Dr. Christopher Shuman for providing the opportunity of a lifetime – to do fieldwork in Greenland! Without his help and connections this thesis would not be what it is; and also Dr. Robert Hudson for his willingness to sit on this committee. I would also like to thank Dr. Richard Walker for access to the TIMS instrument for this work – it made all the difference. I would also like to thank Bozwell Wing for his help over the years. I would also like to acknowledge the support of the EPA Star Fellowship program (U915356), NASA (51-622-83-72WBS), and the NSF for providing financial and field support.

I would also like to thank Dr. W. R. Kelly. He is a true inspiration and true Renaissance man. I am grateful for his willingness to have endless conversations about this research, science in general, and everything else under the sun – I have learned a great deal from you, and I thank you for your help and guidance in all matters and through this process.

Thanks also go to Adam Davis and Lori Keith for simply listening and being my closest friends. Finally, I also want to thank Antone Neugass, the sunshine in my life, for his love, patience, and support; in turn I offer my love to you forever.

Table of Contents

List of Tables

List of Figures

Chapter 1: Introduction

"Understanding Earth's major biogeochemical cycles and their interaction with the global climate" are two of several "Grand Challenges" in environmental research for the next generation recently identified by the National Resource Council (NAS, 2000). The biogeochemical cycling of sulfur and the formation of sulfate aerosol particles in the atmosphere have important consequences for global climate and are not fully understood. Sulfate aerosols interact "directly" with incoming solar and outgoing terrestrial radiation through scattering and absorption and "indirectly" function as cloud condensation nuclei (CCN) that influence the concentration and size of droplets as well as their surface reflectivity, and the radiative properties of clouds (IPCC, 1995). Submicrometer aerosols, in particular, are efficient at scattering solar radiation because they have dimensions close to the wavelengths of visible light. The majority of these are derived from gas-to-particle conversion of anthropogenic sulfur dioxide (SO_2) emissions. These submicron aerosols, with a residence time in the atmosphere of a few days to a week, are able to influence atmospheric composition both downwind of industrialized areas and in remote areas of the world (Polian et al., 1986). Snow and ice cores provide archives of atmospheric sulfate aerosols in many remote regions of the Earth including polar, temperate, and tropical environments. Sulfur isotope composition measurements of these aerosols may provide information on the degree of influence anthropogenic contributions have on the natural sulfur cycle, and ultimately global climate, through time.

1.1 Statement of the Problem

In the 1990's researchers recognized the need to determine the origin of submicron sulfate aerosols in order to assess the impact of increasing anthropogenic sulfur emissions on the natural atmospheric sulfur cycle and global climate. Assessing the global influence of anthropogenic activity in the northern hemisphere on the climate is becoming increasingly more important with the growing population and continued reliance, especially in the third world, on burning coal for energy. Sulfur isotopic composition of remote marine and polar sulfate aerosols sampled directly through the collection of atmospheric aerosols on filters, has been used to identify anthropogenic inputs to distant regions (Nriagu et al., 1991; Calhoun et al., 1991; Li et al., 1993; Norman et al., 1999; Patris et al., 2000b). A problem faced by investigators in these studies was the need to combine samples to obtain sufficient amounts of sulfur to perform isotopic measurements. This large sample requirement can mask seasonal changes in sources. Furthermore, sampling the atmosphere directly only permits current and future changes in contributions to be assessed. There is also a lack of historical data in which to put human influence upon the global atmospheric sulfur budget into context.

In recognition of this, Patris et al. (2002, 2000a) examined the isotopic signatures of a shallow Antarctic ice core and of a discontinuous set of Greenland ice core samples, using continuous flow isotope ratio mass spectrometry (CF-IRMS), to examine the potential variations in sulfate sources through time to assess the current and historical changes in source contributions to these environments. However, the sulfate concentrations in these ice core samples were typically on the order of 25 to 150 ng/g, which tests the limits of isotope ratio mass spectrometry (IRMS). The studies of Patris et

al. (2002, 2000a) required composite samples of 1 to 2.5 L of meltwater (with a density of 0.5 g/mL this corresponds to approximately 2 to 5 kg of ice volume) for analysis, which masked seasonal and sub-seasonal shifts in isotope composition. A significant advancement would be the capability to measure the seasonal isotopic signatures. The techniques presented herein hold such a promise.

1.2 Research Objectives

In order to gain insight into the dynamic global atmospheric sulfur cycle, which varies on a seasonal basis, and the relative importance of natural and anthropogenic sulfur in forcing global climate change, higher-resolution (seasonal and sub-seasonal time scales) data is required to minimize the masking effects associated with combining samples. The primary objectives of this research were to develop an analytical technique for measurement of isotope composition and concentration of sulfur in low concentration environments and to characterize the seasonal shifts of sulfur isotope composition and concentration of sulfate in snowpits from polar and temperate sites impacted by industrial activity. The specific objectives for this research were the following:

1) To develop a double spike (internal standard) technique for use with multi-collector thermal ionization mass spectrometry (MC-TIMS) to measure the sulfur isotopic composition and concentration of low-concentration sulfur (< 1 μg S) samples.
2) To demonstrate the capabilities of the new technique by measuring the isotopic composition and concentration of internationally recognized standards.

3) To test the new double spike technique on snow samples with ppb levels of sulfate collected from the Inilchek Glacier, a high elevation glacier in Kyrgyzstan and Summit, Greenland.
4) To determine the relative seasonal contributions of anthropogenic (fossil fuel burning) and natural (marine biogenic, sea spray, dust) sulfur sources to the sulfate from the Inilchek and Summit.
5) Examine the advantages of the new technique for sulfur isotope measurements of small concentration samples.

The additional high-resolution isotopic data could potentially provide: 1) a more detailed reconstruction of the dynamic (changing on seasonal and sub-seasonal timescales) atmospheric sulfur cycle in both Arctic and temperate environments, 2) the ability to examine the seasonal changes in sulfur sources, including anthropogenic, and the role these contributions play in the global sulfur cycle and in climate forcing, and 3) the necessary field data to test the assumptions employed in atmospheric sulfur cycling models, thus improving their predictive ability. Understanding the role human activities play in the rapidly changing sulfur biogeochemical cycle and global climate is important to humankind and is required to make informed environmental policy decisions.

1.3 Outline of Thesis

Chapter 1 introduces the objectives of this research and an outline of the research goals. Chapter 2 provides background information on the major source contributors to the site locations of this study including their sulfur emission rates and sulfur isotopic variations. The chapter also outlines the necessary requirements for mass balance model calculations. A description of why the two site locations were chosen as well as the

sampling scheme and protocols used in this study are included in Chapter 3 along with the methods employed for dating the snowpit samples. Chapter 4 describes the experimental details of the new double spike technique including the chemical and mass spectrometric procedures and the data reduction and data analysis methods used for the snowpit samples. In Chapter 5 a detailed assessment of the double spike method for instrumental fractionation correction is presented and discussed. In addition, the isotope composition and concentration results for available sulfur isotopic and concentration standards are presented and discussed. Chapter 6 demonstrates the capability of the new double spike method to measure the sulfur isotopic composition and concentration of snowpit samples collected from the Inilchek Glacier, Kyrgyzstan and Summit, Greenland with ppb (ng/g) or μmole/L levels of sulfate. The geochemical and isotopic composition results for the samples in addition to the mass balance results used to determine the relative seasonal contributions of anthropogenic and natural sulfur sources to sulfate in these regions are presented. Finally, Chapter 7 provides a summary and examination of the advantages of the new technique for sulfur isotope measurements of small concentration samples.

Chapter 2: Background

Sulfur compounds in the atmosphere are of natural (sea spray, dust, marine biogenic, and volcanic) and anthropogenic (fossil fuel burning) origin and occur in gaseous (H_2S (hydrogen sulfide), CH_3SCH_3(dimethylsulfide - DMS), CH_3SSCH_3 (dimethyldisulfide - DMDS), CH_3SH (methyl mercaptan), COS (carbonyl sulfide), CS_2 (carbon disulfide), SO_2 (sulfur dioxide)), liquid ($H_2SO_3^-$ (bisulfite), SO_4^{2-} (sulfate), and SO_3^{2-} (sulfite), CH_3SO_2OH (methane sulfonic acid – MSA)), and solid (sulfates, and S^o) phases. The main sulfur species in snow and ice of remote regions are sulfate and methanesulfonic acid (MSA) derived from DMS oxidation; however, the sulfur isotope composition of sulfate is the tracer species typically used as it represents a combination of sources and allows source contributors to be assessed. The most significant contributors to sulfate in snow and ice are primary and secondary aerosols derived from seawater sulfate (sea-salt (ss) sulfate) and non-sea water sulfate (non-sea-salt (nss) sulfate/excess (xs) sulfate). The nss-sulfate fraction for the two study sites in this research includes sulfate derived from: 1) the oxidation of marine biogenic dimethylsulfide (DMS), 2) the oxidation of anthropogenic SO_2 emissions (H_2S is not considered as the emissions are much lower (< 10 %) than that of SO_2 (Brimblecombe et al., 1989)), 3) the direct injection of sulfate particulates from anthropogenic emissions, and 4) particulate sulfate from dust.

This study analyzed samples from two different geographic locations in the northern hemisphere. Samples were collected from Summit, Greenland (3238 m; 72.58°N, 38.53°W) (Figure 2.1) and the Inilchek Glacier, Kyrgyzstan (5100 m; 42.16°N, 80.25°E) (Figure 2.2). The Summit site is located at the highest point on the ice cap

approximately at the center of Greenland. The Inilchek Glacier is located in the Tien Shan region of Central Asia along the boundaries of eastern Kyrgyzstan and western China. From here on the sites will be referred to as "Summit" and "Inilchek". Table 2.1

Table 2.1. Main source contributors to nss-sulfate to study site locations.

	Sulfate Dust (SO_4^{2-})	Marine Biogenic (DMS → SO_2 → SO_4^{2-})	Anthropogenic (SO_2 → SO_4^{2-})
Summit, Greenland	Y	Y	Y
Inilchek Glacier,	Y	N	Y

Y = Yes, N = NO (Kreutz and Sholovitz, 2000; Pruett et al., 2004; Patris et al., 2002; Neftel et al., 1985; Finkel et al., 1986; Mayewski et al., 1986; Mayewski et al., 1990; Legrand et al., 1997)

and Figure 2.3 and 2.4 show the major possible sources and there locations contributing to nss-sulfate in snow of the two locations examined in this study.

In the following sections, information on the emission rates of sulfur from the major source contributors to the study locations are given as well as the sulfur isotopic abundance variations typical of these sources. In addition, requirements for the mass balance models used in this research are outlined, and the specific source contributors used in the mass balance models for each site are provided.

2.1 Sulfur Emission Rates of Major Source Contributors

The emission rates of the major possible source contributors and their corresponding sulfur isotopic composition ranges are shown in Figure 2.5. The total emission of sulfur to the atmosphere, excluding sea-salt contribution, in a given year ranges from 78 to 95 Tg (10^{12} g) S yr^{-1}, not including dust or sea salt, with the most significant contribution being emitted from anthropogenic sources (65 to 73 Tg S) as SO_2

Figure 2.1. Location of the Summit site in Greenland (3238 m; 72.58°N, 38.53°W).

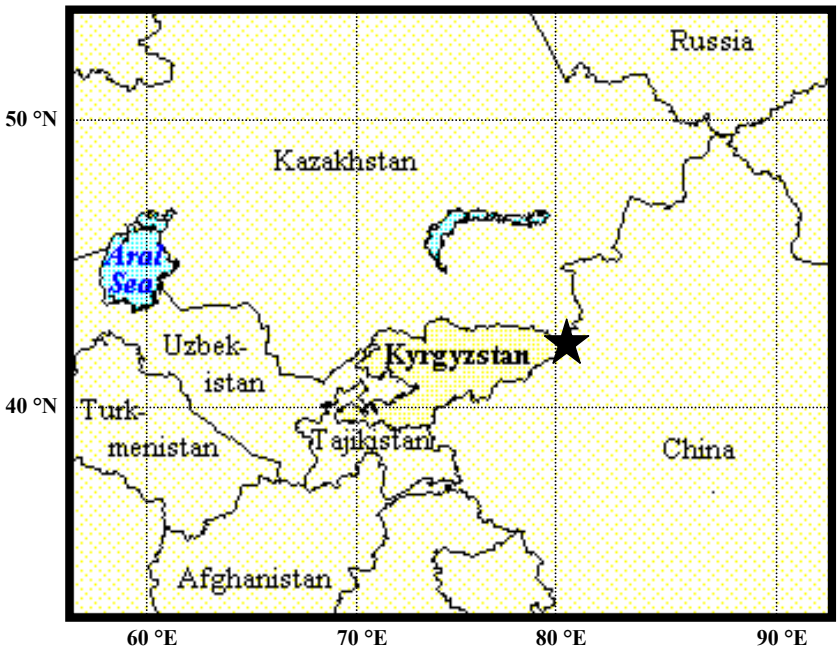

Figure 2.2. Location of the Inilchek Glacier in Kyrgystan (5100 m; 42.16°N, 80.25°E).

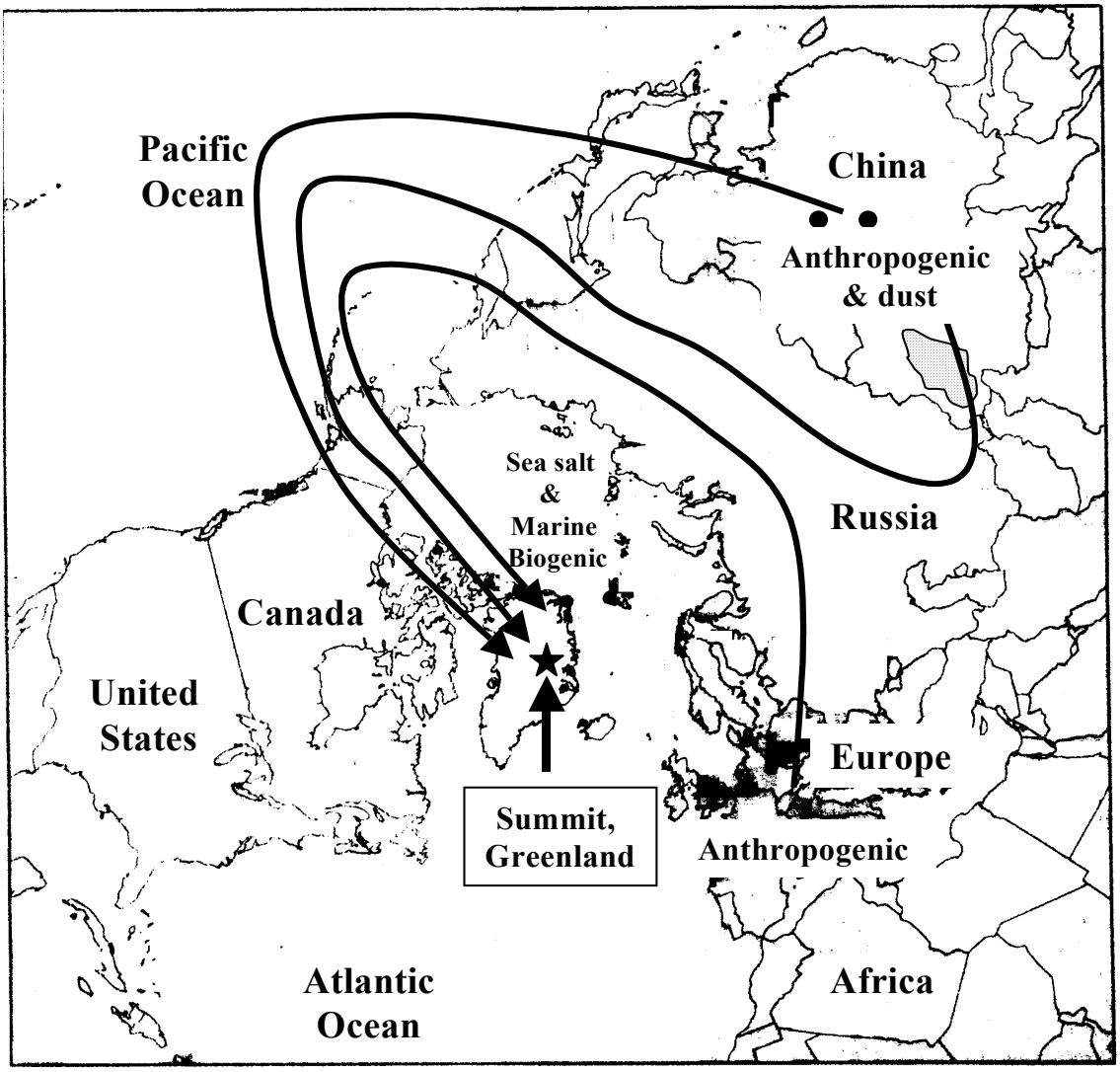

Figure 2.3. Location of the major sulfate sources (sea salt, marine biogenic, anthropogenic, and dust) contributing to Summit, Greenland. The black arrows highlight the dominant wind directions responsible for transporting anthropogenic and dust sulfate to the region (Christensen, 1997; Bory et al., 2002; Bory et al., 2003, Bory et al., 2003). Sea salt and marine biogenic are from local (Atlantic) sources. Figure modified after Christensen (1997).

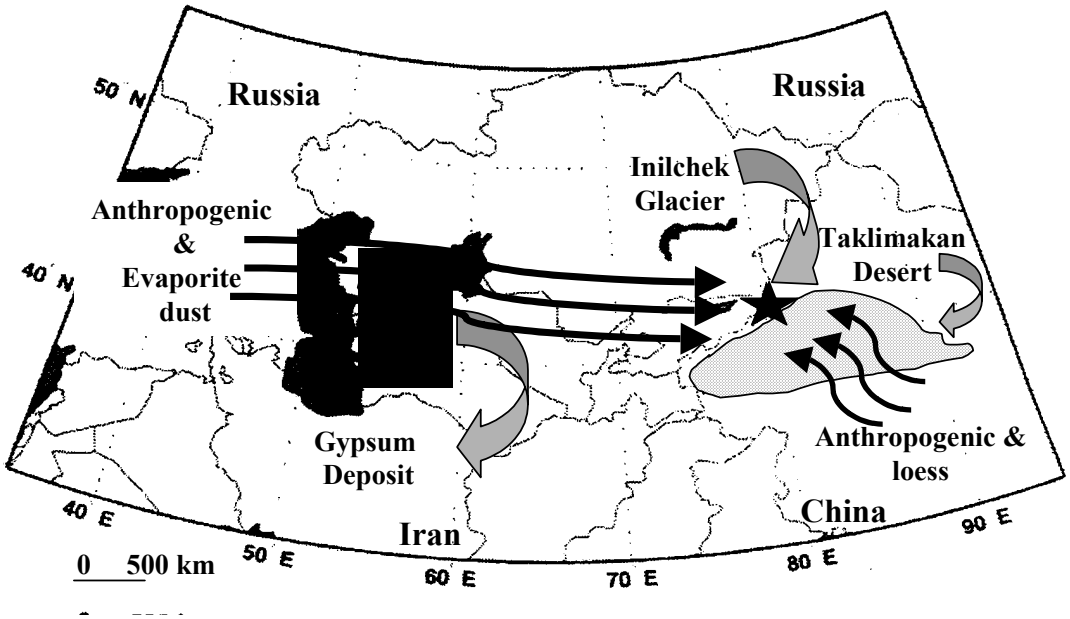

Figure 2.4. Location of the major sulfate sources (anthropogenic and dust) contributing to the Inilchek Glacier. The grey arrows highlight the major dust sources and the black arrows highlight the dominant wind directions responsible for transporting both anthropogenic and dust sulfate to the region (Wake et al, 1994; Claquin et al., 1999; Kreutz and Sholkovitz, 2000; Kreutz et al., 2001; Pruett et al., 2004) . Figure modified after Kreutz and Sholkovitz (2000).

(95%). A smaller portion is emitted directly as sulfate (~ 2 Tg S yr^{-1}) from anthropogenic sources. Anthropogenic sources today contribute approximately 80% of the total global sulfur emissions (Chin et al., 2000a; 2000b) with 90-94% being contributed from the northern hemisphere and roughly 10% or less from the southern hemisphere (Berresheim et al., 1995). Natural sources deliver about 20% (including oceanic sulfur flux) to the total sulfur emissions into the atmosphere. Natural emissions (volcanic and DMS) account for 13 to 22% of the total sulfur budget. The portion attributed to volcanic SO_2 emissions is approximately 3 to 6 Tg S yr^{-1}, which is approximately 3 to 8% of the total S budget. DMS accounts for about 10 to 20% of the S budget ranging from 10 to 16 Tg S yr^{-1} (Chin et al., 2000a, 2000b; Koch et al., 1999; Barth et al., 2000; Rasch et al., 2000). The dust contribution is less well constrained but has been estimated to contribute up to 20 Tg S yr^{-1} (Brimblecombe et al., 1989). In the present temperate time period dust influence is likely to be greater regionally (arid regions) than globally. Furthermore, the amount of dust reaching Summit, Greenland is likely smaller than that reaching the Inilchek Glacier due to its greater distance from terrigenous sources. Finally, the sea-salt sulfate flux is significant, but estimates are highly uncertain ranging from 131 to 275 Tg S yr^{-1} (Andreae and Jaeschke, 1992).

The dominance of anthropogenic sources to the sulfur emission budget seen today began with the industrial age. Anthropogenic sulfur emissions have been increasing since the late 19^{th} century surpassing natural emissions in the northern hemisphere by about 1910 (Dignon and Hameed, 1989; Lefohn et al., 1999) and on a global scale during the 1950s (Spiro et al., 1992). This historical trend is documented in Greenland ice cores where increasing nss-sulfate levels have been recorded over one hundred years coincident

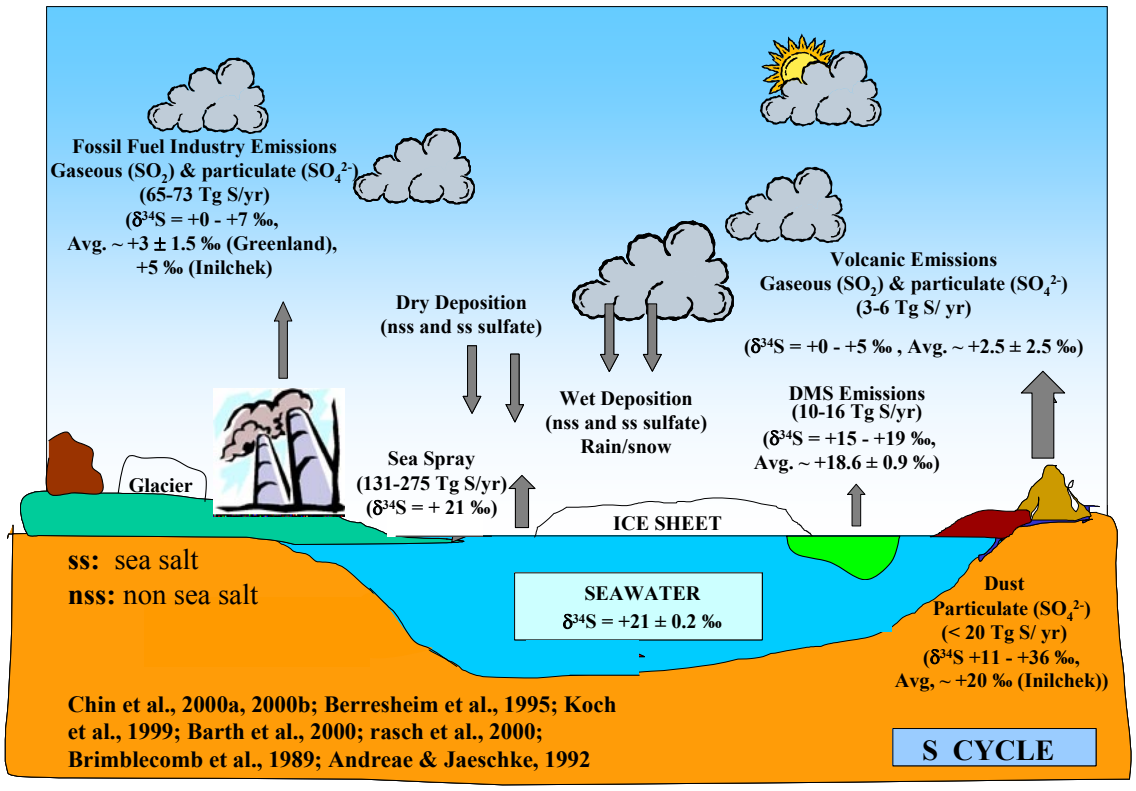

Figure 2.5. Emission rates of the major possible source contributors and their corresponding sulfur isotopic composition ranges. Tg = 10^{12} g. Diagram courtesy of Stephen Long, National Insitute of Standards and Technology.

with industrial activity (Neftel et al., 1985; Finkel et al., 1986; Mayewski et al., 1986; Mayewski et al., 1990; Legrand et al., 1997; Patris et al., 2002) from an average of 22 ppb (1870-1900) to 84 ppb (1968-1984). Similarly, nss-sulfate in ice cores obtained from Asian regions (Dasuopu Glacier (Himalayan Mountains),Tibet; Inilchek Glacier (Tien Shan Mountains), Kyrgyzstan) is believed to be at least partially due to anthropogenic activity (Kreutz and Sholkovitz, 2000; Thompson et al., 2000, Pruett et al., 2004). Based on $\delta^{34}S$ measurements of nss-sulfate and mass balance models, Antarctic nss-sulfate levels, on the other hand, are primarily attributed to the oxidation of marine biogenic dimethylsulfide (DMS) (Patris et al., 2000a; Legrand et al., 1984, 1991) demonstrating the variable spatial distribution and importance of anthropogenic and natural sulfur in different regions of the globe.

2.2 Sulfur Isotope Variations in Sulfate Precursors

The relative isotopic abundances of sulfur typically found in nature are ^{32}S = 95%, ^{33}S = 0.75%, ^{34}S = 4.2%, and ^{36}S = 0.015% (Figure 2.6). The variability in stable sulfur isotopes observed in nature is caused by mass fractionation during biogeochemical processing or by photochemical reactions in the atmosphere. These isotopic abundance variations are usually reported in terms of the $^{34}S/^{32}S$ abundance ratio because these are the two most abundant isotopes; therefore, this ratio can be measured with greater precision. Since the isotope effects are commonly small, fractional differences in the sample isotope ratios are reported in delta notation, where the delta values are relative to a standard material (in this study the standard used was Vienna Canyon Diablo Troilite (VCDT) , $\delta^{34}S$ = -0.3‰). These differences are expressed in parts per thousand (per mille):

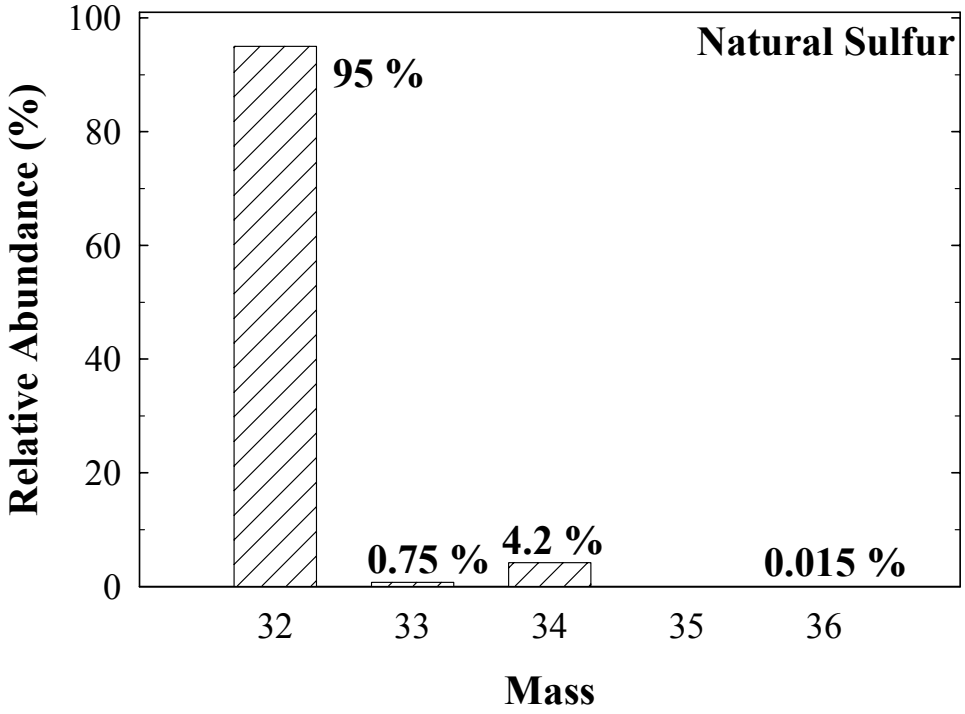

Figure 2.6. Relative abundance of the four stable isotopes of sulfur in nature.

$$\delta^{34}\mathrm{S}\,(‰) = \left(\frac{\left(\frac{^{34}\mathrm{S}}{^{32}\mathrm{S}}\right)_{\text{sample}}}{\left(\frac{^{34}\mathrm{S}}{^{32}\mathrm{S}}\right)_{\text{standard}}} - 1 \right) \times 1000 \qquad \text{Eqn. 2.1}$$

The Canyon Diablo troilite standard was originally chosen as a sulfur isotopic standard because the iron sulfide (FeS), troilite, was available in relatively large quantities and was considered homogenous in composition and representative of the primordial Earth.

The most likely sulfate precursors identified above can potentially have an enormous range of $\delta^{34}S$ values from -30 to +40‰ (references below). Figure 2.7 shows the range of $\delta^{34}S$ values for the main sulfate contributors to the site locations of this study. The range in values, however, is commonly reduced upon mixing of sources over large scales by atmospheric transport.

2.2.1 Marine Biogenic

The sulfur isotope composition of biogenically-derived DMS was first measured by Calhoun et al. (1991). They determined that due to assimilatory sulfate reduction DMS had a $\delta^{34}S$ value of +17 ± 1.9‰ (Figure 2.7) and that the resulting nss-sulfate values, due to oxidation of DMS, ranged from +14 to +22‰; suggesting an approximate 5‰ fractionation from ss-sulfate with a $\delta^{34}S$ value of +21 ± 0.2‰ (Rees et al., 1978). Other researchers obtained $\delta^{34}S$ values of aerosol sulfate within this range (Patris et al., 2000b; McArdle et al., 1998); however, the findings of Patris et al. (2000a) ($\delta^{34}S$ = +18.6 ± 0.9‰) suggest a value of approximately +18‰, at the center of this range, is likely a better representative of the marine biogenic signature due to the limited influence of continental sulfur contribution to their samples.

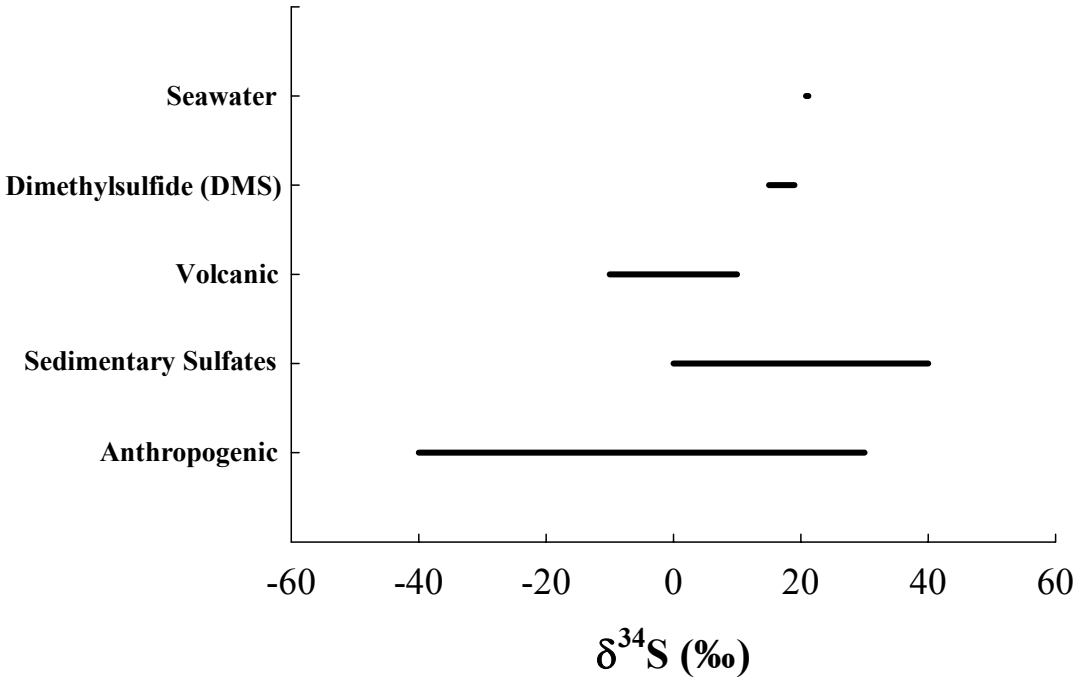

Figure 2.7. $\delta^{34}S$ values for the main sulfate contributors to the site locations of this study.

2.2.2 Volcanic

SO_2 emitted from volcanoes has been shown to be quite variable and has $\delta^{34}S$ values ranging from -10 to +10‰ (Nielsen, 1991) (Figure 2.7); however, this spread is reduced to 0 to +5‰ with mixing over large scales by atmospheric transport (Newman et al., 1991). Gaseous emissions from non-eruptive volcanic activities typically have values closer to 0‰. $\delta^{34}S$ values have been found to be quite uniform at +2.6 ± 0.3‰ (Newman et al., 1991) and +2.5 ± 2.5‰ (Patris et al., 2000a) during non-eruptive years. Conversely, SO_2 from an eruption can fractionate during oxidation to sulfate leading to an increasingly isotopically depleted gaseous plume (up to 10‰); however, for this to occur oxidation must proceed within the erupted plume (Castleman et al., 1974).

2.2.3 Dust

Sulfate dust derived from terrigenous sources is mainly associated with calcium sulfate ($CaSO_4$) and magnesium sulfate ($MgSO_4$). The main source regions of dust reaching Summit (Figure 2.3) are from the Takla Makan desert and the inner Mongolian deserts of northern China, including the Tengger and Mu Us (Bory et al., 2003; Bory et al., 2003; Bory et al., 2002). Dust inputs from the Taklimakan dominate during the dusty spring months while dust inputs from the Tengger and Mu Us dominate during the remainder of the year (summer through winter) during the low-dust season (Bory et al., 2003). The predominant contributor of dust to the Inilchek Glacier site is evaporitic deposits located in Central Asia (Figure 2.4) and from loess deposits in China (Kreutz et al., 2001; Wake et al., 1994; Kreutz and Sholkovitz, 2000, Pruett et al., 2004). Claquin et

al. (1999) determined that the largest source of soil gypsum in the world lies between the Caspian and Aral Seas just to the west of the Inilchek Glacier and that the prevailing synoptic meteorological conditions and large scale mixing events favor atmospheric transport to the region. Aizen et al. (1997) determined that winds have been observed to carry dust from the Taklimakan Desert basin to the Inilchek Galcier. Presently, the isotopic signatures for the dust sources contributing to the Greenland site are not well-known and enormously variable, ranging from 0 to 40‰ (Figure 2.7) representative of most sedimentary sulfates (Nielsen et al., 1991; Patris et al., 2002). The $\delta^{34}S$ value of the evaporitic dust being contributed to the Inilchek Glacier site is expected to be close to that of evaporating seawater sulfate (+21 ± 0.2‰; Raab and Spiro, 1991). However, throughout geologic time the sulfur isotope composition of seawater has changed. The various evaporite deposits of different ages in Asia have a range of reported $\delta^{34}S$ values from +10.8 to +35.5‰ (Krouse and Grinenko, 1991), with a mean value similar to that of seawater at +20‰.

2.2.4 Anthropogenic

Like volcanic emissions, anthropogenic SO_2 gas emitted from fossil fuel burning (combustion of coal, refining oil, and gas) and the roasting of sulfide ores also exhibits highly variable isotope composition, ranging from -40 to +30‰ (Figure 2.7). Measurements of flue gas from coal combustion, however, typically range from -1 to +3‰ (Nielsen, 1974). $\delta^{34}S$ values from the combustion of refining oil and gas have a similarly small range (+4.8 to +5.4‰; Nielsen, 1974). The roasting of sulfide ores is also a major source of atmospheric SO_2 and has an average $\delta^{34}S$ value of +3.4‰ (Grinenko and Grinenko, 1974). Anthropogenic source locations contributing to the two sites of this

study are variable. The Summit site is exposed to anthropogenic sources derived from primarily Asia, Europe, Russia, (Figure 2.3) where in the winter and early spring months a persistent anticyclone over Northern Asia forces some of the air pollution from Europe and Russia to the Arctic region (Christensen, 1997). The anthropogenic contribution to the Inilchek Glacier is likely coming from Central Asia, including countries of the former Soviet Union (FSU) and China, (Kreutz and Sholkovitz, 2000; Pruett et al., 2004) as evidenced in the lower Ca^{2+} and SO_4^{2-} concentrations of precipitation coming from the south and east (Kreutz and Sholkovitz, 2000; Wake et al., 1992) (Figure 2.4). Sulfate contributed to both of these regions is transported long distances and tends to be well-mixed; consequently, $\delta^{34}S$ values are expected to lie within the range of 0 to +7‰ (Nriagu and Coker, 1978; Cortecci and Longinelli, 1970; Saltzman et al., 1983; Herut et al., 1995; Wadleigh et al., 1996; Ohizumi et al., 1997). The $\delta^{34}S$ values for the anthropogenic contribution determined by regression analysis to the Inilchek Glacier averages around + 5‰ ($\delta^{34}S$ = +5.4‰ (Kreutz and Sholkovitz, 2000) and +4.8‰ (Pruett et al, 2004)) while in Greenland $\delta^{34}S$ values concentrate around the +3 to +5‰ (Patris et al., 2002; Nriagu et al., 1991; Li et al., 1993; Norman et al., 1999) range (+3 ± 1.5‰ (Patris et al., 2002); + 5.0 ± 0.9‰ (Li et al., 1993)).

2.3 Mass Balance Model Requirements

In order to use sulfur isotopes as a source tracer it is necessary to determine whether the isotope compositions are distinguishable and whether the isotope distribution is preserved during chemical transformation in the atmosphere. The average $\delta^{34}S$ values for the four primary sulfur sources contributing to sulfate to snow and ice for the two

study sites are shown in Table 2.2. It is immediately obvious that the seawater sulfate and evaporite dust of the Inilchek Glacier have similar compositions and could pose a

Table 2.2. Average $\delta^{34}S$ values of the four primary sulfur sources contributing to sulfate in snow of the two study sites.

	$\delta^{34}S$	Reference
Seawater	+21 ± 0.2‰	Rees et al., 1978
Marine Biogenic	+18.6 ± 0.9‰	Calhoun et al., 1991; Patris et al., 2000a
Dust	+20‰ (Inilchek Glacier)	Kreutz and Sholkovitz, 2000; Pruett et al., 2004
	N/A (Greenland)	
Anthropogenic	+5‰ (Inilchek Glacier)	Patris et al., 2000
	+3 ± 1.5‰ (Greenland)	Kreutz and Sholkovitz, 2000; Pruett et al., 2004

N/A – average is not available.

potential problem for isotope mass balance models. The Inilchek Glacier, however, is likely to be free of influence from direct marine sources due to its long distance from a seawater source. In addition the major ion ratios and the synoptic meteorology of the region suggest that there is minimal contribution from sea salt for any of the major ion species including SO_4^{2-} (Pruett et al., 2004; Kreutz et al., 2001; Wake et al., 1992; Wake et al., 1990). It is also obvious that the very large range of $\delta^{34}S$ values for the sedimentary sulfates potentially contributing sulfate to Greenland can pose a problem for mass balance calculations. In this case the $\delta^{34}S$ value used was determined using the model of Patris et al. (2002) where the isotopic value and the uncertainty are determined assuming the extreme case, where the $\delta^{34}S$ value is 20‰ apart from the remaining $\delta^{34}S_{nss}$ ($f_{mb}\delta_{mb} + f_a\delta_a$). Thus, for example, if the measured contribution of dust to a sample is 2% this would be multiplied by 20 ± 20‰, assuming the extreme case, to yield 0.4 ± 0.4‰.

Volcanic sulfate typically has $\delta^{34}S$ values (+2.5 ± 2.5‰ (Patris et al.,2000a; Patris et al., 2002)) similar to anthropogenic signatures for the two study sites (+3 ± 1.5‰ (Patris et al., 2002); + 5.0 ± 0.9‰ (Li et al., 1993)), which also presents a challenge when using mass balance models. For the Inilchek Glacier region the volcanic contribution was eliminated from the isotope mass balance models because there are no known active volcanic centers (Pruett et al., 2004) and there is no evidence for global-scale explosive activity during 2000 when the snowpit samples were collected. In fact, there is no apparent evidence, for example increases in SO_4^{2-} concentration, in Asian ice core records of major global volcanic eruption events such as Aguing, Krakatau, or Tambora (Kang et al., 2002). To a first approximation the volcanic contribution to the Greenland site was excluded from the isotope mass balance models due to the relatively small contribution from volcanic emissions to the total anthropogenic sulfur being emitted to the atmosphere (< 6.5%). In addition there is no evidence for global scale explosive volcanic activity during the time period (2000-2001) represented by the snowpit samples. Based on the determination of the sulfate sources that are the likely dominant contributors to the study locations, the measured isotope compositions together with estimates of the isotopic signatures taken from the literature are combined with the chemical concentration results to evaluate the fractional contributions of the various source contributions.

To use sulfur isotopic composition to distinguish sulfur sources, not only is it necessary to establish whether the isotope compositions of the sources are distinguishable, it is also essential to determine whether the isotope distribution is preserved during chemical transformation in the atmosphere (e.g., $SO_2 \rightarrow SO_4^{2-}$). The

dominant sulfur species being emitted to the atmosphere are dimethylsulfide (DMS) from ocean surfaces and sulfur dioxide (SO_2) from anthropogenic emissions. DMS is the main reduced sulfur species important in the production of nss-sulfate (Andreae, 1985; Bates et al., 1987; Berresheim, 1987). Other reduced sulfur species including, carbon disulfide (CS_2), hydrogen sulfide (H_2S), carbonyl sulfide (COS) and methyl mercaptan (CH_3SH) are also likely to contribute to sulfate formation over the remote oceans; however, the sea-air transfer of these compounds is only a few percent compared to DMS (Andreae, 1985).

The DMS isotope composition is governed by the assimilatory reduction process. Phytoplankton obtain sulfate from the seawater for the synthesis of organosulfur compounds. Sulfate is assimilated from the oceans ($\delta^{34}S = +21 \pm 0.2‰$), reduced inside the cell, and fixed into amino acids and other organic compounds (Andreae and Jaeschke, 1992). Microbial degradation liberates the chemically unstable reduced sulfur (DMS) to the environment where it is oxidized either to sulfate or MSA. The fractionation between sea salt and DMS via assimilatory reduction has not been directly measured; however, fractionation is known to occur during biological processing but it is suggested to be relatively small (1 to 3‰) with the lighter isotope concentrating in the product DMS (Chambers and Trudinger, 1979). Calhoun et al. (1991) determined the sulfur isotope composition of DMS to be $+17.0 \pm 1.9‰$, which falls within the predicted range expected with assimilatory sulfate reduction. DMS can also be transferred to the atmosphere via sea-air exchange to produce sulfate during subsequent atmospheric oxidation. Isotope fractionation associated with transfer to the atmosphere is thought to be negligible. Once in the atmosphere, the residence time of DMS is approximately 1 to 3 days due to the

reaction with the hydroxyl (OH) radical or with NO_3^- to form SO_2 and MSA. In general, the OH species dominates during daylight and NO_3^- at night; however, the relative importance of these two oxidation pathways is likely a function of latitude, altitude, and season, which control the OH_x and NO_x atmospheric concentrations (Berresheim et al., 1995). Hynes et al. (1986) identified two primary reaction channels for the DMS + OH reaction: 1) hydrogen abstraction where hydrogen is removed from DMS to yield the radical CH_3SCH_2 and water, and 2) OH addition, where a OH is added to the sulfur atom in DMS to yield $(CH_3)SOH$. The second major oxidative species, NO_3^-, reacts to form CH_3SCH_2, similar to the hydrogen abstraction channel, and HNO_3. These radical species further react to form SO_2 and sulfate (discussed below) and/or MSA by multi-step processes. Kinetic isotope effects associated with the DMS + OH reaction to form SO_2 have not been measured but examination of the oxidation of other reduced species, specifically H_2S, suggests a 2 to 3‰ fractionation where SO_2 is enriched in ^{32}S relative to reactant H_2S (Krouse and van Everdingen, 1983).

Many of the sources (anthropogenic and DMS oxidation) contributing to nss-sulfate in snow are emitted as SO_2. SO_2 oxidation to sulfate proceeds either by gaseous (homogeneous) or aqueous (heterogeneous) phase oxidation. The primary homogeneous gas phase oxidation pathway in the atmosphere is the reaction initiated by the OH radical (Atkinson et al., 1997) and is summarized as:

$$SO_{2(gas)} + OH_{(gas)} + M \rightarrow HOSO_2 + M \qquad \text{R. 2.1}$$

$$HOSO_{2(gas)} + O_{2(gas)} \rightarrow SO_{3(gas)} + HO_{2(gas)} \qquad \text{R. 2.2}$$

$$SO_{3(gas)} + H_2O_{(aq)} + M \rightarrow H_2SO_4 + M \qquad \text{R. 2.3}$$

The SO_3 formed in reaction 2.2 either hydrates or is incorporated into an existing aerosol to produce H_2SO_4. Saltzman et al. (1983) and Tanaka et al. (1994) determined that these reactions are likely to be kinetically driven and are expected to result in sulfate that is isotopically lighter than SO_2.

The heterogeneous pathway is another dominant oxidation mechanism of SO_2, and is typically more important than the gas phase reaction, particularly in the warm months and in the existence of clouds. This oxidation pathway commonly starts in cloud droplets or on the surface of wet aerosol particles where the primary step is the dissolution of SO_2 in water and its equilibration to form bisulphite (H_2SO_3) and sulphite (SO_3^{2-}):

$$SO_{2(gas)} \leftrightarrow H_2SO_{3(dissolved)} \qquad \text{R. 2.4}$$

$$H_2SO_{3(dissolved)} \leftrightarrow HSO_3^-{}_{(aq)} + H^+_{(aq)} \qquad \text{R. 2.5}$$

or

$$H_2SO_{3(dissolved)} \leftrightarrow SO_3^{2-} + 2\,H^+_{(aq)} \qquad \text{R. 2.6}$$

In reactions 2.5 and 2.6 equilibrium isotope effects occur where a large fractionation (+20 ‰; k = 1.02) is expected, with the heavier isotope concentrating in the HSO_3^- and SO_3^{2-} (Saltzman et al., 1983). The transformation of HSO_3^- and SO_3^{2-} to SO_4^{2-} typically proceeds by reaction with strong oxidants such as hydrogen peroxide (H_2O_2) and/or ozone (O_3), and/or with O_2 in the presence of catalysts (e.g. Fe(III) and Mn(II), OH, NO_3, NO_2, SO_5^-, etc.). Catalyzed reactions are important when transition metal concentrations are high, otherwise the primary oxidation mechanisms are H_2O_2 (pH < 5) and O_3 (pH > 5) (Berresheim et al., 1995; Liang and Jacobson, 1999; Penkett et al., 1979; Seinfield and Pandis, 1998; Savarino et al., 2000). The three mechanisms that oxidize HSO_3^- are

irreversible and isotopic equilibrium is not reached with sulfate. Consequently, these reactions are characterized by kinetic isotope effects where the sulfate produced is isotopically lighter than the HSO_3^- due to the preferential oxidation of the lighter isotope (Newman et al., 1991; Saltzman et al., 1983). Saltzman et al. (1983) determined, however, that the associated fractionation for the three kinetic reactions that can oxidize HSO_3^- is of much smaller magnitude (k = 1.001); hence the sulfate produced is isotopically heavier or enriched in ^{34}S primarily because of the larger fractionation (20‰) associated with the equilibrium isotope effect. Ultimately, ^{34}S is favored in the product SO_4^{2-} for heterogeneous oxidation reactions of SO_2, whereas ^{32}S is favored during homogeneous oxidation reactions, suggesting compensating heterogeneous and homogeneous oxidation pathways that result in minimal isotopic fractionation during SO_2 oxidation. It is important to note that if the ratio of homogenous over heterogeneous S(IV) oxidation should increase, as proposed during the last glacial period, that $\delta^{34}S$ values would be lower due to ^{32}S being favored in this reaction (Savarino et al., 2000; Alexander et al., 2003). For this study, the ratio of homogenous over heterogeneous S(IV) oxidation is expected to be approximately equal, as suggested by Saltzman et al. (1983), for an anthropogenically influenced atmosphere. Consequently, the total fractionation falls between the two reaction end members and is small. Overall, the chemical oxidation of SO_2 and DMS to SO_4^{2-} results in small isotope fractionations that allow the original distinguishable isotopic signatures to be preserved for source identification.

2.4 Summary

This chapter has provided information on the emission rates of sulfur from the major sources, both natural and anthropogenic, that impact the study sites, and details the typical sulfur isotopic abundance variations encountered for these sources. Furthermore, the specific source contributors used in the mass balance models for each site are provided. Lastly, the requirements that need to be satisfied in order to employ the mass balance models used in this research are highlighted.

Chapter 3: Sampling Protocols

Knowledge of the origin of submicron sulfate aerosols in a regional and global context is required to assess the impact of increasing anthropogenic sulfur emissions on the natural atmospheric sulfur cycle and on global climate. This chapter highlights the reasons for selecting the study site locations and focuses on the sampling strategies established to assure representative data collection and the protocols established for the collection and handling of trace sulfur samples from these regions. The dating methods used for the samples collected from each site are also described.

3.1 Study Site Selection

Samples were collected from snowpits (Figure 3.1.a and 3.1.b) of approximately 2 – 4 m depth, representing just less than 1 year for the Inilchek Glacier and just over 1 ½ years for Summit, Greenland. The primary reason these Northern Hemisphere sites were chosen was because of their exposure to anthropogenic emissions (Neftel et al., 1985; Finkel et al., 1986; Mayewski et al., 1986; Mayewski et al., 1990; Legrand et al., 1997; Kreutz and Sholkovitz, 2000; Pruett et al., 2004). Analysis of meltwater samples from these locations allows the degree of anthropogenic influence in these sensitive regions to be examined. The two sites were also chosen to minimize factors (melting, sublimation, condensation) that may affect the chemical and isotopic record via remobilization of ions. This can cause either an increase or decrease in the concentration of ionic constituents. Both site locations have negligible summer melt (0%) (Kreutz and Sholkovitz, 2000; Alley and Anandarkrishnan, 1995) and high accumulation rates, > 21 cm water equivalent per year for Summit (Johnsen et al., 1992) and > 100 cm water equivalent per

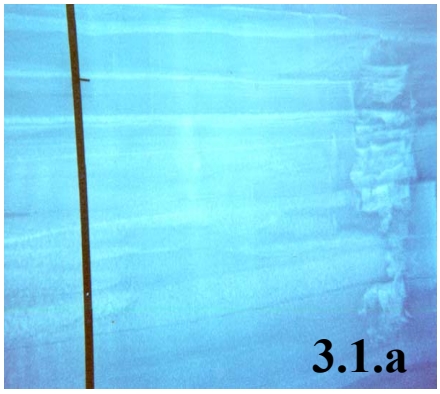

Figure 3.1.a and 3.1.b. The snowpit wall – lighter layers deposited in warmer months and darker layers deposited in colder months (3.1.a) and the 2 m snowpit from above with Dr. Christopher Shuman (3.1.b) for scale. Samples were taken May 2001, Summit, Greenland (3238 m; 72.58°N, 38.53°W).

year for Inilchek (Kreutz and Sholkovitz, 2000, Pruett et al., 2004). The high accumulation rates and sufficient winter and summer precipitation provide a larger mass per unit time in which to examine the potential seasonal changes in the isotope record.

3.2 Sampling Scheme & Protocols

Snowpit samples collected from Summit were sampled by myself and Dr. Christopher Shuman, National Aeronautics and Space Administration (NASA), at 2 cm intervals for major ion and sulfur isotopic analysis. The volume of sample collected for major ion analysis was approximately 60 mL and for sulfur isotope composition was approximately 180 mL, assuming a snow density of 0.3 g/L. All sampling equipment, including scrapers and shovels, was rinsed with methanol and purified water and soaked for 24 hours in purified water prior to use. Samples were placed into pre-cleaned low-density polyethylene (LDPE) containers sequentially washed by rinsing and soaking three times with Milli-Q 18 mΩ water. LDPE was chosen for sampling as less metal is introduced during manufacture. Samples for density measurements were taken in parallel every 3 cm to convert the original sample depths to water equivalent depth (WED) and samples for hydrogen isotope measurements were also taken every 3 cm in order to date the snowpit samples as will be described later (see also Shuman et al., 1995, 1998). All samples were then packed into insulated shipping containers and transported on dry ice to the National Institute of Standards and Technology (NIST) and the Institute for Quaternary Studies at the University of Maine for processing. Samples were stored at –25°C in a dedicated freezer until analysis. Collection and analysis procedures are detailed in ITASE (International Trans-Antarctic Scientific Expedition) “200 years of

Past Antarctic Climate and Environmental Change" Science and Implementation Plan (www.antcrc.utas.edu.au) (ITASE, 2000).

The samples collected from the Inilchek Glacier were obtained by Professor Karl Kreutz, University of Maine, during a 2000 expedition. Snowpit samples were sampled at 5 cm intervals for major ion concentrations and density. Samples for deuterium and oxygen isotope measurements for dating the snowpit were also taken at 5 cm intervals. One-liter samples for sulfur isotopic analysis were collected at an interval of 10 cm. Samples were placed into pre-cleaned containers and stored below –15°C until analysis. All sampling was done using the ITASE procedures. Samples were packed into insulated shipping containers and transported frozen to the University of Maine, and processed in a dedicated cold room (temperature < -12°C) using established techniques for ultra-clean sample preparation. Samples were then shipped to NIST for sulfur isotope analysis.

Major ion (Na^+, K^+, NH^{4+}, Mg^{2+}, Ca^{2+}, Cl^-, NO_3^-, SO_4^{2-} and methane sulfonic acid (MSA)) measurements for both the Summit and Inilchek snowpit samples were performed at the University of Maine with a dedicated Dionex DX-500 ion chromatograph. Anions were analyzed with an AS-II column using 6 mM sodium hydroxide (NaOH) eluent and cations were analyzed with a CS-12A column using 25 mM MSA eluent. The uncertainties for all the species were ± 5% (Kreutz, personal communication). The sulfate concentrations determined were used as a guide for sample spiking and in general the concentrations were in good agreement with the sulfate concentrations determined with the double spike technique.

3.3 Dating

Accessing the high-resolution (seasonal) sulfur isotopic record of snow and ice not only requires an analytical technique capable of measuring low concentration samples, but also necessitates dating techniques that are also of sufficient resolution to observe seasonal time-series data. The snowpit samples from Summit were dated using the deuterium isotope record. δD measurements were performed at the Institute of Artic and Alpine Research (INSTAAR) at the University of Colorado at Boulder on a Micromass SIRA Series II Dual Inlet mass spectrometer using standard carbon dioxide (CO_2) equilibration techniques (Vaughn et al., 1998). Data are reported in delta notation (δD) relative to the international water standard SMOW. The reproducibility on the δD measurements based on replicate analyses of multiple standard measurements - Vienna Standard Mean Ocean Water (VSMOW) was approximately ± 0.3‰ (1σ).

The specific method used for dating the Summit snowpit samples is described by Shuman et al. (1995, 1998) and uses a combination of the seasonal changes in the hydrogen isotope (δD) ratios, where negative δD values indicate colder temperatures and more positive values indicate warmer temperatures, and automatic weather station (AWS) temperature data. The AWS was located approximately 1 km from the field site in this study. The method relies on the close correlation of the stable isotope (δD) depth series to the surface temperature time series at a site. The stable isotope depth record can be used as a proxy for the "surface" temperature record as long as accumulation occurs relatively consistently throughout the year. The two records are compared using a qualitative point-pairing technique that is directed by the maxima, minima, and inflections in the shape of the profiles. Once complete, the stable isotope "depth" profile

is now correlated to the automated weather station temperature "dated" (time-series) profile to link the depth profile with time. The uncertainty is typically ± 2 weeks at these depths (Shuman et al., 1995, 1998).

The Inilchek samples were dated using the deuterium and oxygen isotope record and details are given in Kreutz and Sholkovitz (2000) and Pruett et al. (2004). The deuterium and oxygen isotopes were measured at the University of Maine using standard carbon dioxide (CO_2) equilibration techniques (similar to the method used for the Summit samples by INSTARR) on a VG SIRA II mass spectrometer. Data are reported in traditional delta notation ($\delta^{18}O$ and δD, refer to Chapter 2, section 2.2) relative to the international water standard SMOW. The analytical precision based on replicate analyses of samples and international standards for $\delta^{18}O$ is ± 0.05‰ (1σ) and for δD is ± 0.3‰ (1σ). The uncertainty is similar to that of the Summit samples with ± 2 weeks near the surface.

3.4 Summary

Chapter 3 described the reasons for selection of the two northern hemisphere site locations and focuses on the sampling strategies established to assure representative data collection and the protocols established for the collection and handling trace sulfur samples, and minimizing sample contamination during handling from these regions. The dating methods (δD for Greenland and δD and $\delta^{18}O$ for the Inilchek Glacier samples) used for the samples collected from each site were also described.

Chapter 4: Experimental Procedures

Sulfur isotope composition measurements are typically made using gas source Isotope Ratio Mass Spectrometers (IRMS) and these techniques are capable of precisions of 0.2‰ on sample sizes ≥ 33 μg S (≈ 1 μmole S). To obtain enough sample (≥ 33 μg S) for sulfur isotope composition analysis of snow and ice, 300 to 1000 g of meltwater are required based on the typical sulfate concentration ranges encountered (25 to 100 ng/g (ppb)) (Patris et al., 2000a, b & 2002). Global atmospheric sulfur cycling is a dynamic process that varies on short timescales and these large of sample requirement can mask seasonal changes in S sources.

Thermal ionization mass spectrometry (TIMS) has been used for many years in the geological community to measure trace element concentrations with high precision. However, the use of TIMS for isotope composition measurements for sulfur has been limited due to the poor precisions (± 1-2‰) resulting from instrumental fractionation effects. The fundamental limitation to the accuracy and precision in isotopic measurements by TIMS is mass fractionation during ion production in the source. Therefore, the measured ratio at the detector differs from the true ratio and changes with time. This fractionation is thought to follow Rayleigh-like fractionation as expressed in the equation below,

$$R_{ij}^{\text{Measured}} = R_{ij}^{\text{Corrected}} \sqrt{\frac{m_j}{m_i}} \left[1 - F\right]^{\left(\sqrt{\frac{m_j}{m_i}} - 1\right)} \qquad \text{Eqn. 4.1}$$

where R is the ratio of the lighter isotope, m_i, over the heavy, m_j, and 1-F is the fraction of reservoir remaining on the filament. During vaporization ^{32}S is enriched in the vapor

and depleted in the reservoir. As the reservoir is depleted there is less ^{32}S available and the vapor curve decreases as does the reservoir curve. This effect is illustrated in Figure 4.1.a., which shows an example of a Rayleigh-generated vapor curve for the $^{32}S/^{34}S$ ratio and the associated depletion of the 2 curves with time and depletion of the reservoir. One hundred percent of the reservoir is still remaining when f = 1 and the reservoir is completely depleted at f = 0. Ideally the ratio being measured at the detector would be unchanging with depletion of the reservoir or through an analysis and the true ratio in the source could be determined as shown by the line with a slope of 0 in Figure 4.1a. Figure 4.1.b shows the vapor curve $^{32}S/^{34}S$ ratios recast in $\delta^{34}S$ notation. In this figure, the curve has a positive slope because as ^{32}S is being removed, the vapor is becoming more enriched in ^{34}S resulting in heavier $\delta^{34}S$ values with depletion of the reservoir (this is due to how $\delta^{34}S$ is expressed with the heavy isotope over the lighter isotope, refer Section 2.2). Again, the ideal situation would be that the ratio would be unchanging with depletion of the reservoir (slope = 0). Ultimately, the key to determining the true ratio in the source and to improving the precision in the TIMS isotope composition measurements is to correct for this instrumental fractionation or the changing ratio. To do this a well-characterized $^{33}S/^{36}S$ double spike can be used to determine a fractionation factor (α) that corrects for the instrumental fractionation (changing ratio) thereby providing the true $^{32}S/^{34}S$ ratio in the source. The $^{33}S/^{36}S$ double spike has the added advantage that it also allows small concentration samples to be measured for both concentration and isotope composition, because it acts as a chemical carrier by adding to the total sulfur mass in the sample. This is a significant advantage over the gas source technique that is limited to only isotope composition measurements.

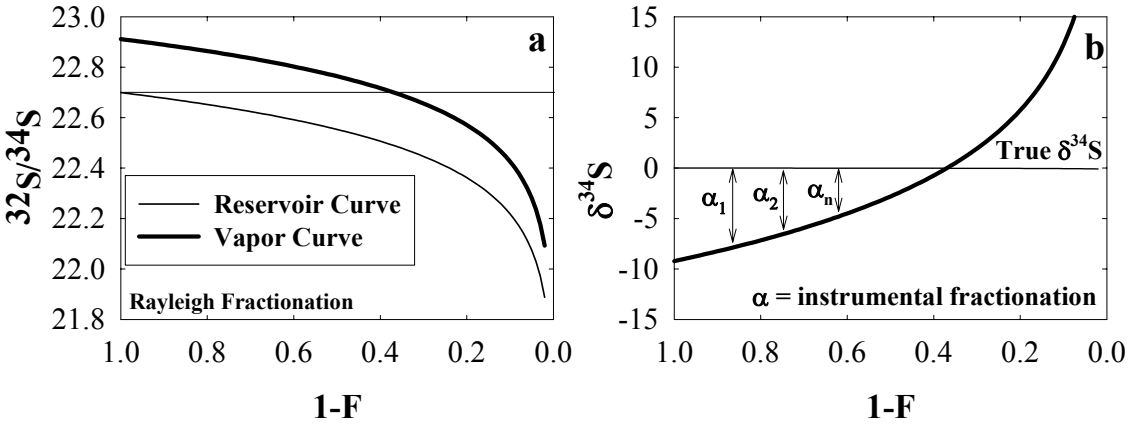

Figure 4.1. Instrumental fractionation curves modeled as Rayleigh fractionation for the $^{32}S/^{34}S$ ratio (a) and $\delta^{34}S$ (b). The α_1, α_2, and α_n show the net instrumental fractionation through time.

This chapter provides a detailed description of the double spike analytical technique, including a detailed description of sample preparation and mass spectrometric procedures, followed by an overview of the data reduction and data analysis techniques used in this research.

4.1 Double Spike

The Double Spike technique has proven successful for barium, calcium, cesium, molybdenum, lead, and iron isotopic measurements (Eugster et al., 1969; Dietz et al. 1962; Russell et al., 1978; Moore et al., 1974; Todt et al., 1996; Skulan et al., 1997; Johnson et al., 1999) but has yet to be used for the sulfur isotopic system. The sulfur system is ideally suited for this technique because of the low natural abundance of the spike isotopes (atomic abundances: $^{33}S \approx 0.75\%$, $^{36}S \approx 0.015\%$ (refer Section 2.2)) thus only small corrections are required. The $^{33}S/^{36}S$ spike used in this study was prepared from solutions of $^{33}SO_4^{2-}$ and $^{36}SO_4^{2-}$ that were prepared from elemental sulfur produced in the former Soviet Union (Table 4.1 and Figures 4.2.a and b). The spike materials are

Table 4.1 Atom Percent Abundances for the Enriched Isotopes				
		^{33}S		
Isotope	^{32}S	**^{33}S**	^{34}S	^{36}S
Percentage (at. %)	0.05	99.9 ± 0.05	0.02	< 0.003
		^{36}S		
Isotope	^{32}S	^{33}S	^{34}S	**^{36}S**
Percentage (at. %)	0.15	0.02	0.05	99.78 ± 0.05

the highest purity available with the ^{33}S spike isotope being 99.9 ± 0.05 atom % and the ^{36}S spike isotope being 99.78 ± 0.05 atom %. The atom abundances for the minor

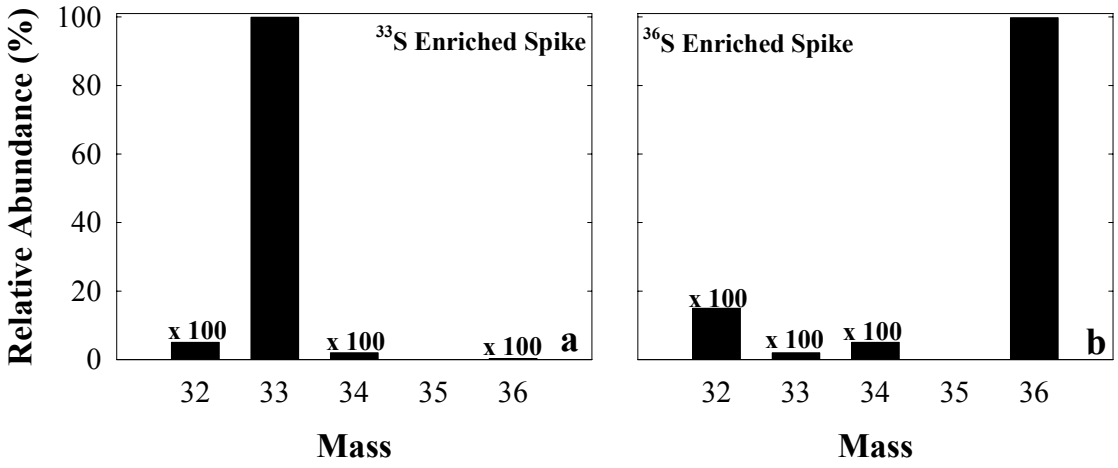

Figure 4.2. Relative atom abundances for sulfur masses 32, 33, 34, and 36 for the ^{33}S enriched spike (a) and for the ^{36}S enriched spike (b). The minor isotopes are multiplied by 100 to illustrate how insignificant these are relative to the spike abundances.

isotopes for both spikes are negligible as can be seen in Figures 4.2.a and b. The enriched ^{33}S and ^{36}S solid spike materials were converted to sulfate by oxidation with 6 g of high purity Fisher Optima nitric acid (HNO_3) in a sealed Carius tube at 240°C (Paulsen and Kelly et al., 1984). After dissolution the tube was opened and the contents were transferred to a 50 mL beaker, rinsing the Carius tube with quartz distilled water. High-purity sodium carbonate (Na_2CO_3) was added to yield a Na/S atom ratio of 4 to provide sufficient Na to act as a counter-cation to prevent a loss of S as sulfuric acid during heating. The solution was then evaporated to dryness and the nitrates destroyed by repeated additions of 5 mL high purity Fisher Optima hydrochloric acid (12 N HCl) and evaporation. This last step is extremely important because nitrates destroy the reducing capability of the reduction (Thode) solution (refer to Section 4.2). The dried spike materials (now in sulfate form) were dissolved in 5 mL high purity Fisher Optima HCl and transferred to 500 mL high-density-polyethylene (HDPE) bottles using quartz-distilled water. The final volume for $^{33}SO_4^{2-}$ was approximately 72 g and for $^{36}SO_4^{2-}$ approximately 53 g. The gravimetric concentrations were approximately 1,300 μg/g for ^{33}S and 175 μg/g for ^{36}S.

The double spike was prepared gravimetrically to yield a $^{33}S/^{36}S$ molar ratio of approximately 1. A spike mixture of 1:1 (^{33}S:^{36}S) is the optimum ratio required to minimize magnification in uncertainty and contribution of ^{32}S and ^{34}S from the spike to the natural sample, over the range of spike to sample ratios likely to be encountered. Figure 4.3 shows the error amplification ratio (E(R)) for a 1:1 spike mixture for spike:sample molar ratios from 0.01 to 10. The equation used to calculate the error using the $^{34}S/^{33}S$ ratio is:

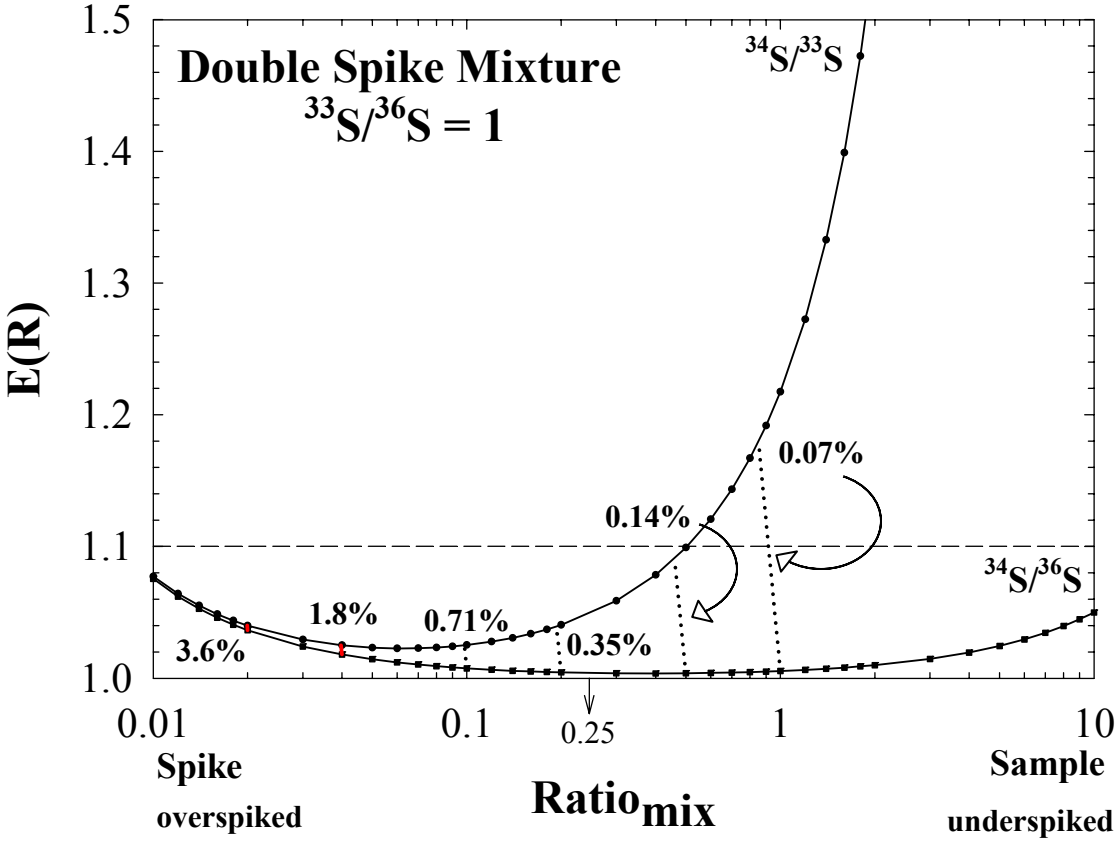

Figure 4.3. Error amplification ratio for spike:sample molar ratios of 0.01 to 10 for a double spike mixture of 1:1. The percent values are the contribution of ^{34}S from the spike to the sample and the dotted lines between the two curves are the tie lines that show the $Ratio_{mix}$ that corresponds with the ^{34}S contribution. The optimum range for sample spiking is a $Ratio_{mix}$ range of 0.1 to 0.25.

$$E(R) = \frac{\left[\left(\frac{^{33}S}{^{34}S}\right)_{measured} \times \left(1 - \left(\frac{^{34}S}{^{33}S}\right)_{sample}\left(\frac{^{33}S}{^{34}S}\right)_{tracer}\right)\right]}{\left[\left(\left(\frac{^{33}S}{^{34}S}\right)_{tracer} - \left(\frac{^{33}S}{^{34}S}\right)_{measured}\right) \times \left(\left(\frac{^{34}S}{^{33}S}\right)_{sample}\left(\frac{^{33}S}{^{34}S}\right)_{measured} - 1\right)\right]} \qquad \text{Eqn. 4.2}$$

The error amplification curves in this case were calculated for the $^{34}S/^{33}S$ and $^{34}S/^{36}S$ ratios because most of the error is coming from ^{34}S as it is the lowest abundance isotope even with the addition of the double spike. As a result, the count rate on the ^{34}S isotope is the fundamental limitation on the measurement precision. The optimum situation is to limit the contribution of ^{34}S from the spike to the sample (percent contributions of ^{34}S from the spike to the sample are shown for the respective tie lines that link the two curves ($^{34}S/^{33}S$ and ^{34}S /^{36}S)) and to limit the error magnification to 1.1% or lower. It was determined that a $Ratio_{mix}$ range of approximately 0.1 to 0.25 was the optimum range for sample spiking, which requires approximately 1 mole of spike to be added to approximately 1-2 moles of natural sample (e.g., Figure 4.4). This range in the $Ratio_{mix}$ limits the percent contribution of ^{34}S to 0.35% - 0.71% and the error magnification is kept to a minimum on both curves (< 1.1%).

The concentration of the 1:1 double spike was determined by calibrating it against a dilute solution prepared gravimetrically from Standard Reference Material (SRM) 3154 (Sulfur Spectrometric Solution). This SRM was certified coulometrically as well as gravimetrically and the combined uncertainty on the certificate was 0.3%, relative (SRM Certificate 3154, NIST). Assuming that the concentration of S was equal to twice the hydrogen ion concentration, the coulmetric determinations were in excellent agreement

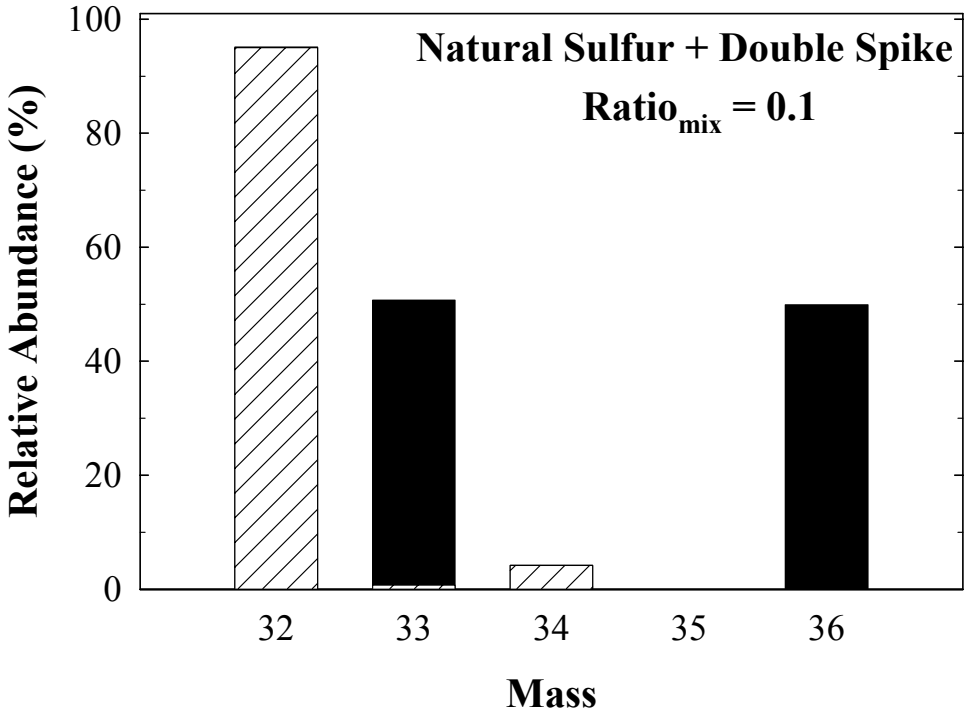

Figure 4.4. Relative abundances of the four isotopes for a natural sample mixed with the double spike in a Ratio$_{mix}$ = 0.1. The $^{32}S/^{33}S$ ratio is about 2:1.

with the less precise gravimetric values (SRM Certificate 3154, https://srmors.nist.gov/view_detail.cfm?srm=3154). The spike concentration was then established by mixing the assayed SRM with the spike in 30 mL polycarbonate bottles and carrying these samples through the same chemical and mass spectrometric procedures used for samples and standards (refer to Section 4.2 below). The concentration for double spike mix 1 (DS #1) was 0.68291 ± 0.00116 μmoles S/g (1s) based on six mixes (Table 4.2). The relative standard deviation for these six determinations was 0.170%. A second double spike mix was prepared as the first was depleted after completing test analyses of standards. The concentration for double spike mix 2 (DS #2) was 0.65355 ± 0.00158 μmoles S/g (1σ) based on six mixes (Table 4.2). The relative standard deviation for these six determinations was 0.242%.

The isotopic composition of the $^{33}S/^{36}S$ double spike mixtures, given in Table 4.2 and Figure 4.5.a and 4.5.b, were determined using sample sizes ranging from approximately 50 to 291 μg S. The sample sizes were chosen both to minimize the effect of the blank, which is typically less then 0.1 μg based on our accumulated blank record

Table 4.2. Sulfur Concentration and Compositions of Double Spike #1 and #2 (atom %).

Double Spike #1				
Sulfur [ ] (μmoles/g)	**^{32}S**	**^{33}S**	**^{34}S**	**^{36}S**
0.68291± 0.00116 (1s)	0.36	49.38	0.032	50.23
Double Spike #2				
Sulfur [ ] (μmoles/g)	**^{32}S**	**^{33}S**	**^{34}S**	**^{36}S**
0.65355 ± 0.00158 (1s)	0.38	48.96	0.031	50.63

covering 3 years (n=37), and to minimize the amount of spike used. Ratio measurements

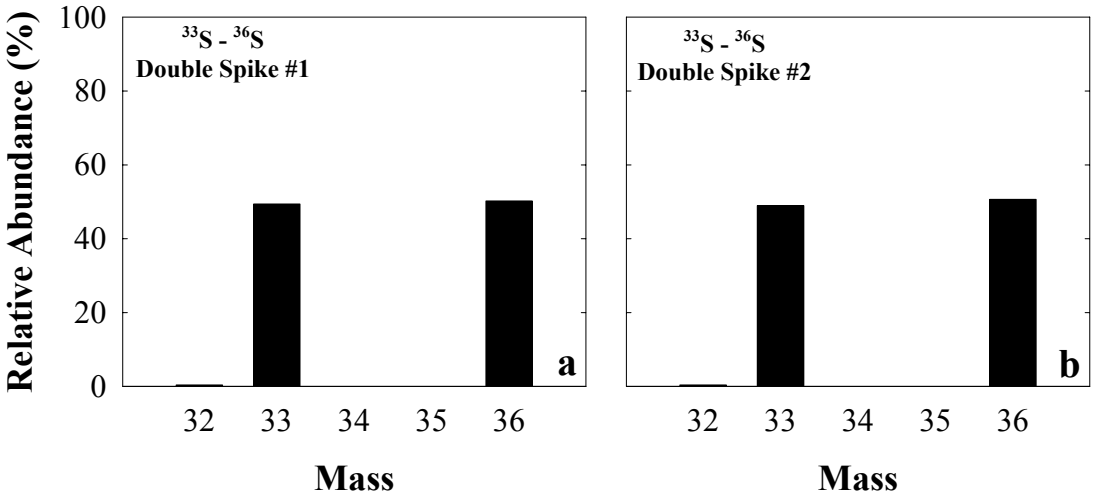

Figure 4.5 Relative abundance of the four isotopes for double spike mixtures #1 (a) and #2 (b).

for DS #1 were made on a single sector 12" radius NIST designed mass spectrometer (these were the only measurements done on the NIST designed mass spectrometer) equipped with a Faraday collector and ratios measurements for DS #2 were made on a VG Sector 54 multi-collector mass spectrometer at the University of Maryland. The signal intensity on ^{33}S and ^{36}S was typically greater then 2V (10^{11} Ω feedback resistor) in both cases. The ratio measurements were corrected for both instrumental fractionation and blank to obtain the corrected isotopic composition. To correct for instrumental fractionation a fractionation factor was determined by comparing the $^{107}S/^{109}S$ measured (raw uncorrected) ratio to the absolute $^{107}S/^{109}S$ ratio of IAEA-S-1 ($^{107}S/^{109}S = 22.6504$; Ding et al., 2001) using the exponential law [The mass spectrometric procedure of this technique is based on the production of AsS^+ (arsenic sulfide). Because As (arsenic) is mono-nuclidic, the sulfur mass spectrum (32, 33, 34, and 36) is shifted to higher mass by 75 amu (atomic mass units); 107, 108, 109, 111]. The fractionation factor was then used to correct the remaining measured ratios ($^{107}S/^{108}S$, $^{109}S/^{108}S$, and $^{111}S/^{108}S$) for instrumental fractionation. The $^{107}S/^{109}S$ ratio of IAEA-S-1 was used because it is the most precise of the ratios and therefore is the best approximation of instrumental fractionation. The instrumentally-corrected double spike composition values were then corrected for blank. The composition of the blank is uncertain but likely varies by 40‰ (refer to Section 5.2.2 for details); however, the concentration is relatively well-characterized, as shown earlier, and is typically less the 0.1 μg. Although the composition is uncertain the sample/blank ratio was kept relatively high (> 250 up to 1000) to minimize the effect of this uncertainty and reduce spike consumption. In addition, the DS composition was calibrated against IAEA-S-1. If the DS isotope

composition is correct, repeated measurements of the spiked standard (standard was optimally spiked (2:1 molar ratio standard:spike)) and with a standard:blank molar ratio of (> 2000/1) should yield an average $\delta^{34}S$ within the absolute reference value provided by the Institute for Reference Materials and Measurements (IRMM, Belgium) of –0.30 ± 0.12‰ (Ding et al., 2001). The $\delta^{34}S$ obtained was –0.32 ± 0.04‰ (1σ, n = 4) for DS #1 and -0.31 ± 0.13‰ (1σ, n = 8) for DS #2 after blank correction (refer to Section 4.3 for details on blank correction) (refer to Appendix A for further details on the individual measurements). Both results were within the stated uncertainty of IRMM for this standard suggesting the DS compositions had been corrected appropriately and are close to the true value. It is important to note that all calibration mixes had ^{34}S signal intensities above 100 mV and it was expected these data would provide the best measurement accuracy for the double spike calibration.

4.2 Chemical and Mass Spectrometric Procedures

The chemical and mass spectrometric methods used in this research are similar to that described by Paulsen and Kelly (1984); however, the sample preparation steps including the drying procedures and the reduction procedures have been modified to accommodate the different matrix (snow and ice) and large sample volumes. Typically, samples are first dried under flowing argon (Ar) and then diluted to yield an approximately 5 mL sample size. The sample is added to a reducing solution – hydriodic, hydrochloric, and hypophosphorous acids - (HI-HCl-H_3PO_2) (Thode et al., 1961), where sulfate is chemically reduced to hydrogen sulfide (H_2S) and trapped in an arsenic-ammonia (As-NH_3) solution. Sulfur is then precipitated as arsenic sulfide (As_2S_3) with the addition of HCl. Arsenic sulfide precipitates are then rinsed with 18 MΩ Milli-

Q water and re-dissolved in an As-NH_3 solution to yield a ratio of As/S = 2 and a [S] = 0.1 g/L. From this mixture approximately 1.5 μg of sulfur is loaded on a Re filament with silica gel and placed into a multi-collector thermal ionization mass spectrometer for isotope analysis.

4.2.1 Reagents

The preparation of the reducing solution followed that described by Thode et al. (1961) using Sigma Aldrich HI (125 mL), Sigma Aldrich H_3PO_2 (61 mL), and high purity Fisher Optima HCl (205 mL). The mixed solution was refluxed under a nitrogen (N_2) stream (0.2 L/min.) at 120°C for 3 hours to remove any sulfur as H_2S. The As-NH_3 solutions were prepared from a saturated ammonia solution prepared by bubbling high-purity NH_3 through a water scrubber and into quartz-distilled water chilled with ice (Kuehner et al., 1972). Both solutions were prepared by dissolving SRM 83c (As_2O_3) in saturated NH_3 solution. The first solution, which is used to trap the H_2S, was 1000 μg of As/mL and the dilution solution was approximately 312 μg of As/mL. Silica gel was prepared by fusing high-purity quartz with sodium carbonate (Na_2CO_3) and washed with quartz-distilled water (Kelly, personal communication). The silica gel was mixed with phosphoric acid, (H_3PO_4) prepared from high-purity P_2O_5 and quartz-distilled water, to yield 20 μg of silica gel/μL of 0.4 M H_3PO_4. The Si gel and H_3PO_4 are premixed in a ratio designed to maximize signal level and stability (Paulsen and Kelly, 1984).

4.2.2 Chemical Preparation (Sample, Test Standards, and Blank)

The melting and drying procedures for the samples focused on minimizing sample contamination (blank). First, samples were allowed to melt in their sample containers

over night at room temperature on the benchtop in a Class 10 clean laboratory. Second, samples were spiked optimally using a 5 mL plastic syringe (2 moles of natural to 1 mole of spike, refer to section 4.1) prior to drying the samples to add a counter cation (Na) to minimize loss of sample during the drying process. Third, the samples were dried on a hotplate in 250 to 400 mL Pyrex flasks with a 1 cm diameter 45° sidearm within a HEPA filtered glove box (to limit atmospheric sulfur particle contribution) contained in Class 10 clean laboratory. This sidearm construction was designed to reduce the cross section of the opening to the atmosphere to reduce chemical blank. The flasks were heated to dryness under a flowing stream of Ar and samples were converted to the chloride form by the addition of 1 mL of high-purity HCl (Fisher Scientific) and 4 mL of 18 MΩ MilliQ and heated to dryness again (Ar was brought into the glove box via stiff Teflon tubing containing an inline filter to absorb sulfur particles in the gas). The additions of HCl eliminate the nitrates, which interfere with the reduction step (Section 4.2.3). The dried samples were dissolved in 1 mL of high-purity HCl and 5 mL of 18 MΩ MilliQ water, and transferred to 30 mL polycarbonate bottles for storage until reduction.

Two different methods were used for the chemical preparation of the standards based on the purpose of the standard (testing the technique) or the sample concentration being measured. For standards being used to test the technique and for higher concentration samples, the standard and spike were added directly into 30 mL polycarbonate bottles. Aliquots of the spike solution were added by weight to the standards using a 5 mL plastic syringe to yield approximately 5 mL per batch. This would allow for 3 analyses per batch. For samples with lower concentration representative dilute solutions of the spike materials were prepared. Aliquots of the

dilute standard solution were taken and spiked accordingly and processed as described above for the samples.

Standards and high concentration samples were processed in groups of four; 3 standards or samples and 1 blank. Low concentration samples were processed in groups of 5; 2 samples, 2 standards (IAEA-S-1 and IAEA-S-2), and 1 blank. As with the standards, the chemical processing of the blanks was based on whether the blank was to be processed with test standards or high or low concentration samples. For blanks associated with high concentration samples and test standards 2 mL of 18 MΩ MilliQ water and 2 mL of high-purity HCl was added to 30 mL polycarbonate bottles and spiked typically with 0.5 g of spike. For blanks processed with low concentration samples and standards, a representative volume (volume similar in magnitude to that required for real samples) of 18 MΩ MilliQ water was added to a Pyrex flask and spiked with approximately 0.5 g of spike solution and dried as described above for the samples.

4.2.3 Reduction Chemistry

All samples were put through the reduction procedure within 24 hours of chemical preparation. Fifteen milliliters of the reducing solution was refluxed for 45 min at 120°C with nitrogen (N_2) gas injected through a sidearm (0.12 L/min) and then cooled. The sample was then transferred to the reduction flask (see Figure 4.6) and refluxed for 45 minutes. The sulfate in the sample was reduced to H_2S and flushed out of the flask through a 10 mL distilled water trap and then trapped in a 15 mL centrifuge tube containing 1 mL of the aqueous As-NH_3 solution (solution 1, Section 4.2.1). During the collection step the As-NH_3 solution was cooled in an ice bath to minimize loss of NH_3. Retention of the NH_3 is necessary to keep the pH of the capture solution at 11, which was

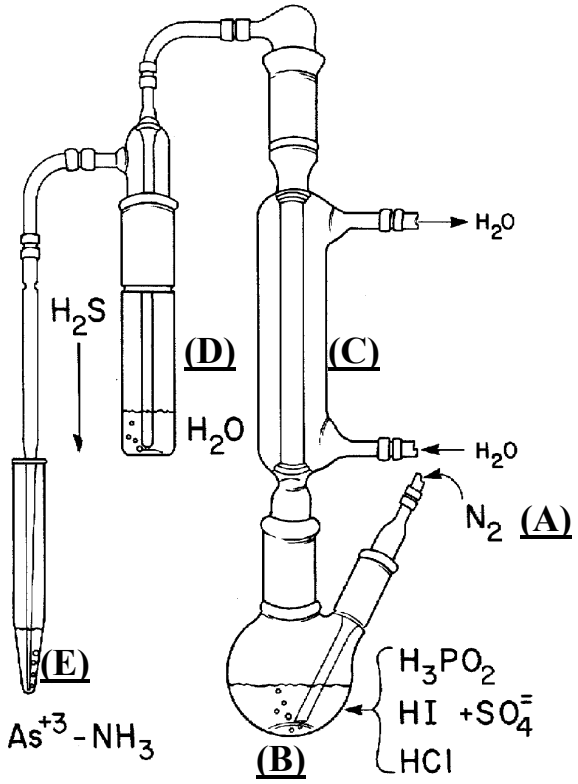

Figure 4.6. Schematic of the reduction apparatus for reducing sulfate to arsenic sulfide. (A) N_2 inlet, (B), reduction flask, (C) condenser, (D) water trap, and (E) arsenic-ammonia (AS-NH_3) trap solution.

needed to convert H_2S to HS^- for better yields. The trapped sulfur was then precipitated as arsenic sulfide (As_2S_3) with the addition of high-purity HCl. Samples smaller than 5 μg can be recovered using this technique. The precipitate is then centrifuged for 10 min to remove the As_2S_3 particles from the solution. The supernatant was then removed with a Pasteur pipette. The arsenic sulfide precipitate was then washed and centrifuged 3 times with 10 mL portions of 18 MΩ Milli-Q water. The cleaned As_2S_3 was then re-dissolved in an As-NH_3 solution (solution 2, Section 4.2.1) to yield a ratio of As/S = 2 and a [S] = 0.1 g/L. An important feature of this reduction chemistry is that for all samples, whether natural samples or standards, the resulting arsenic sulfide precipitate is the same and not affected by impurities because the reduction solution reduces only sulfate.

4.2.4 Mass Spectrometry

The primary thermal ionization mass spectrometer used in this study was the University of Maryland multi-detector VG Sector 54 equipped with 7 Faraday collectors and a turret for 20 samples. The mass spectrometric procedure is based on the production of AsS^+ (arsenic sulfide) molecular ions from a single rhenium filament using silica gel to enhance ionization. Again, because As (arsenic) is mono-nuclidic, the sulfur mass spectrum (32, 33, 34, and 36) is shifted to higher mass by 75 amu (atomic mass units); 107, 108, 109, 111.

Rhenium filaments were fabricated from zone refined Re ribbon (H. Cross Co. – Thickness: 0.0012”, Width: 0.030”, length: 1500) and out-gassed initially for 5 minutes at 2 A at 10^{-6} torr followed by two 2 minute cycles of 5 s flashings at 3.5 A at 10^{-6} torr. Filaments were typically stored for one week before use. Samples were loaded on the Re

filaments in a laminar flow hood. Details of the loading procedure are described in Paulsen and Kelly (1984). In brief, the Si gel/H_3PO_4 solution is placed in an ultrasonic bath for 10 min to facilitate the suspension of the Si gel particles. The solution is then shaken vigorously prior to each loading and 5 μl were placed in the center of the filament using 5 cm length 0.030" i.d. intramedic polyethylene tubing attached to a 21 gauge hypodermic needle affixed to a syringe. A 0.9 A current is applied until the solution is dry. Fifteen microliters (≈ 1.5 μg) of the As_2S_3 sample solution is then added as droplets to the dried Si gel. With the addition of the first drop of the sample the filament current is raised to 1.6 A. The remainder of the sample is added and then the sample is evaporated to dryness. The current is then increased and the sample dried at a red glow for about 1-2 s. The sample solutions were aged for a minimum of 12 hours before loading for optimum signal intensity and stability. It is important to note that because the same amount of As_2S_3 sample solution is loaded regardless of what is being analyzed (samples or standards) the signal intensities will be the same, as along as they are spiked similarly. As a consequence, the precision of the $\delta^{34}S$ measurements will be the same for samples and standards regardless of the sample amount processed.

All samples were placed into the mass spectrometer turret immediately upon completion of loading to minimize exposure to room atmosphere. Once samples were loaded the pressure in the source was reduced to below 2 x 10^{-7} mbar with the addition of liquid N_2 to the source cold finger. The filament was initially heated to approximately 1.5 A (~ 700°C) for 5 minutes and then incrementally heated to a final current of roughly 1.8 A (~ 1000°C). The signal intensity commonly gave an AsS^+ ion beam of 1 to 3.5 V for mass 107 and 30 to 90 mV for 109 (10^{11} Ω feedback resistor) after focusing for

maximum intensity. Data collection began approximately 20-30 minutes after commencing filament heating. Five data blocks were collected each block consisting of 10 integrations of all masses (^{107}S, ^{108}S, ^{109}S, and ^{111}S) using an integration time of 10 s on peak. Background signals were read before each set using an integration time of 10 s. Typical run time was about 25 minutes. The integration time on the background was increased to 45 s later in the study for samples with low signal intensity < 15 mV on mass 109. Above 15 mV the statistics between the two routines was typically similar for each ratio pair.

4.3 Data Reduction

4.3.1 Sulfur Isotope Composition

The $^{107}S/^{109}S$ ($^{32}S/^{34}S$) natural isotopic ratios were extracted from the mass spectrometric measurements using an iterative calculation scheme similar to that used in previous double spike applications (Eugster et al., 1969, Russell et al., 1978, Skulan et al., 1997, and Johnson et al., 1999). In this technique the instrumental fractionation and the natural isotope composition are successively refined until the values converge. The basic derivation of the equations used in the iterative scheme is given in Text Box 1. The step-by-step description below describes how these equations were used to derive the true ratio $^{107}S/^{109}S$ ($^{32}S/^{34}S$) in the source.

1) A first approximation or trial value for the $^{108}S/^{111}S$ ($^{33}S/^{36}S$) ratio of the double spike was calculated from the first unmixing equation (Equation 2 in Text Box 1) given below:

$$\left(\frac{^{33}S}{^{36}S}\right)_{tracer}^{TRUE} = \left(\frac{^{33}S}{^{36}S}\right)_{mix}^{Measured} + \left[\left(\frac{^{33}S}{^{36}S}\right)_{mix}^{Measured}\left(\frac{^{36}S}{^{32}S}\right)_{sample} - \left(\frac{^{33}S}{^{32}S}\right)_{sample}\right] \times \left[\frac{\left(\frac{^{32}S}{^{36}S}\right)_{tracer} - \left(\frac{^{32}S}{^{36}S}\right)_{mix}^{Measured}}{\left(\frac{^{32}S}{^{36}S}\right)_{mix}^{Measured}\left(\frac{^{36}S}{^{32}S}\right)_{sample} - 1}\right] \quad \text{Eqn. 4.3}$$

2) This trial value for the $^{108}S/^{111}S$ ($^{33}S/^{36}S$) ratio of the double spike derived from the equation above was compared to the true or assumed $^{108}S/^{111}S$ ($^{33}S/^{36}S$) ratio (determined from direct measurements of the spike itself) to calculate a fractionation factor (α). The true and measured ratios are related by the following laws:

$$\alpha = \frac{\left(\frac{R_m}{R_c} - 1\right)}{\Delta M_{ij}} \qquad \text{linear}$$

$$\alpha = \left(\frac{R_m}{R_c}\right)^{\frac{1}{\Delta M_{ij}}} \qquad \text{power} \qquad \text{Eqn. 4.4}$$

$$\alpha = \frac{\ln\left(\frac{R_m}{R_c}\right)}{\ln\left(\frac{M_i}{M_j}\right)} \qquad \text{exponential}$$

where R_m is the ($^{108}S/^{111}S$) measured ratio, R_c is the assumed or true ($^{108}S/^{111}S$) ratio of the double spike, M_i is the light isotope, M_j is the heavy isotope, and α is the fractionation factor expressing the degree of fractionation.

3) The newly calculated α was then used to correct the measured ratios in both unmixing equations, unmixing equation 1 (Eqn. 2 in Text Box 1 and Eqn. 4.3) and unmixing equation 2 (Eqn. 3 in Text Box 1 and Eqn. 4.5 below)

Text Box 1 – Basic Derivation of Equations:
The atom balance relationship for the mixture of a $^{33}S/^{36}S$ internal standard (tracer) is:

$$\left(\frac{^{33}S}{^{36}S}\right)_{mix}^{TRUE} = \frac{(^{33}S)_{sample} + (^{33}S)_{tracer}}{(^{36}S)_{sample} + (^{36}S)_{tracer}} \qquad \text{Eqn. 1}$$

The tracer is then mixed with a sample:

$$\left(\frac{^{33}S}{^{36}S}\right)_{tracer}^{TRUE} = \left(\frac{^{33}S}{^{36}S}\right)_{mix}^{Measured} + \left[\left(\frac{^{33}S}{^{36}S}\right)_{mix}^{Measured}\left(\frac{^{36}S}{^{32}S}\right)_{sample} - \left(\frac{^{33}S}{^{32}S}\right)_{sample}\right] \times \left[\frac{\left(\frac{^{32}S}{^{36}S}\right)_{tracer} - \left(\frac{^{32}S}{^{36}S}\right)_{mix}^{Measured}}{\left(\frac{^{32}S}{^{36}S}\right)_{mix}^{Measured}\left(\frac{^{36}S}{^{32}S}\right)_{sample} - 1}\right] \qquad \text{Eqn. 2}$$

where the right hand side of the equation subtracts out the contribution of the spike from the sample to yield the true ratio in the tracer that was added to the sample (left hand side of the equation). The isotope composition of the sample is given by the relationship below:

$$\left(\frac{^{32}S}{^{34}S}\right)_{sample}^{TRUE} = \left(\frac{^{32}S}{^{34}S}\right)_{mix}^{Measured} + \left[\left(\frac{^{32}S}{^{34}S}\right)_{mix}^{Measured}\left(\frac{^{34}S}{^{33}S}\right)_{tracer} - \left(\frac{^{32}S}{^{33}S}\right)_{tracer}\right] \times \left[\frac{\left(\frac{^{34}S}{^{33}S}\right)_{mix}^{Measured}\left(\frac{^{33}S}{^{34}S}\right)_{sample} - 1}{\left(\frac{^{34}S}{^{33}S}\right)_{tracer} - \left(\frac{^{34}S}{^{33}S}\right)_{mix}^{Measured}}\right] \qquad \text{Eqn. 3}$$

In this equation the spike contribution is removed from the sample to yield the true ratio in the sample. The two equations above are the unmixing equations, which yield the true $^{33}S/^{36}S$ tracer ratio and the true $^{32}S/^{34}S$ sample ratio. In reality the true ratios are **NOT** input into the right hand side of these equations, but rather measured ratios that have been perturbed by mass fractionation during vaporization from the filament (instrumental fractionation). The true and measured ratios are related by the following relationship:

$$\left(\frac{^{i}S}{^{j}S}\right)_{tracer}^{TRUE} = \left(\frac{^{i}S}{^{j}S}\right)^{Measured} f(\alpha;\Delta Mij) \qquad \text{Eqn. 4}$$

where j is the heavy isotope and i is the light isotope. The first term on the right hand side of the equation is the measured ratio from the mass spectrometer and the second term is the fractionation factor whether for the linear, power, or exponential case. The true $^{32}S/^{34}S$ sample ratio ratios are related to the values in the VCDT (Vienna Canyon DiabloTroilite - $\delta^{34}S$ = -0.3 ‰) standard by:

$$\left(\frac{^{i}S}{^{j}S}\right)_{sample} = \left(\frac{^{i}S}{^{j}S}\right)_{VCDT} f\left(\beta;\Delta M_{ij}\right) \qquad \text{Eqn. 5}$$

where the second factor on the right hand side of the equation is the degree of natural fractionation (β) of the sample relative to the VCDT standard due to geochemical and biogeochemical processing.

Continuation of Text Box 2 – Basic Derivation of Equations:

Natural fractionation, similar to instrumental fractionation, can fractionate mass by the following laws linear, power, or exponential. These fractionation functions are given below:

$$f(\beta;\Delta M_{ij}) = (1+\beta\Delta M_{ij}) \quad \text{linear}$$

$$f(\beta;\Delta M_{ij}) = (1+\beta)^{\Delta M_{ij}} \quad \text{power} \qquad \text{Eqn. 6}$$

$$f(\beta;\Delta M_{ij}) = \left(\frac{M_i}{M_j}\right)^{\beta} \quad \text{exponential}$$

β is related to the traditional $\delta^{34}S$ notation by the following:

$$\delta^{34}S = \left[\frac{\left(\frac{^{34}S}{^{32}S}\right)_{sample}}{\left(\frac{^{34}S}{^{32}S}\right)_{VCDT}}\right] \times 10^3 = \left[\frac{1}{1+2\beta} - 1\right] \qquad \text{Eqn. 7}$$

NOTE: The values for the tracer and sample ratios used in the unmixing equations (Eqns. 2 & 3) have been corrected for both instrumental fractionation and blank (refer to Section 4.1 for details on the tracer (double spike).

$$\left(\frac{^{32}S}{^{34}S}\right)^{TRUE}_{sample} = \left(\frac{^{32}S}{^{34}S}\right)^{Measured}_{mix} + \left[\left(\frac{^{32}S}{^{34}S}\right)^{Measured}_{mix}\left(\frac{^{34}S}{^{33}S}\right)_{tracer} - \left(\frac{^{32}S}{^{33}S}\right)_{tracer}\right] \times \left[\frac{\left(\frac{^{34}S}{^{33}S}\right)^{Measured}_{mix}\left(\frac{^{33}S}{^{34}S}\right)_{sample} - 1}{\left(\frac{^{34}S}{^{33}S}\right)_{tracer} - \left(\frac{^{34}S}{^{33}S}\right)^{Measured}_{mix}}\right] \quad \text{Eqn. 4.5}$$

4) The corrected ratios were then plugged back into the two unmixing-equations to derive a first trial value for the natural sample $^{107}S/^{109}S$ ($^{32}S/^{34}S$) ratio and the associated $\delta^{34}S$ value, a NEW double spike $^{108}S/^{111}S$ ($^{33}S/^{36}S$) ratio value, and a new α. The natural sample $^{107}S/^{109}S$ ratio was used with IRMM's absolute natural composition value for VCDT ($^{107}S/^{109}S = 22.6436$, $\delta^{34}S = -0.3$ ‰) to obtain the natural $\delta^{34}S$ value for the natural sample (Eqn.7 Text Box 1). These 3 steps are repeated until both α and $\delta^{34}S$ values convergence.

To summarize, a fractionation factor (α) representing instrumental fractionation was derived from the relationships in equations 4.3 and 4.4. This fractionation factor was then used to correct all measured ratios in unmixing equations 4.3 and 4.5 for instrumental fractionation to obtain the true $^{32}S/^{34}S$ sample ratio. This ratio is then compared to the standard VCDT to obtain the $\delta^{34}S$ value or the natural isotope composition.

An important consideration when employing the correction laws above is what masses should be used as inputs into the correction equations. It is necessary to be aware that the species observed at the detector may not be the species that is vaporizing off the filament. Knowledge of the molecular species being produced upon vaporization of the sample from the filament is important for determining which masses to use in the correction equations. If the incorrect masses are used, drift in the results can occur. For further details refer to Appendix B.

The $\delta^{34}S$ values obtained from the iterative calculation scheme above are not the true $\delta^{34}S$ values of the standards/samples but are modified due to contribution from the blank. The method used for blank correction was similar to that described in Hayes (2002). In this method, the $\delta^{34}S$ values derived from the iterative equations are blank-corrected to obtain the true $\delta^{34}S$ value using the following equations with the second equation being the associated error propagation equation.

$$\delta^{34}S_{\text{sample}}^{\text{blankcorrected}} = \frac{\eta_{\text{measured}}\delta_{\text{measured}} - \eta_{\text{blank}}\delta_{\text{blank}}}{\eta_{\text{measured}} - \eta_{\text{blank}}} \qquad \text{Eqn. 4.6}$$

$$\sigma^2\delta^{34}S^{\text{blankcorrected}} = \frac{1}{\left(\eta_{\text{measured}} - \eta_{\text{blank}}\right)^2} \times$$

$$\left[\left(\frac{\eta_{\text{blank}}\left(\delta_{\text{blank}} - \delta_{\text{measured}}\right)}{\eta_{\text{measured}} - \eta_{\text{blank}}}\right)^2 \sigma\eta^2_{\text{measured}} + \eta^2_{\text{measured}}\sigma\delta^2_{\text{measured}}\right] + \qquad \text{Eqn. 4.7}$$

$$\frac{1}{\left(\eta_{\text{measured}} - \eta_{\text{blank}}\right)^2} \times \left[\left(\frac{\eta_{\text{measured}}\left(\delta_{\text{measured}} - \delta_{\text{blank}}\right)}{\eta_{\text{measured}} - \eta_{\text{blank}}}\right)^2 \sigma\eta^2_{\text{blank}} + \; - \eta^2_{\text{blank}}\sigma\delta^2_{\text{blank}}\right]$$

In these equations $\eta_{measured}$ is the concentration of the measured sample/standard in μmoles derived from isotope dilution, η_{blank} is the concentration of the blank in μmoles also derived from isotope dilution, $\delta_{measured}$ is the instrumentally-corrected $\delta^{34}S$ value of the sample/standard, δ_{blank} is the $\delta^{34}S$ value of the blank determined by either direct measurement or by the scale contraction method (see below), $\sigma\eta^2_{measured}$ is derived from the 1σ uncertainty on the concentration measurements for the sample/standard, $\sigma\eta^2_{blank}$ is derived from the 1σ uncertainty determined from the pooled blanks run with each group of standards and samples, $\sigma\delta^2_{measured}$ is derived from the external standard deviation (1σ) uncertainty for the standards and the samples. For the samples the standard deviation was derived from the pooled standard deviation for duplicate measurements (n=5). The resulting standard deviation was similar to that for the standards as the measurement precisions are the same as long as the signal intensities are similar (refer to 4.2.4 Mass Spectrometry). The $\sigma\delta^2_{blank}$ is either a best estimate from direct measurements or is derived from the 1σ uncertainty results from a Monte Carlo simulation (refer to the next paragraph).

The sulfur isotope composition of the blank is typically the main source of uncertainty in the error propagation equation 4.7. As sample sizes decrease blank effects

become more significant making the determination of the composition all that much more critical. In this work $\delta^{34}S$ values for the blank were either directly measured or derived using a method similar to that used to correct $\delta^{34}S$ values for scale expansion/contraction (linearity) in gas source measurements. As sample sizes get smaller, the $\delta^{34}S$ of the blank causes the $\delta^{34}S$ of the measured sample/standards to deviate from their true value similar to the scale expansion/contraction effect seen with the SO_2 gas source techniques. In this case the deviation is not due to linearity effects related to the instrument, but purely to the uncertainty of the blank concentration and $\delta^{34}S$ value of the blank. To determine the $\delta^{34}S$ value of the blank the following equation was used:

$$\delta^{34}S_{blankcorrected} = x\delta^{34}S_{measured} + y \qquad \text{Eqn. 4.8}$$

where x and y are a factor and offset determined by the simultaneous solution of two equations that use the internal absolute $\delta^{34}S$ values determined for IAEA-S-1 and IAEA-S-2 and the instrumentally-corrected $\delta^{34}S$ ($\delta^{34}S_{measured}$) values for IAEA-S-1 and IAEA-S-2 (all natural sample $\delta^{34}S$ values fall within the range of these 2 standards). The isotope composition value of the blank is when the instrumentally-corrected $\delta^{34}S$ value equals the blank-corrected $\delta^{34}S$. Using the uncertainties of the internal absolute $\delta^{34}S$ values and the instrumentally-corrected $\delta^{34}S$ values, 1000 points were produced using the Monte Carlo method. These points were than used to generate the x and y factors in equation 4.8 to determine an uncertainty for the blank composition.

4.3.2 Sulfur Concentration

One of the major advantages of the double spike technique is not only can the natural isotopic composition be obtained, but the concentration both in the natural sample

and the blank can also be determined by isotope dilution (ID). Isotope dilution analysis is based on the chemical equilibration of a known amount of an enriched isotope (in this case ^{33}S (^{108}S)) with the isotopes of the element being determined and the measurements of the isotopic ratio in the resulting mix. The technique is inherently accurate because after the spike is mixed with the sulfur in the sample only isotopic ratios need to be measured, and these ratios can be measured with high accuracy and precision. Furthermore, because only isotopic ratios need to be measured the accuracy of the determination is independent of chemical yields. In this work, the $^{32}S/^{33}S$ fractionation corrected ratio was used to calculate the [S]. The measured ratio in the mixture is given by the following atom balance relationship:

$$\left[\frac{^{32}S}{^{33}S}\right]_{mixture} = \frac{\left(^{32}S\right)_{sample} + \left(^{32}S\right)_{tracer}}{\left(^{33}S\right)_{sample} + \left(^{33}S\right)_{tracer}} \qquad \text{Eqn. 4.9}$$

where the numerator and the denominator equal the sum of the moles of ^{32}S and ^{33}S, respectively, in the sample and the spike (t. Rearrangement of equation 4.9 gives:

$$\left(^{32}S\right)_{sample} = \left(^{33}S\right)_{tracer} \frac{\left(\frac{^{32}S}{^{33}S}\right)_{tracer} - \left(\frac{^{32}S}{^{33}S}\right)_{mixture}}{\left(\frac{^{32}S}{^{33}S}\right)_{mixture}\left(\frac{^{33}S}{^{32}S}\right)_{sample} - 1} \qquad \text{Eqn. 4.10}$$

Assuming that the amount of tracer added is known, it is clear that the moles of ^{32}S in the sample can be determined from the measurement of isotopic ratios alone. The concentration of sulfur in the sample is given in the following:

$$C_{sample} = \frac{\left(^{32}S\right)_{sample}(\text{at.wt.})}{\left(^{32}A\right)(\text{wt.})} \times 10^{6}\,\mu g\ g^{-1} \qquad \text{Eqn. 4.11}$$

where the numerator is the product of the moles of ^{32}S and the atomic weight of sulfur in the sample and the denominator is the product of the fractional abundance of ^{32}S in the sample and the sample weight in grams. The specific data input into the equations above are as follows:

1) The ^{107}S and ^{108}S atom abundances used in the ID equation above for the double spike were corrected for instrumental fractionation and blank (refer to Section 4.1), those used for the standards (IAEA-S-1, IAEA-S-2, and IAEA-S-3) were the absolute values determined by IRMM (Ding et al., 2001), and those used for the natural samples were approximated by calculating the natural fractionation (β) from the absolute $^{107}S/^{109}S$ ratio determined from our iterative calculations and correcting the $^{107}S/^{108}S$, $^{109}S/^{108}S$, and the $^{111}S/^{108}S$ ratios, assuming fractionation follows an exponential law, to derive the corrected ^{107}S and ^{108}S atom abundances, and for the blank from the raw uncorrected data.

2) The atomic weights used in the ID equation to convert moles to grams are calculated from the absolute atom abundances from IRMM for the standards, from the approximated atom abundances for the samples (refer to above), and from the raw data for the blank.

The atom abundances and the atomic weight for the blank were the best available approximation for the blank as we could not obtain the corrected $^{107}S/^{109}S$ from the iterative calculations as the blanks were overspiked. The effect of isotope composition of the blank on the concentration; however, is minimal.

4.4 Data Analysis

The geochemical and corrected sulfur isotope data obtained were used to characterize the seasonal sulfur isotopic shifts and to estimate the relative contributions of anthropogenic (fossil fuel burning) and natural (sea salt, dust, and marine biogenic) sulfur sources using chemical and isotope mass balance models. Based on literature findings indicating that anthropogenic, dust, and marine biogenic sulfur are the primary contributors to nss-sulfate of Greenland, estimates of the mass fractions for each contributor was assessed using a three-source model. In this case the measured isotopic composition was broken down into the terms representative of the source contributors:

$$\delta_{measured} = f_{ss}\delta_{ss} + f_{nss}\delta_{nss} = f_a\delta_a + f_d\delta_d + f_{mb}\delta_{mb} \qquad \text{Eqn. 4.12}$$

where $\delta_{measured}$ is the measured $\delta^{34}S$ of the sample, δ_{ss}, δ_{nss}, δ_a, δ_d, δ_{mb} are the isotopic signatures of the sea salt, non-sea-salt, anthropogenic, dust, and marine biogenic components and f_{ss}, f_{nss}, f_a, f_d, and f_{mb}, are the mass fractions of the components.

Using the three-component source model for Greenland, we can start establishing the fractional components with the most well-defined component, the sea-salt contribution with $\delta^{34}S$ of +21 ± 0.2‰ (Rees et al., 1978). The fractional contribution (f_{ss}) is calculated assuming the mass ratio of SO_4^{2-} to Na^+ is 0.25 in bulk seawater and that this ratio holds for sea-salt in ice:

$$f_{ss} = \frac{k\left[Na^+\right]}{\left[SO_4^{2-}\right]} \qquad \text{Eqn 4.13}$$

The non-sea-salt fraction is $f_{nss} = 1\text{-}f_{ss}$. The non-sea-salt sulfur isotope composition can then be derived from $\delta_{measured} = f_{ss}\delta_{ss} + (1\text{-}f_{ss})\delta_{nss}$ and is calculated as:

$$\delta_{nss} = \frac{\delta_{measured} - f_{ss}\delta_{ss}}{1 - f_{ss}} \qquad \text{Eqn. 4.14}$$

The non-sea-salt sulfate component further consists of the anthropogenic, continental dust, and marine biogenic contributions. The continental dust fraction of sulfate is derived from the nss-calcium content (magnesium can also be used however the concentration of Ca^{2+} was larger and therefore better known). The mass ratio for soil and dust emissions is $SO_4^{2-}/Ca^{2+} = 0.18$ (Legrand et al., 1997). Combining this data with the $\delta^{34}S$ values from the literature we can derive the marine biogenic and anthropogenic fractions being contributed to Greenland on seasonal timescales.

Based upon the literature and location of the Inilchek Glacier site, anthropogenic and evaporite dust were determined to be the main contributors to nss-sulfate (Kreutz & Sholkovitz, 2000; Pruett et al., 2004). The measured isotopic composition in this case can be equated to the sum of the two terms representative of each contributor:

$$\delta_{measured} = \delta_{nss} f_{nss} = f_a\delta_a + f_d\delta_d \qquad \text{Eqn. 4.15}$$

where δ_a and δ_d are the isotopic signatures of the anthropogenic and dust components and f_a and f_d are the mass fractions of the components. If f_d is equal to x and f_a is therefore 1-x, then we can rewrite Eqn. 4.15 as:

$$\delta_{nss} f_{nss} = (1-x)\delta_a + (x)\delta_d \qquad \text{Eqn. 4.16}$$

Combining the mass fraction components with the ^{34}S values from the literature we can examine the changes in sulfate source contributions to the Inilchek region using equation 4.16 over time.

Chapter 5: Standards: Analytical Results and Discussion

The new double spike method for $\delta^{34}S$ and concentration measurements was tested using international reference materials with accepted sulfur isotope composition and sulfur concentration. In this study, three international isotopic standards available from the International Atomic Energy Agency (IAEA-S-1, IAEA-S-2, and IAEA-S-3) were used along with two standards from McMaster University, Canada (prepared by C.E. Rees) to test the double spike technique for sulfur isotope composition determination. SRM 2724b (Sulfur in Diesel Fuel Oil) was used to test the technique for sulfur concentration determination. This chapter specifically provides: 1) a detailed assessment of the double spike method for instrumental fractionation correction, 2) the isotope composition results for the IAEA and McMaster standards using the new double spike technique and an evaluation of this technique by comparing the results to those of other laboratories, and 3) the concentration results for SRM 2724b and the isotopic standards using the new technique.

5.1 Instrumental Fractionation Correction: Results and Discussion

One of the main purposes of using the double spike method is to correct for instrumental fractionation to improve the measurement precisions obtained for the $^{32}S/^{34}S$ measured ratios and subsequent $\delta^{34}S$ values. Figures 5.1.a – c show the raw $\delta^{34}S$ values for individual TIMS runs of arsenic sulfide of the 3 international standards IAEA-S-1, S-2, and S-3, prior to correction for instrumental fractionation (open circles), and the $\delta^{34}S$ values after correction for instrumental fractionation (closed circles) using the iterative method described in Chapter 4. It is important to note that: 1) the figures show the

correction of the raw data for fractionation by the *exponential* correction case only, 2) the scale for the axes are the same for all plots (the range in the ordinate is 10‰) and 3) the double spike has been removed from both; therefore, the difference between the two sets of points is solely due to instrumental fractionation. Table 5.1 shows the uncorrected and the corrected $\delta^{34}S$ values for IAEA-S-1 (Figure 5.1.a), IAEA-S-2 (Figure 5.1.b), and IAEA-S-3 (Figure 5.1.c). The observed fractionation for each standard is

Table 5.1. Uncorrected and Corrected $\delta^{34}S$ values for IAEA-S-1, S-2, and S-3.

	IAEA-S-1			IAEA-S-2			IAEA-S-3		
	$\delta^{34}S$	1σ	$2\sigma_m$	$\delta^{34}S$	1σ	$2\sigma_m$	$\delta^{34}S$	1σ	$2\sigma_m$
Uncorrected	-1.37	0.47	0.13	17.43	1.07	0.30	-32.27	0.84	0.24
Corrected	-0.31	0.24	0.067	22.65	0.20	0.056	-32.45	0.21	0.058

All $\delta^{34}S$ values are in per mil (‰VCDT defined by $\delta^{34}S$ = -0.30‰).

consistent with a Rayleigh-like fractionation curve (Figure 4.1.b) as indicated by the positive slope for the uncorrected $\delta^{34}S$ data. For IAEA-S-1 and S-3 there is a factor of two improvement in the measurement precision between the uncorrected and corrected data, while IAEA-S-2 shows a factor of 5 improvement in the measurement precision. Typically the improvement in precision for the standards mixed with double spike #1 (DS #1) ranged from a factor of just above 1 to 6, averaging around 1.5 for IAEA-S-1, 3.8 for IAEA-S-2, and 3.5 for IAEA-S-3. The smaller improvement in measurement precision for IAEA-S-1 is likely due to the lower signal intensity of the ion beam for mass 109 for some of the early runs. The improvement in precision for the standards mixed with double spike #2 (DS #2) had a similar range to those for DS #1 and ranged from a factor of just above 1 to 4 with an average of approximately 2.2 for IAEA- S-1 and about 1.8 for

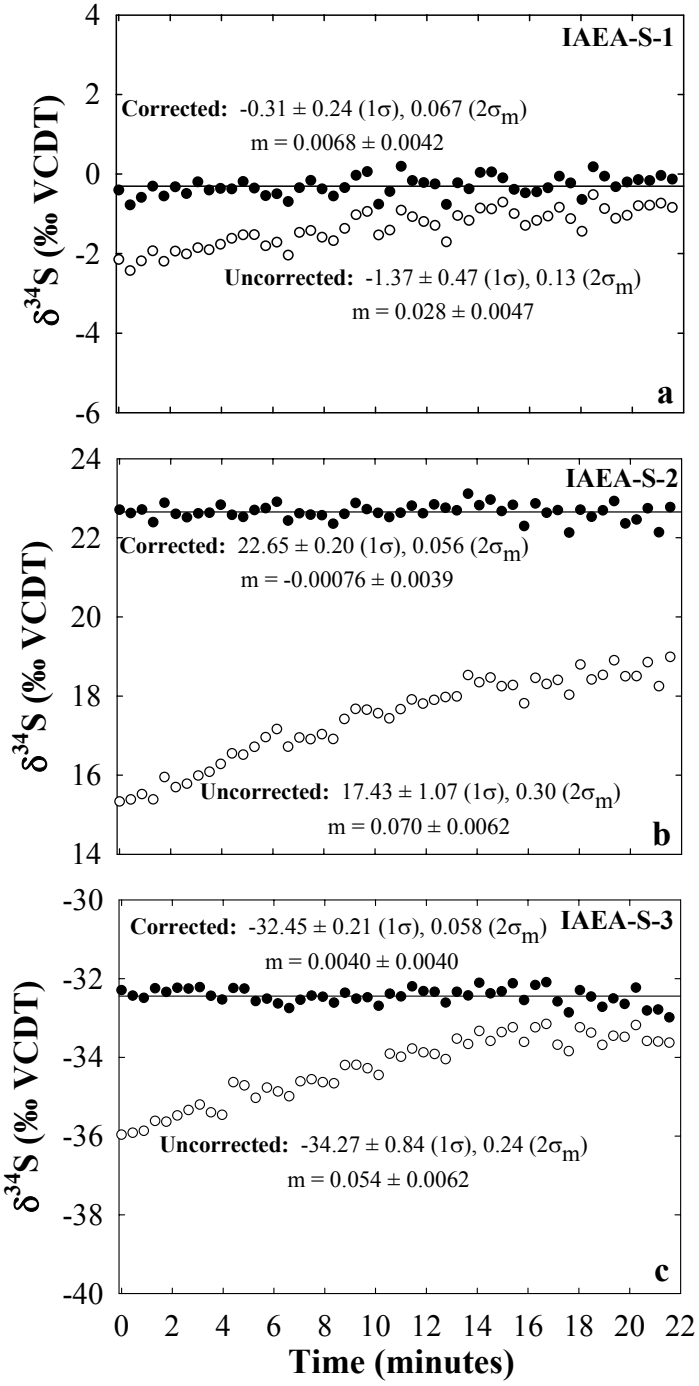

Figure 5.1. Raw $\delta^{34}S$ values and slope (m) for the 3 international standards IAEA-S-1 (a), S-2 (b), and S-3 (c), prior to correction for instrumental fractionation (open circles) and after correction for instrumental fractionation (closed circles) . The uncertainties reported for the uncorrected and corrected data are 1σ and $2\sigma_m$. Uncertainties for the slopes are 95% confidence intervals (C.I.).

IAEA-S-2 (IAEA-S-3 was not measured with the DS #2 mix as it was outside the isotopic range of our actual samples). Details of the improvement in measurement precision for each sample can be found in Appendix A.

Another way to determine whether the double spike technique is adequately correcting for instrumental fractionation is to examine the slope (m) of the uncorrected and corrected data. The uncorrected $\delta^{34}S$ data that includes the instrumental fractionation should have a positive slope (enriching in ^{34}S) if the fractionation follows a Rayleigh-like fractionation (Chapter 4). The corrected data, with instrumental fractionation removed, should have a slope of 0 (Chapter 4). The slopes for the uncorrected and corrected $\delta^{34}S$ values for IAEA-S-1 (Figure 5.1.a), IAEA-S-2 (Figure 5.1.b), and IAEA-S-3 (Figure 5.1.c) are shown in Table 5.2. In each case, the slopes for the uncorrected data were

Table 5.2. Slopes of the Uncorrected and Corrected $\delta^{34}S$ values for IAEA-S-1, S-2, and S-3.

	IAEA-S-1		IAEA-S-2		IAEA-S-3	
	m (slope)	**95% C.I.**	**m (slope)**	**95% C.I.**	**m (slope)**	**95% C.I.**
Uncorrected	0.028	0.0047	0.070	0.0062	0.054	0.0062
Corrected	0.0068	0.0042	-0.00076	0.0039	-0.0040	0.0040

All uncertainties reported are 95% confidence intervals.

positive and significant and the slopes for the corrected data were essentially 0 within uncertainty, demonstrating that the fractionation correction procedure in fact works. IAEA-S-1 shows a slight positive slope after correction, which is interpreted to be due to decreased precision resulting from the decreasing signal intensity on the minor isotope, ^{109}S, over the course of the run, and not due to drift.

The figures above show only the data for the exponential correction case; however, the linear and power laws can also be used for correction of the raw uncorrected data. Figure 5.2 shows the Rayleigh-generated correction curves for the 3 different laws

– linear (there are 2 for the linear case because 2 separate equations can be written for this law), power, and exponential –assuming AsS^+ is being produced (masses 107, 108, 109, and 111) and AsS^+ is used for correction. Assuming that the true $\delta^{34}S$ value is 0‰, it is obvious from this figure that the exponential case is a better choice for instrumental fractionation correction as the corrected exponential curve is closer to the true $\delta^{34}S$ value of 0‰ and the drift from this value over the depletion of the reservoir (1-F) is smaller than for the other correction laws. In addition, the measurement precision after correction typically ranged from approximately 0.20 to 0.60‰ (the precision reported here excludes blank correction); consequently, the difference between the various correction laws cannot be observed with the current precision. Moreover, the curve for the exponential correction has essentially a slope of 0 within the measurement precisions observed (several parts in 10^4 data); hence, we should not observe appreciable drift in the data. Even though the linear and power laws can also be used in this case, the exponential law was employed because examination of the Rayleigh theoretical model clearly demonstrates that the exponential law is better suited for data correction.

Although the curves for the three laws are indistinguishable within the uncertainty of the data, the potential to obtain a part in 10^5 data does exist with newer instrumentation. In this case, knowledge of what point on the fractionation curve analysis begins aids in knowing whether the 3 laws can be distinguished and which is the most appropriate to use for data correction. Figure 5.2 shows that for measurements made when the reservoir is minimally depleted (when the reservoir is still near 100%) the correction laws would be distinguishable for parts in 10^5 data and that the exponential

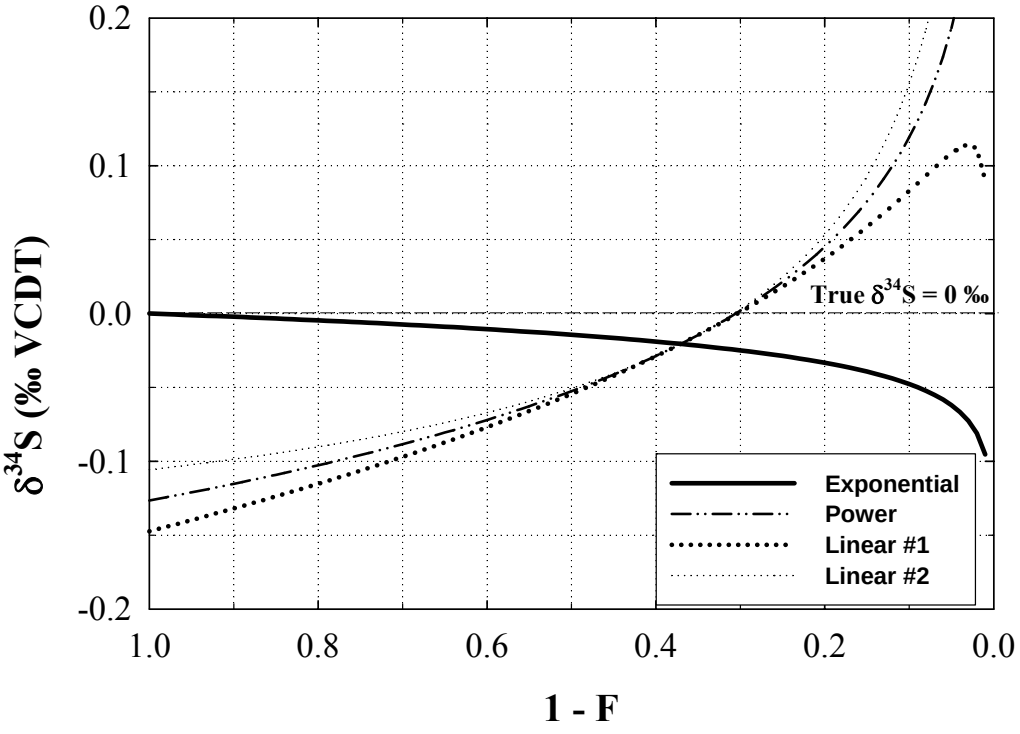

Figure 5.2. Rayleigh-generated correction curves for the 3 different laws - linear, power, and exponential - assuming AsS^+ is being produced (masses 107, 108, 109, and 111) and AsS^+ is used for correction.

law is a better model of the true value. For measurements made further along on the fractionation curve, analysis starting at approximately 60% depletion, it becomes more difficult to distinguish between the three laws even with several parts in 10^5 precision. In this study, it was found that the point on the fractionation curve where analysis begins and ends could be determined through modeling. The top three figures in Figures 5.3.a – f (Figures 5.3.a-c) are the same three figures in Figure 5.1, which show the uncorrected $\delta^{34}S$ data (open circles) and the corrected $\delta^{34}S$ data (closed circles) for the three standards IAEA-S-1, S-2, and S-3. The bottom three figures (Figures 5.3.d–f) show the Rayleigh-generated curves (thin solid lines with positive slope) for each of the three standards and the corresponding corrected curves for the exponential case (thick solid lines). Again, the curves generated assume production of AsS^+ and correction using AsS^+. The Rayleigh curves were generated using the absolute $^{107}S/^{109}S$ ratios (22.6504 (S-1), 22.1424 (S-2), and 22.3933 (S-3)) for each of the standards reported by the Institute for Reference Materials and Measurements (IRMM) (Ding et al., 2001). Assuming the actual data follows Rayleigh-like fractionation, which is suggested by the positive slope of the uncorrected data shown in Figures 5.1.a – c, the uncorrected data with the double spike removed, can be plotted on the modeled Rayleigh curves to ascertain the points at which an analysis begins and ends. The scale for the y-axis on the bottom three plots is 10‰ and for the top three plots the scale is 16‰. This is to show the complete fractionation curve starting from 100% of the reservoir being on the filament to 0% remaining on the filament. The uncorrected data (open circles) for IAEA-S-1 (Figure 5.3.a) range from approximately –2‰ at the start of analysis to approximately –1‰ at the end. The vertical

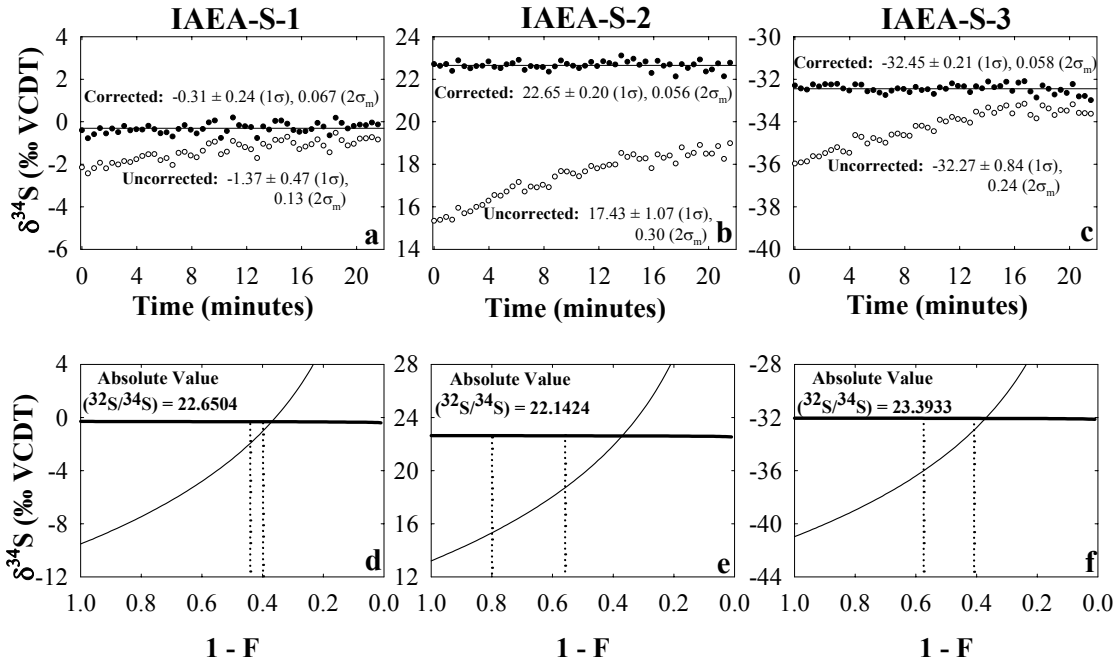

Figure 5.3. The top three figures (Figures 5.3.a – c) are the same three figures in Figure 5.1 that show the uncorrected (open circles) $\delta^{34}S$ data, prior to correction, and the corrected $\delta^{34}S$ data (closed circles) for the three standards IAEA-S-1, S-2, and S-3. The uncertainties reported for the uncorrected and corrected data are 1σ and $2\sigma_m$. Uncertainties for the slopes are 95 % confidence intervals (C.I.). The bottom three figures (Figures 5.3.d – f) show the Rayleigh-generated curves (thin solid lines with positive slope) for each of the three standards and the corresponding corrected curves for the exponential case (thick solid lines). The vertical dotted lines in Figures 5.3.d-f bracket where on the model Rayleigh fractionation curve the true data plot. The scale for the y-axis on the bottom three plots is 10‰ and for the top three plots the scale is 16‰.

dotted lines in Figure 5.3.d bracket where on the model Rayleigh fractionation curve these true data plot. For this analysis about 55% of the reservoir was depleted before the analysis began. In Figure 5.3.e (IAEA-S-2) the sample analysis began just after 20% of the reservoir was depleted where as in Figure 5.3.f (IAEA-S-3) analysis began when approximately 42% of the reservoir was depleted. The sample for IAEA-S-3 was the most fractionated while that for IAEA-S-2 was the least fractionated. For all three standards approximately 40 to 50% on average, of the reservoir was depleted before analysis began (refer to Appendix A for details on individual analyses) and in a typical run the change in per mil over the time of data collection as a result of isotopic fractionation averaged about 2‰ (details in Appendix A). For data with a precision of several parts in 10^4, as in this study, the important message to take away from Figures 5.3.d-f is that it is not important where on the fractionation curve measurements are taken because the changing ratio caused by instrumental fractionation is removed with the double spike technique; thus, the measurements made are of the true ratio and follow along a straight line with a slope of 0. Taking into consideration that sample analysis typically begins when about 40 to 50% of the sample reservoir is depleted, it is clear from Figure 5.2 and Figures 5.3.a–f that the 3 laws are still indistinguishable for parts in 10^5 data. Only under the extreme conditions, low (< 20%) and highly (> 80%) fractionated, do the laws become distinguishable. In these cases the exponential law would have to be employed to obtain data of the highest precision and accuracy.

5.2 Standards : Isotope Composition Results and Discussion

It has been demonstrated that the double spike technique provides a factor of two to five improvement in measurement precision and yields corrected $^{32}S/^{34}S$ ratios that are

consistent; yet, whether the technique yields the correct $\delta^{34}S$ values, in the absolute sense, still needs to be assessed. The results for the isotopic standards (IAEA-S-1, IAEA-S-2, and IAEA-S-3, 2 McMaster) with known sulfur isotope composition used to test the new double spike method for $\delta^{34}S$ determination are shown below. Details of the individual data and uncertainty results discussed below are found in Appendix A.

5.2.1 Double Spike #1

The $\delta^{34}S$ results for the standards IAEA-S-1, S-2, and S-3 measured using DS #1 are shown in Table 5.3 and Figures 5.4, 5.5, and 5.6. Figures 5.4.a, 5.5.a, and 5.6.a show the $\delta^{34}S$ values for the individual measurements while Figures 5.4.b, 5.5.b, and 5.6.b show the average $\delta^{34}S$ values determined from the individual measurements for each of the

Table 5.3. $\delta^{34}S$ Results for IAEA-S-1, S-2, and S-3 measured using DS #1.

						Signal Intensity (mV)	
	$\delta^{34}S$ (‰ VCDT)	**1σ**	**$2\sigma_m$**	**n**	**Sample size (μmoles S)**	**Start**	**End**
IAEA-S-1	-0.32	0.04	0.04	4	1.00 - 1.34	100 - 140	60 - 100
IAEA-S-2	22.65	0.04	0.03	7	0.40 – 1.05	42 - 169	20 - 105
IAEA-S-3	-32.47	0.07	0.05	8	0.70 – 1.09	67 – 150	31 - 83

n = number of analyses.

standards with the corresponding consensus value reported by Taylor et al. (2000). The $\delta^{34}S$ consensus values reported by Taylor et al. (2000) are based on $\delta^{34}S$ measurements made of the three standards using sulfur hexafluoride (SF_6) techniques and include values of isotope ratio measurements and values calculated from absolute ratio measurements. The average $\delta^{34}S$ value determined for IAEA-S-1 was –0.32 ± 0.04‰ (1σ) (Figure 5.4.b) and overlaps the consensus value assigned for IAEA-S-1, –0.3‰ (Taylor et al., 2000). The $\delta^{34}S$ result for IAEA-S-2 was 22.65 ± 0.04‰ (1σ), (Figure 5.5.b) and for IAEA-S-3 –32.47 ± 0.07‰ (1σ) (Figure 5.6.b). Both were within the uncertainty of the

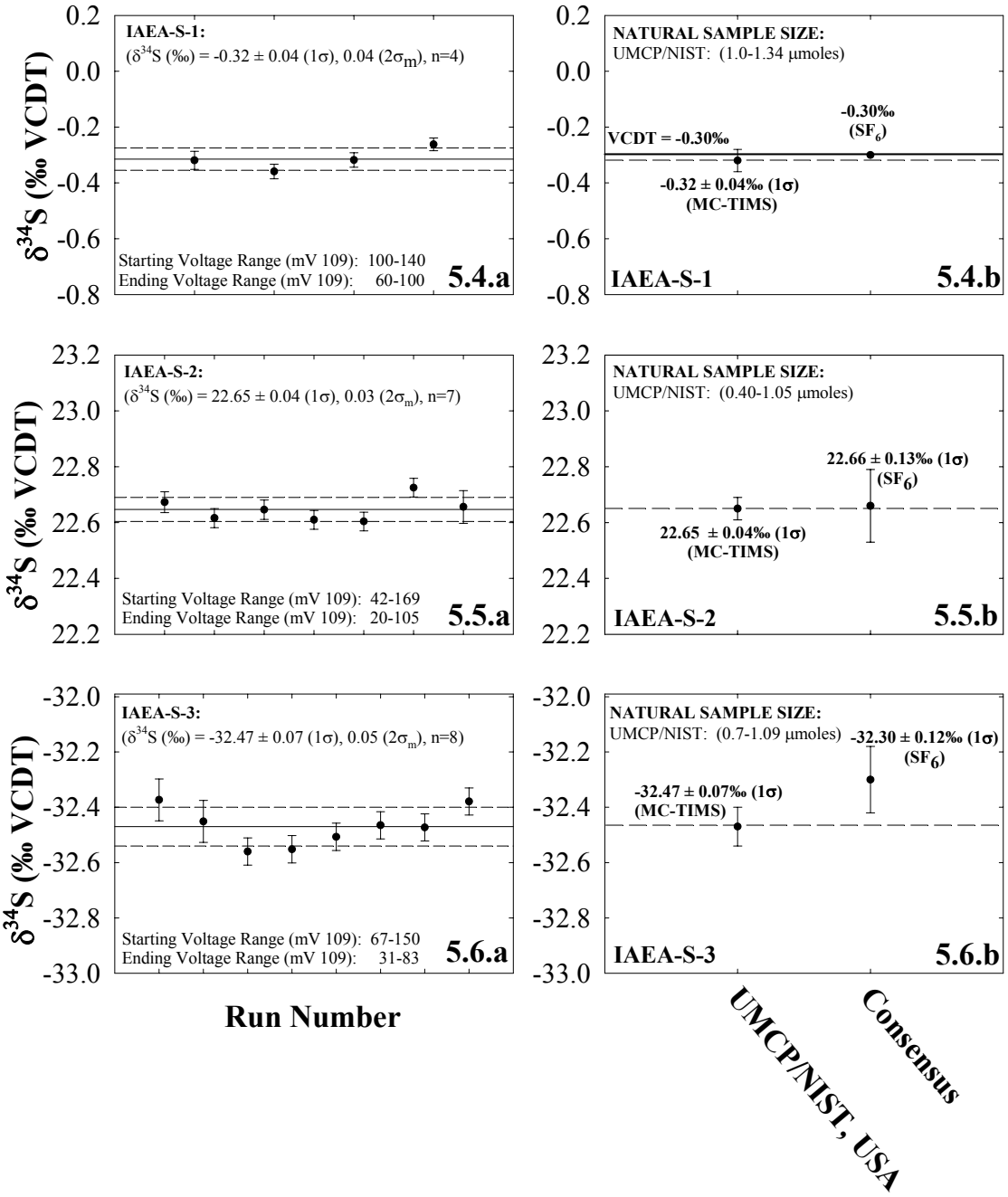

Figures 5.4-5.6a,b. $\delta^{34}S$ results for the standards IAEA-S-1, S-2, and S-3 measured using DS #1. $\delta^{34}S$ values for the individual measurements are shown in Figures (a) while the average $\delta^{34}S$ value determined from the individual measurements is shown with the corresponding consensus value reported by Taylor et al. (2000) in Figures (b). The uncertainties reported for the average $\delta^{34}S$ value are 1σ (the mean (solid line) and 1σ (dashed lines) highlighted in Figures (a)) and $2\sigma_m$.

consensus values set at 22.66 ± 0.13‰ (1σ) for IAEA-S-2 (Taylor et al., 2000) and -32.30 ± 0.12‰ (1σ) for IAEA-S-3 (Taylor et al., 2000). The signal intensities on the minor isotope, mass ^{109}S, at the start of analysis were typically above 50 mV with the exception of the IAEA-S-1 runs which were above 100 mV in signal intensity. The signal intensities at the end of analysis were typically below 100 mV. Sample sizes used for $\delta^{34}S$ analysis ranged from 0.40 to 1.34 μmoles S. The range in sample sizes used by the consensus laboratories was approximately 3 to 30 μmoles S (Taylor et al., 2000). For each standard, the natural sample sizes used for measurement in this study were smaller (0.40 to 1.34 μmoles S) than that used by the laboratories that contributed to the consensus value. The results for all the standards measured are in excellent agreement with the consensus values reported by Taylor et al. (2000) considering the very different (double spike MC-TIMS) technique used in this research and the very different sample sizes.

The samples shown in Figure 5.4.a,b for IAEA-S-1 were those samples specifically used for calibration of the spike. These samples were used because the signal intensity on the minor isotope, mass ^{109}S, was above 100 mV when starting sample analysis, yielding the best possible data results. Figure 5.7.a shows additional results for IAEA-S-1 that were used to check the double spike technique itself and Figure 5.7.b shows these results relative to the reported consensus value. The $\delta^{34}S$ value determined was –0.35 ± 0.17‰ (1σ) (Figure 5.7.a) for sample sizes 0.43 to 1.98 μmoles S. The range in signal intensity for these samples was 18 to 98 mV at the start and 15 to 45 mV at the end of analysis. Again the $\delta^{34}S$ value determined overlaps the consensus value reported –0.30‰ (Taylor et al., 2000) (Figure 5.7.b).

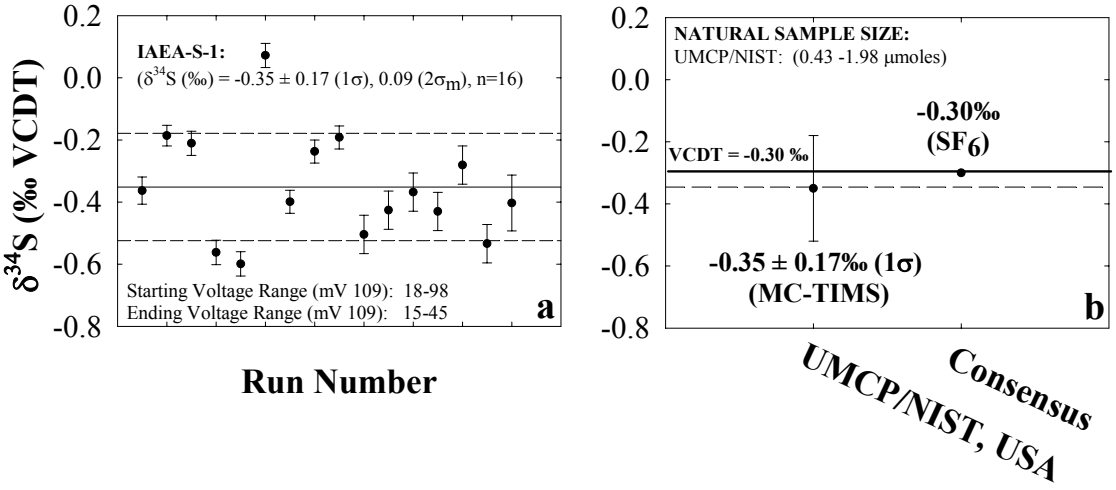

Figure 5.7.a,b. Additional $\delta^{34}S$ results for IAEA-S-1 using DS #1. Figure 5.7.a shows the results for the individual measurements and Figure 5.7.b shows the average of these results relative to the reported consensus value by Taylor et al. (2000). The uncertainties reported for the average $\delta^{34}S$ value are 1σ (the mean (solid line) and 1σ (dashed lines) highlighted in Figure (a)) and $2\sigma_m$.

Two additional standards (SL #7 and SL #9) from McMaster University, prepared by C.E. Rees, were also used as an additional test of the double spike technique. SL #7 was chosen because it was reported to have a highly enriched $\delta^{34}S$ value of approximately + 49‰. SL #9 was chosen because it was the counterpart to IAEA-S-2 with a value of approximately –19‰. The results are shown in Table 5.4 and Figures 5.8 and 5.9. Figures 5.8 and 5.9 show the $\delta^{34}S$ values for each individual measurement (a)

Table 5.4. $\delta^{34}S$ Results for the McMaster Standards measured using DS #1.

						Signal Intensity (mV)	
	$\delta^{34}S$ (‰ VCDT)	1σ	$2\sigma_m$	n	Sample size (μmoles S)	Start	End
SL #7	50.71	0.11	0.08	3	≈ 1.38	91 - 135	51 - 80
SL #9	-19.19	0.06	0.05	3	≈ 1.47	58 - 150	23 - 47

n = number of analyses

and the average $\delta^{34}S$ value of the two standards with the corresponding value reported by Rees (1978) (b) whose measurements were done by the SF_6 method. The average $\delta^{34}S$ value for SL #7 was +50.71 ± 0.11‰ (1σ) (Figures 5.8.a & b) and the average value for SL #9 was –19.19 ± 0.06‰ (1σ) (Figures 5.9.a & b). The sample size used for the $\delta^{34}S$ measurements averaged just under 1.5 μmoles S for both standards. The signal intensity for the minor isotope were typically greater than 50 mV at the start of analysis and below 80 mV at the end of sample analysis. The values reported by Rees (1978) were +48.77‰ and –19.51‰ (Figures 5.8.b and 5.9.b). Only one measurement of each of the standards was performed by Rees (1978); therefore, an uncertainty on the value is not available. It is obvious that even if a 1σ uncertainty of 0.10 ‰ is assumed, which is a typical uncertainty encountered for the $\delta^{34}S$ measurements of standards, the values determined by the double spike method are different then those determined by Rees (1978). For

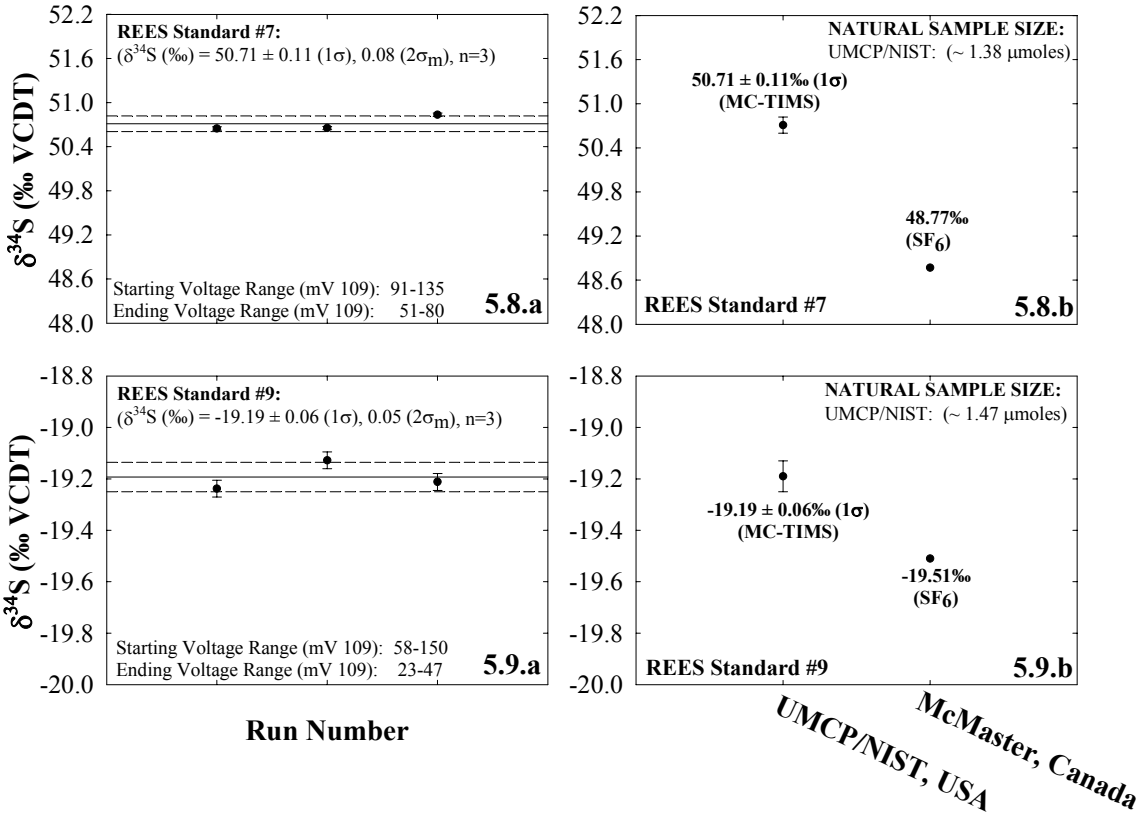

Figure 5.8 - 5.9.a,b. $\delta^{34}S$ values for the McMaster standards measured using DS #1. The $\delta^{34}S$ values for the individual measurements are shown in Figures (a) and the average $\delta^{34}S$ value determined from the individual measurements are shown with the corresponding value reported by Rees (1978) (b). The uncertainties reported for the average $\delta^{34}S$ value are 1σ (the mean (solid line) and 1σ (dashed lines) highlighted in Figures (a)) and $2\sigma_m$.

SL #7 the reported value is almost 2‰ different from the measured values whereas the reported value is only about 0.3‰ different than the measured values for SL #9. This difference may potentially be caused by leakages from the unknown sample and reference gas sides of the switching (changeover) valve (inlet leakages), background ion current, and/or any zero offset in the collector amplifiers related to the gas source instrument used and built by Rees (1978). Memory effects caused by mixing of the sample and standard within the inlet lines of this particular gas source instrument were considered to be negligible for the SF_6 measurements relative to those listed above. The double spike method uses the TIMS, a solid source technique for isotope analysis; thus, memory effects are eliminated. All the mechanisms listed above can potentially cause the $\delta^{34}S$ values to deviate from their true value. This could contribute to the deviations observed between the data reported by Rees (1978) and those in this study. Even though the $\delta^{34}S$ results for the McMaster standards reported in this study were significantly different then those reported by Rees (1978) and may indicate a problem with the double spike technique, the results for the IAEA isotopic standards strongly suggest otherwise.

5.2.2 Double Spike #2

The isotopic standards IAEA-S-1 and S-2 were also measured using DS #2 and the $\delta^{34}S$ results are shown in Table 5.5 and Figures 5.10 and 5.11, respectively. DS #2 was

Table 5.5. $\delta^{34}S$ Results for IAEA-S-1 and S-2 measured using DS #2.

						Signal Intensity (mV)	
	$\delta^{34}S$ (‰ VCDT)	1σ	$2\sigma_m$	n	Sample size (μmoles S)	Start	End
IAEA-S-1	-0.31	0.13	0.09	8	0.73 – 2.35	102 - 167	15 - 65
IAEA-S-2	22.60	0.06	0.05	5	1.04 – 1.22	110 - 166	15 - 53

n = number of analyses

prepared from the same stock solutions as DS #1. These were the only standards measured with DS #2 as they bracketed the $\delta^{34}S$ values expected for the snowpit samples from Greenland and the Inilchek Glacier. Figures 5.10.a and 5.11.a show the $\delta^{34}S$ value for each individual measurement while Figures 5.10.b and 5.11.b show the average $\delta^{34}S$ values (Taylor et al., 2000). The average $\delta^{34}S$ value for IAEA-S-1 was –0.31 ± 0.13‰ (1σ) (Figure 5.10.b). This value both overlaps the assigned consensus value for IAEA-S-1 (Taylor et al., 2000) and is within the range of that determined using DS #1 (-0.32 ± 0.04‰ (1σ)). Because the signal intensity of the minor isotope (^{109}S) for these samples was greater then 100 mV they were used for the calibration of the spike. The $\delta^{34}S$ result for IAEA-S-2 was 22.60 ± 0.06 ‰ (1σ) (Figure 5.11.b). Again the value determined lies within the uncertainty of the consensus value set at 22.66 ± 0.13‰ (1σ) (Taylor et al., 2000) and lies within the value determined using DS #1 (22.65 ± 0.04‰ (1σ)). The signal intensities for mass 109 were greater then 100 mV at the start of analysis and less then 50 mV at the end. The sample sizes used for analysis were again smaller (0.73 to 2.35 μmoles S) than that used for $\delta^{34}S$ analysis by researchers employing gas source techniques. Figure 5.12 shows additional IAEA-S-1 samples that were measured with DS #2, with Figure 5.12.a showing the individual results and Figure 5.12.b showing the results relative to the reported consensus value. The $\delta^{34}S$ value determined was –0.34 ± 0.12‰ (1σ), 0.12 ($2\sigma_m$), (n = 4) for sample sizes ranging from 0.89 to 1.32 μmoles S. The range in signal intensity for these samples was 17 to 64 mV at the start and 24 to 40 mV at the end of analysis. The average $\delta^{34}S$ value determined overlaps the consensus value reported by Taylor et al. (2000) and is within the range determined using DS #1

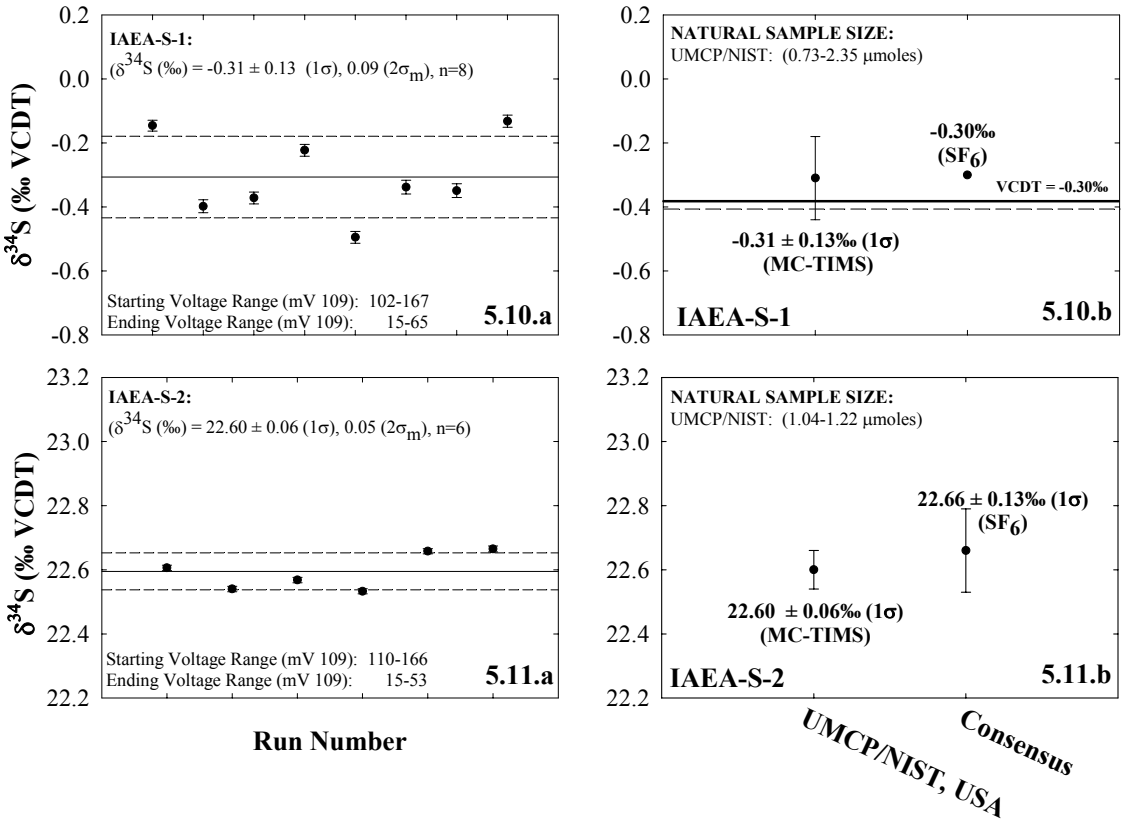

Figure 5.10 – 5.11a,b. $\delta^{34}S$ results for IAEA-S-1 and S-2 measured using DS #2. Figures 5.10.a and 5.11.a show the $\delta^{34}S$ value for each individual measurement while Figures 5.10.b and 5.11.b show the average $\delta^{34}S$ value for each of the standards with the corresponding consensus value reported by Taylor et al. (2000). The uncertainties reported for the average $\delta^{34}S$ value are 1σ (the mean (solid line) and 1σ (dashed lines) highlighted in Figures (a)) and $2\sigma_m$.

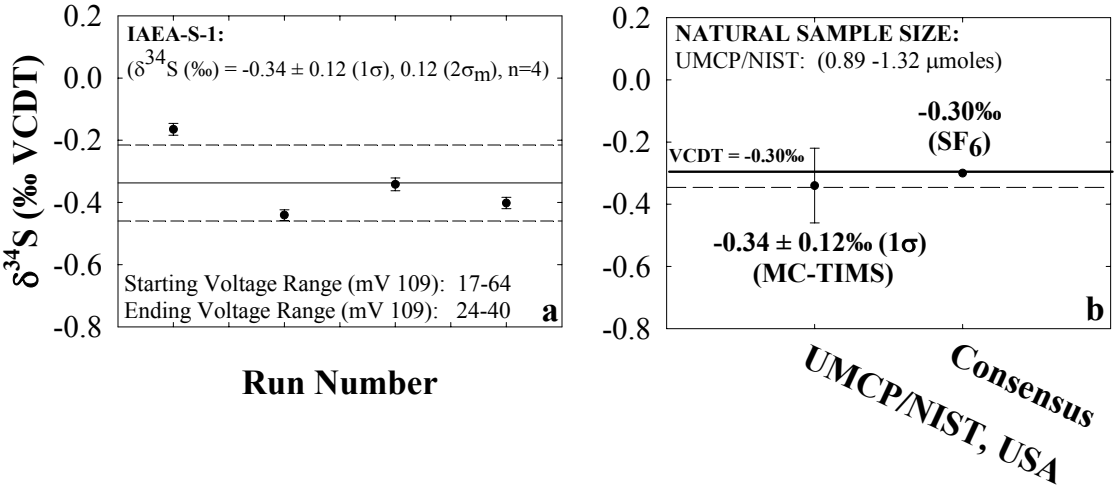

Figure 5.12.a,b. Additional $\delta^{34}S$ results for IAEA-S-1 using DS #2. Figure 5.12.a shows the individual results and Figure 5.12.b shows the results relative to the reported consensus value (Taylor et al., 2000). The uncertainties reported for the average $\delta^{34}S$ value are 1σ (the mean (solid line) and 1σ (dashed lines) highlighted in Figures (a)) and $2\sigma_m$.

(–0.35 ± 0.17‰ (1σ)). The variability seen in the S-1 samples used for spike calibration is likely the due to the inclusion of samples having lower signal intensity for the minor isotope and not due to variations in sample size or blank (discussed below). Figure 5.13 suggests that no correlation exists between sample size and the resulting $\delta^{34}S$ values, which is another indicator that blank is not a factor in the variability observed at these sample sizes.

All reported $\delta^{34}S$ values for both DS #1 and DS #2 have been corrected for blank (individual uncertainties for the blank-corrected $\delta^{34}S$ measurements are shown in Appendix A). In this case, the blank for the standards was determined to be from Si gel and the As-NH_3 dilution solution and control the blank isotope composition. This conclusion, was deduced from experiments that showed when 10 times less reducing solution was used in the extraction there was no change in the average blank concentration. This suggests the variability observed in the blanks is coming from the loading portion of the procedure. Based on this determination the blank composition used in the Hayes (2002) correction scheme (+36.6‰, n = 2) was determined by direct measurement where only Si gel and As-NH_3 were added to the filament. The same Si gel and As-NH_3 solution was used for all the standards measured; thus, the blank composition should be constant. The uncertainty in the composition, however, is likely quite large due to the limited ability to directly measure the composition of the blank on such small concentrations; thus, the $\sigma\delta^2_{blank}$ used in the error propagation equation 4.7 was set at 1600 (± 40‰). This is likely an overestimation of the uncertainty for the $\delta^{34}S$ of the blank; however, because the natural sample sizes used in this part of the study were

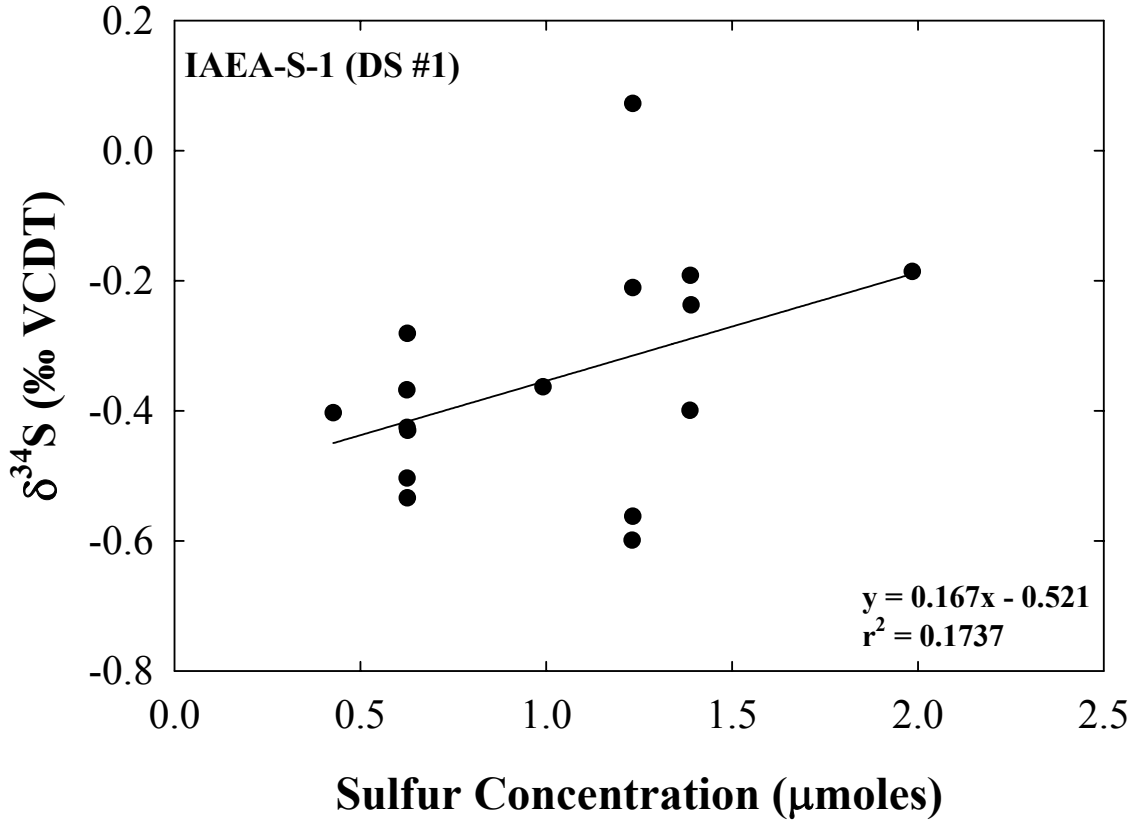

Figure 5.13. $\delta^{34}S$ values versus S concentration (μmoles). The variability observed at these sample sizes suggests that no correlation exists between sample size and $\delta^{34}S$ values.

relatively large (sample to blank ratios were 900 to 8,000 (Appendix A)) the effect of the uncertainty on the blank composition is quite small. Even if the uncertainty ($\sigma\delta^2_{blank}$) was set at 4 (± 2‰) the resulting calculated uncertainty is < 0.01‰ different than when using a ± 40‰ uncertainty; ultimately, falling within the measurement precision for the all the standards. The procedural loading blank concentration used in the Hayes (2002) correction scheme (Eqn. 4.7) was 0.00042 μmoles for standards run with DS #1 and 0.00022 μmoles for standards run with DS #2.

The potential of the double spike technique to yield highly accurate and precise data on a variety of sample sizes was demonstrated early on in the study through modeling calculations. The data reported above indicate precisions better the 0.20‰. To check the accuracy and precisions of the standards data, the $\delta^{34}S$ values for the three IAEA standards determined using DS #1 and DS #2 were compared to those determined by other laboratories (Table 5.6 and Figures 5.14.a – c). All of the other laboratories employed the SF_6 method for sulfur isotope analysis with the exception of USGS (refer to Table 5.6 for definition) that used the SO_2 method. Figure 5.14.a show the results reported by each laboratory for IAEA-S-1. The average $\delta^{34}S$ values reported for IAEA-S-1 by all the laboratories including this work, are the same within the stated uncertainties, which range from 0.04‰ to 0.16‰ (1σ). The average $\delta^{34}S$ values reported in this study (NIST/UMCP), –0.32 ± 0.04‰ (1σ) for DS #1 and –0.31 ± 0.13‰ (1σ) for DS #2, were for sample sizes of 0.73 to 2.35 μmoles S. These are considerably smaller then the sample sizes used by the other laboratories (3 to 30 μmoles S). The results for IAEA-S-2 for all the laboratories are shown in Figure 5.14.b. Again the average $\delta^{34}S$ values reported by the other laboratories are in good agreement with those from this

Table 5.6. $\delta^{34}S$ values reported by each laboratory for IAEA-S-1, S-2, and S-3.			
IAEA-S-1			
	$\delta^{34}S$ (‰ VCDT)	**1σ**	**Sample Size (μmoles S)**
NIST/UMCP DS #1	-0.32	0.04	1.00 – 1.34
NIST/UMCP DS #2	-0.31	0.13	0.73 – 2.35
IMD[a]	-0.30	0.16	≈ 16
IRMM[a]	-0.30	0.12	20 - 30
USGS #1[b]	-0.30	0.12	13
USGS #2[b]	-0.30	0.12	10
IAEA-S-2			
NIST/UMCP DS #1	22.65	0.04	0.40 – 1.05
NIST/UMCP DS #2	22.60	0.06	1.03 – 1.22
IMD[a]	22.67	0.15	≈ 16
IRMM[a]	22.64	0.11	20 - 30
GSC[c]	22.66	0.81	3 - 6
USGS #1[b]	22.67	0.09	13
USGS #2[b]	22.67	0.11	10
IAEA-S-3			
NIST/UMCP DS #1	-32.47	0.07	0.70 – 1.09
IMD[a]	-32.55	0.12	≈ 16
IRMM[a]	-32.06	0.11	20 - 30
GSC[c]	-32.24	0.38	3 - 6

a Ding et al. (2001)
b Qi and Coplen (2003)
c Taylor et al. (2000)

NIST/UMCP (National Institute of Standards and Technology/University of Maryland, Maryland, USA (this work))
IMD (Institute of Mineral Deposits, Beijing, China)
IRMM (Institute for Reference and Measurements, Geel, Belgium)
GSC (Geological Survey of Canada, Ottawa, Canada)
USGS (United States Geological Survey, Virginia, USA)

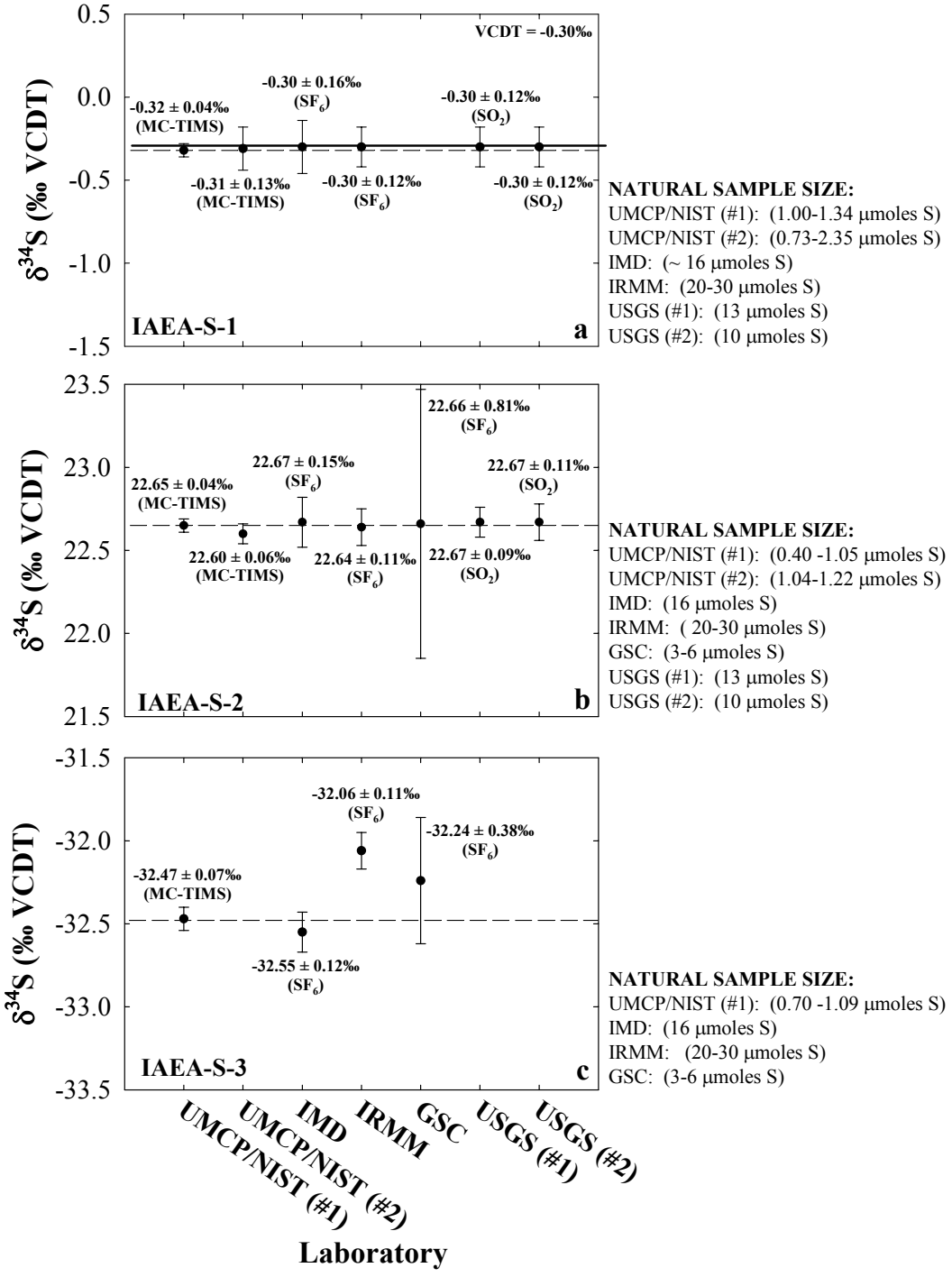

Figure 5.14.a-c. $\delta^{34}S$ values reported by each laboratory for the isotopic standards IAEA-S-1 (a), S-2 (b), and S-3 (c). The natural sample sizes used for analysis by each laboratory are listed to the right of each figure. Uncertainties are reported as 1σ.

study, 22.65 ± 0.04‰ (1σ) and DS #1 and 22.60 ± 0.06‰ (1σ), within the stated 1σ uncertainties (0.04‰ to 0.81‰). The larger uncertainties reported by GSC compared to those for other laboratories is attributed to the high reactivity of Ag_2S with F_2 during laser micro-analysis (Taylor et al., 2000). The sample sizes used for analysis were also considerably smaller (0.4 to 1.22 μmoles S) than those used by other laboratories. The results for IAEA-S-3 are shown in Figure 5.14.c. In this case, all the laboratories show agreement among each other within the stated 1σ uncertainties (0.07‰ to 0.38‰) with the exception of IRMM. The results reported for this study and those reported by IMD are significantly different than that reported by IRMM even at the 2σ level. The value reported by GSC is not significantly different from IRMM's; however, this is due to the larger uncertainty reported by this laboratory. Based on these results, the agreement between laboratories is very good considering the variability in sample size and techniques used. The data results show that the double spike technique is competitive with other techniques presently used for sulfur isotope analysis and allows for the measurement of even smaller samples.

5.3 Standards: Concentration Results and Discussion

The data results using the double spike technique clearly demonstrate an improvement in measurement precision (by a factor of ≈ 2 to 5) and that the accurate natural isotopic compositions are obtained. Another added advantage of using the double spike is that the concentration in the natural samples/standard can also be simultaneously determined by isotope dilution (ID). For example, SRM 2724b (Sulfur in Diesel Fuel Oil) was used to test the double spike technique for concentration determinations. The concentration results for the standards (IAEA-S-1, IAEA-S-2,

IAEA-S-3, SL #7, and SL #9) used to test the double spike method for isotope composition determination are also shown; however, these solutions were prepared gravimetrically and the original calculated S concentration value has subsequently changed over time. Nonetheless, the measurements made using the two different double spike mixtures show the precisions obtainable and the repeatability of the new method.

SRM 2724b (Sulfur in Diesel Fuel Oil) is a certified reference material available from NIST. The results from this work are shown in Table 5.7 relative to the certified value reported by NIST. The blank-corrected concentration determined using the double spike method is in excellent agreement with the certified value of 426.5 ± 5.7 μg/g and is

Table 5.7. Sulfur concentration of SRM 2724b (S in Diesel Fuel Oil)

	S Concentration (μg/g)
This Work[a]	424.6 ± 1.4 (n=3)
SRM Certified Value[a]	426.5 ± 5.7

a uncertainties for both are expressed as expanded uncertainties and are calculated according to the method in the NIST/ISO Guide (GUM, 1994). The expanded uncertainties are based on a 95% confidence interval.

well within the 95% confidence interval.

The blank-corrected concentration results determined using DS #1 and DS #2 for the isotope composition standards are shown in Table 5.8. Inspection of Table 5.8 shows that both spike mixtures (DS #1 and DS #2) give concentration results for IAEA-S-1 and S-2 that are well within the 95% confidence interval of each other and show the repeatability of the technique. The concentration results for IAEA-S-3, SL #7, and SL #9 were 304.3 ± 1.0 μg/g (0.20 (1σ), 0.07% RSD, n = 8), 448.8 ± 1.5 μg/g (0.38 (1σ), 0.08% RSD, n = 3), and 422.7 ± 1.4 μg/g (0.28 (1σ), 0.07% RSD, n = 3), respectively. The relative standard deviations (RSDs) obtained ranged from 0.07% to 0.27%, which are

Table 5.8. Sulfur Concentration Results for the 3 IAEA Standards and 2 McMaster Standards measured using DS #1 and DS #2.										
	DS #1					DS #2				
	[S] (μg/g)	95% C.I.[a]	1σ	RSD (%)	n	[S] (μg/g)	95% C.I.[a]	1σ	RSD (%)	n
IAEA-S-1	296.0	1.0	0.68	0.23	22	296.4	1.1	0.61	0.21	8
IAEA-S-2	264.5	0.9	0.50	0.19	11	264.4	1.1	0.72	0.27	7
IAEA-S-3	304.3	1.0	0.20	0.07	8					
SL #7	448.8	1.5	0.38	0.08	3					
SL #9	422.7	1.4	0.28	0.07	3					

a uncertainties for both are expressed as expanded uncertainties and are calculated according to the method in the NIST/ISO Guide (GUM, 1994). The expanded uncertainties are based on a 95% confidence interval. n = number of analyses.

similar to or better then that obtained using the existing ID technique that uses an enriched ^{34}S spike.

5.4 Summary

This chapter has shown the double spike technique to be an excellent analytical method for sulfur isotope composition and concentration determination for standard materials. The technique provides a factor of 2 – 5 improvement in measurement precision, yielding precisions of approximately 0.20‰ to 0.60‰, prior to blank correction, for the $\delta^{34}S$ measurements. This demonstrates the ability of the technique to suitably correct for instrumental fractionation. The present measurement precision (several parts in 10^4) suggests all three correction laws could be used; however, if the Rayleigh model is correct, then the exponential law is better suited for correction of the data. In addition, it was also found that the point on the fractionation curve where analysis begins and ends could be determined, revealing that analysis typically began when the reservoir was 40 – 50% depleted. For ratio data with measurement precisions

of 0.01% as obtained in this study, the three correction laws are indistinguishable at this point on the curve. If the precision were to increase to 0.001%, it is likely that small differences would be observed.

The isotope composition results for the IAEA standards demonstrate excellent agreement with the other laboratories considering the different techniques and the differing sample sizes used for determination. Furthermore, the uncertainties reported in this work are typically lower than those reported by the other laboratories, which all used larger samples. Clearly, the data results show that the double spike technique is competitive with the other established techniques presently used for sulfur isotope analysis. Although the $\delta^{34}S$ results for the McMaster standards reported by Rees (1978) were significantly different than those reported in this study and may indicate a problem with the double spike technique, the results for the IAEA isotopic standards suggest otherwise. Moreover, the data reported by Rees (1978) includes only one analysis and may potentially be influenced by leakages, background, and/or offset in the collector amplifiers.

The concentration results for SRM 2724b (Sulfur in Diesel Fuel Oil) was in excellent agreement with previously certified value and were well within the certified 95% confidence interval given. In addition, both spike mixtures (DS #1 and DS #2) gave values that are well within the 95% confidence interval of each other demonstrating the repeatability of the technique. Lastly, the relative standard deviations (RSDs) obtained for the data were similar to or better then that obtained using the existing ID technique that employs an enriched ^{34}S spike.

Chapter 6: Snowpit Samples: Analytical Results and Discussion

The Ice Core Working Group published a report in 2003 highlighting recommendations for future U.S. ice coring activities one of which was to support the development of analytical techniques for small samples for all measurements including stable isotope measurements. Towards this end, the primary objective of this research was to develop an analytical technique capable of determining isotope composition and concentration of sulfur in low concentration environments, in particular in snow and ice. The $\delta^{34}S$ results reported in Chapter 5 demonstrate that the double spike technique has the capability to measure isotope composition on much smaller samples and with precisions comparable to or better than those obtained using gas source mass spectrometric techniques that require larger sample volume/mass.

To examine seasonal or "event" scale changes in the atmospheric sulfur cycle at a given site requires that the smallest sample possible be used for analysis. To date, studies that have used gas source IRMS for $\delta^{34}S$ measurements to explore sulfate sources, transport pathways, and contribution to the atmospheres of central Asia and remote Greenland have required > 1 μmole which typically requires 1 to 2.5 L of meltwater (Kreutz and Sholkovitz, 2000; Pruett et al., 2004; Patris et al., 2002) for $\delta^{34}S$ analysis due to the low ppb level concentrations. The reported precisions are typically ± 1‰ or better; however, this large sample requirement precludes a detailed high-resolution ice core record necessary for determining seasonal changes in $\delta^{34}S$ values. This chapter demonstrates the ability of the new double spike method to measure the isotopic

composition and sulfur concentration of snowpit samples with ppb (ng/g) or μmole/L levels of sulfate using 300 mL or less meltwater, which are the smallest snow samples ever measured. The geochemical and isotopic composition results are presented for the snowpit samples collected from the Inilchek and Summit along with the mass balance results used to determine the relative seasonal contributions of anthropogenic (fossil fuel burning) and natural sulfur (marine biogenic, sea spray, dust) sources to sulfate in these regions.

6.1 Inilchek Glacier

Analysis of the samples from the Inilchek snowpit were performed first because the sulfate concentrations were typically larger and the accumulation rate at this site location is higher than at Summit; thus, providing the maximum mass per unit volume (and time) in which to test the new double spike technique. In addition, the larger sulfate concentrations in conjunction with the documented exposure of the site to anthropogenic emissions (Kreutz and Sholkovitz, 2000; Pruett et al., 2004) makes the Inilchek location an excellent test site for this new analytical technique.

6.1.1 Results

6.1.1.a Dating Results

Accessing the high-resolution (seasonal) sulfur isotopic record of any snowpit requires dating techniques that are of sufficient resolution to examine seasonal time-series data. Both the deuterium isotope ratio (δD) and oxygen isotope ratio ($\delta^{18}O$) values were used to date the Inilchek snowpit and are shown in Figure 6.1. Both isotope records serve as proxies for surface temperature at a site, where more depleted values (negative

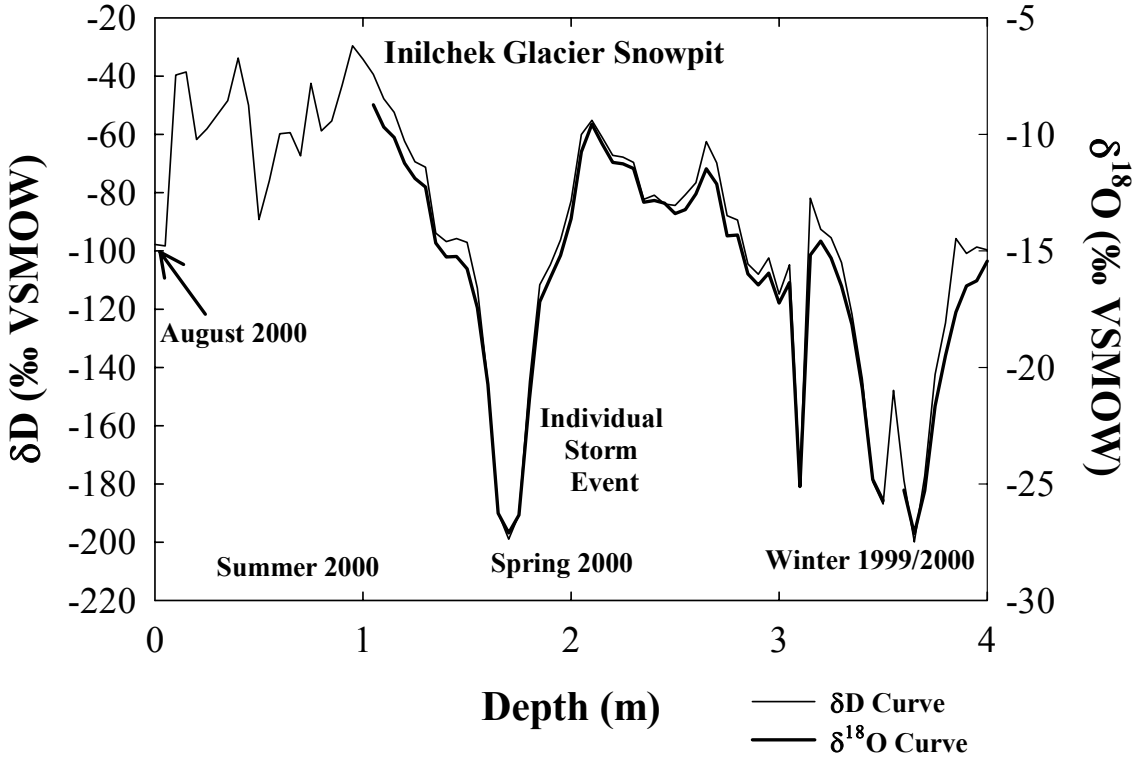

Figure 6.1. Deuterium isotope ratio (δD) and oxygen isotope ratio ($\delta^{18}O$) curves used to date the 2000 Inilchek snowpit. δD uncertainties are ± 0.3‰ and $\delta^{18}O$ uncertainties are ± 0.05‰. Samples collected by Dr. Karl Kreutz, University of Maine.

delta values) represent colder temperatures and more enriched values (positive delta values) represent warmer temperatures. The δD values in the Inilchek snowpit ranged from –29.6‰ to –200‰ (thin solid line in Figure 6.1) while the $\delta^{18}O$ values ranged from –8.7 ‰ to –27.1‰ (thick solid line in Figure 6.1). A firn core previously obtained from the same location on the Inilchek shows a clear seasonal $\delta^{18}O$ trend with $\delta^{18}O$ values typically higher than –20‰ in the summer and values as low as –35‰ in winter (Kreutz et al., 2001). The snowpit in this study shows two points of minima at 1.7 and 3.65 m, where the $\delta^{18}O$ values are both –27.1‰. Based on the accumulation rate for this location (> 140 cm water equivalent $yr^{-1} \approx 3.2$ m snow; Kreutz and Sholkovitz, 2000; Pruett et al., 2004) the minima at 1.7 m is not likely snow deposited during the winter but snow deposited during an individual spring/summer storm event whereas the minima at 3.65 m is likely snow deposited during the winter months. Additional δD and $\delta^{18}O$ data from snowpit samples collected nearby, also by Dr. Karl Kreutz, and within a month of the one in this study, show no corresponding drop of this degree in δD and $\delta^{18}O$ at 1.7 m (Figure 6.2). Assuming that snow is being deposited and not lost at these other site locations the excursion observed is likely an individual storm event. The range of $\delta^{18}O$ values for the winter was typically –27.1‰ to –20‰ and is comparable to that determined by others for this location (Kreutz et al., 2001; Pruett et al., 2004). The $\delta^{18}O$ values for snow deposited during the spring and summer months, with the exception of the individual storm event, were typically heavier than –15‰, ranging from –8.7‰ to –15‰. Again this is comparable to that determined previously for this location by Kreutz et al. (2001) and Pruett et al. (2004).

The δD record shows excellent agreement and correlation with the $\delta^{18}O$ record.

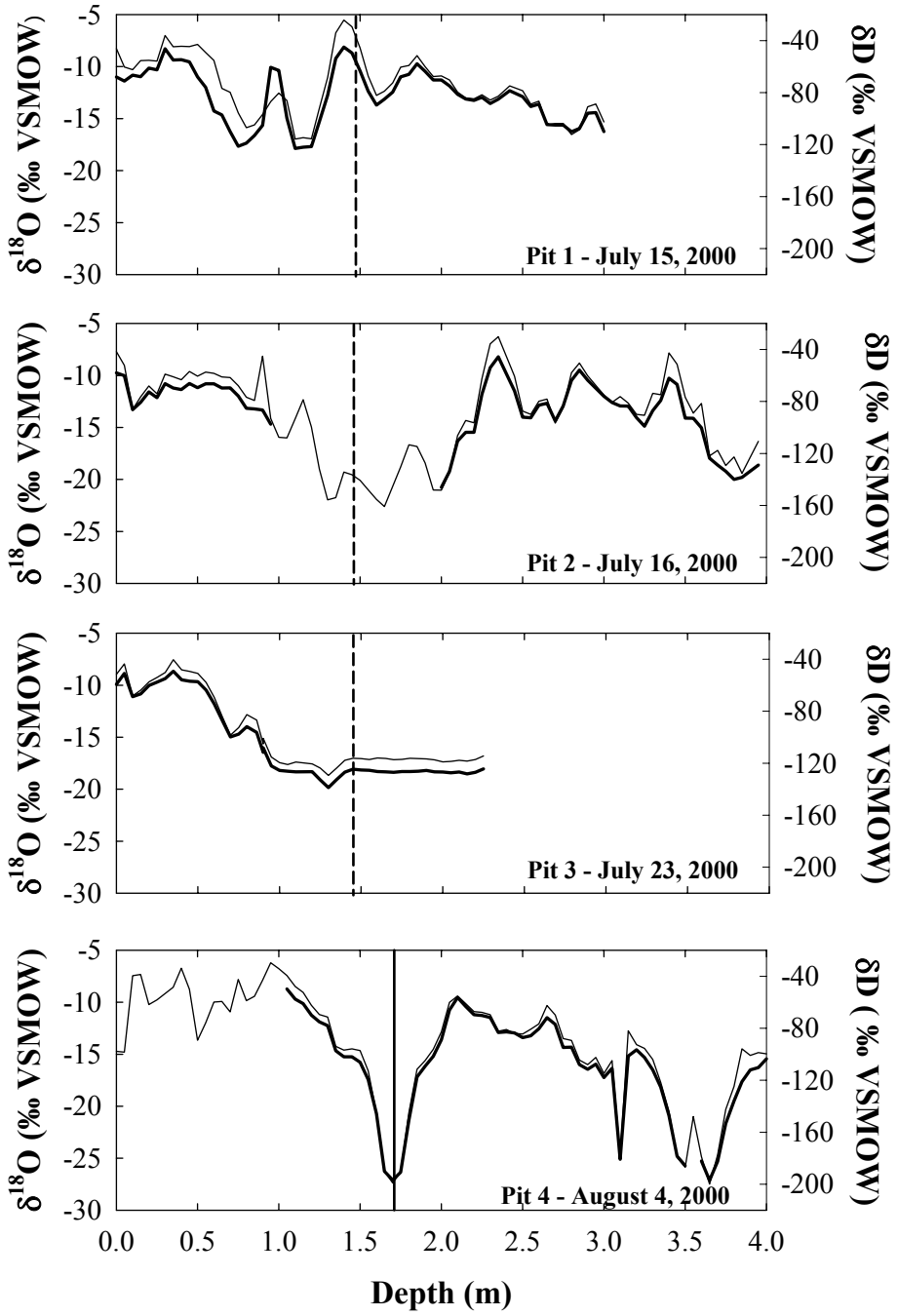

Figure 6.2. Additional δD and $\delta^{18}O$ data from snowpit (Pit 1 through Pit 3) samples collected nearby and within a month of the one in this study. Solid line marks 1.7 m. Please note that the 1.7 m will be shifted by approximately 2 to 3 weeks to the left in the first three snowpits because the pits were collected at an earlier date (the dashed lines mark the approximate location). Samples collected by Dr. Karl Kreutz, University of Maine.

The δD values for the two minima in the curve were –199‰ and –200‰, respectively. The range of values for snow deposited in winter was typically –200‰ to –120‰. For snow deposited during the spring and summer months the δD values typically ranged from –120‰ to –30‰, with the exception of the individual storm event. Based on the seasonal trend in both isotope records, the snowpit likely represents precipitation occurring over approximately a 9-month period. The samples taken for sulfur isotopic analysis, therefore, provide a continuous $\delta^{34}S$ record from winter 1999/2000 to August of 2000 with each sample representing approximately 2 weeks.

6.1.1.b Major Ion Results

Major ion concentration data for all the soluble species measured in the snowpit are presented in Figure 6.3 (refer to Appendix C for details). Broadly speaking, all the major ion species show similar trends, with concentrations peaking between 1 and 2 m (late spring/early summer) and again around 3.5 m (winter). The background interval concentrations of all major ions are < 1 μmole L^{-1} except for NH_4^+. The concentration ranges of the data fall within the ranges determined for both the 1999 Tien Shan snowpit (Pruett et al., 2004) and the 3 snowpits (Pits #1 – 3) dug at the same site location from July to August of the same year (Table 6.1). Furthermore, the mean concentrations found in the present snowpit were similar to those determined for the three other snowpits for all the ionic species with the exception of Ca^{2+}, which was almost a factor of two higher, and Mg^{2+} and NO_3^-, which were about a factor of 1.5 higher in the case of Mg^{2+} and about a factor of 1.5 lower in the case of NO_3^- (Table 6.2). It is important to consider that the mean concentrations are to demonstrate the similarity in the seasonal data of this site to other nearby locations.

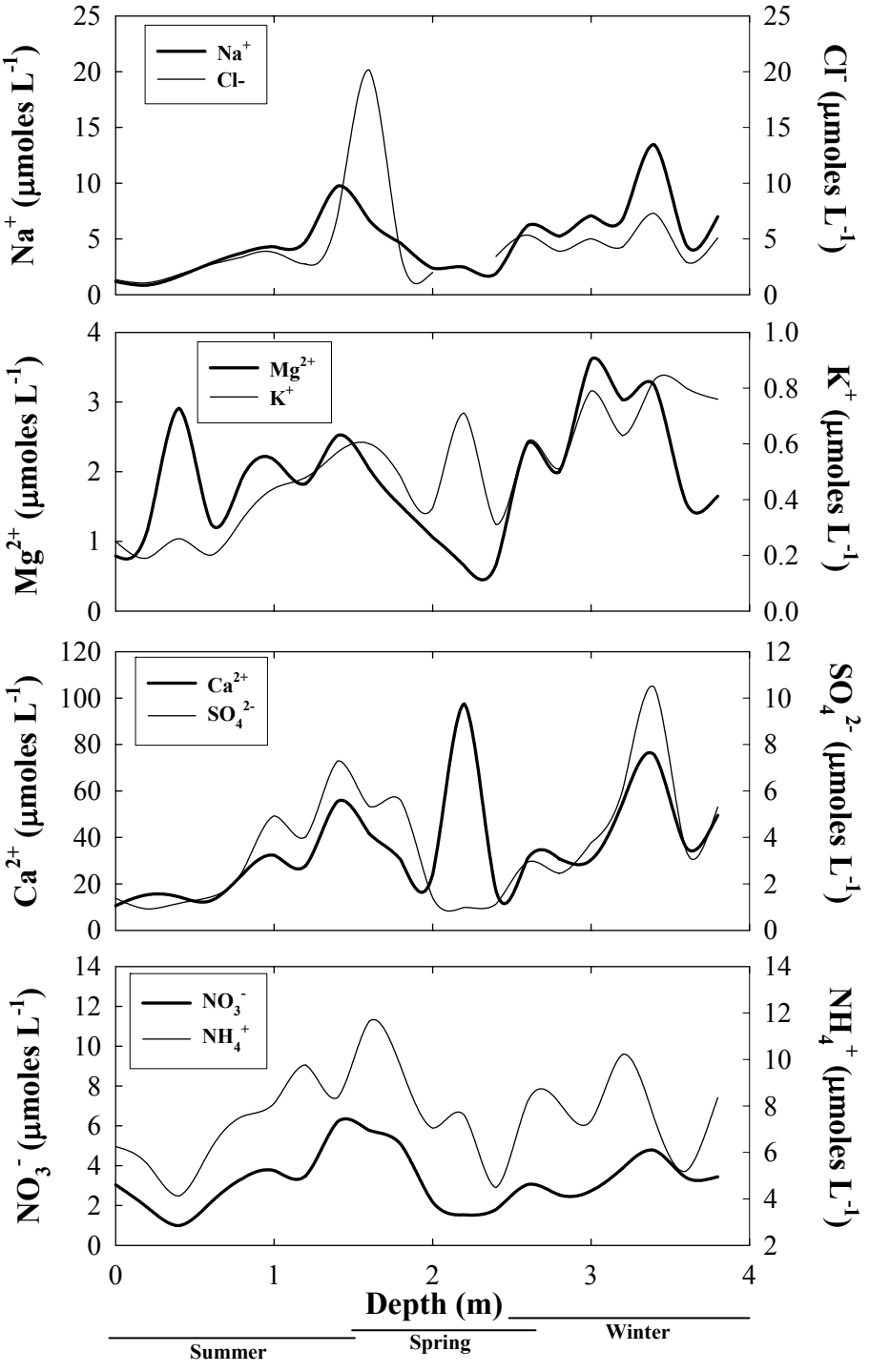

Figure 6.3. Major ion concentration data for all the soluble species measured in the Inilchek snowpit. The surface of the snowpit is to the left at 0 m. Refer to Appendix C for measurement details. Samples collected by Dr. Karl Kreutz, University of Maine.

Table 6.1. Major ion concentration ranges for the 2000 Inilchek snowpit of this work, the 1999 Tien Shan snowpit, and the 3 snowpits (Pits #1 – 3) dug at the same time as the snowpit in this work.					
	2000 snowpit (This work)	**1999 snowpit (Pruett et al., 2004)**	**Pit 1 (07-15-2000)**	**Pit 2 (07-16-2000)**	**Pit 3 (07-23-2000)**
Na^+	0.86 – 13.46	0 – 30	0.83 – 38.63	0.58 – 52.59	1.39 – 47.12
NH_4^+	4.13 – 11.64	0 – 10	2.26 – 19.41	2.49 – 22.16	2.80 – 13.79
K^+	0.19 – 0.83	0 – 6	0.11 – 3.05	0.09 – 4.39	0.14 – 1.48
Ca^{2+}	10.60 – 97.54	0 – 25	0.39 – 75.19	0.98 – 90.93	1.63 – 64.50
Mg^{2+}	0.65 – 3.24	0 – 3.5	0.05 – 3.51	0.04 – 4.39	0.33 – 5.02
Cl^-	1.07 – 20.16	0 – 20	0.34 – 32.91	0.33 – 46.06	0.72 – 49.90
NO_3^-	0.99 – 6.21	0 – 15	0.47 - 22.75	0.47 – 32.26	0.31 – 7.56
SO_4^{2-}	0.92 – 10.46	0 – 10	0.11 - 19.90	0.08 – 23.52	0.11 – 16.19

All concentrations are in μmoles L^{-1}. All snowpits were dug by Professor Karl Kreutz.

Table 6.2. Mean concentrations of the major ionic species for the 2000 Inilchek snowpit of this work and the 3 snowpits (Pits #1 – 3) dug at the same time.				
	2000 snowpit (This work)	**Pit 1 (07-15-2000)**	**Pit 2 (07-16-2000)**	**Pit 3 (07-23-2000)**
Na^+	4.87 ± 3.10	5.66 ± 6.46	5.83 ± 9.03	7.29 ± 7.80
NH_4^+	7.56 ± 1.92	8.21 ± 3.89	7.83 ± 3.78	7.08 ± 2.01
K^+	0.51 ± 0.21	0.62 ± 0.50	0.53 ± 0.47	0.59 ± 0.46
Ca^{2+}	35.55 ± 22.03	18.59 ± 15.69	19.81 ± 19.36	19.62 ± 12.47
Mg^{2+}	1.90 ± 0.86	1.16 ± 0.87	1.28 ± 1.10	1.57 ± 1.02
Cl^-	4.57 ± 4.14	4.31± 5.68	5.08 ± 8.01	6.25 ± 7.99
NO_3^-	3.25 ± 1.39	4.18± 3.42	4.61 ± 5.27	4.20 ± 2.11
SO_4^{2-}	3.61 ± 2.36	3.58 ± 3.78	3.84 ± 4.60	2.73 ± 2.88

All concentrations are in μmoles L^{-1}. All snowpits were dug by Professor Karl Kreutz.

6.1.1.c $\delta^{34}S$ and Sulfate Concentration Results

The variability observed in the major ion concentrations make it difficult to distinguish between the two main sources, anthropogenic emissions and evaporite dust, contributing sulfate to these regions and therefore understanding the degree of anthropogenic influence on the sulfur cycle at this location. The distinct variability of stable sulfur isotopes ($\delta^{34}S$) in nature, however, provides a useful chemical tool for tracing these two sources of sulfate-sulfur and can be used to assess the relative proportions of anthropogenic versus evaporite dust being contributed to the region. $\delta^{34}S$ values (solid triangles) and the corresponding sulfate concentration data (grey circles) in time (depth) series for the samples collected for this study are shown in Figure 6.4. All concentration and $\delta^{34}S$ results are reported in Appendix C. The amount of meltwater used for sulfur isotope analysis by the double spike technique ranged from 108 to 358 mL, and averaged 191 mL, which is considerably less then the 1 L used by previous researchers for analysis of samples from this region (Pruett et al., 2004). It is important to note that the samples used in this study were collected for gas source analysis of $\delta^{34}S$. Therefore, even though higher-resolution is attainable with the double spike technique, as demonstrated by the smaller amount of meltwater required for analysis (108 to 358 mL), the resolution of this record is consistent with that of 1 L of meltwater. Sulfate concentrations ranged from 0.92 ± 0.009 μmoles L^{-1} SO_4^{2-} to 10.46 ± 0.08 μmoles L^{-1} SO_4^{2-} and averaged 3.61 μmoles L^{-1} SO_4^{2-}. The range in uncertainties, expressed as an expanded 95% confidence interval, was 0.008 to 0.08 μmoles L^{-1} SO_4^{2-}. The range in $\delta^{34}S$ values was from 2.6 ± 0.1‰ (2σ) to 7.6 ± 0.10‰ (2σ) and averaged 5.8‰. The range in 2σ for the individual $\delta^{34}S$ measurements was 0.10 to 0.12‰ for sample sizes

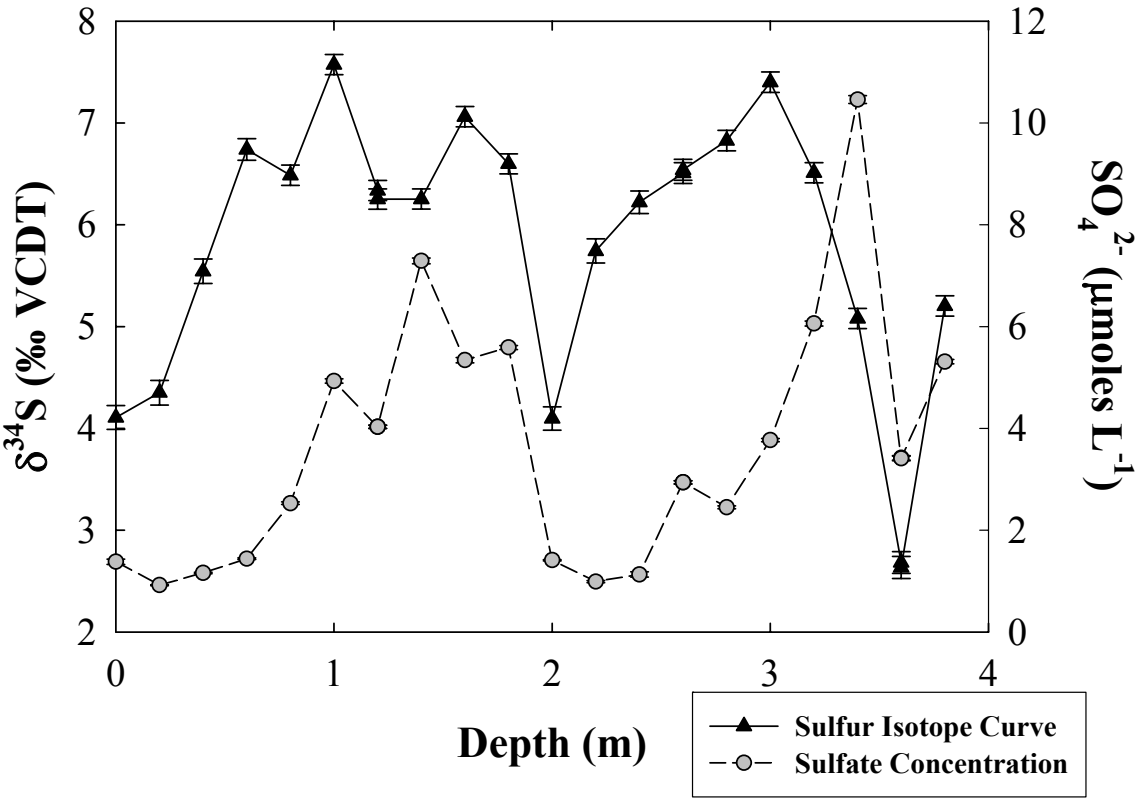

Figure 6.4. $\delta^{34}S$ values (solid triangles) and the corresponding sulfate concentration data (grey circles) in time (depth) series for the Inilchek samples. All error bars are 2σ.

ranging from 0.26 to 1.82 μmoles S. An additional 6 samples collected from 2 separate fresh snow events on July 31 and August 3, 2000 were also measured for sulfate concentration and $\delta^{34}S$ (refer to Appendix C). The sulfate averaged 4.29 ± 0.51 μmoles L^{-1} (95% C.I.) for the July 31st snow event and 1.13 ± 0.55 μmoles L^{-1} (95% C.I.) for the August 3rd event. The $\delta^{34}S$ values ranged from 2.8‰ to 3.1‰ for the July 31st event and averaged 3.0 ± 0.33‰ (2σ) (n = 3) while the range for the August 3rd event was 2.3‰ to 2.4‰ and averaged 2.4 ± 0.12‰ (2σ) (n = 3). Because the samples were taken simultaneously, the $\delta^{34}S$ values are expected to have the same or similar $\delta^{34}S$ values within an individual snow event, which the data support. The range in sample sizes used for these analyses was 0.10 to 0.65 μmoles S. If these samples are viewed as triplicate analyses of the same sample, it is clear that the double spike technique is capable of precisions better then 0.35‰ (2σ) on sample sizes of 0.10 μmoles S.

The high precision obtained for the $\delta^{34}S$ values for all the samples in this part of the study results from the high measurement precision, low blanks, and the relatively high precision determination of the blank composition. The $\delta^{34}S$ measurement precision was derived from the pooled standard deviation for duplicate sample measurements (n = 5) and was 0.22 ‰ (1σ). The procedural blank concentrations for this portion of the study were quite low and averaged 0.0028 ± 0.00079 μmoles S (1σ) for the larger sample sizes (0.43 to 1.83 μmoles) and 0.0032 ± 0.0026 μmoles S (1σ) for the smaller sample sizes (0.10 to 0.44 μmoles). The blank composition determined using Eqn. 4.8 (refer to Chapter 4 section 4.3) was 8.8 ± 0.06 ‰ (1σ). Using the double spike combined with the relatively well-characterized blank concentration and isotope composition yields the high

precisions observed for the individual blank-corrected $\delta^{34}S$ measurements.

In other locations such as the Arctic (Nriagu et al., 1991, Norman et al., 1999) seasonal trends have been observed in the $\delta^{34}S$. Figure 6.5 shows the $\delta^{34}S$ values (solid triangles) with the corresponding δD curve in time (depth) series. Samples with low $\delta^{34}S$ values were deposited during each season represented in this snowpit; winter, spring, and summer. Pruett et al. (2004) also observed low $\delta^{34}S$ values in snow deposited in the summer months. $\delta^{34}S$ values that are ^{34}S-enriched appear to occur during the height of spring and summer suggesting that a possible weak seasonal trend may exist; yet, a longer term record is required to determine the strength of the seasonality at this site.

6.1.1.d Mass Balance Results

To assess whether there exists a seasonal trend exhibited by the Inilchek snowpit the fractions of the anthropogenic contribution and the evaporite sulfate contribution to the snowpit samples of this study were estimated using a two-component mixing model. In this model, the measured isotopic composition can be resolved using Eqn. 4.15 ($\delta_{measured} = f_{nss}\delta_{nss} = f_a\delta_a + f_d\delta_d$) and Eqn. 4.16 ($\delta_{nss}f_{nss} = (1\text{-}x)\delta_a + (x)\delta_d$), where δ_a and δ_d are the isotopic signatures of the anthropogenic and dust components and f_a (1-x)and f_d (x) are the mass fractions of these components. Examination of the seasonal changes in the relative amounts of sulfate being contributed by the two sources (anthropogenic and evaporite dust) to this region was determined using $\delta^{34}S$ values from the literature. The $\delta^{34}S$ value used in the model for the evaporite dust was +20‰ while that used for the anthropogenic was 0‰. The $\delta^{34}S$ value used for the anthropogenic component is lighter than that used in previous studies for this location ($\delta^{34}S$ = +5.4‰ (Kreutz and Sholkovitz, 2000) and +5 ‰ (Pruett et al, 2004)) because Pruett et al. (2004) suggested that two

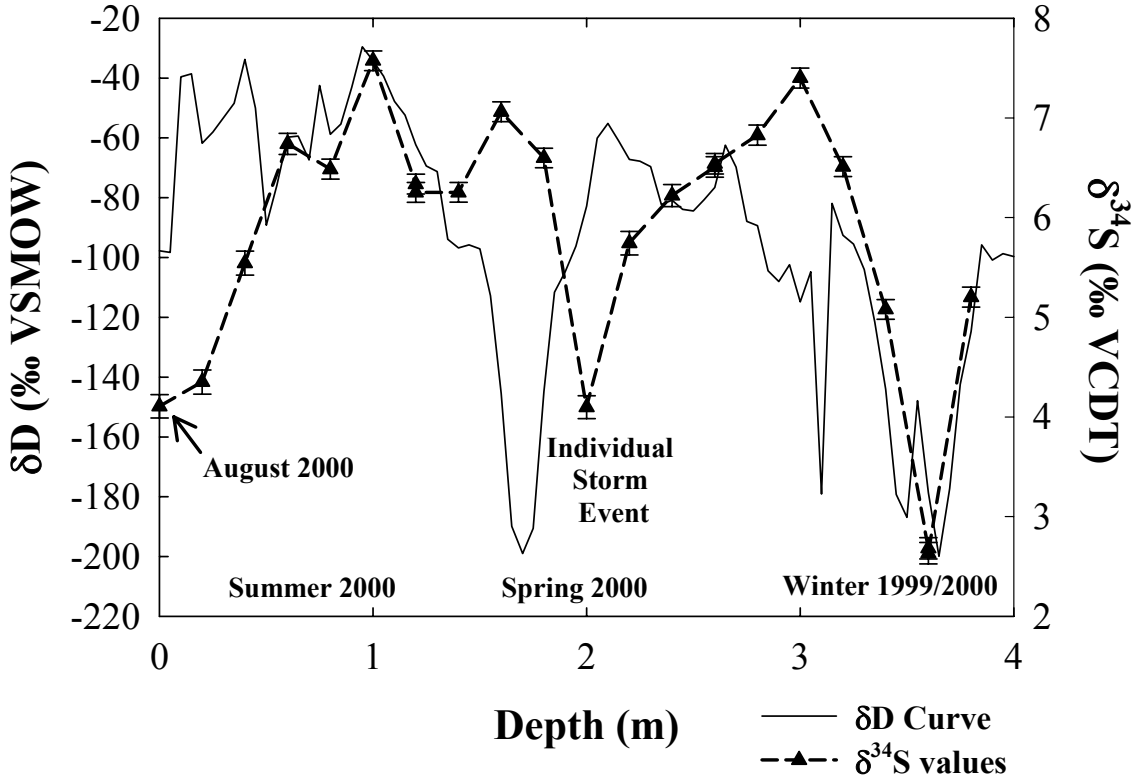

Figure 6.5. $\delta^{34}S$ values (solid triangles) and the corresponding δD curve in time (depth) series for the Inilchek samples. Precision in the δD data are ± 0.3‰ Error bars for the $\delta^{34}S$ measurements are 2σ.

samples with anomalously low $\delta^{34}S$ values could not be accounted for using the end-member composition of +5‰, suggesting the end-member composition used may not be appropriate. These authors suggested that the anomalous samples could be explained by the uncertainty in the $\delta^{34}S$ value of the anthropogenic end-member. Changing the end-member value by approximately 4‰ accommodates these low $\delta^{34}S$ values. This change in the end-member composition is not outside the $\delta^{34}S$ values observed for coals from the former Soviet Union (< 0‰) (Wedepohl, 1978) and Bohemia (-1.4‰ to 0.1‰) (Krouse and Grinenko, 1991). Consequently, for this study 0‰ was used for the anthropogenic end-member.

The uncertainties in the $\delta^{34}S$ values of the end-members for this study are quite large and can significantly effect the calculated relative percent contributions. To determine the uncertainty contributed by the end-members a sensitivity analysis was performed using the range extremes of the end-members in the mass balance equations. For the evaporite dust end-member the range of reported $\delta^{34}S$ values was +10.8‰ to +35.5‰ (Krouse and Grinenko, 1991). The range in $\delta^{34}S$ values for the anthropogenic end-member was +5‰ to –5‰. Taking into account these uncertainties the calculated uncertainty on the relative contributions averages to 37%. This is much larger then the uncertainty coming from the experimental error (0.53%) on δ_{nss}. Contrary to the findings of Patris et al. (2002), whose experimental error was the main contributor to the uncertainty on their contribution estimates, the uncertainty from the experimental error in this study was very small due to the better precision of the measurements. Consequently, the uncertainty on the relative contributions of the end-members results from the large uncertainty of the end-member $\delta^{34}S$ values and not experimental error.

Based on the above starting assumptions, the relative percent contribution of each end-member (evaporite (black bar) dust and anthropogenic (grey bar)) is shown in Figure 6.6. The estimated contribution of each to the total sulfate concentration is shown in Figure 6.7. Error bars have not been placed on the estimates in Figure 6.6 and 6.7 because the exact end-member $\delta^{34}S$ value is not known. We note that this technique including the large uncertainties; however, is a common method for estimating SO_4^{2-} source contributions to other regions (Norman et al., 1999, Pruett et al., 2004). The data show that the anthropogenic sulfate contribution dominates the snowpack during the winter to summer months of 2000 in this location. The sulfate that accumulated in the snowpack in 2000 showed that 71% on average was contributed from anthropogenic sources and 29% on average was contributed from evaporite dust. The lowest $\delta^{34}S$ values observed show a large anthropogenic input (≈ 81%) paired with a low dust input (19%) (marked by back slashes in Figures 6.6 and 6.7). The highest $\delta^{34}S$ values observed show an increased input of dust (≈ 37%), almost a factor of 2 higher dust input relative to the samples with the lowest $\delta^{34}S$ values. The corresponding anthropogenic contribution averaged 63% (marked by horizontal slashes in Figures 6.6 and 6.7). The remainder of the $\delta^{34}S$ values lie between the two extremes and are marked by open boxes in Figures 6.6 and 6.7. During times of negligible dust sulfate deposition (marked by the letter X in Figure 6.7), the amount of anthropogenic sulfate deposition is also low but accounts for a large fraction (≈ 73%) of the sulfate deposited. Increased deposition of both evaporite and anthropogenic sulfate appears to occur in the late spring/early summer and winter months (marked by a star in Figure 6.7). The samples taken during the July 31st and

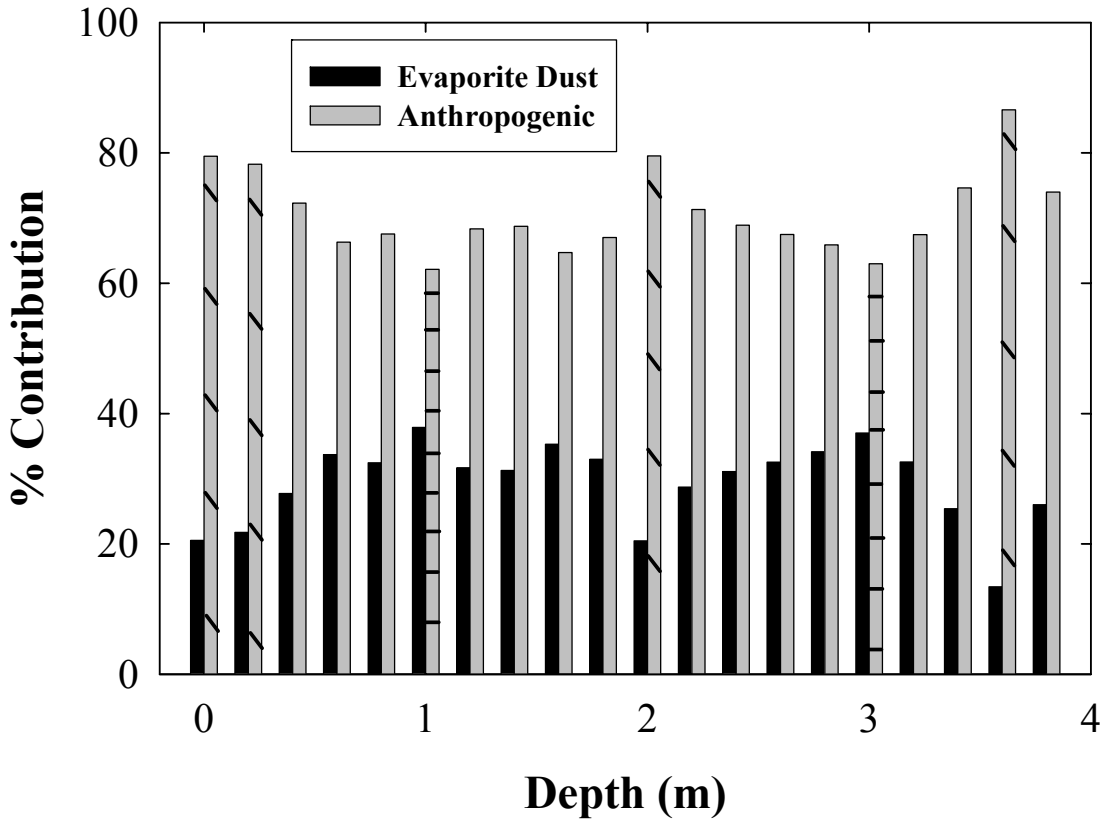

Figure 6.6. Relative percent contributions of each end-member, anthropogenic (grey bar) and evaporite dust (black bar) for the Inilchek site. The back slashes mark the samples with the lowest $\delta^{34}S$ values, the horizontal slashes mark the samples with the highest observed $\delta^{34}S$ values, and the open boxes mark the samples with $\delta^{34}S$ values that lie between the lowest and highest.

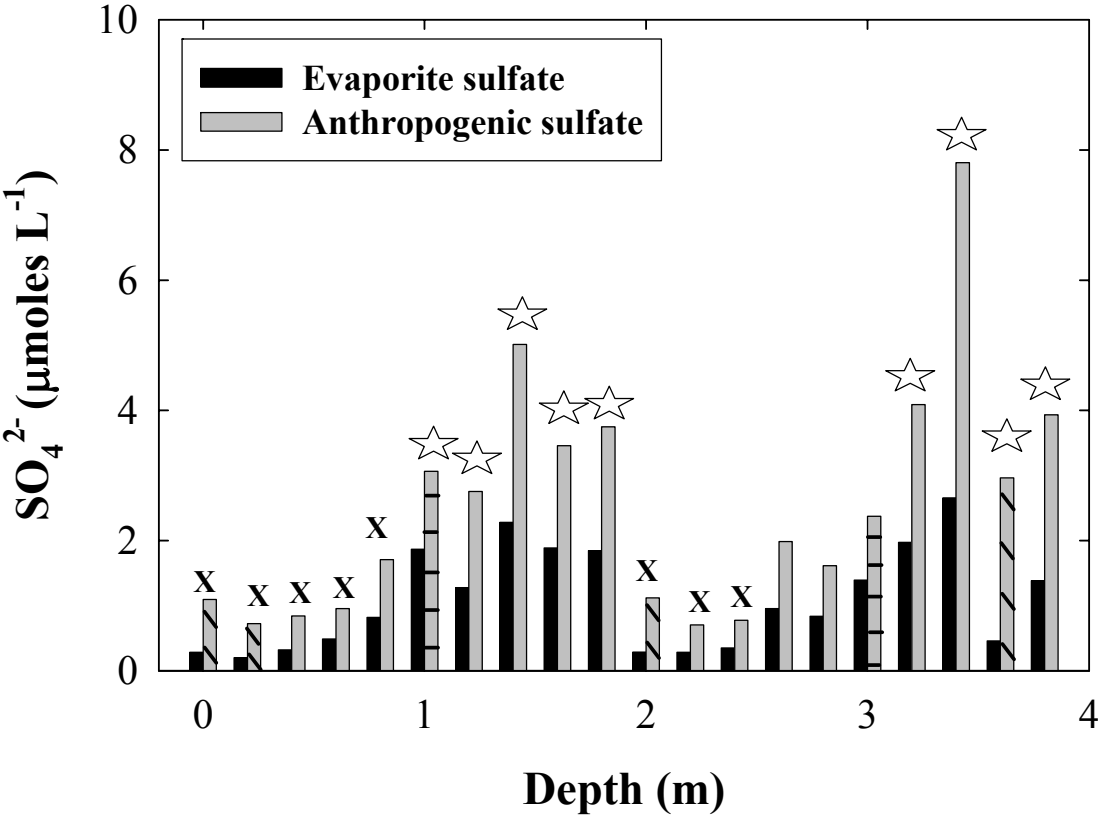

Figure 6.7. Estimates of the contribution of evaporite dust and anthropogenic sulfate to the total sulfate concentration in each snowpit sample, anthropogenic (grey bar) and evaporite dust (black bar) for the Inilchek site. The back slashes mark the samples with the lowest $\delta^{34}S$ values, the horizontal slashes mark the samples with the highest observed $\delta^{34}S$ values, the open boxes mark the samples with $\delta^{34}S$ values that lie between the lowest and highest, X marks times of negligible deposition of anthropogenic and dust sulfate, and the star marks times of increased deposition of anthropogenic and dust sulfate.

August 3rd snow events show an even larger contribution of anthropogenic sulfate of approximately 87%, with the contribution during the August 3rd event being slightly higher at 88% and the July 31st event slightly lower at 85%. The fraction of dust being contributed is approximately 13% with the July 31st event contributing more (15%) and the August 3rd event slightly less (12%). It is important to note that because of the large uncertainty on the relative contributions (37%), the results reported above are circumspect. It is obvious that the dust contribution could also dominate rather than the anthropogenic contribution. Although further constraints or better characterization of the isotope composition of the dust fraction is required to reduce this uncertainty; the range in the sulfur isotope composition of the dust fraction likely clusters around +20‰, which does not preclude the findings observed in this study.

6.1.2 Discussion

A summary of all the data results for the Inilchek snowpit, including δD, $\delta^{18}O$, major ion, and the $\delta^{34}S$, are shown versus depth and time in Figure 6.8. The major ion data (Figure 6.8.c-g) show that concentrations tend to be higher in the winter and late spring/early summer months compared to the late summer months. Typically the snowpit chemistry records from the Tien Shan region show a pattern of low concentration intervals punctuated by relatively brief increases in ion concentration (Pruett et al., 2004; Wake et al., 1992; Kreutz et al., 2001; Kreutz and Sholkovitz, 2000). Kreutz et al. (2001) and Kreutz and Sholkovitz (2000) attribute this pattern in the major ion chemistry, including sulfate, to a significant flux of evaporite dust. This snowpit record, however, does not exhibit any obvious dust events as have been observed previously (Pruett et al., 2004; Wake et al., 1992; Kreutz et al., 2001; Kreutz and Sholkovitz, 2000) and likely

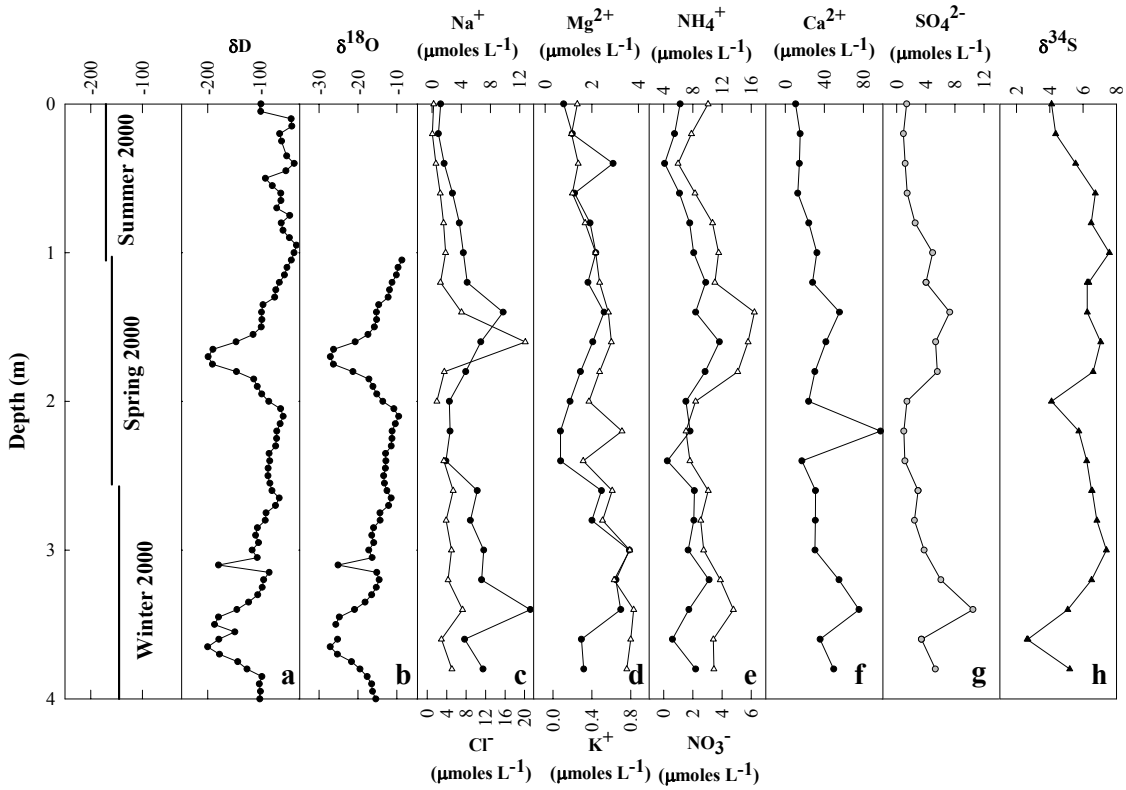

Figure 6.8.a-h. Summary figure of all the data results for the Inilchek snowpit including δD and $\delta^{18}O$ (a-b), major ion (c-g), and the $\delta^{34}S$ (h), are shown versus depth and time. The open triangles (c-g) refer to the elements listed along the bottom of the graph.

represents "background" conditions. As mentioned in Chapter 2 the predominant contributor of dust to the Inilchek Glacier site is evaporite deposits located in Central Asia and loess from the Taklimakan Desert basin in China (Kreutz et al., 2001; Wake et al, 1994; Kreutz and Sholkovitz, 2000, Pruett et al., 2004) and that the prevailing synoptic meteorological conditions favor atmospheric transport to the Inilchek region (Claquin et al., 1999, Aizen et al., 1997) (Figure 2.1). Kreutz and Sholkovitz (2000) suggest that during the summer months the transport of dust from the west to east associated with the Northern Hemisphere jet stream is typically higher resulting in increased deposition of Ca^{2+} and SO_4^{2-}. The data here show increased inputs of both species during early summer and then again in the winter months. The summer increase is likely caused by an increase in atmospheric convective transport (Doscher et al., 1996, Kreutz and Sholkovitz, 2000). The cause of the increase observed in winter is unknown but may be due to changes in the local- to regional-scale atmospheric circulation (Kreutz and Sholkovitz, 2000) in conjunction with increased energy use.

The other primary source contributing to the Inilchek snowpit chemistry records is of anthropogenic origin. Based on the prevailing wind directions, anthropogenic contributions are likely coming from both the former Soviet Union and China (Figure 2.1) (Kreutz and Sholkovitz, 2000; Pruett et al., 2004). The variability in the $\delta^{34}S$ data allows for the examination of the "background" conditions and an understanding of the changes in the contributions from the two sources under these conditions through time. The $\delta^{34}S$ (Figure 6.8.h) and sulfate concentration (Figure 6.8.g) data from this study show that a poor correlation ($r^2 = 0.027$) exists between the two. A study by Pruett et al. (2004), however, found a significant positive correlation ($r = 0.87$) between $\delta^{34}S$ and

sulfate concentration (Pruett et al., 2004) for a snowpit collected from the Inilchek in 1999, however, the regression is dominated largely by one high dust value (represented by a high sulfate concentration). Regression of only the low concentration samples yields a poor correlation as observed in this study (Kreutz, personal communication) suggesting these samples are representative of "baseline" conditions. Ignoring the high dust value, the $\delta^{34}S$ values for the 1999 Inilchek snowpit were typically < 10‰ (ranging from approximately 1 to 10‰), which is similar to the range found in this study and is similar to the one value with low sulfate concentration and low $\delta^{34}S$ value (+ 5.4‰) found in a firn core from the Tien Shan in 1998, which was attributed to anthropogenic sources. This suggests that under "baseline" conditions, anthropogenic sources tend to dominate.

The mass balance results show the Inilchek region is in fact strongly impacted by anthropogenic inputs with an average of 71 % of the total sulfate being contributed from this source throughout most of the year. In addition, anthropogenic contribution to the total sulfate concentration dominates no matter whether the overall total sulfate deposition is high or low. The total sulfate deposition, like most of the major ions, appears to be higher in the late spring/early summer and winter months and lower in early spring showing a potentially weak seasonal trend. Although the specific transport strength is not well established the observed variability is likely caused by changes in the local- to regional-scale atmospheric circulation in the region as suggested by Kreutz and Sholkovitz (2000).

6.2 Summit

The samples obtained from Summit were analyzed after the Inilchek samples

because the mass per unit volume (and time) was lower. Because of the lower sulfate concentration and exposure to anthropogenic emissions, the Summit site presented an attractive challenge for the newly-developed double spike technique.

6.2.1 Results

6.2.1.a Dating Results

The dating technique used to date the Greenland snowpit is discussed in Shuman et al. (1995, 1998) and is based on that described in Chapter 3 Section 3.3. Briefly, the technique relies on the relationship of the stable isotope depth series (δD) to surface temperature at a site. The δD record is a proxy for the surface temperature record assuming accumulation occurs throughout the year, which is the case at Summit. Comparison is made between the proxy temperature δD record and the actual surface temperature record obtained from an automatic weather station (AWS) located approximately 1 km from the field site using a qualitative point-pairing technique that is directed by the maxima, minima, and inflections in the shape of the profiles. Figure 6.9.a shows the surface temperature versus time and Figure 6.9.b shows the δD stable isotope versus depth. The tie lines between the two curves link the depth profile with the time profile. The surface temperature for the snowpit ranged from 224°K to 263°K, with the warmer temperatures, typically above 250°K, occurring in the summer months (May through September), and the cooler temperatures, typically below 240°K, occurring in the winter months (November to March). δD values in the snowpit ranged from –319‰ to –176‰ (Figure 6.9.b) and fall within the δD range, -350‰ to –200‰, for the Summit site previously determined by Shuman et al.(1995). δD values in the summer months are generally above -230‰ and in the winter months below –250‰. In Figure 6.10 the tie

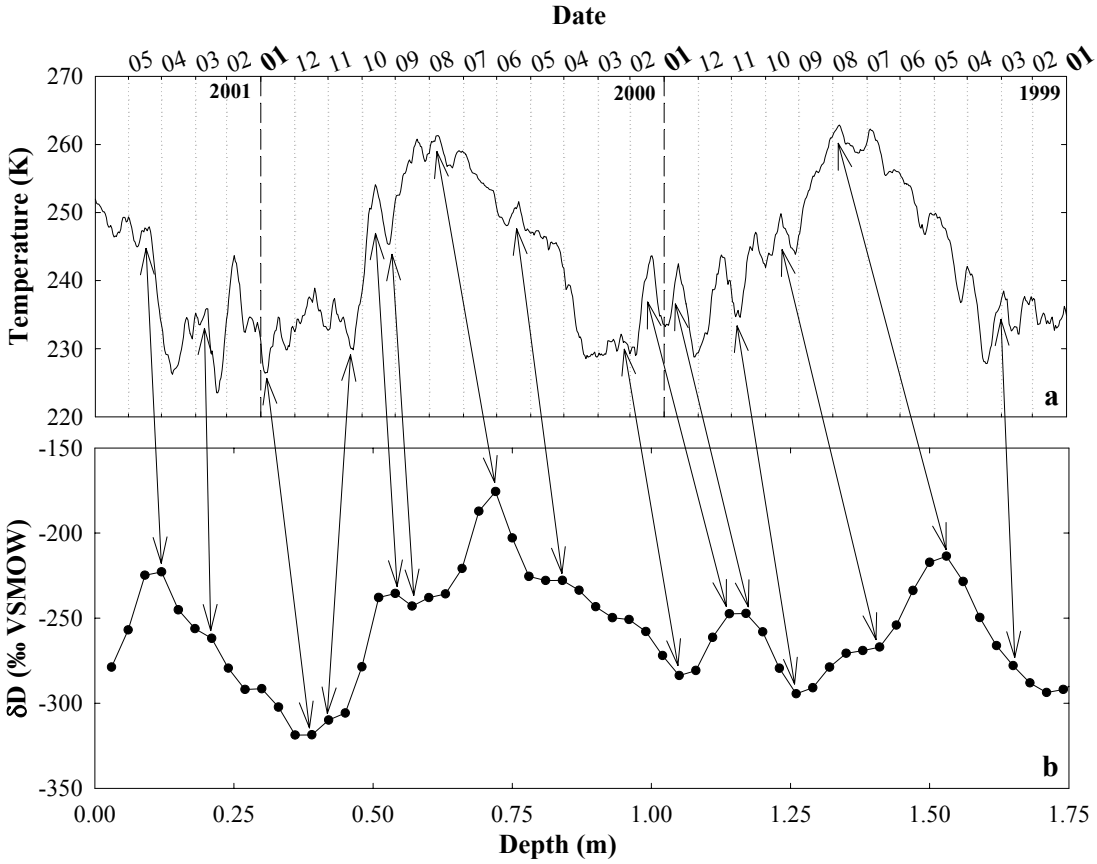

Figure 6.9. The composite temperature record (14 day Average) from the automatic weather station (AWS) located approximately 1 km from the snowpit collection site (72.58°N, 38.50°W) (a) and the δD record used to link the depth profile with time (b) for the Greenland snowpit. The tie lines connect the maxima, minima, and points of inflection between the two curves linking depth with time. Negative δD values indicate cooler temperatures and positive values indicate warmer temperatures. Surface of the snowpit is to the left at 0 m which marks the date the snowpit was dug (May 7-8, 2001). Uncertainties for the δD and temperature measurements were ± 0.3‰ (1σ) and ± 2°K (1σ).

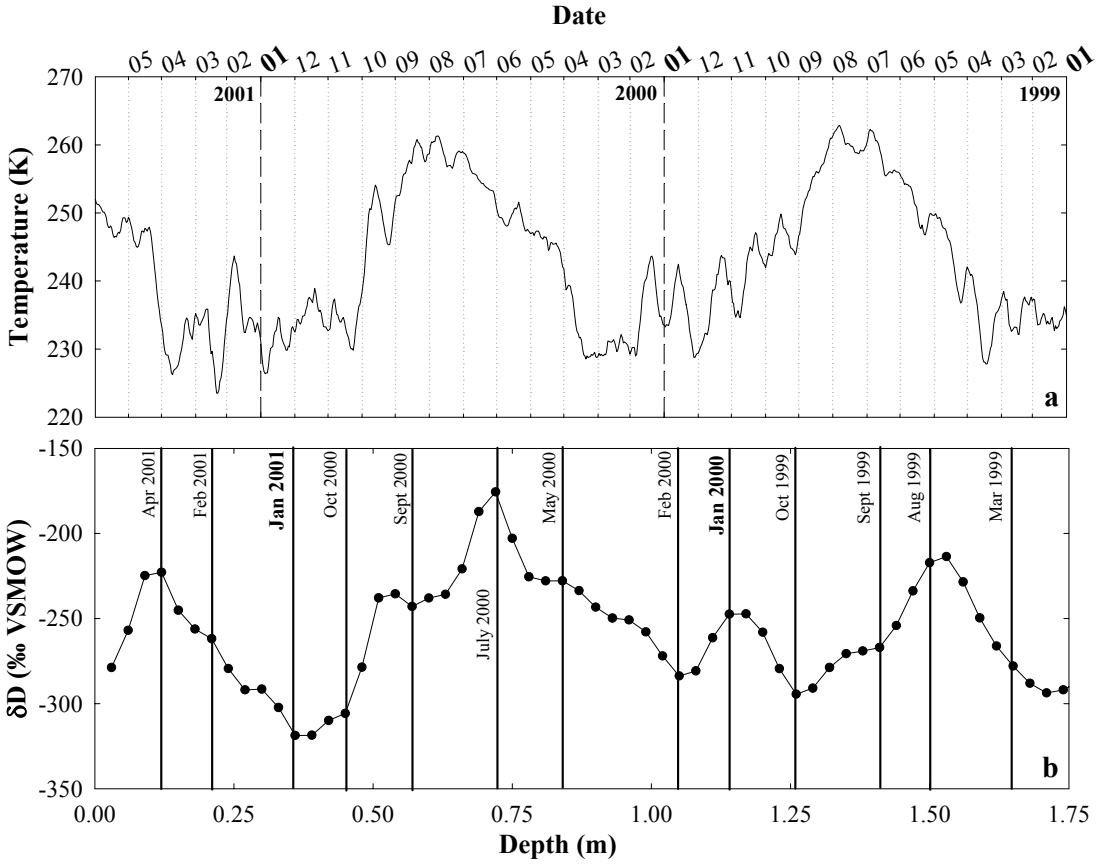

Figure 6.10. The composite temperature record (14 day Average) from the automatic weather station (AWS) (72.58°N, 38.50°W) (a) and the δD record used to link the depth profile with time (b) for the Greenland snowpit. The tie lines have been removed and replaced with solid vertical lines to highlight time in (b) for the Greenland snowpit. Surface of the snowpit is to the left at 0 m which marks the date the snowpit was dug (May 7-8, 2001). Uncertainties for the δD and temperature measurements were ± 0.3 ‰ (1σ) and ± 2°K (1σ).

lines between the two records have been replaced with vertical solid lines highlighting time in Figure 6.10.b. Based on the clear seasonal trend in both records, the snowpit extends back approximately 21 months representing a continuous $\delta^{34}S$ record from mid-August 1999 to the beginning of May 2001. Each sample represents approximately 1.5 months. The uncertainty in the dates is approximately ± 2 weeks.

6.2.1.b Major Ion Results

All the major ion species measured in the Greenland snowpit were the same as those measured in the Inilchek snowpit except, instead of NH_4^+, methane sulphonate (a derivative of MSA) was measured. The concentration data for the snowpit are presented in Figure 6.11 (refer to Appendix C for details) with the mean concentrations and 2σ uncertainties reported in Table 6.3. In general, all the major ion species show seasonal trends that are typical for the region. Both Na^+, with concentrations ranging from 0.01 to 0.89 μmoles L^{-1}, and Mg^{2+}, with concentrations ranging from 0 to 0.16 μmoles L^{-1}, peak in concentration from Feburary to April of 2000 and then again from March to April in 2001. Potassium concentrations, which range from 0 to 0.12 μmoles L^{-1}, tend to have a similar profile to that of Mg^{2+} but with baseline concentrations being slightly higher. The Ca^{2+} concentrations, which range from 0 to 0.88 μmoles L^{-1}, peak

Table 6.3. Mean concentrations of the major ionic species for the Greenland snowpit.

Na^+	K^+	Mg^{2+}	Ca^{2+}	Cl^-	NO_3^-	SO_4^{2-}	MS
0.23 ± 0.26	0.03 ± 0.02	0.01 ± 0.06	0.13 ± 0.34	0.48 ± 0.28	1.91 ± 3.10	0.43 ± 0.46	0.02 ± 0.04

All concentrations are in μmoles l^{-1}. Uncertainties reported are 2σ.

in April/May of 2000 and 2001, at approximately the same time as Na^+ and Mg^{2+}. The Cl^- concentrations ranged from 0.32 to 1.00 μmoles L^{-1} and peak in April of both 2000

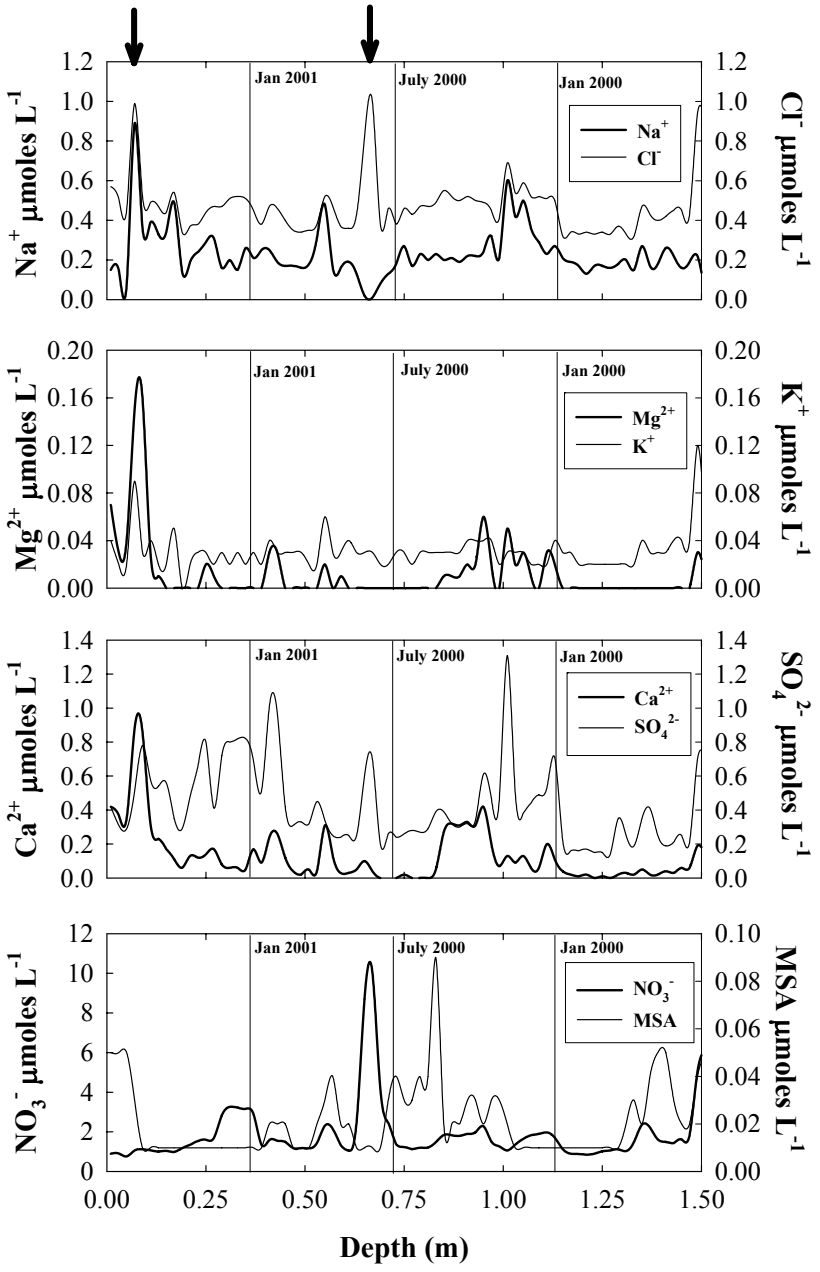

Figure 6.11. Major ion concentration data for all soluble species measured in the Greenland snowpit. The surface of the pit is to the left at 0 m. The vertical lines highlight time for each profile. The first solid black arrow highlights the cation peak while the second highlights the anion peak. The total sulfate concentration is shown here. Refer to Appendix C for measurement details. Uncertainties for all ions are ± 5% (1σ).

and 2001. An additional peak was observed in the summer of 2000. Nitrate concentrations ranged from 0.76 to 10.05 μmoles L^{-1} and show a clear peak in concentration during the summer (August) of 2000. Methane sulphonate shows a peak in the spring (April to May in 2000 and 2001) similar to NO_3^- but an additional peak also occurs in the summer (July to August in 2000). A broad minimum in concentration occurs from November to February 1999/2000 and 2000/2001. The concentrations ranged from 0.01 to 0.09 μmoles L^{-1}. Finally, the SO_4^{2-} concentration ranged from 0.14 to 1.31 μmoles L^{-1}, with peaks in concentration generally occurring from February to April/May of 2000 and then again from January through May of 2001. There is a distinct peak exhibited by all the anions (Cl^-, NO_3^-, and SO_4^{2-}) in August of 2000 and another distinct peak is exhibited by the cations (Na^+, Mg^{2+}, and Ca^{2+}) in April of 2001.

Hg concentrations in Arctic snow, like the ions above, have demonstrated strong seasonality with the concentrations peaking just after polar sunrise and progressively declining to negligible concentrations in the winter (Lindberg et al., 2001, 2002; Mann et al., in press). Based on this observation, it was expected that the Hg(II) concentrations should peak starting in March/April, when polar sunrise occurs for this site, and after the

winter peak observed in the nss-SO_4^{2-} concentrations. Figure 6.12 shows the nss-SO_4^{2-}concentrations of the snowpit samples taken for the present study and the total Hg mercury concentrations of samples taken from a firn core less than two meters away with the δD snowpit record. The concentrations for the nss-SO_4^{2-} ranged from 0.16 ± 0.09 to 0.92 ± 0.06 μmoles L^{-1}, and peak concentrations were observed in March to April of 2000 and again in January to February of 2001. The ranges in uncertainties, expressed as an expanded 95% confidence interval, were 0.01 to 0.09 μmoles L^{-1}. The Hg

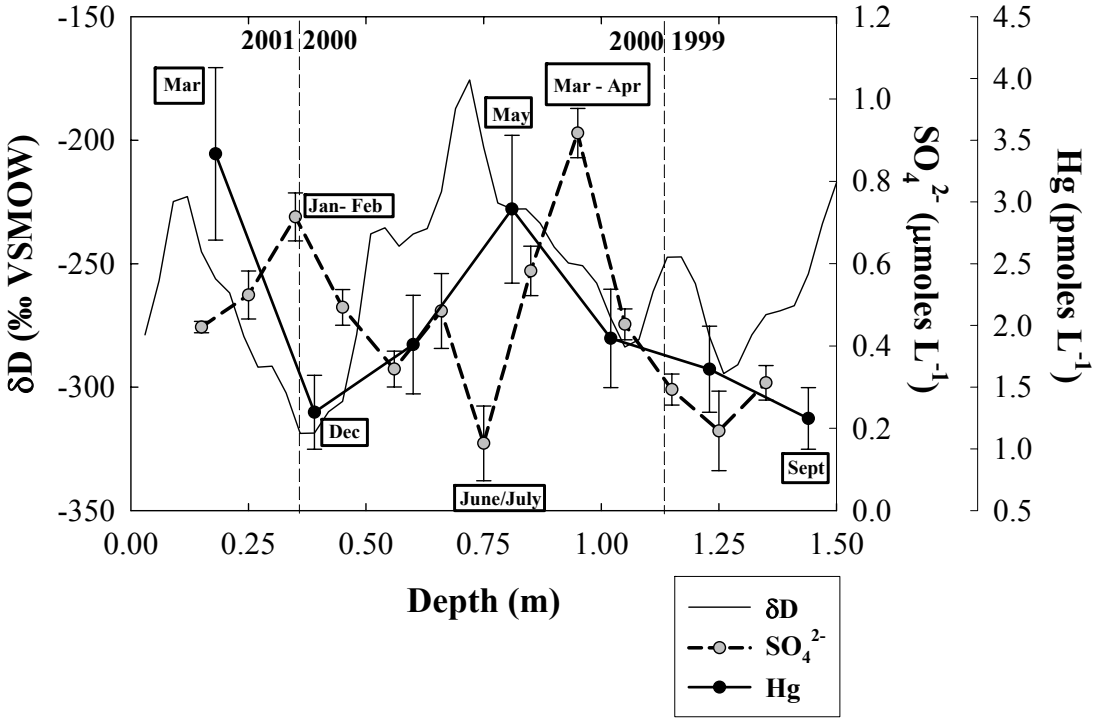

Figure 6.12. Nss-SO_4^{2-} and total Hg concentrations with the δD record for the Greenland snowpit. Surface of the snowpit is to the left at 0 m. Extreme concentrations are identified by boxes containing dates. The uncertainties for the concentration measurements are expressed as an expanded 95% confidence interval (GUM, 1994). The uncertainty for the δD is ± 0.3‰ (1σ).

concentrations range from 1.2 ± 0. 2 to 3.4 ± 0. 7 pmoles L^{-1} (95% confidence level) (Mann et al., in press) and peak just after nss-SO_4^{2-} in May of 2000 and March of 2001.

Similar to Hg, MSA concentrations also exhibit strong seasonality with peaks in concentration typically occurring in the spring months just after nss-SO_4^{2-} concentrations peak (Li and Barrie, 1993; Hopke et al., 1995). Figure 6.13 shows the nss-SO_4^{2-} concentration and the MSA concentration with the δD record. The MSA concentrations ranged from 0.01 to 0.09 μmoles L^{-1} peaking in May of 2000 and April/May of 2001. Minimum in concentrations occurred from October to February of 1999 to 2000 and again from December to March 2000 to 2001.

6.2.1.c $\delta^{34}S$ and Sulfate Concentration Results

The relative proportions of the major sources of sulfate-sulfur, anthropogenic and natural (sea salt, marine biogenic, and dust), being contributed to the Summit site were identified, like the Inilchek, by using the stable sulfur isotope data. $\delta^{34}S_{nss}$ values (solid triangles) and the corresponding sulfate concentration data (grey circles) in time (depth) series for the samples collected are shown in Figure 6.14. All concentration and $\delta^{34}S$ results are reported in Appendix C. The amount of meltwater used for sulfur isotope analysis in this portion of the study ranged from 209 to 307 mL, and averaged 272 mL, which is considerably less then the 1 to 2.5 L used by Patris et al. (2002) for analysis of samples from this region. In this case we were able to obtain higher-resolution data, approximately 9 analyses per year with each analysis representing approximately 1.5 months. Patris et al. (2002) samples represented anywhere from 3 to 8 years of time. The concentrations for the nss-SO_4^{2-} were reported above and again ranged from 0.16 ± 0.09 to 0.92 ± 0.06 μmoles L^{-1} (95% C. I.). This is an order of magnitude smaller than

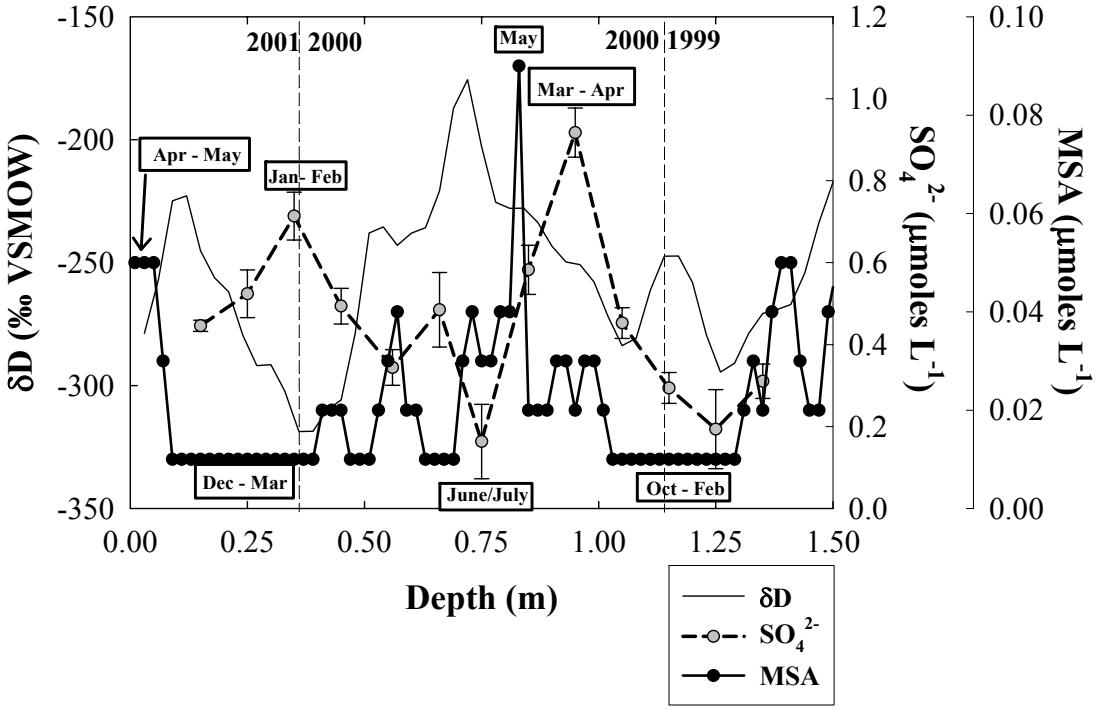

Figure 6.13. Nss-SO_4^{2-} and MSA concentrations with the δD record for the Greenland snowpit. Surface of the snowpit is to the left at 0 m. Dates in boxes highlight concentration extremes. The uncertainties for the Nss-SO_4^{2-} concentration measurements are expressed as an expanded 95% confidence interval (GUM, 1994) and for the MSA are ± 5% (1σ). The uncertainty for the δD is ± 0.3‰ (1σ).

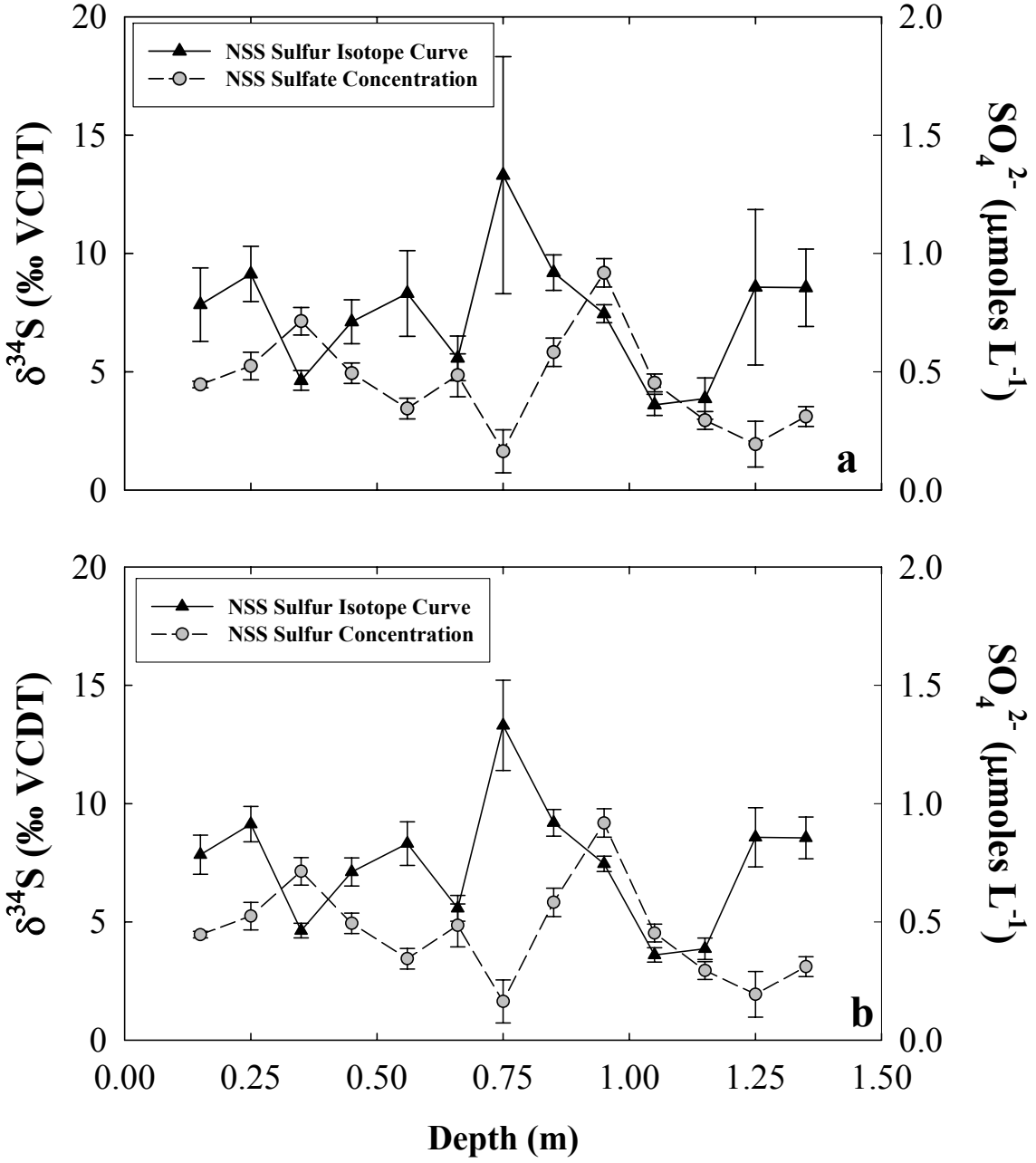

Figure 6.14. $\delta^{34}S_{nss}$ values and corresponding nss-SO_4^{2-} concentration data in time (depth) series for the Greenland snowpit. The $\delta^{34}S_{nss}$ values with the actual uncertainties obtained are in (a) while the uncertainties shown in (b) are estimates using a lower blank concentration. All uncertainties are 2σ.

the concentrations observed for the Inilchek samples. The $\delta^{34}S_{nss}$ values shown in Figure 6.14.a range from 3.6 ± 0.45‰ (2σ) to 13.3 ± 5.01‰ (2σ) and average 7.5‰. The range in 2σ for the individual $\delta^{34}S$ measurements was 0.38‰ to 5.01‰ for sample sizes ranging from 0.05 to 0.29 μmoles S. The $\delta^{34}S$ measurement precision for this sample set was the same as that used for the Inilchek samples at 0.22‰ (1σ), and was based on the pooled standard deviation of duplicate sample measurements (n = 5). This value was used because for duplicate measurements on the Greenland samples there was not enough sample available. Moreover, because the signal intensities at mass ^{109}S, the fundamental limitation to measurement precision, were similar in range (8 to 66 mV) to that of the Inilchek (6 to 72 mV) we would expect the measurement precisions to be similar. The blank composition determined using Eqn. 4.8 was -0.40 ± 0.17‰ (1σ). The uncertainty was approximately a factor of two worse then the uncertainty determined for the blank composition used for correction of the Inilchek samples, yet the uncertainty is still relatively small.

The uncertainties (ranging from 0.38‰ to 5.01‰ (2σ)) determined were quite large for this sample set relative to those determined for the Inilchek samples (0.10‰ to 0.12‰ (2σ)) and only the extreme $\delta^{34}S_{nss}$ values are distinguishable from one another (Figure 6.14.a). These large uncertainties were because of the increased blank concentration and the smaller sample size used for analysis in this portion of the study. The open circles in Figure 6.15 show that as sample size decreases the precisions (2σ) degrade considerably, particularly below 0.15 μmoles S. The average blank concentration for this portion of the study was 0.017 ± 0.0063 μmoles S (1σ), which is just under an order of magnitude larger then the average blank concentration obtained for

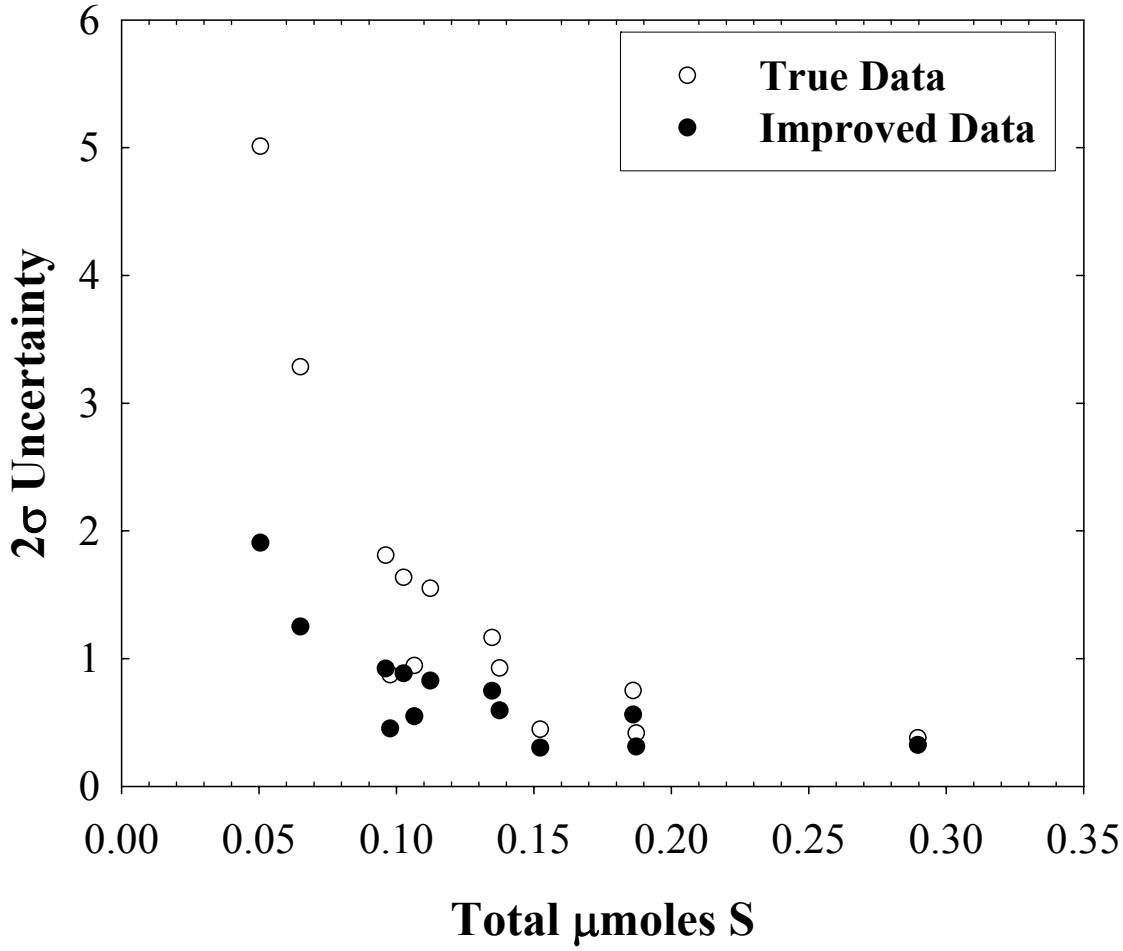

Figure 6.15. Total sample size used for analysis with the resulting 2σ uncertainty for the Greenland samples. The open circles are for the actual uncertainties obtained and the closed circles are for the uncertainties obtained using a lower blank concentration.

the Inilchek Glacier samples (0.0028 ± 0.00079 μmoles S (1σ), 0.0032 ± 0.0026 μmoles S (1σ)). Although the exact cause of this increase has not been determined it is likely owing to the change in argon gas suppliers at NIST. Argon gas was used in the dry down step to sweep out moisture, to keep the samples under an inert atmosphere, and limit exposure to oxygen. An increase in the blank concentrations occurred when the supply of argon was changed from Roberts Oxygen to Airgas. It is important to note that the $\delta^{34}S$ measurement precisions after correction for instrumental fractionation, but prior to blank correction, ranged from 0.32‰ to 1.20‰ (2σ), which are better than the precisions obtained after the samples have been corrected for blank (0.38‰ to 5.01‰ (2σ)). This demonstrates that the degradation of the precision on the individual measurements was caused by the increase in blank concentration combined with the smaller sample sizes used for analysis and does not result from a decrease in instrumental measurement precision.

The blanks determined during the measurement of the Greenland samples are not representative of the typical blank normally achieved using this technique. This is demonstrated by the lower blank measured for both the standards as well as the Inilchek samples. As a consequence, an estimate of what precisions are obtainable using this technique for the Greenland samples are shown in Figure 6.14.b. The $\delta^{34}S_{nss}$ values (solid triangles) and corresponding 2σ uncertainties were determined using the procedural blank (0.0032 ± 0.0026 μmoles S (1σ)) and blank composition uncertainty (0.06‰ (1σ)) determined for the Inilchek Glacier samples in Eqn 4.7. The resulting uncertainties in this case ranged from 0.30‰ to 1.91‰ (2σ), with the largest uncertainty corresponding to the sample of smallest size 0.06 μmoles S. The uncertainties

determined here are in some cases almost a factor of three better than those previously determined. The closed circles in Figure 6.15 show the improvement in the precision of the data for the various samples sizes used for analysis. The improvement in precision observed demonstrates that if the blank were lowered and the uncertainty in the blank composition were small, then most of the $\delta^{34}S_{nss}$ values would be distinguishable and significant from one another (Figure 6.14.b).

Examination of the $\delta^{34}S_{nss}$ values and the nss-SO_4^{2-} in Figures 6.14.a and 6.14.b appear to show poor correlation ($r^2 = 0.11$) similar to the Inilchek data. A strong seasonal trend in the $\delta^{34}S_{nss}$ values, however, does appear to exist as shown in Figures 6.16.a and 6.16.b, where the $\delta^{34}S_{nss}$ values are shown with the δD curve. The $\delta^{34}S_{nss}$ data in 6.16.a show the true uncertainties and 6.16.b show the improved uncertainties. Lower $\delta^{34}S_{nss}$ values (3.6‰, 3.9‰, and 4.6‰) occur in the winter months (January to February) while the higher $\delta^{34}S_{nss}$ values (13.3‰) occur in the summer months (June-July). The remaining $\delta^{34}S_{nss}$ values (5.6‰ to 9.2‰) lie between the two extremes.

6.2.1.d Mass Balance Results

To determine the relative seasonal importance of the source contributors, anthropogenic and natural, and the proportions of each contributing to the deposited sulfate at this site a three-component mixing model was used. In this case the measured isotopic composition was resolved using Eqn. 4.12 ($\delta_{measured} = f_{ss}\delta_{ss} + f_{nss}\delta_{nss} = f_{mb}\delta_{mb} + f_a\delta_a + f_d\delta_d$) where $\delta_{measured}$ is the measured $\delta^{34}S$ of the sample, δ_{ss}, δ_{nss}, δ_{mb}, δ_a, δ_d are the isotopic signatures of the sea salt, non-sea-salt, marine biogenic, anthropogenic, and dust components and f_{ss}, f_{nss}, f_{mb}, f_a, and f_d are the corresponding mass fractions. The relative contributions were determined using the $\delta^{34}S$ values from the literature. The $\delta^{34}S$ value

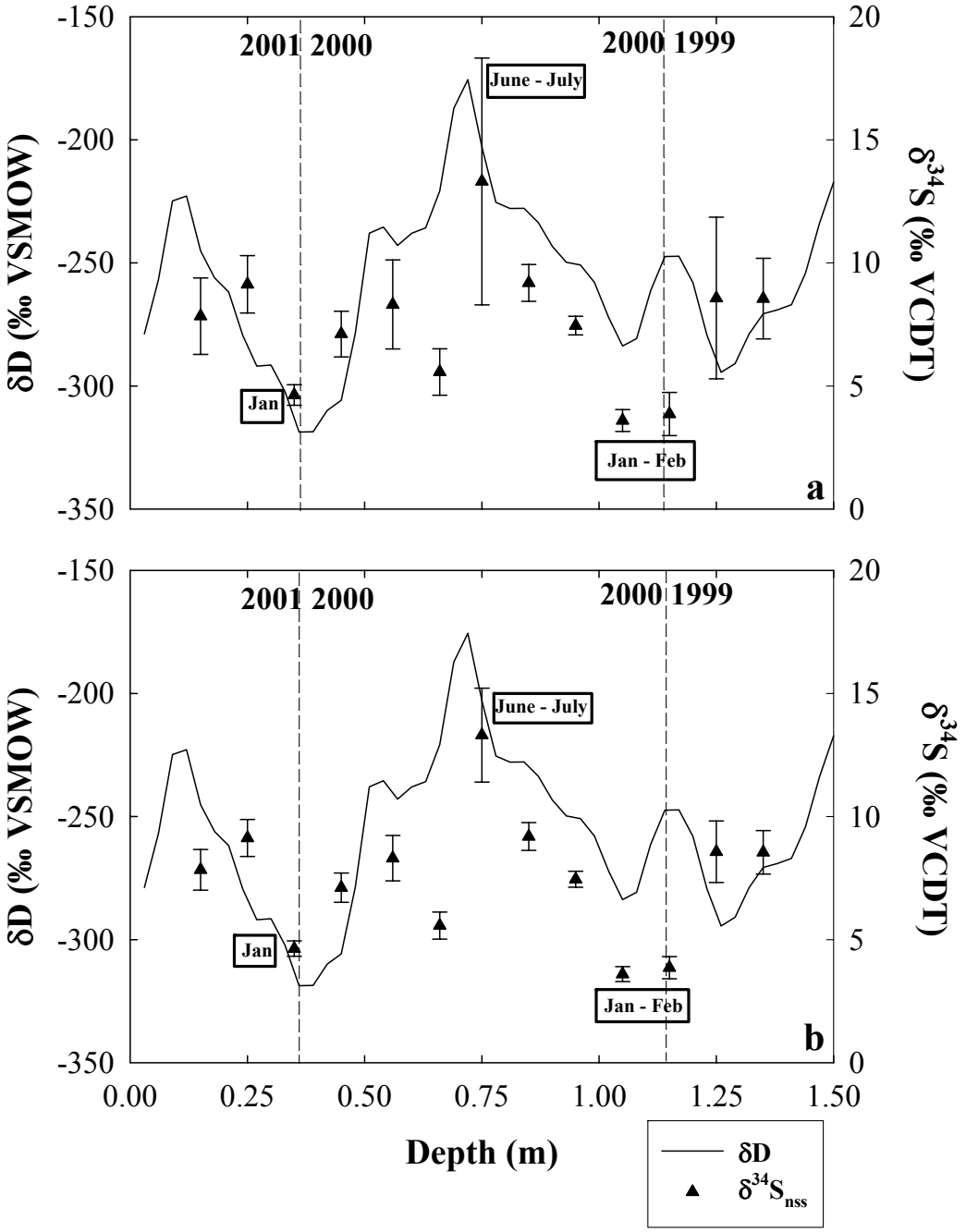

Figure 6.16. $\delta^{34}S_{nss}$ values shown with the δD curve for the Greenland snowpit. The $\delta^{34}S_{nss}$ values with the actual uncertainties obtained are in (a) while the uncertainties shown in (b) are estimates using a lower blank concentration. Dates in the boxes highlight extremes in $\delta^{34}S_{nss}$ values. All uncertainties are 2σ.

used for the sea salt component was +21 ± 0.2‰ (Rees et al., 1978). For the marine biogenic component the value used was +18.6 ± 0.9‰ (Patris et al., 2002; Calhoun et al., 1991) and for the anthropogenic component the $\delta^{34}S$ value used was +3 ± 1.5‰ (Patris et. al., 2002). The $\delta^{34}S$ value used for the dust component was determined using the model of Patris et al., 2002, where the isotopic value and the uncertainty are determined assuming the extreme case, where the $\delta^{34}S$ value is 20‰ apart from the remaining $\delta^{34}S_{nss}$ ($f_{mb}\delta_{mb} + f_a\delta_a$). Thus, for example, if the measured contribution of dust to a sample is 2% this would be multiplied by 20 ± 20‰, assuming the extreme case, to yield 0.4 ± 0.4‰.

A sensitivity analysis was performed using the uncertainties of the input parameters (δ_{nss}, δ_{mb}, δ_a, δ_d) to the mass balance equation, to identify the component contributing the largest portion of uncertainty to the relative contribution estimates. It was determined that the uncertainty on the anthropogenic composition, +1.5‰ (1σ), and the uncertainties on the δ_{nss} (ranging from 0.19‰ to 2.5‰ (1σ)) contributed approximately ± 14% and ± 5%, respectively, to the relative contribution estimates. The uncertainties contributed from the marine biogenic (δ_{mb}), with an uncertainty of ± 0.9‰ (1σ), and the dust component (δ_d), with a range of uncertainties from ± 0.08 to 0.57‰ (1σ), to the relative contribution calculations was < 2% for both. In this case the uncertainty coming from the experimental error on δ_{nss}, ± 5%, is larger than the uncertainty from this component for the Inilchek samples (0.53%), which is expected because of the degraded precisions obtained due to the blank problems in this portion of the study. Although this is the case, the uncertainty contributed to the relative contribution calculations by the anthropogenic component is still larger at ± 14%.

The relative contributions of each component (sea salt (black bar), marine biogenic (light gray bar with diagonal lines), anthropogenic (darker grey bar with diagonal lines), and dust (light grey bar with cross hatch)) and the estimated contribution of each to the total sulfate concentration of each sample calculated by the procedure above are shown in Figures 6.17 and 6.18, respectively. Similar to the Inilchek samples, the contribution of sulfate from anthropogenic sources dominates the snowpack throughout most of time period represented by the snowpit (mid 1999 to May 2001) with the exception of during the summer months in 2000, June and July, when the marine biogenic contribution to the total sulfate was larger. On average 74% of the sulfate being contributed to Summit over the time covered by the snowpit, was from anthropogenic sources while 3.4% was from sea salt, 24% was from marine biogenic sources, and < 2% was from dust sources. The lower $\delta^{34}S_{nss}$ values (marked by back slashes in Figures 6.17 and 6.18) (3.6‰, 3.9‰, and 4.6‰) that were measured during the winter months show that almost 100% of the sulfate is from anthropogenic sources and the range was from 92% to 103%. The ^{34}S-enriched $\delta^{34}S_{nss}$ value observed in June/July of 2000 (marked by horizontal slashes in Figures 6.17 and 6.18) is associated with a larger input, 60%, of marine biogenic sulfate with a heavier $\delta^{34}S_{nss}$ value. The contribution from anthropogenic sources was only 38% at this time. The remaining $\delta^{34}S_{nss}$ values that lie between these two extremes (marked by open boxes in Figures 6.17 and 6.18) show that the marine biogenic contribution is more significant then during the winter months and less significant than in the summer months. In addition, the total sulfate deposited in the winter and spring months is typically larger (marked by stars in Figure 6.18) than during the summer and fall months. and the August 3rd event slightly less (12%). Again it is

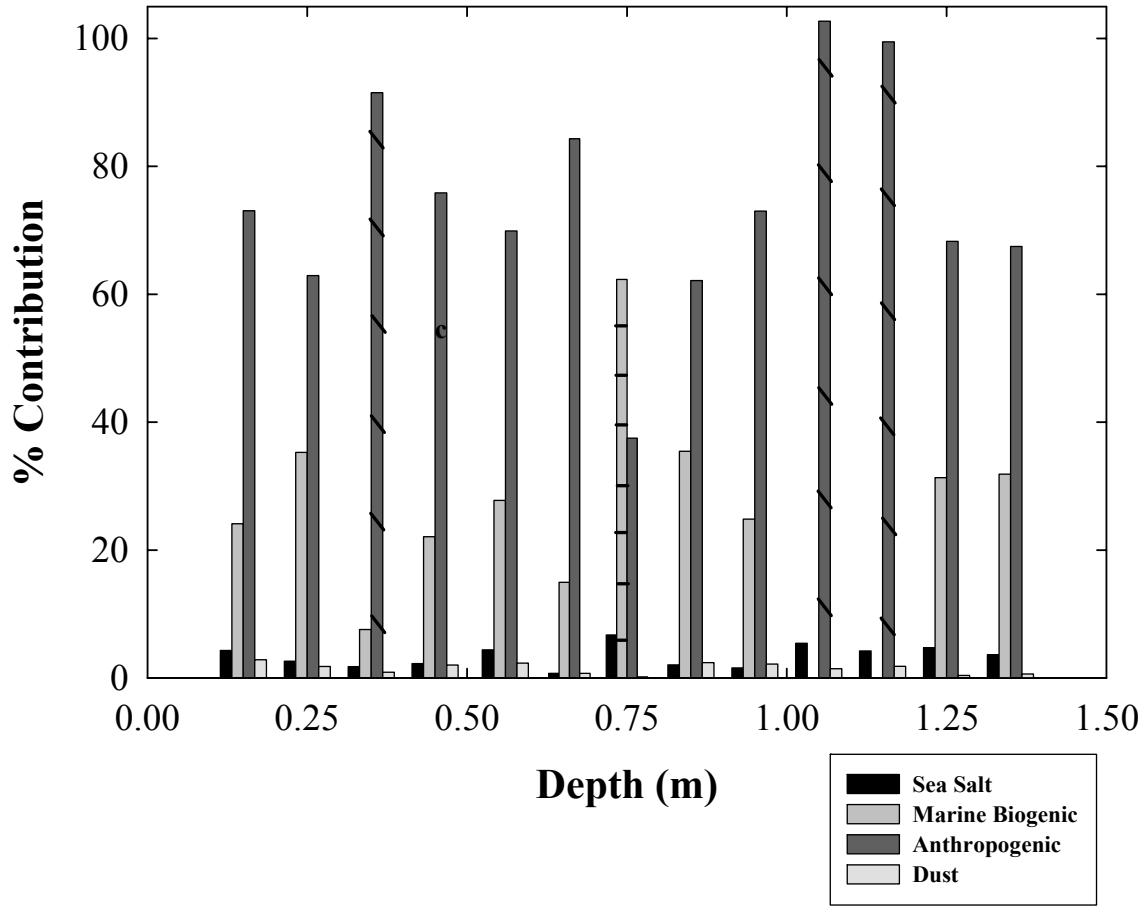

Figure 6.17. Relative contributions in percent for each sulfate source contributor for the Greenland snowpit samples: sea salt, marine biogenic, anthropogenic, and dust. The back slashes mark samples with the lowest $\delta^{34}S_{nss}$ values, the horizontal slashes mark the sample with the highest observed $\delta^{34}S_{nss}$ value , and the open boxes marks samples with $\delta^{34}S_{nss}$ values that lie between the lowest and highest values.

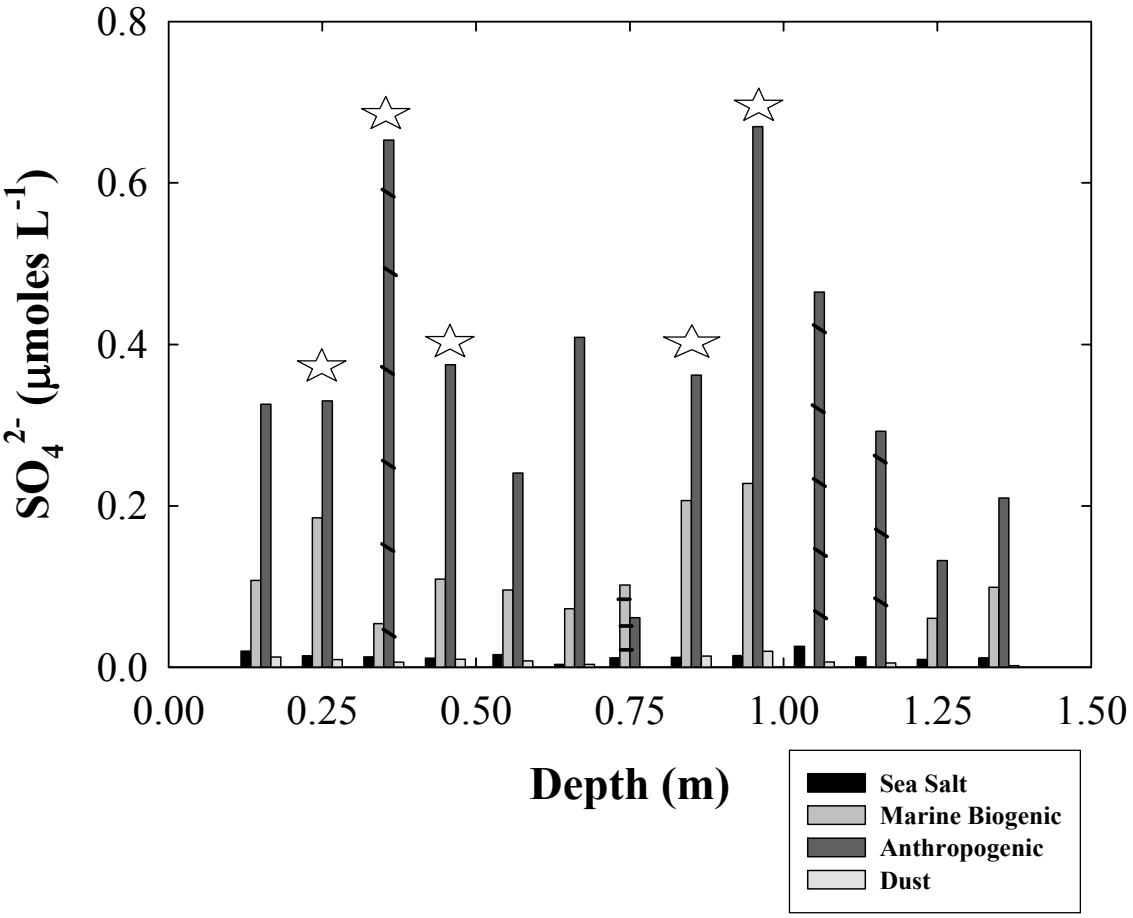

Figure 6.18. Estimated contribution to the total sulfate for each source contributor for the Greenland samples: sea salt, marine biogenic, anthropogenic, and dust. Again, the back slashes mark the lowest $\delta^{34}S_{nss}$ values, the horizontal slashes mark the highest observed $\delta^{34}S_{nss}$ value, and the open boxes mark the $\delta^{34}S_{nss}$ values that lie between the lowest and highest values. The stars mark the samples with the highest total sulfate concentrations.

important to note that because of the uncertainty on the calculated relative contributions (14%), the results need to be considered carefully. In this case, although better characterization of the isotope composition of the anthropogenic fraction would reduce the uncertainty; the uncertainty reported does not change the findings observed in this study, unlike that for the Inilchek samples.

6.2.2 Discussion

The δD and temperature data, the major ion data, and the $\delta^{34}S$ data are all shown versus depth and time in Figure 6.19 to provide a summary of the data results. The major ion species show seasonal trends that are similar to those that have been previously identified for this region. Sodium (Figure 6.19.b) and magnesium (Figure 6.19.c) concentrations, which peak from Feburary to April of 2000 and then again from March to April of 2001, exhibit a trend similar to that identified by Li and Barrie (1993) and Toom-Sauntry and Barrie (2002) in atmospheric filter and snow samples from Alert, Canada (located on Ellesmere Island). Calcium (Figure 6.19.d) concentrations, which peak twice, once in April/May of 2000 and then again at the same time in 2001, and at approximately the same time as Na^+ and Mg^{2+}, were also seen to peak at a similar time at Alert by Toom-Sauntry and Barrie (2002) and by Colin et al. (1997) for snowpit samples collected from Dye 3 in Greenland (southwest of Summit site at 65.11°N and 43.5°W). At the Alert site Toom-Sauntry and Barrie (2002) found Cl^- to peak in December to 3 February while ice core samples collected by Finkel et al. (1986) showed Cl^- to be highly variable only periodically showing peaks in concentration in the winter at the Dye location. The Cl^- (Figure 6.19.b) concentrations in this study, peaked in April of both 2000 and 2001. An additional peak was observed in the summer of 2000 demonstrating

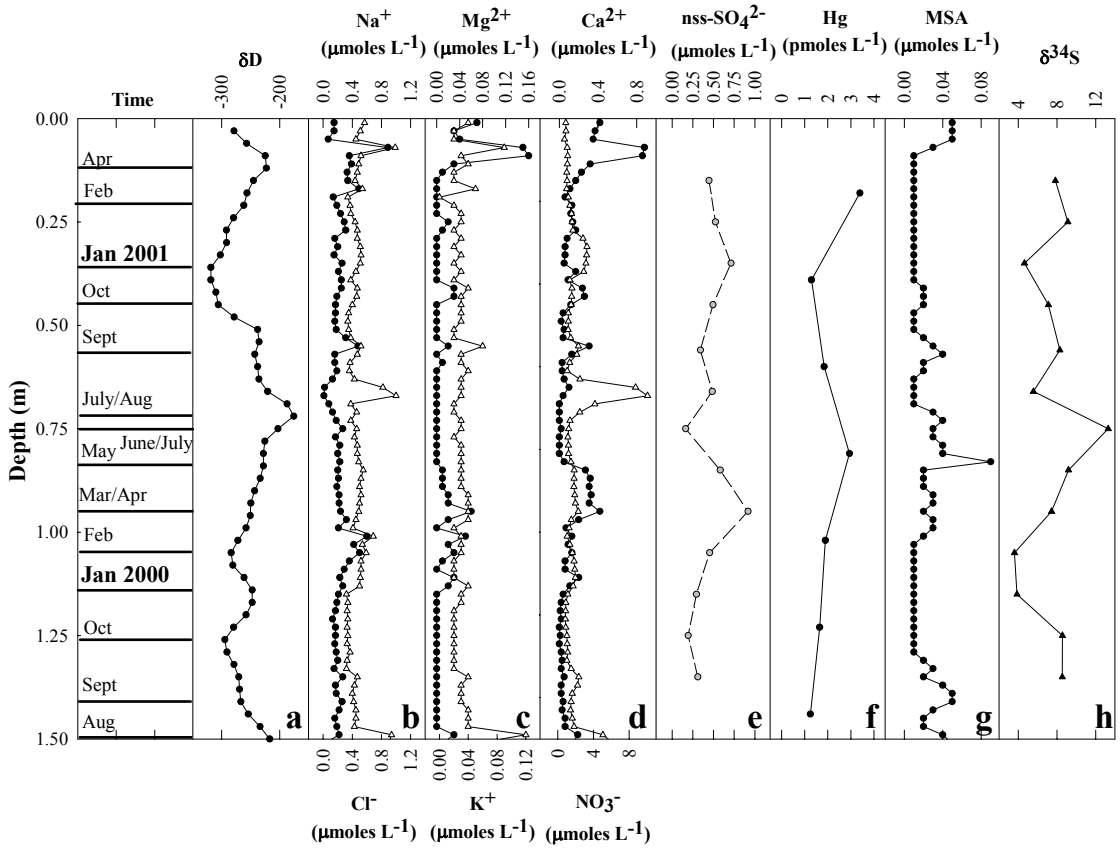

Figure 6.19.a-h. Summary figure of all the data results for the Summit snowpit including δD (a), major ion (b-g), and the $\delta^{34}S$ (h), are shown versus depth and time. The open triangles (c-g) refer to the elements listed along the bottom of the graph.

the variability observed by Finkel et al. (1986). Like that observed by Toom-Sauntry and Barrie (2002), Fischer et al. (1998), and Finkel et al. (1986) in atmospheric filter samples from Alert, Canada and in firn core and snowpit samples from Greenland, nitrate (Figure 6.19.d) concentrations showed a clear peak in concentration during the summer months (August). A spring peak in methane sulphonate ((Figure 6.19.g) (April to May in 2000 and 2001) was observed in addition to a peak in the summer (July to August in 2000). Li and Barrie (1993), Li et al. (1993), and Colin et al. (1997) found the same seasonal trend for methane sulphonate in atmospheric filter samples and in snowpit samples from Alert, Canada and Summit, Greenland. Finally, the seasonal SO_4^{2-} (Figure 6.19.e) concentration variations, with peaks in concentration generally occurring in the winter to early spring months of both 2000 and 2001, are typical of the seasonal trend observed by Finkel et al. (1986), Colin et al. (1997), Li and Barrie (1993), Fischer et al. (1998) (shallow firn core), and Norman et al. (1999) for these high latitude locations. The similarity between the seasonality observed at Summit and of that observed at the Dye 3 site suggests that the two sites may be impacted by the same air masses and with similar timing (Mayewski et al., 1990). In addition, the large anion peak in August of 2000 may be attributed to a large storm event that brought in a larger proportion of sea salt to the region, while the large cation peak in April 2001 may be associated with an increase in dust contribution. Mass balance results used to determine whether the cause of this peak was increased dust input was not possible because this sample was lost. In general, peaks in cation concentration occur in the spring months of both 2000 and 2001 and are likely associated with inputs from the Taklimakam desert in China (Bory et al., 2003). The timing of the peaks correspond with the most active period for dust storms in eastern

Asia. During the spring months, cold air outbreaks from Siberia cause cold fronts and cyclonic activity that lift large amounts of lithogenic material to high altitudes (up to 8000 m) to be transported north into the westerlies towards the Pacific (Sun et al., 2001) and to Greenland (Barrie, 1995; Bory et al., 2003) (Figure 2.1). It is important to note that the overall dust contribution is quite small (< 5%) and that the main sources of nss-SO_4^{2-} to this region are anthropogenic and marine biogenic.

Similar to the major cation data, the nss-SO_4^{2-} (Figure 6.19.e), Hg (Figure 6.19.f), and MSA (Figure 6.19.g) concentrations also exhibit strong seasonality, with nss-SO_4^{2-} concentrations peaking just prior to Hg and MSA. The seasonal trend in the nss-SO_4^{2-} was not observed in samples from the Arctic until the commencement of industrial activity (Finkel et al., 1986; Toom-Sauntry and Barrie 2002; Goto-Azuma et al., 2001; Norman et al., 1999; Colin et al., 1997; Li and Barrie 1993; Li et al., 1993). The increases in the sulfate concentration during the winter and spring months occur because the transport of air pollution from the mid-latitudes to the Arctic is strongest during this time of year and scavenging by precipitation is lowest; thus, sulfur species do not fall out prior to reaching the Arctic (Li and Barrie, 1993; Davidson et al., 1993). In addition, just after polar sunrise the photochemical production of aerosols and gases that are more readily scavenged by snow allow for the observed increase in sulfate at this time (Finkel et al., 1986). Conversely, the typically lower values in summer occur because northward transport of air masses is weaker and higher precipitation causes sulfur species to fall out prior to reaching the Arctic. The increases observed in the Hg and MSA concentrations during the spring months are attributed to polar sunrise. The increases in the Hg concentration are likely a combination of increased northward transport of air pollution

from the mid-latitudes and the photochemical oxidation of this pool of Hg during polar sunrise. The dominant species of Hg in the atmosphere is gaseous mercury (Hg°). The increased Hg concentrations observed at this site are likely related to Arctic polar Mercury Depletion events (AMDEs) where during polar sunrise this pool of Hg° is oxidized to reactive Hg(II) in the atmosphere resulting in depletion of gaseous Hg (Hg°) (Schroeder et al., 1998; Lu et al., 2001; Lindberg et al., 2002; Steffen et al., 2002). This reactive Hg(II) can then be rapidly deposited to the snow surface as mercuric chloride or mercury oxide species causing springtime peaks in the mercury content within the snowpack (Lindberg et al., 2001; Lu et al., 2001; Steffen et al., 2002; Mann et al., in press). It is expected that the Hg(II) concentration would peak after the nss-SO_4^{2-} because for Hg to be deposited to the snow surface it must be photochemically oxidized to the reactive form, Hg(II), prior to deposition; therefore, polar sunrise first must occur which for this site is sometime in March/April. The similarity in the physical and chemical mechanisms responsible for the nss-SO_4^{2-} and Hg concentration peaks suggest the Hg trend, peaking in the spring, also commenced with industrial activity. MSA concentrations also exhibit strong seasonality with peaks in concentration typically occurring in the spring months just after nss-SO_4^{2-} and concentration minimums occurring in the fall and winter months. The maxima are caused by the increase in seawater biogenic activity that occurs in the spring while the minima are the result of inhibited biogenic activity during the winter months. Because of the reduced biogenic activity the source of the precursor to MSA, DMS, is inhibited (Li et al., 1993) thus resulting in the lower concentrations observed.

The main sources contributing to the variations in the observed $\delta^{34}S_{nss}$ are anthropogenic and marine biogenic sulfate. The $\delta^{34}S_{nss}$ values (Figure 6.19.h) in the winter months, when most of the sulfate being contributed to the region is primarily from anthropogenic sources, were expected to be closer to +3 ± 1.5‰, the $\delta^{34}S$ value of anthropogenic sulfate determined by Patris et al. (2002) for the Summit location. The $\delta^{34}S_{nss}$ values for the summer were expected to be closer to that of marine biogenic sulfate, +18.6 ± 0.9‰ (Patris et al., 2002, Calhoun et al., 1991). In this case the $\delta^{34}S_{nss}$ values appear to follow the trend expected with values being lower in winter, closer to +3‰, and higher in the summer, closer to +18.6‰. The $\delta^{34}S_{nss}$ values that lie between the two extremes are likely a mixture of sulfate from anthropogenic and marine biogenic sources as well as other sulfate sources such as sea salt and dust. Examination of the mass balance results (Figure 6.17 and 6.18) show that samples with low $\delta^{34}S_{nss}$ values (marked with back slashes in Figures 6.17 and 6.18) are dominated by anthropogenic input at almost 100%. The one sample that has a higher $\delta^{34}S_{nss}$ value (marked with horizontal slashes in Figures 6.17 and 6.18) is dominated by marine biogenic input with 60% of the sulfate coming from this source. For the $\delta^{34}S_{nss}$ values (marked with open boxes in Figures 6.17 and 6.18) that lie within the two extremes, a larger proportion of the total sulfate is coming in from ^{34}S-enriched marine biogenic sources while the proportion being contributed from the sea salt and dust components remain relatively constant. Consequently, the $\delta^{34}S_{nss}$ values observed in spring/early summer and then again in late summer/fall are due to a larger contribution from the marine biogenic source. The increase in sulfate being contributed from this source, particularly in the spring when the $\delta^{34}S_{nss}$ values first begin to become more ^{34}S-enriched, corresponds to

the increase in sea water biogenic activity. This results in an increase of marine biogenic sulfate contribution. In addition, the total sulfate deposited in the winter and spring is typically larger (marked by stars in Figure 6.18) and likely is the result of increased northward transport and lowered scavenging by precipitation during this time of year.

The range in the relative anthropogenic contribution identified for the winter months, 92% to 103%, suggests that the isotope composition used for the anthropogenic end-member may not be appropriate. Using the $\delta^{34}S$ value of +1.5‰, which lies within the uncertainty reported by Patris et al. (2002), the range becomes 83% to 94% and averages 89%. This may be a better estimate of the anthropogenic contribution. The contributions to the total sulfate from the other contributors, in this case, remains the same for the sea salt and dust fraction yet the contribution from the marine biogenic fraction increases to 31% overall. Whether +3‰ or +1.5‰ is used in the model the anthropogenic fraction remains the largest contributor to the total sulfate deposited at this location throughout most of the year.

6.3 Summary

The $\delta^{34}S$ results for the Inilchek samples demonstrate that this new method, that couples thermal ionization with an internal double spike, is fully capable of sulfur isotope determination of snow samples with ppb levels of sulfate. Because of the high measurement precision, low blank concentrations, and relatively precise determination of the blank composition, the uncertainties on the individual $\delta^{34}S$ measurements were approximately 0.10 ‰. These precisions were obtained using less meltwater, 108 mL to 358 mL, and on smaller sample sizes, 0.10 to 1.82 μmoles S, and rival the precisions obtained by gas source techniques for larger sample sizes.

The $\delta^{34}S$ measurements presented here for Greenland are the first high-resolution measurements obtained for this location. The amount of meltwater used for sulfur isotope analysis in this portion of the study ranged from 209 to 307 mL, and averaged 272 mL, representing sample sizes ranging from 0.05 to 0.29 μmoles S. The smaller sample requirement allowed for approximately 9 analyses per year with each analysis representing approximately 1.5 months. The uncertainties (0.38‰ to 5.01‰ (2σ)) determined for this portion of the study were quite large relative to those determined for the Inilchek samples (0.10‰ to 0.12‰ (2σ)). In this case the large uncertainties were because of the increased blank concentration and the smaller sample size used for analysis. It is important to note that the larger uncertainties observed are not caused by a decrease in instrumental measurement precision but to the increase in the blank concentration combined with smaller sample sizes used for $\delta^{34}S$ analysis. Furthermore, estimates of the precisions that are obtainable, 0.30‰ to 1.91‰ (2σ), using the double spike technique on sample sizes ranging from 0.05 to 0.29 μmoles S, demonstrate that if the blank concentration is lowered and the uncertainty in the blank composition is small, that up to a factor of three improvement in the uncertainties can occur. In this case the precisions obtained would be similar to those of gas source techniques but for much smaller sample sizes, almost an order of magnitude smaller. Moreover, this improvement is attainable because the blank concentrations determined during the measurement of the Summit samples are not typical of blank concentrations normally achieved using this technique and are likely the result of the change in argon gas suppliers which can be easily remedied.

The geochemical and mass balance results for the Inilchek and Summit sites show anthropogenic inputs tend to dominate through most of the year averaging 75%. For Summit, the exception is in the summer months when the marine biogenic contribution is larger. In addition, the Inilchek region appears to show only a weak seasonal trend in sulfate deposition with increased deposition in late spring/early summer and winter, which may be cause by increased convective transport or increased energy use and changes in the local- to regional- atmospheric circulation patterns. The Summit site shows a strong seasonality, both in $\delta^{34}S_{nss}$ values and in the timing of sulfate deposition. In the winter months the $\delta^{34}S_{nss}$ values are ^{34}S-depleted and in the summer months the $\delta^{34}S_{nss}$ values are ^{34}S-enriched. When seawater biogenic activity is operating, larger amounts of marine biogenic sulfate are being contributed to the site. In the spring and fall months the contribution from this marine biogenic source is greater causing the $\delta^{34}S_{nss}$ values to be ^{34}S-enriched relative to the $\delta^{34}S_{nss}$ values observed during the winter months. During the winter and late spring months sulfate deposition is larger due to the increased northward transport of air pollution from the mid-latitudes.

Chapter 7: Conclusions

The main objectives of this research were to develop an analytical technique for the measurement of isotope composition and concentration of sulfur in low concentration snow, and through model constraints to characterize the seasonal shifts in $\delta^{34}S$ of sulfate in snowpits from polar and temperate sites impacted by industrial activity. The capability of the new double spike technique developed here for high-precision $\delta^{34}S$ and sulfur concentration measurements was demonstrated by measuring internationally accepted sulfur standards with known sulfur isotope composition and sulfur concentration and by measuring snowpit samples with low sulfur concentrations. The sulfur isotope data obtained for the snowpit samples from the Inilchek Glacier, Kyrgyzstan and Summit, Greenland was used along with other geochemical data to calculate the relative seasonal contributions of anthropogenic (fossil fuel burning) and natural (sea salt, marine biogenic, and dust) sulfur sources to sulfate of the two high-elevation study sites. The high-resolution isotopic data obtained for the Greenland snowpit samples allowed for a more detailed reconstruction of the dynamic atmospheric sulfur cycle that has not previously been attainable by other analytical techniques.

7.1 Summary of Results

The limitation to the accuracy and precision in isotopic measurements by TIMS is instrumental fractionation. Using the new double spike method developed here the instrumental fractionation was quantified and corrected. The results for the internationally accepted standards show that a factor of two to five improvement in measurement precision (0.01%) is attainable and that the double spike technique is

"accurate" because the correct values for the standards are obtained. It is shown that all three correction laws (linear, power, and exponential) may be used, however, the Rayleigh theoretical model suggests that the exponential law is best suited for correction of the data as minimal drift is observed in the corrected data. If the measurement precision were to increase by an order of magnitude to 0.001%, small differences in the three correction laws may be observed and determination of where on the fractionation curve analysis begins, allows the identification of which law is appropriate for correction. As a result of the improved method, it is shown that the TIMS measurements, on considerably smaller sample sizes, are comparable to or better than that achieved by gas source mass spectrometric techniques.

The double spike technique also allows for the simultaneous determination of sulfur concentration by isotope dilution. The concentration results for SRM 2724b (Sulfur in Diesel Fuel Oil) show excellent agreement with the previously certified value and were well within the certified 95% uncertainty. In addition, the concentration results for the standards used to test the capability of this technique for isotope composition measurement show that both spike mixtures (DS #1 and DS #2) gave values that are well within the 95% confidence interval of each other, thus demonstrating the repeatability of the technique. The relative standard deviations (RSDs) obtained for the data were similar to or better than that obtained using the existing isotope dilution technique that employs an enriched ^{34}S spike.

The $\delta^{34}S$ results for the Inilchek and Greenland samples show the new double spike technique to be an invaluable method for sulfur isotope determination of snow samples with ppb levels of sulfate. In the case of the Inilchek samples, because of the

high measurement precision, low blank concentrations, and relatively precise determination of the blank composition, uncertainties of approximately ± 0.10‰ (2σ) on the individual $\delta^{34}S$ measurements were obtainable. These precisions were determined using less meltwater, 108 mL to 358 mL, and on smaller sample sizes, 0.10 to 1.82 μmoles S, than are typically used for gas source methods of sulfur isotope composition analysis and rival the precisions obtained by these techniques for larger sample sizes. The $\delta^{34}S$ measurements for Greenland are the first high-resolution measurements obtained for this location. The amount of meltwater used for sulfur isotope analysis in this portion of the study ranged from 209 to 307 mL, and averaged 272 mL. This is considerably less than the 1 to 2.5 L used in previous research. The uncertainties determined were quite large, averaging ± 1.5‰ (2σ), relative to those determined for the Inilchek samples. The larger uncertainties were because of the increased blank concentration and the smaller sample size used for analysis in this portion of the study. If the blank concentration is lowered and the uncertainty in the blank composition reduced, estimates of the precisions obtainable, averaging ± 0.75‰ (2σ), show that up to a factor of two to three improvement in the uncertainties on sample sizes ranging from 0.05 to 0.29 μmoles S is attainable with the double spike technique. In this case the precisions obtained would be similar to those of gas source techniques for snow samples but for much smaller sample sizes, 0.1 μmole S rather than 1 μmole S, which is almost an order of magnitude smaller. Moreover, it is important to note that these are the first $\delta^{34}S$ measurements that include a correction for blank, and demonstrate that blanks must be measured to assess the accuracy of the $\delta^{34}S$ data.

The elemental and sulfur isotope data obtained for snowpit samples showed that the main sulfate contributors to the Inilchek Glacier in Kyrgyzstan were anthropogenic and evaporite dust, while at the Summit, Greenland site these were mostly anthropogenic and marine biogenic in origin. Overall, the results show that anthropogenic inputs tend to dominate, averaging almost 75%, for both sites. The anthropogenic contributor dominates throughout the year in the Inilchek region, while in Greenland the influence of anthropogenic sources wanes during the summer months when the marine biogenic contribution increases.

The $\delta^{34}S_{nss}$ values of the two site locations appear to exhibit quite different seasonal behaviors. The $\delta^{34}S_{nss}$ values in the Inilchek snowpit do not appear to demonstrate any seasonality in the $\delta^{34}S_{nss}$ values, while the $\delta^{34}S_{nss}$ values observed in the Greenland snowpit exhibit strong seasonality, with the values ^{34}S-depleted in the winter months and ^{34}S-enriched in the summer months. The ^{34}S-depleted winter values were attributed to larger anthropogenic contribution while the ^{34}S-enriched summer values were attributed to the peak in seawater biogenic activity. In the spring and fall months the $\delta^{34}S_{nss}$ typically lie between the extreme values observed in summer and winter. At times of the year when sea water biogenic activity is operating, this ^{34}S-enriched component is being mixed with the ^{34}S-depleted anthropogenic component causing the $\delta^{34}S_{nss}$ values to be ^{34}S-enriched relative to the $\delta^{34}S_{nss}$ values observed during the winter months and ^{34}S-depleted relative to the $\delta^{34}S_{nss}$ values observed during the summer months.

At both site locations, total sulfate concentrations appear to increase during specific times of the year. In the Inilchek snowpit sulfate abundance increased during both the late spring/early summer and winter months; the late spring/early summer increase has

been attributed to more active convective transport in the atmosphere (Doscher et al., 1996, Kreutz and Sholkovitz, 2000), while winter increases are attributed to a combination of increased energy use and changes in the local- to regional- atmospheric circulation (Barrie, 1995; Kreutz and Sholkovitz, 2000). In the Summit snowpit the winter enhancement of sulfate concentration is likely caused by the increased transport of air pollution from the mid-latitudes and decreased scavenging by precipitation during this time of year (Li and Barrie, 1993).

7.2 Advantages and Benefits

The double spike technique offers numerous advantages and benefits beyond what the gas source techniques for sulfur isotope analysis are able to provide. Table 7.1

Table 7.1. List comparing the new Double Spike technique to the existing gas source techniques.

	Double Spike Technique	**Gas Source Technique**
	Internal Standard	External Standard
Sample Size	< 1 μmole S	≥ 1 μmole S
Precision & Sample Size (standards)	± 0.04 to 0.17‰ (1σ) for 0.40 to 1.34 μmoles S	± 0.10 to 0.16‰ (1σ) 10 to 30 μmoles S[a]
Precision & Sample Size (Snow samples)		
Inilchek Glacier	± 0.1‰ (1σ) for 0.10 to 1.83 μmoles S	± 0.5‰ (1σ) for ≥ 1 μ mole S[b]
Summit, Greenland	True (± 0.38 to 5.01‰) for 0.05 to 0.29 μmoles S	≤ ± 1‰ (1σ) for ≥ 1 μmole S[c]
	Estimated (± 0.30 to 1.91‰) for 0.05 to 0.29 μmoles S	
Meltwater Required		
Inilchek Glacier	Average 191 mL	1L
Summit, Greenland	Average 272 mL	1 to 2.5L

a Taylor et al, 2000, b Pruett et al., 2004, c Patris et al., 2002

summarizes some of the main advantages of this new technique relative to gas source. First, the double spike technique uses an internal standard rather than an external

standard. The internal standard is intrinsically accurate because only isotope ratios need to be measured; therefore complete recovery of the sample is not required for unbiased results, unlike techniques that use external standards. In addition, mass fractionation that may be caused by loses during drying and/or chemical reduction of the sample is accounted for by adding the spike upfront prior to sample processing. This is a considerable advantage for small sample sizes (< 1 μmole S) where loses can result in potentially large biases without the use of an internal standard. Another major advantage is the smaller sample volumes and consequently smaller sample sizes required. In addition, the precisions obtained are equal to or better then those obtained for large sample sizes using the gas source technique. The combination of these advances allows for access to the high-resolution temporal record contained in snow. In addition, other benefits that are also provided by the double spike method include: 1) a more complete understanding of instrumental mass fractionation during ion production using Si gel as an emitter; 2) a better constraint on where analysis begins and ends on the fractionation curve, 3) an improved understanding of blank effects on small samples of the size used in this study, and 4) an independent assessment of the biases among laboratories for the $\delta^{34}S$ standard values reported.

7.3 Implications for the Future

The new double spike technique has reduced the sample size required for sulfur isotope analysis by as much as a factor of 10. As the isotopic results show for the Inilchek and Summit snowpit samples, this significant reduction provides better access to the high-resolution temporal record contained in snow. Applying this technique to ice cores will extend the high-resolution temporal record back in time to establish a timeline

of changes in the atmospheric sulfur cycle. Ice cores are typically 8 cm in diameter. Taking the lowest amount of sample needed for analysis, 0.1 μmole S, and assuming an average concentration in Greenland ice of 25 ppb, a 3 cm section, approximately 150 mL of water, would be needed for sulfur isotope analysis by the double spike method. This is assuming an ice density of 1 g/cm^3. Assuming a density of around 0.5 g/cm^3 a 6 cm section would be needed. This size section is considerably smaller than the section length used, 40 cm to 100 cm (yielding 1 to 2.5 L sample volume), by Patris et al. (2002) for analysis of ice core samples from Greenland by the gas source technique. The double spike technique, consequently, has the potential to allow for a more detailed reconstruction of the atmospheric sulfur cycle and the understanding of changes in sources and sinks through time. This becomes particularly important when examining periods in geologic history where abrupt changes (< a decade) in climate occur.

Appendices

Appendix A – Details of all individual measurements for all standard measurements (IAEA-S-1, S-2, S-3, SL#7, and SL#9) using Double Spike #1 and #2.

A.1. Details of all individual measurements for all standard measurements (IAEA-S-1, S-2, S-3, SL#7, and SL#9) using Double Spike #1.

Double Spike #1

Sample ID	Sulfur #	S (ppm)	Total S (umoles) excluding blank
IAEA-S-1 (calibration)	**S-2635**	295.3	0.99
IAEA-S-1 (calibration)	**S-2651**	295.6	1.23
IAEA-S-1 (calibration)	**S-2652**	295.9	1.23
IAEA-S-1 (calibration)	**S-2654(3)**	295.8	1.39
	Avg	**295.6**	**1.2**
IAEA-S-1 (additional)	**S-2634**	295.5	0.99
IAEA-S-1 (additional)	**S-2636**	295.9	1.98
IAEA-S-1 (additional)	**S-2648**	295.7	1.23
IAEA-S-1 (additional)	**S-2649**	295.7	1.23
IAEA-S-1 (additional)	**S-2650**	295.3	1.23
IAEA-S-1 (additional)	**S-2650b**	295.6	1.23
IAEA-S-1 (additional)	**S-2653**	295.5	1.39
IAEA-S-1 (additional)	**S-2653a**	296.1	1.39
IAEA-S-1 (additional)	**S-2654(4)**	295.7	1.39
IAEA-S-1 (additional)	**S-2663b**	295.6	0.63
IAEA-S-1 (additional)	**S-2664**	295.6	0.63
IAEA-S-1 (additional)	**S-2664b**	295.5	0.63
IAEA-S-1 (additional)	**S-2665**	296.2	0.63
IAEA-S-1 (additional)	**S-2666**	295.8	0.63
IAEA-S-1 (additional)	**S-2666b**	296.0	0.63
IAEA-S-1 (additional)	**S-26674**	297.1	0.43
	Avg	**295.8**	**1.0**
IAEA-S-2	**2682a**	264.2	0.79
IAEA-S-2	**2694**	263.9	0.97
IAEA-S-2	**2695**	264.2	0.97
IAEA-S-2	**2702**	265.1	1.05
IAEA-S-2	**2703**	265.4	1.05
IAEA-S-2	**2704**	265.1	1.05
IAEA-S-2	**2727**	264.3	0.39
	Avg	**264.6**	**0.9**

Double Spike #1 continued

Sample ID	Sulfur #	$\delta^{34}S$ (per mil) raw	1σ	2σ	$2\sigma_m$
IAEA-S-1 (calibration)	**S-2635**	**-2.12**	0.55	1.09	0.15
IAEA-S-1 (calibration)	**S-2651**	**-0.17**	0.31	0.62	0.09
IAEA-S-1 (calibration)	**S-2652**	**0.50**	0.47	0.94	0.13
IAEA-S-1 (calibration)	**S-2654(3)**	**-1.03**	0.38	0.75	0.11
	Avg	**-0.71**	**0.43**	**0.85**	**0.12**
	1σ	**1.13**			
	$2\sigma_m$	**1.13**			
IAEA-S-1 (additional)	**S-2634**	**-2.89**	0.86	1.72	0.24
IAEA-S-1 (additional)	**S-2636**	**-4.00**	0.60	1.20	0.17
IAEA-S-1 (additional)	**S-2648**	**-5.09**	0.89	1.77	0.25
IAEA-S-1 (additional)	**S-2649**	**-2.83**	0.77	1.54	0.22
IAEA-S-1 (additional)	**S-2650**	**-2.62**	0.57	1.14	0.16
IAEA-S-1 (additional)	**S-2650b**	**-1.99**	0.57	1.15	0.16
IAEA-S-1 (additional)	**S-2653**	**-1.60**	0.83	1.66	0.24
IAEA-S-1 (additional)	**S-2653a**	**-0.52**	0.61	1.21	0.17
IAEA-S-1 (additional)	**S-2654(4)**	**-3.36**	0.54	1.08	0.15
IAEA-S-1 (additional)	**S-2663b**	**-2.89**	0.73	1.45	0.21
IAEA-S-1 (additional)	**S-2664**	**-1.51**	0.82	1.63	0.23
IAEA-S-1 (additional)	**S-2664b**	**0.06**	0.65	1.30	0.18
IAEA-S-1 (additional)	**S-2665**	**-2.31**	0.68	1.35	0.19
IAEA-S-1 (additional)	**S-2666**	**-1.17**	0.48	0.97	0.14
IAEA-S-1 (additional)	**S-2666b**	**-0.48**	0.89	1.78	0.25
IAEA-S-1 (additional)	**S-26674**	**-0.03**	0.72	1.45	0.20
	Avg	**-2.08**	**0.70**	**1.40**	**0.20**
	1σ	**1.46**			
	$2\sigma_m$	**0.73**			
IAEA-S-2	**2682a**	**21.15**	1.12	2.25	0.32
IAEA-S-2	**2694**	**20.88**	0.75	1.50	0.21
IAEA-S-2	**2695**	**19.51**	1.07	2.14	0.30
IAEA-S-2	**2702**	**22.18**	1.04	2.08	0.29
IAEA-S-2	**2703**	**22.52**	0.50	0.99	0.14
IAEA-S-2	**2704**	**22.88**	0.51	1.03	0.15
IAEA-S-2	**2727**	**17.91**	0.65	1.31	0.19
	Avg	**21.01**	**0.81**	**1.61**	**0.23**
	1σ	**1.78**			
	$2\sigma_m$	**1.35**			

Double Spike #1 continued

Sample ID	Sulfur #	$\delta^{34}S$ (per mil) corrected for instrumental fractionation	1σ	2σ	$2\sigma_m$
IAEA-S-1 (calibration)	**S-2635**	**-0.30**	0.29	0.57	0.08
IAEA-S-1 (calibration)	**S-2651**	**-0.35**	0.20	0.41	0.06
IAEA-S-1 (calibration)	**S-2652**	**-0.31**	0.24	0.47	0.07
IAEA-S-1 (calibration)	**S-2654(3)**	**-0.25**	0.23	0.45	0.06
	Avg	**-0.30**	**0.24**	**0.48**	**0.07**
	1σ	**0.04**			
	$2\sigma_m$	**0.04**			
IAEA-S-1 (additional)	**S-2634**	**-0.35**	0.88	1.76	0.25
IAEA-S-1 (additional)	**S-2636**	**-0.18**	0.70	1.39	0.20
IAEA-S-1 (additional)	**S-2648**	**-0.20**	0.89	1.77	0.25
IAEA-S-1 (additional)	**S-2649**	**-0.55**	0.61	1.22	0.17
IAEA-S-1 (additional)	**S-2650**	**-0.59**	0.33	0.67	0.09
IAEA-S-1 (additional)	**S-2650b**	**0.09**	0.78	1.56	0.22
IAEA-S-1 (additional)	**S-2653**	**-0.39**	0.50	1.01	0.14
IAEA-S-1 (additional)	**S-2653a**	**-0.23**	0.36	0.71	0.10
IAEA-S-1 (additional)	**S-2654(4)**	**-0.18**	0.40	0.79	0.11
IAEA-S-1 (additional)	**S-2663b**	**-0.48**	0.82	1.64	0.23
IAEA-S-1 (additional)	**S-2664**	**-0.40**	0.45	0.91	0.13
IAEA-S-1 (additional)	**S-2664b**	**-0.34**	0.24	0.49	0.07
IAEA-S-1 (additional)	**S-2665**	**-0.40**	0.61	1.22	0.17
IAEA-S-1 (additional)	**S-2666**	**-0.26**	0.58	1.17	0.17
IAEA-S-1 (additional)	**S-2666b**	**-0.51**	0.27	0.54	0.08
IAEA-S-1 (additional)	**S-26674**	**-0.37**	0.39	0.79	0.11
	Avg	**-0.33**	**0.55**	**1.10**	**0.16**
	1σ	**0.17**			
	$2\sigma_m$	**0.09**			
IAEA-S-2	**2682a**	**22.68**	0.23	0.46	0.06
IAEA-S-2	**2694**	**22.62**	0.21	0.41	0.06
IAEA-S-2	**2695**	**22.65**	0.20	0.39	0.06
IAEA-S-2	**2702**	**22.62**	0.25	0.51	0.07
IAEA-S-2	**2703**	**22.61**	0.15	0.30	0.04
IAEA-S-2	**2704**	**22.73**	0.15	0.30	0.04
IAEA-S-2	**2727**	**22.67**	0.43	0.86	0.12
	Avg	**22.65**	**0.23**	**0.46**	**0.07**
	1σ	**0.04**			
	$2\sigma_m$	**0.03**			

Double Spike #1 continued

Sample ID	Sulfur #	$\delta^{34}S$ (per mil) blank-corrected	1σ	2σ	Voltage on mass 109 (^{34}S)
IAEA-S-1 (calibration)	**S-2635**	**-0.32**	0.03	0.06	100-60
IAEA-S-1 (calibration)	**S-2651**	**-0.36**	0.03	0.05	125-73
IAEA-S-1 (calibration)	**S-2652**	**-0.32**	0.03	0.05	133-54
IAEA-S-1 (calibration)	**S-2654(3)**	**-0.26**	0.02	0.05	140
	Avg	**-0.31**	**0.03**	**0.05**	
	1σ	**0.04**			
	$2\sigma_m$	**0.04**			
IAEA-S-1 (additional)	**S-2634**	**-0.36**	0.04	0.09	18-15
IAEA-S-1 (additional)	**S-2636**	**-0.19**	0.03	0.07	23-21
IAEA-S-1 (additional)	**S-2648**	**-0.21**	0.04	0.08	19
IAEA-S-1 (additional)	**S-2649**	**-0.56**	0.04	0.08	18-40
IAEA-S-1 (additional)	**S-2650**	**-0.60**	0.04	0.08	43-25
IAEA-S-1 (additional)	**S-2650b**	**0.07**	0.04	0.08	25-20
IAEA-S-1 (additional)	**S-2653**	**-0.40**	0.04	0.07	32-23
IAEA-S-1 (additional)	**S-2653a**	**-0.24**	0.04	0.07	98-41
IAEA-S-1 (additional)	**S-2654(4)**	**-0.19**	0.04	0.07	47-45
IAEA-S-1 (additional)	**S-2663b**	**-0.50**	0.06	0.12	26-16
IAEA-S-1 (additional)	**S-2664**	**-0.43**	0.06	0.12	42-25
IAEA-S-1 (additional)	**S-2664b**	**-0.37**	0.06	0.12	40-24
IAEA-S-1 (additional)	**S-2665**	**-0.43**	0.06	0.12	27-24
IAEA-S-1 (additional)	**S-2666**	**-0.28**	0.06	0.12	44-18
IAEA-S-1 (additional)	**S-2666b**	**-0.53**	0.06	0.12	86-15
IAEA-S-1 (additional)	**S-26674**	**-0.40**	0.09	0.18	92-15
	Avg	**-0.35**	**0.05**	**0.10**	
	1σ	**0.17**			
	$2\sigma_m$	**0.09**			
IAEA-S-2	**2682a**	**22.67**	0.04	0.07	42-20
IAEA-S-2	**2694**	**22.62**	0.03	0.07	79-25
IAEA-S-2	**2695**	**22.65**	0.03	0.07	50-20
IAEA-S-2	**2702**	**22.61**	0.03	0.07	65-23
IAEA-S-2	**2703**	**22.60**	0.03	0.07	169-105
IAEA-S-2	**2704**	**22.73**	0.03	0.07	169-95
IAEA-S-2	**2727**	**22.66**	0.06	0.12	87-31
	Avg	**22.65**	**0.04**	**0.08**	
	1σ	**0.04**			
	$2\sigma_m$	**0.03**			

Double Spike #1 continued

Sample ID	Sulfur #	Voltage on 34 (@ end)	Sample/ Blank Molar Ratio	µgrams natural	µmoles of natural	Sample /Spike Ratio Molar Ratio
IAEA-S-1 (calibration)	**S-2635**	60	2334	32	0.99	1.8
IAEA-S-1 (calibration)	**S-2651**	73	2904	40	1.23	2.1
IAEA-S-1 (calibration)	**S-2652**	54	2908	40	1.23	2.1
IAEA-S-1 (calibration)	**S-2654(3)**	100	3271	45	1.39	2.4
		Avg	**2854**	**39**	**1.21**	
IAEA-S-1 (additional)	**S-2634**	15	2336	32	0.99	1.8
IAEA-S-1 (additional)	**S-2636**	21	4677	64	1.98	1.8
IAEA-S-1 (additional)	**S-2648**	19	2905	40	1.23	2.1
IAEA-S-1 (additional)	**S-2649**	40	2905	40	1.23	2.1
IAEA-S-1 (additional)	**S-2650**	25	2901	39	1.23	2.1
IAEA-S-1 (additional)	**S-2650b**	20	2905	40	1.23	2.1
IAEA-S-1 (additional)	**S-2653**	23	3269	44	1.39	2.4
IAEA-S-1 (additional)	**S-2653a**	41	3275	45	1.39	2.4
IAEA-S-1 (additional)	**S-2654(4)**	45	3270	44	1.39	2.4
IAEA-S-1 (additional)	**S-2663b**	16	1475	20	0.63	1.9
IAEA-S-1 (additional)	**S-2664**	25	1475	20	0.63	1.9
IAEA-S-1 (additional)	**S-2664b**	24	1474	20	0.63	1.9
IAEA-S-1 (additional)	**S-2665**	24	1478	20	0.63	1.9
IAEA-S-1 (additional)	**S-2666**	18	1475	20	0.63	1.9
IAEA-S-1 (additional)	**S-2666b**	15	1476	20	0.63	1.9
IAEA-S-1 (additional)	**S-26674**	15	1007	14	0.43	1.9
		Avg	**2394**	**33**	**1.02**	
IAEA-S-2	**2682a**	20	1872	25	0.79	1.7
IAEA-S-2	**2694**	25	2277	31	0.97	1.8
IAEA-S-2	**2695**	20	2280	31	0.97	1.8
IAEA-S-2	**2702**	23	2472	34	1.05	1.8
IAEA-S-2	**2703**	105	2475	34	1.05	1.8
IAEA-S-2	**2704**	95	2472	34	1.05	1.8
IAEA-S-2	**2727**	31	914	12	0.39	1.8
		Avg	**2109**	**29**	**0.89**	

Double Spike #1 continued

Sample ID	Sulfur #	Improvement in Precision Uncor to Cor	Range in per mil for Uncorrected Data	Approximate reservoir Depleted before analysis (%)
IAEA-S-1 (calibration)	**S-2635**	1.9	-5--3.4	38
IAEA-S-1 (calibration)	**S-2651**	1.5	-2.4--1.7	55
IAEA-S-1 (calibration)	**S-2652**	2.0	-2.1--075	54
IAEA-S-1 (calibration)	**S-2654(3)**	1.7	-1.7--1.2	57
	Avg	**1.8**		**51**
IAEA-S-1 (additional)	**S-2634**	1.0	-5.5--4.5	35
IAEA-S-1 (additional)	**S-2636**	0.9	-6.3--5.8	30
IAEA-S-1 (additional)	**S-2648**	1.0	-7.5--6.2	20
IAEA-S-1 (additional)	**S-2649**	1.3	-5.8--3.8	30
IAEA-S-1 (additional)	**S-2650**	1.7	-6.5--4.5	35
IAEA-S-1 (additional)	**S-2650b**	0.7	-3.8--4	--
IAEA-S-1 (additional)	**S-2653**	1.7	-4.2--2.2	45
IAEA-S-1 (additional)	**S-2653a**	1.7	-3.0--1.6	52
IAEA-S-1 (additional)	**S-2654(4)**	1.4	-5.5--4.5	35
IAEA-S-1 (additional)	**S-2663b**	0.9	-5.2--4.8	40
IAEA-S-1 (additional)	**S-2664**	1.8	-4.8--2.6	40
IAEA-S-1 (additional)	**S-2664b**	2.7	-3--1.1	52
IAEA-S-1 (additional)	**S-2665**	1.1	-5--3.9	38
IAEA-S-1 (additional)	**S-2666**	0.8	-3.5--3	50
IAEA-S-1 (additional)	**S-2666b**	3.3	-4.3--1.5	42
IAEA-S-1 (additional)	**S-26674**	1.8	-3.5--0.8	50
	Avg	**1.5**		**40**
IAEA-S-2	**2682a**	4.9	17-20	38
IAEA-S-2	**2694**	3.7	17.3-20	38
IAEA-S-2	**2695**	5.4	15-19	20
IAEA-S-2	**2702**	4.1	18-21.5	40
IAEA-S-2	**2703**	3.3	19.5-21	46
IAEA-S-2	**2704**	3.5	19.9-21.2	55
IAEA-S-2	**2727**	1.5	14.9-16	20
	Avg	**3.8**		**37**

Double Spike #1 continued

Sample ID	Sulfur #	S (ppm)	Total S (umoles) excluding blank
IAEA-S-3	**2708**	304.3	0.71
IAEA-S-3	**2710**	304.1	1.09
IAEA-S-3	**2711**	304.1	1.09
IAEA-S-3	**2712**	304.0	1.09
IAEA-S-3	**2714**	304.4	1.09
IAEA-S-3	**2715**	304.6	1.09
IAEA-S-3	**2716**	304.4	1.09
	Avg	**304.3**	**1.04**
SL#7	**S-2758**	449.3	1.38
SL#7	**S-2759**	448.6	1.38
SL#7	**S-2760**	448.6	1.38
	Avg	**448.8**	**1.4**
SL#9	**S-2770**	423.0	1.47
SL#9	**S-2771**	422.5	1.47
SL#9	**S-2772**	422.6	1.47
	Avg	**422.7**	**1.5**

Double Spike #1 continued

Sample ID	Sulfur #	$\delta^{34}S$ (per mil) raw	1σ	2σ	$2\sigma_m$
IAEA-S-3	**2708**	**-32.36**	0.99	1.97	0.28
IAEA-S-3	**2710**	**-32.88**	0.68	1.36	0.19
IAEA-S-3	**2711**	**-33.27**	0.85	1.70	0.24
IAEA-S-3	**2712**	**-33.54**	0.62	1.23	0.17
IAEA-S-3	**2714**	**-36.32**	0.56	1.12	0.16
IAEA-S-3	**2715**	**-32.57**	0.84	1.68	0.24
IAEA-S-3	**2716**	**-32.27**	0.55	1.11	0.16
	Avg	**-33.32**	**0.73**	**1.45**	**0.21**
	1σ	**1.40**			
	$2\sigma_m$	**0.99**			
SL#7	**S-2758**	**49.50**	1.01	2.03	0.29
SL#7	**S-2759**	**48.49**	0.83	1.66	0.23
SL#7	**S-2760**	**47.65**	0.47	0.93	0.13
	Avg	**48.55**	**0.77**	**1.54**	**0.22**
	1σ	**0.93**			
	$2\sigma_m$	**1.07**			
SL#9	**S-2770**	**-18.14**	0.81	1.61	0.23
SL#9	**S-2771**	**-20.38**	0.61	1.21	0.17
SL#9	**S-2772**	**-20.51**	0.66	1.32	0.19
	Avg	**-19.67**	**0.69**	**1.38**	**0.20**
	1σ	**1.33**			
	$2\sigma_m$	**1.54**			

Double Spike #1 continued

Sample ID	Sulfur #	$\delta^{34}S$ (per mil) corrected fro instrumental fractionation	1σ	2σ	$2\sigma_m$
IAEA-S-3	**2708**	**-32.41**	0.21	0.41	0.06
IAEA-S-3	**2710**	**-32.53**	0.27	0.53	0.07
IAEA-S-3	**2711**	**-32.52**	0.20	0.40	0.06
IAEA-S-3	**2712**	**-32.48**	0.18	0.35	0.05
IAEA-S-3	**2714**	**-32.44**	0.18	0.37	0.05
IAEA-S-3	**2715**	**-32.44**	0.21	0.41	0.06
IAEA-S-3	**2716**	**-32.35**	0.16	0.31	0.04
	Avg	**-32.45**	**0.20**	**0.40**	**0.06**
	1σ	**0.06**			
	$2\sigma_m$	**0.05**			
SL#7	**S-2758**	**50.64**	0.24	0.49	0.07
SL#7	**S-2759**	**50.65**	0.23	0.47	0.07
SL#7	**S-2760**	**50.83**	0.28	0.56	0.08
	Avg	**50.71**	**0.25**	**0.50**	**0.07**
	1σ	**0.11**			
	$2\sigma_m$	**0.08**			
SL#9	**S-2770**	**-19.22**	0.40	0.79	0.11
SL#9	**S-2771**	**-19.11**	0.26	0.53	0.07
SL#9	**S-2772**	**-19.20**	0.31	0.62	0.09
	Avg	**-19.18**	**0.32**	**0.65**	**0.09**
	1σ	**0.06**			
	$2\sigma_m$	**0.04**			

Double Spike #1 continued

Sample ID	Sulfur #	$\delta^{34}S$ (per mil) blank-corrected	1σ	2σ	Voltage on mass 109 (^{34}S)
IAEA-S-3	**2708**	**-32.45**	0.08	0.15	67-31
IAEA-S-3	**2710**	**-32.56**	0.05	0.10	80-39
IAEA-S-3	**2711**	**-32.55**	0.05	0.10	101-59
IAEA-S-3	**2712**	**-32.51**	0.05	0.10	144-83
IAEA-S-3	**2714**	**-32.47**	0.05	0.10	75-51
IAEA-S-3	**2715**	**-32.47**	0.05	0.10	102-38
IAEA-S-3	**2716**	**-32.38**	0.05	0.10	150-55
	Avg	**-32.48**	**0.05**	**0.11**	
	1σ	**0.06**			
	$2\sigma_m$	**0.04**			
SL#7	**S-2758**	**50.65**	0.02	0.04	116-51
SL#7	**S-2759**	**50.65**	0.02	0.04	91-53
SL#7	**S-2760**	**50.84**	0.02	0.04	135-80
	Avg	**50.71**	**0.02**	**0.04**	
	1σ	**0.11**			
	$2\sigma_m$	**0.08**			
SL#9	**S-2770**	**-19.24**	0.03	0.06	58-23
SL#9	**S-2771**	**-19.13**	0.03	0.06	131-47
SL#9	**S-2772**	**-19.21**	0.03	0.06	150-36
	Avg	**-19.19**	**0.03**	**0.06**	
	1σ	**0.06**			
	$2\sigma_m$	**0.04**			

Double Spike #1 continued

Sample ID	Sulfur #	Voltage on 34 (@ end)	Sample/ Blank Molar Ratio	µgrams natural	µmoles of natural	Sample/Spike Ratio Molar Ratio
IAEA-S-3	**2708**	31	1602	23	0.71	2.1
IAEA-S-3	**2710**	39	2461	35	1.09	2.4
IAEA-S-3	**2711**	59	2462	35	1.09	2.4
IAEA-S-3	**2712**	83	2461	35	1.09	2.4
IAEA-S-3	**2714**	51	2464	35	1.09	2.4
IAEA-S-3	**2715**	38	2465	35	1.09	2.4
IAEA-S-3	**2716**	55	2464	35	1.09	2.4
		Avg	**2340**	**33**	**1.04**	
SL#7	**S-2758**	51	3261	44	1.38	2.2
SL#7	**S-2759**	53	3256	44	1.38	2.2
SL#7	**S-2760**	80	3256	44	1.38	2.2
		Avg	**3258**	**44**	**1.38**	
SL#9	**S-2770**	23	3473	47	1.47	2.4
SL#9	**S-2771**	47	3469	47	1.47	2.4
SL#9	**S-2772**	36	3470	47	1.47	2.4
		Avg	**3471**	**47**	**1.47**	

Double Spike #1 continued

Sample ID	Sulfur #	Improvement in Precision Uncor to Cor	Range in per mil for Uncorrected Data	Approximate reservoir Depleted before analysis (%)
IAEA-S-3	**2708**	4.8	-36--33	42
IAEA-S-3	**2710**	2.6	-35.5--33.4	43
IAEA-S-3	**2711**	4.3	-36.5--34	40
IAEA-S-3	**2712**	3.5	-36.5--34.5	40
IAEA-S-3	**2714**	3.1	-39--37	20
IAEA-S-3	**2715**	4.1	-36--33.5	44
IAEA-S-3	**2716**	3.6	-35--33	45
		3.7		**39**
SL#7	**S-2758**	4.2	45.3-46.6	
SL#7	**S-2759**	3.6	46-49.3	
SL#7	**S-2760**	1.7	45.2-47.5	
		3.1		
SL#9	**S-2770**	2.0	-21--19	
SL#9	**S-2771**	2.3	23--21	
SL#9	**S-2772**	2.1	-23.2--21	
		2.2		

Appendix A.2 - Details of all individual measurements for all standard measurements (IAEA-S-1 and S-2) using Double Spike #2.

Double Spike #2

Sample ID	Sulfur #	S (ppm)	Total S (μmoles) excluding blank	$\delta^{34}S$ (per mil) raw	1σ	2σ	$2\sigma_m$
IAEA-S-1 (calibration)	**S-2774**	296.8	1.77	**-3.30**	0.75	1.49	0.21
IAEA-S-1 (calibration)	**S-2815**	296.2	0.85	**1.17**	0.59	1.18	0.17
IAEA-S-1 (calibration)	**S-2832**	295.9	1.13	**-1.72**	0.63	1.25	0.18
IAEA-S-1 (calibration)	**S-2838**	297.6	1.10	**0.05**	0.80	1.59	0.22
IAEA-S-1 (calibration)	**S-2840**	297.8	1.10	**-6.71**	0.91	1.81	0.26
IAEA-S-1 (calibration)	**S-2859c**	295.9	0.73	**-0.85**	0.76	1.52	0.21
IAEA-S-1 (calibration)	**S-2860**	297.0	0.73	**-2.38**	0.44	0.88	0.12
IAEA-S-1 (calibration)	**S-2865**	297.2	0.98	**-0.24**	0.65	1.31	0.19
			Avg	**-1.75**	**0.69**	**1.38**	**0.20**
			1σ	**2.46**			
			$2\sigma_m$	**1.74**			
IAEA-S-1 (additional)	**S-2792**	296.7	0.89	**-0.29**	0.83	1.66	0.23
IAEA-S-1 (additional)	**S-2830**	296.4	1.13	**-2.08**	0.60	1.21	0.17
IAEA-S-1 (additional)	**S-2858**	295.7	0.73	**-2.31**	0.72	1.45	0.20
IAEA-S-1 (additional)	**S-2866**	297.0	0.98	**-2.14**	0.61	1.23	0.19
			Avg	**-1.70**	**0.69**	**1.38**	**0.20**
			1σ	**0.95**			
			$2\sigma_m$	**0.95**			
IAEA-S-2	**S-2822r**	263.8	1.15	**24.68**	1.32	2.64	0.37
IAEA-S-2	**S-2823r**	264.7	1.16	**22.24**	0.41	0.83	0.12
IAEA-S-2	**S-2824**	267.3	1.17	**24.03**	0.45	0.89	0.13
IAEA-S-2	**S-2835**	265.5	1.22	**22.59**	0.50	1.00	0.14
IAEA-S-2	**S-2836**	265.0	1.21	**21.76**	0.52	1.04	0.15
IAEA-S-2	**S-2877**	263.4	1.04	**24.11**	0.69	1.38	0.19
			Avg	**23.23**	**0.65**	**1.30**	**0.18**
			1σ	**1.19**			
			$2\sigma_m$	**0.97**			

Double Spike #2 Continued

Sample ID	Sulfur #	$\delta^{34}S$ (per mil) corrected for instrumental fractionation	1σ	2σ	$2\sigma_m$
IAEA-S-1 (calibration)	**S-2774**	**-0.14**	0.18	0.36	0.05
IAEA-S-1 (calibration)	**S-2815**	**-0.39**	0.29	0.59	0.08
IAEA-S-1 (calibration)	**S-2832**	**-0.36**	0.27	0.54	0.08
IAEA-S-1 (calibration)	**S-2838**	**-0.22**	0.59	1.17	0.17
IAEA-S-1 (calibration)	**S-2840**	**-0.49**	0.35	0.69	0.10
IAEA-S-1 (calibration)	**S-2859c**	**-0.33**	0.15	0.31	0.04
IAEA-S-1 (calibration)	**S-2860**	**-0.34**	0.20	0.40	0.06
IAEA-S-1 (calibration)	**S-2865**	**-0.12**	0.38	0.76	0.11
	Avg	**-0.30**	**0.30**	**0.60**	**0.09**
	1σ	**0.13**			
	$2\sigma_m$	**0.09**			
IAEA-S-1 (additional)	**S-2792**	**-0.16**	0.25	0.49	0.07
IAEA-S-1 (additional)	**S-2830**	**-0.43**	0.41	0.81	0.12
IAEA-S-1 (additional)	**S-2858**	**-0.33**	0.28	0.55	0.08
IAEA-S-1 (additional)	**S-2866**	**-0.39**	0.51	1.03	0.16
	Avg	**-0.33**	**0.36**	**0.72**	**0.11**
	1σ	**0.12**			
	$2\sigma_m$	**0.12**			
IAEA-S-2	**S-2822r**	**22.61**	1.14	2.28	0.32
IAEA-S-2	**S-2823r**	**22.54**	0.33	0.66	0.09
IAEA-S-2	**S-2824**	**22.57**	0.20	0.40	0.06
IAEA-S-2	**S-2835**	**22.54**	0.23	0.45	0.06
IAEA-S-2	**S-2836**	**22.66**	0.28	0.57	0.08
IAEA-S-2	**S-2877**	**22.67**	0.36	0.72	0.10
	Avg	**22.60**	**0.42**	**0.85**	**0.12**
	1σ	**0.06**			
	$2\sigma_m$	**0.05**			

Double Spike #2 Continued

Sample ID	Sulfur #	$\delta^{34}S$ (per mil) blank-corrected	1σ	2σ
IAEA-S-1 (calibration)	**S-2774**	**-0.15**	0.02	0.03
IAEA-S-1 (calibration)	**S-2815**	**-0.40**	0.02	0.04
IAEA-S-1 (calibration)	**S-2832**	**-0.37**	0.02	0.04
IAEA-S-1 (calibration)	**S-2838**	**-0.22**	0.02	0.04
IAEA-S-1 (calibration)	**S-2840**	**-0.50**	0.02	0.04
IAEA-S-1 (calibration)	**S-2859c**	**-0.34**	0.02	0.04
IAEA-S-1 (calibration)	**S-2860**	**-0.35**	0.02	0.04
IAEA-S-1 (calibration)	**S-2865**	**-0.13**	0.02	0.04
	Avg	**-0.31**	**0.02**	**0.04**
	1σ	**0.13**		
	$2\sigma_m$	**0.09**		
IAEA-S-1 (additional)	**S-2792**	**-0.17**	0.02	0.04
IAEA-S-1 (additional)	**S-2830**	**-0.44**	0.02	0.03
IAEA-S-1 (additional)	**S-2858**	**-0.34**	0.02	0.04
IAEA-S-1 (additional)	**S-2866**	**-0.40**	0.02	0.04
	Avg	**-0.34**	**0.02**	**0.04**
	1σ	**0.12**		
	$2\sigma_m$	**0.12**		
IAEA-S-2	**S-2822r**	**22.61**	0.01	0.02
IAEA-S-2	**S-2823r**	**22.54**	0.01	0.02
IAEA-S-2	**S-2824**	**22.57**	0.01	0.02
IAEA-S-2	**S-2835**	**22.53**	0.01	0.02
IAEA-S-2	**S-2836**	**22.66**	0.01	0.02
IAEA-S-2	**S-2877**	**22.67**	0.01	0.02
	Avg	**22.60**	**0.01**	**0.02**
	1σ	**0.06**		
	$2\sigma_m$	**0.05**		

Double Spike #2 Continued

Sample ID	Sulfur #	Voltage on 34	Voltage on 34 (@ end)	Sample/ Blank Molar Ratio	µgrams natural	µmoles of natural
IAEA-S-1 (calibration)	**S-2774**	122-65	65	8046	57	1.77
IAEA-S-1 (calibration)	**S-2815**	154-30	30	3850	27	0.85
IAEA-S-1 (calibration)	**S-2832**	167-23	23	5124	36	1.13
IAEA-S-1 (calibration)	**S-2838**	152-15	15	4977	35	1.10
IAEA-S-1 (calibration)	**S-2840**	118-15	15	4981	35	1.10
IAEA-S-1 (calibration)	**S-2859c**	102-62	62	3303	23	0.73
IAEA-S-1 (calibration)	**S-2860**	129-49	49	3315	23	0.73
IAEA-S-1 (calibration)	**S-2865**	127-27	27	4462	32	0.98
			Avg	**4757**	**34**	**1.05**
IAEA-S-1 (additional)	**S-2792**	64-29	29	4046	29	0.89
IAEA-S-1 (additional)	**S-2830**	39-24	24	5133	36	1.13
IAEA-S-1 (additional)	**S-2858**	61-40	40	3301	23	0.73
IAEA-S-1 (additional)	**S-2866**	17-24	24	4458	32	0.98
			Avg	**4234**	**30**	**0.93**
IAEA-S-2	**S-2822r**	123-15	15	5236	37	1.15
IAEA-S-2	**S-2823r**	166-?	> 15	5255	37	1.16
IAEA-S-2	**S-2824**	145-53	53	5306	38	1.17
IAEA-S-2	**S-2835**	124-45	45	5510	39	1.22
IAEA-S-2	**S-2836**	132-32	32	5501	39	1.21
IAEA-S-2	**S-2877**	110-19	19	4703	33	1.04
			Avg	**5255**	**37**	**1.16**

Double Spike #2 Continued

Sample ID	Sulfur #	Sample/ Spike Ratio Molar Ratio	Improvement in Precision Uncor to Cor	Range in per mil for Uncorrected Data	Approximate reservoir Depleted before analysis (%)
IAEA-S-1 (calibration)	**S-2774**	2.1	4.2	-6.1--3.8	30
IAEA-S-1 (calibration)	**S-2815**	2.1	2.0	-1.5-0.3	55
IAEA-S-1 (calibration)	**S-2832**	2.0	2.3	4.5--3	42
IAEA-S-1 (calibration)	**S-2838**	1.9	1.4	2.6--1	53
IAEA-S-1 (calibration)	**S-2840**	1.9	2.6	-10--7	n/a
IAEA-S-1 (calibration)	**S-2859c**	2.3	4.9	-3.7--1.2	48
IAEA-S-1 (calibration)	**S-2860**	2.4	2.2	-4.5--3.5	42
IAEA-S-1 (calibration)	**S-2865**	2.0	1.7	-3--1	52
		Avg	**2.7**		**46**
IAEA-S-1 (additional)	**S-2792**	2.0	3.4	-3.5--1	50
IAEA-S-1 (additional)	**S-2830**	2.0	1.5	-4.5--3.3	42
IAEA-S-1 (additional)	**S-2858**	2.3	2.6	-5--3.1	40
IAEA-S-1 (additional)	**S-2866**	2.0	1.2	-5--3	40
		Avg	**2.2**		**43**
IAEA-S-2	**S-2822r**	2.1	1.2	22-26	60
IAEA-S-2	**S-2823r**	2.1	1.3	20-21.2	52
IAEA-S-2	**S-2824**	2.1	2.2	22-23	60
IAEA-S-2	**S-2835**	2.2	2.2	20-21.5	52
IAEA-S-2	**S-2836**	2.2	1.8	19.6-21	51
IAEA-S-2	**S-2877**	1.8	1.9	20.9-22.5	55
		Avg	**1.8**		**55**

Appendix B - Molecular Species Production during Vaporization

Previous mass spectrometric studies of bulk and thin-film arsenic trisulfide (As_2S_3) samples have suggested that As_2S_3 may vaporize to: 1) AsS (g) (masses 107, 108, 109, and 111) (Faure et al., 1973), 2) As_nS_n, where n = 1-4 (mass 246, 247, 248, and 250) a compilation of various arsenic sulfide species (Pashinkin et al., 1974), or 3) to As_4S_6 molecules (mass 492, 493, 494, and 496) (Mills et al., 1974; Janai et al., 1978). Although As_4S_6 was not detected in their work due to the suggested very short lifetime ($< 10^{-6}$ s), Janai et al. (1978) suggest that because of the presence of almost all of its possible fragments and $As_4S_5^+$, which is not a known molecular form, bulk As_2S_3 evaporates as As_4S_6 molecules. It is thought that upon ionization the As_4S_6 molecule becomes highly unstable and fragments to $As_4S_5^+$ and lower mass ions like AsS^+. In fact mass spectrometric analyses performed by Janai et al., (1978) of arsenic trisulfide upon thermal vaporization showed that above 300°C the most abundant observed species was arsenic sulfide (AsS^+). Indeed other arsenic sulfide species are produced as well (e.g. $As_4S_4^+$, $As_3S_3^+$, $As_2S_2^+$) and if taken together with their relative abundance the resulting masses produced are 246, 247, 248 and 250. All the measurements in the above studies thermally vaporized bulk or thin-film As_2S_3.

In this work, the arsenic trisulfide was loaded on to a filament with Si gel to enhance ionization. The temperature for analysis in this work was 950°C to 1000°C. The boiling points for As_2S_3, As_2O and As metal are 700°C, 400°C, and 610°C, respectively, well below 950°C, yet these species are observed at the elevated temperatures used for analysis. These observations taken together suggest arsenic trisulfide forms a compound ($NH_3 \bullet H_2O \bullet AsS_3^-$) with the Si gel and increases the boiling

point for these species. The specific mechanism of ion formation from Si gel is not well understood but it is likely that the primary species being vaporized from the filament in this case is AsS^+.

Although it remains unclear which molecular species may be vaporizing or being produced and ultimately which masses to use in the correction equations is still uncertain, it can be shown that the corrections are not sensitive to the assumed molecule. Figures B.1.a-f show Rayleigh-generated correction curves for the exponential (thick solid lines) and power (dash/dotted lines) laws with Figures B.1.a-c showing the curves generated assuming vaporization as the various species mentioned above - AsS^+ (masses 107, 108, 109, and 111), As_nS_n (masses 246, 247, 248, and 250) and As_4S_6 (masses 492, 493, 494, and 496) - and using masses 107, 108, 109, and 111 in the correction equations. Figures B.1.d-f show the same curves but masses 246, 247, 248, and 250 are used in the correction equations. The short dashed lines in each figure highlight the uncertainty, ± 0.2‰, commonly obtained using the double spike technique. Because of the relatively heavy masses of the arsenic sulfide species the deviations of the corrected curves from the true $\delta^{34}S$ values is quite small for both the power and exponential cases (< 0.15‰), with the largest deviation observed being for the power correction case when using masses 107 to 111 for correction (Figure B.1.a). For the measurement precisions typically obtained using the double spike technique, ± 0.20 to 0.60‰ (prior to blank-correction), the figures show that it does not matter whether masses 107 - 111 or 246 - 250 are used because the correction curves are indistinguishable within this uncertainty.

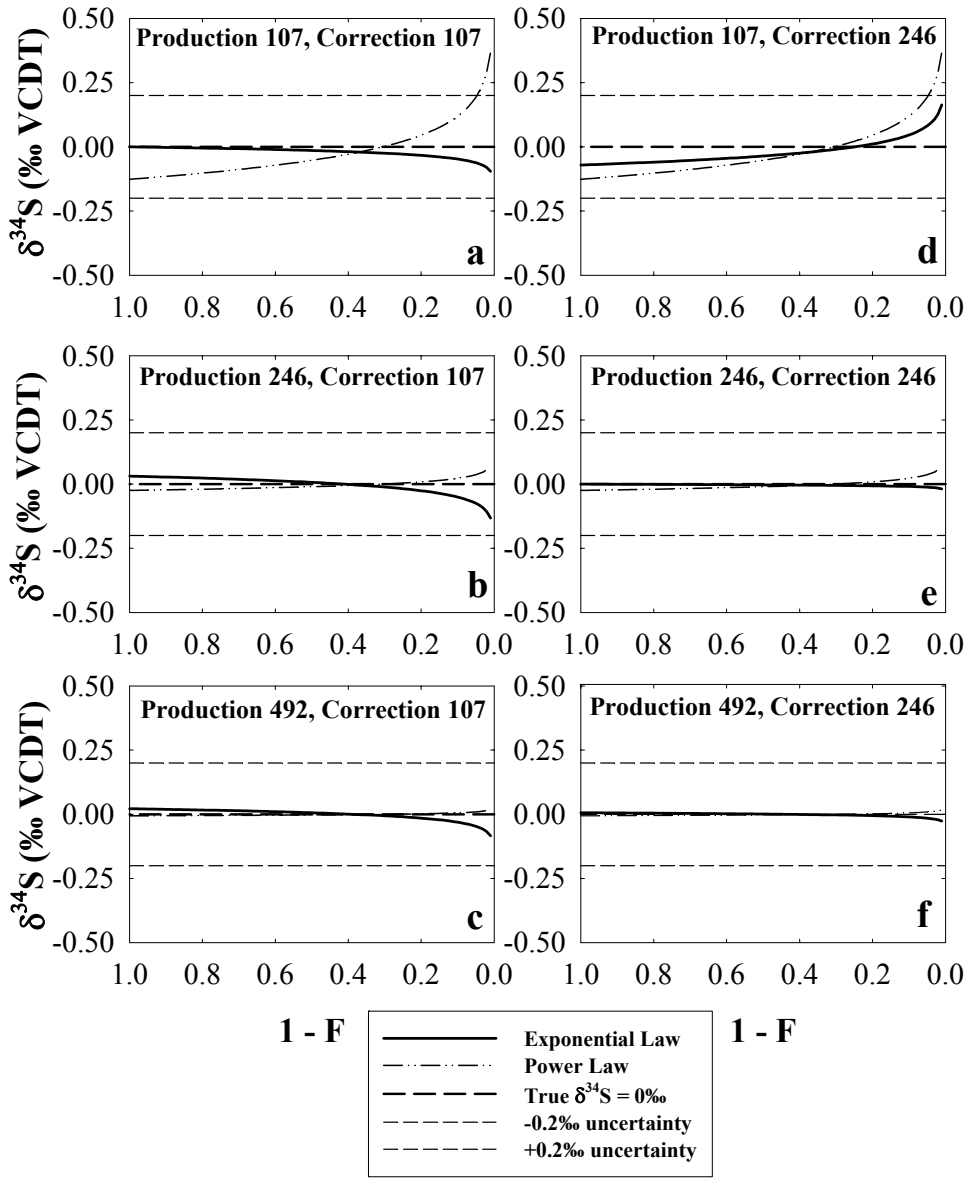

Figure B.1.a-f. Rayleigh-generated correction curves for the power (thick solid lines) and exponential (dash/dotted lines) laws. The curves in Figures B.1.a-c were generated assuming vaporization as - AsS^+ (masses 107, 108, 109, and 111) (Figure B.1.a), As_nS_n (masses 246, 247, 248, and 250) (Figure B.1.b) and As_4S_6 (masses 492, 493, 494, and 496) (Figure B.1.c) – and masses 107, 108, 109, and 111 were used for correction. Figures B.1.d-f show the same curves but masses 246, 247, 248, and 250 are used in the correction equations. The short dashed lines in highlight the uncertainty, ± 0.2‰, commonly obtained using the double spike technique.

Moreover, curves derived using heavier masses in the correction equations (e.g. 492-496) will not be significantly different than what is shown in Figure B.1.f). In this work the masses used in the correction equations are the masses of the AsS^+ spectrum based on both the findings of Janai et al. (1978), who determined from direct observation this species to be the most abundant species produced when vaporized at 300°C, and that in this work the arsenic trisulfide is in a compound form with Si gel.

Appendix C - Details of all individual measurements for the Inilchek (C.1) and Summit (C.2) samples.

C.1.1 Major Ion Data for the snowpit and fresh snow events from the Inilchek.

Inilchek Glacier **All concentrations are in μmoles L^{-1}**

Snowpit samples			Depth (m)	Na^+	NH_4^+	K^+	Mg^{2+}	Ca_2^+	Cl^-	NO_3^-	SO_4^{2-}
TS00-	PIT4-	1	0.00	1.18	6.25	0.25	0.79	10.60	1.34	3.04	1.38
TS00-	PIT4-	2	0.20	0.86	5.50	0.19	1.16	15.30	1.07	1.90	0.92
TS00-	PIT4-	3	0.40	1.65	4.13	0.26	2.91	14.41	1.81	0.99	1.16
TS00-	PIT4-	4	0.60	2.80	6.15	0.20	1.26	12.73	2.70	2.15	1.44
TS00-	PIT4-	5	0.80	3.75	7.55	0.33	1.92	24.01	3.38	3.35	2.53
TS00-	PIT4-	6	1.00	4.30	8.11	0.44	2.17	32.32	3.78	3.76	4.93
TS00-	PIT4-	7	1.20	4.81	9.76	0.48	1.83	27.92	2.75	3.50	4.03
"	"	"									4.03
TS00-	PIT4-	8	1.40	9.73	8.36	0.57	2.52	55.49	7.05	6.21	7.29
TS00-	PIT4-	9	1.60	6.68	11.64	0.60	2.04	41.64	20.16	5.78	5.34
TS00-	PIT4-	10	1.80	4.60	9.67	0.48	1.51	30.26	3.51	5.07	5.59
TS00-	PIT4-	11	2.00	2.38	7.05	0.37	1.06	23.96	1.99	2.18	1.41
TS00-	PIT4-	12	2.20	2.47	7.61	0.71	0.65	97.54		1.53	0.99
TS00-	PIT4-	13	2.40	1.89	4.49	0.31	0.66	17.04	3.43	1.80	1.13
TS00-	PIT4-	14	2.60	6.20	8.20	0.61	2.41	30.93	5.35	3.05	2.94
"	"	"									2.94
TS00-	PIT4-	15	2.80	5.25	8.13	0.51	2.00	30.76	3.89	2.53	2.45
TS00-	PIT4-	16	3.00	7.08	7.36	0.79	3.61	30.39	5.02	2.74	3.77
TS00-	PIT4-	17	3.20	6.78	10.22	0.63	3.03	55.00	4.29	3.88	6.06
TS00-	PIT4-	18	3.40	13.46	7.44	0.83	3.24	75.46	7.29	4.77	10.46
TS00-	PIT4-	19	3.60	4.47	5.20	0.80	1.55	35.70	2.93	3.40	3.42
"	"	"									3.41
TS00-	PIT4-	20	3.80	6.99	8.36	0.76	1.65	49.54	5.09	3.44	5.31
			Avg	**4.87**	**7.56**	**0.51**	**1.90**	**35.55**	**4.57**	**3.25**	**3.61**
			Std (1σ)	**3.10**	**1.92**	**0.21**	**0.86**	**22.03**	**4.14**	**1.39**	**2.36**

Fresh snow samples			Na^+	NH_4^+	K^+	Mg^{2+}	Ca_2^+	Cl^-	NO_3^-	SO_4^{2-}
TS00-	FS7/31-	10	0.60	16.81	0.74	0.52	5.82	1.27	8.26	4.00
TS00-	FS7/31-	20	0.64	16.45	0.90	0.40	3.75	1.26	6.64	4.44
TS00-	FS7/31-	30	0.66	17.20	0.98	0.46	9.95	26.21	6.70	4.44
		Avg	**0.64**	**16.82**	**0.88**	**0.46**	**6.51**	**9.58**	**7.20**	**4.29**
		Std (1σ)	**0.03**	**0.37**	**0.12**	**0.06**	**3.16**	**14.40**	**0.92**	**0.26**
TS00-	FS8/03-	10	0.70	3.36	0.26	0.12	1.07	0.73	1.97	1.41
TS00-	FS8/03-	20	1.57	2.70	0.34	0.13	0.97	1.13	2.03	1.13
TS00-	FS8/03-	30	2.75	2.12	0.55	0.12	0.49	1.84	1.68	0.86
		Avg	**1.67**	**2.73**	**0.38**	**0.12**	**0.85**	**1.23**	**1.90**	**1.13**
		Std (1σ)	**1.03**	**0.62**	**0.15**	**0.01**	**0.31**	**0.56**	**0.19**	**0.28**

C.1.2 Details of all individual measurements for the Inilchek snowpit using Double Spike #2.

Inilchek Glacier

Sample ID	Sulfur #	Top Depth (cm)	S (ppm) (UM)	S (ppm) (NIST)	Expanded Uncertainty (95% C.I.)	Relative (%)
TS00-PIT4-01	**S-2884**	0	0.03	0.05	0.00085	1.84%
TS00-PIT4-02	**S-2879**	20	0.03	0.03	0.00014	0.47%
TS00-PIT4-03	**S-2894**	40	0.02	0.04	0.00027	0.69%
TS00-PIT4-04	**S-2895**	60	0.03	0.05	0.00028	0.59%
TS00-PIT4-05	**S-2846**	80	0.06	0.08	0.00044	0.52%
TS00-PIT4-06*	**S-2794**	100	0.12	0.17	0.00070	0.42%
TS00-PIT4-07	**S-2847**	120	0.10	0.13	0.00054	0.40%
	S-2847c	120	0.10	0.13	0.00054	0.40%
TS00-PIT4-08*	**S-2795**	140	0.19	0.24	0.00094	0.39%
TS00-PIT4-09	**S-2854**	160	0.14	0.18	0.00085	0.48%
TS00-PIT4-10	**S-2848r**	180	0.10	0.19	0.00066	0.35%
TS00-PIT4-11	**S-2880**	200	0.03	0.05	0.00019	0.41%
TS00-PIT4-12	**S-2889**	220	0.02	0.03	0.00033	1.01%
TS00-PIT4-13	**S-2885**	240	0.03	0.04	0.00084	2.24%
TS00-PIT4-14	**S-2842**	260	0.07	0.10	0.00051	0.51%
	S-2842c	260	0.07	0.10	0.00051	0.51%
TS00-PIT4-15	**S-2820**	280	0.08	0.08	0.00045	0.55%
TS00-PIT4-16	**S-2810r**	300	0.10	0.13	0.00051	0.41%
TS00-PIT4-17	**S-2843**	320	0.16	0.20	0.00080	0.40%
TS00-PIT4-18	**S-2796**	340	0.22	0.35	0.00129	0.37%
TS00-PIT4-19	**S-2855**	360	0.08	0.11	0.00075	0.66%
	S-2855c	360	0.08	0.11	0.00075	0.66%
TS00-PIT4-20	**S-2844**	380	0.13	0.18	0.00073	0.41%
		Avg	**0.09**	**0.12**		
FS7/31-10	**S-2856**	--	0.11	0.13	0.00078	0.58%
FS7/31-20	**S-2811**	--	0.12	0.15	0.00058	0.39%
FS7/31-30*	**S-2812**	--	0.12	0.15	0.00058	0.39%
		Avg	**0.12**	**0.14**		
FS8/3-10	**S-2890**	--	0.04	0.05	0.00035	0.75%
FS8/3-20	**S-2908**	--	0.03	0.04	0.00066	1.75%
FS8/3-30	**S-2909**	--	0.02	0.03	0.00066	2.29%
		Avg	**0.03**	**0.04**		

Inilchek Glacier Continued

Sample ID	Sulfur #	S (ppb) (UM)	S (ppb) (NIST)	Expanded Uncertainty (95% C.I.)
TS00-PIT4-01	**S-2884**	30.75	46.11	0.85
TS00-PIT4-02	**S-2879**	25.14	30.91	0.14
TS00-PIT4-03	**S-2894**	21.68	38.90	0.27
TS00-PIT4-04	**S-2895**	26.85	48.23	0.28
TS00-PIT4-05	**S-2846**	58.77	84.55	0.44
TS00-PIT4-06*	**S-2794**	122.07	165.02	0.70
TS00-PIT4-07	**S-2847**	103.69	134.75	0.54
	S-2847c	103.69	134.74	0.54
TS00-PIT4-08*	**S-2795**	187.63	243.93	0.94
TS00-PIT4-09	**S-2854**	143.99	178.72	0.85
TS00-PIT4-10	**S-2848r**	103.06	187.07	0.66
TS00-PIT4-11	**S-2880**	30.49	47.12	0.19
TS00-PIT4-12	**S-2889**	21.76	33.05	0.33
TS00-PIT4-13	**S-2885**	34.37	37.64	0.84
TS00-PIT4-14	**S-2842**	74.91	98.36	0.51
	S-2842c	74.91	98.35	0.51
TS00-PIT4-15	**S-2820**	75.65	81.90	0.45
TS00-PIT4-16	**S-2810r**	95.75	125.97	0.51
TS00-PIT4-17	**S-2843**	155.79	202.75	0.80
TS00-PIT4-18	**S-2796**	216.72	350.01	1.29
TS00-PIT4-19	**S-2855**	80.99	114.46	0.75
	S-2855c	80.99	114.17	0.75
TS00-PIT4-20	**S-2844**	130.38	177.74	0.73
	Avg	**86.96**	**120.63**	
FS7/31-10	**S-2856**	114.37	133.72	0.78
FS7/31-20	**S-2811**	116.87	148.44	0.58
FS7/31-30*	**S-2812**	117.20	148.59	0.58
	Avg	**116.15**	**143.58**	
FS8/3-10	**S-2890**	38.59	47.10	0.35
FS8/3-20	**S-2908**	28.52	37.89	0.66
FS8/3-30	**S-2909**	23.80	28.70	0.66
	Avg	**30.30**	**37.90**	

Inilchek Glacier Continued

Sample ID	Sulfur #	$\delta^{34}S$ (per mil) raw	1σ	2σ	$2\sigma_m$
TS00-PIT4-01	**S-2884**	**-8.26**	0.52	1.04	0.15
TS00-PIT4-02	**S-2879**	**-3.07**	0.49	0.98	0.14
TS00-PIT4-03	**S-2894**	**-4.34**	1.20	2.40	0.34
TS00-PIT4-04	**S-2895**	**1.62**	0.74	1.47	0.21
TS00-PIT4-05	**S-2846**	**1.53**	0.66	1.31	0.19
TS00-PIT4-06*	**S-2794**	**-10.30**	0.69	1.38	0.20
TS00-PIT4-07	**S-2847**	**2.70**	0.60	1.20	0.17
	S-2847c	**1.45**	0.71	1.43	0.20
TS00-PIT4-08*	**S-2795**	**-8.00**	0.66	1.33	0.19
TS00-PIT4-09	**S-2854**	**-1.51**	0.70	1.40	0.20
TS00-PIT4-10	**S-2848r**	**2.01**	0.43	0.86	0.12
TS00-PIT4-11	**S-2880**	**-3.22**	0.71	1.42	0.20
TS00-PIT4-12	**S-2889**	**-2.27**	0.81	1.61	0.23
TS00-PIT4-13	**S-2885**	**0.30**	0.73	1.46	0.21
TS00-PIT4-14	**S-2842**	**-2.82**	1.15	2.29	0.32
	S-2842c	**-3.97**	0.57	1.14	0.16
TS00-PIT4-15	**S-2820**	**-3.93**	0.76	1.52	0.21
TS00-PIT4-16	**S-2810r**	**-4.78**	0.58	1.16	0.16
TS00-PIT4-17	**S-2843**	**0.90**	0.79	1.57	0.22
TS00-PIT4-18	**S-2796**	**-8.57**	0.78	1.56	0.22
TS00-PIT4-19	**S-2855**	**-7.51**	0.55	1.09	0.15
	S-2855c	**-4.21**	0.54	1.07	0.15
TS00-PIT4-20	**S-2844**	**-4.18**	0.83	1.66	0.24
	Avg	**-3.06**	**0.70**	**1.41**	**0.20**
FS7/31-10	**S-2856**	**-3.74**	0.70	1.41	0.20
FS7/31-20	**S-2811**	**-9.39**	0.54	1.07	0.20
FS7/31-30*	**S-2812**	**-10.20**	1.10	2.19	0.31
	Avg	**-7.78**	**0.78**	**1.56**	**0.23**
FS8/3-10	**S-2890**	**-7.34**	0.81	1.63	0.23
FS8/3-20	**S-2908**	**-7.02**	0.81	1.62	0.23
FS8/3-30	**S-2909**	**-3.61**	0.51	1.03	0.15
	Avg	**-5.99**	**0.71**	**1.42**	**0.20**

Inilchek Glacier Continued

Sample ID	Sulfur #	$\delta^{34}S$ (per mil) corrected for instrumental fractionation	1σ	2σ	$2\sigma_m$
TS00-PIT4-01	**S-2884**	**4.14**	0.21	0.42	0.06
TS00-PIT4-02	**S-2879**	**4.39**	0.22	0.43	0.06
TS00-PIT4-03	**S-2894**	**5.58**	0.94	1.87	0.27
TS00-PIT4-04	**S-2895**	**6.76**	0.53	1.06	0.15
TS00-PIT4-05	**S-2846**	**6.50**	0.34	0.69	0.10
TS00-PIT4-06*	**S-2794**	**7.58**	0.55	1.10	0.16
TS00-PIT4-07	**S-2847**	**6.34**	0.32	0.64	0.09
	S-2847c	**6.26**	0.35	0.70	0.10
TS00-PIT4-08*	**S-2795**	**6.26**	0.59	1.17	0.17
TS00-PIT4-09	**S-2854**	**7.07**	0.27	0.53	0.08
TS00-PIT4-10	**S-2848r**	**6.60**	0.21	0.43	0.06
TS00-PIT4-11	**S-2880**	**4.13**	0.22	0.44	0.06
TS00-PIT4-12	**S-2889**	**5.78**	0.22	0.44	0.06
TS00-PIT4-13	**S-2885**	**6.25**	0.42	0.84	0.12
TS00-PIT4-14	**S-2842**	**6.52**	0.48	0.95	0.13
	S-2842c	**6.56**	0.30	0.59	0.08
TS00-PIT4-15	**S-2820**	**6.84**	0.45	0.89	0.13
TS00-PIT4-16	**S-2810r**	**7.41**	0.23	0.46	0.07
TS00-PIT4-17	**S-2843**	**6.52**	0.43	0.86	0.12
TS00-PIT4-18	**S-2796**	**5.08**	0.37	0.74	0.10
TS00-PIT4-19	**S-2855**	**2.71**	0.36	0.72	0.10
	S-2855c	**2.67**	0.30	0.59	0.08
TS00-PIT4-20	**S-2844**	**5.22**	0.25	0.50	0.07
	Avg	**5.79**	**0.37**	**0.74**	**0.11**
FS7/31-10	**S-2856**	**2.82**	0.36	0.71	0.10
FS7/31-20	**S-2811**	**3.12**	0.32	0.63	0.12
FS7/31-30*	**S-2812**	**3.07**	0.53	1.05	0.15
	Avg	**3.00**	**0.40**	**0.80**	**0.12**
FS8/3-10	**S-2890**	**2.51**	0.29	0.57	0.08
FS8/3-20	**S-2908**	**2.57**	0.52	1.05	0.15
FS8/3-30	**S-2909**	**2.51**	0.20	0.40	0.06
	Avg	**2.53**	**0.34**	**0.67**	**0.10**

Inilchek Glacier Continued

Sample ID	Sulfur #	$\delta^{34}S$ (per mil) blank-corrected	1σ	2σ	$2\sigma_m$
TS00-PIT4-01	**S-2884**	**4.11**	0.06	0.12	2.46
TS00-PIT4-02	**S-2879**	**4.35**	0.06	0.12	2.26
TS00-PIT4-03	**S-2894**	**5.54**	0.06	0.12	1.28
TS00-PIT4-04	**S-2895**	**6.74**	0.05	0.11	1.38
TS00-PIT4-05	**S-2846**	**6.49**	0.05	0.10	1.90
TS00-PIT4-06*	**S-2794**	**7.57**	0.05	0.10	1.25
TS00-PIT4-07	**S-2847**	**6.34**	0.05	0.10	1.89
	S-2847c	**6.25**	0.05	0.10	2.03
TS00-PIT4-08*	**S-2795**	**6.25**	0.05	0.10	1.13
TS00-PIT4-09	**S-2854**	**7.06**	0.05	0.10	2.61
TS00-PIT4-10	**S-2848r**	**6.60**	0.05	0.10	2.02
TS00-PIT4-11	**S-2880**	**4.10**	0.06	0.11	3.21
TS00-PIT4-12	**S-2889**	**5.74**	0.06	0.12	3.66
TS00-PIT4-13	**S-2885**	**6.22**	0.06	0.11	1.75
TS00-PIT4-14	**S-2842**	**6.51**	0.05	0.10	2.41
	S-2842c	**6.54**	0.05	0.10	1.93
TS00-PIT4-15	**S-2820**	**6.83**	0.05	0.10	1.70
TS00-PIT4-16	**S-2810r**	**7.40**	0.05	0.10	2.50
TS00-PIT4-17	**S-2843**	**6.51**	0.05	0.10	1.82
TS00-PIT4-18	**S-2796**	**5.08**	0.05	0.10	2.11
TS00-PIT4-19	**S-2855**	**2.68**	0.05	0.11	1.52
	S-2855c	**2.63**	0.05	0.11	1.81
TS00-PIT4-20	**S-2844**	**5.20**	0.05	0.10	3.36
	Avg	**5.77**	**0.05**	**0.11**	**2.09**
FS7/31-10	**S-2856**	**2.79**	0.05	0.10	1.97
FS7/31-20	**S-2811**	**3.10**	0.05	0.10	1.69
FS7/31-30*	**S-2812**	**3.05**	0.05	0.10	2.08
	Avg	**2.98**	**0.05**	**0.10**	**1.92**
FS8/3-10	**S-2890**	**2.43**	0.09	0.18	2.84
FS8/3-20	**S-2908**	**2.42**	0.17	0.35	1.55
FS8/3-30	**S-2909**	**2.32**	0.23	0.46	2.55
	Avg	**2.39**	**0.16**	**0.33**	**2.31**

Inilchek Glacier Continued

Sample ID	Sulfur #	Voltage on 34	Voltage on 34 (@ end)	Approximate Sample/ Blank Molar Ratio	μmoles of natural
TS00-PIT4-01	**S-2884**	116-51	51	126	0.40
TS00-PIT4-02	**S-2879**	151-50	50	110	0.35
TS00-PIT4-03	**S-2894**	40-6	6	84	0.26
TS00-PIT4-04	**S-2895**	34-25	25	101	0.32
TS00-PIT4-05	**S-2846**	155-23	23	222	0.57
TS00-PIT4-06*	**S-2794**	35-34	34	425	1.19
TS00-PIT4-07	**S-2847**	151-24	24	326	0.92
	S-2847c	165-24	24	326	0.92
TS00-PIT4-08*	**S-2795**	64-19	19	587	1.65
TS00-PIT4-09	**S-2854**	115-33	33	379	1.06
TS00-PIT4-10	**S-2848r**	139-53	53	428	1.20
TS00-PIT4-11	**S-2880**	92-72	72	139	0.44
TS00-PIT4-12	**S-2889**	118-57	57	85	0.27
TS00-PIT4-13	**S-2885**	43-35	35	113	0.29
TS00-PIT4-14	**S-2842**	45-19	19	165	0.43
	S-2842c	136-30	30	165	0.43
TS00-PIT4-15	**S-2820**	25-15	15	178	0.46
TS00-PIT4-16	**S-2810r**	152-50	50	222	0.57
TS00-PIT4-17	**S-2843**	142-21	21	310	0.87
TS00-PIT4-18	**S-2796**	59-29	29	649	1.82
TS00-PIT4-19	**S-2855**	115-30	30	210	0.54
	S-2855c	130-41	41	209	0.54
TS00-PIT4-20	**S-2844**	124-32	32	278	0.78
			Avg	**254**	**0.71**
FS7/31-10	**S-2856**	69-20	20	230	0.60
FS7/31-20	**S-2811**	28-33	33	250	0.65
FS7/31-30*	**S-2812**	30-17	17	245	0.63
			Avg	**242**	**0.63**
FS8/3-10	**S-2890**	113-36	36	74	0.23
FS8/3-20	**S-2908**	47-29	29	41	0.13
FS8/3-30	**S-2909**	147-66	66	33	0.10
			Avg	**49**	**0.16**

Inilchek Glacier Continued

Sample ID	Sulfur #	µgrams natural	Sample/Spike Ratio Molar Ratio	Range of Uncor Data	Per mil Change thru Run
TS00-PIT4-01	**S-2884**	13	3.1	-10--8.4	1.6
TS00-PIT4-02	**S-2879**	11	2.3	-5.5--4	1.5
TS00-PIT4-03	**S-2894**	8	3.4	-6.8--2	4.8
TS00-PIT4-04	**S-2895**	10	2.9	-0.20-0.75	1.0
TS00-PIT4-05	**S-2846**	18	2.9	-1-0.5	1.5
TS00-PIT4-06*	**S-2794**	38	2.6	-12--10.5	1.5
TS00-PIT4-07	**S-2847**	29	2.5	0.5-2.5	3.0
	S-2847c	29	2.5	-1-1.5	2.5
TS00-PIT4-08*	**S-2795**	53	2.3	-10.5--8.5	2.0
TS00-PIT4-09	**S-2854**	34	2.3	-4--2	2.0
TS00-PIT4-10	**S-2848r**	39	3.6	0.3-1.06	1.4
TS00-PIT4-11	**S-2880**	14	2.4	-5.5--4	1.5
TS00-PIT4-12	**S-2889**	9	3.4	-4.5--2.2	2.3
TS00-PIT4-13	**S-2885**	9	2.1	-2.2--0.5	1.7
TS00-PIT4-14	**S-2842**	14	3.0	-6--2.6	3.4
	S-2842c	14	3.0	-6--4	2.0
TS00-PIT4-15	**S-2820**	15	2.0	-6.4--5	1.4
TS00-PIT4-16	**S-2810r**	18	2.3	-7--5	2.0
TS00-PIT4-17	**S-2843**	28	2.2	-1.8--0.2	2.0
TS00-PIT4-18	**S-2796**	58	2.9	-10.6--9	1.6
TS00-PIT4-19	**S-2855**	17	2.5	-9.5--8	1.5
	S-2855c	17	2.5	-6.5-5	1.5
TS00-PIT4-20	**S-2844**	25	2.6	-7--4	3.0
	Avg	**23**	**2.7**		**2.0**
FS7/31-10	**S-2856**	19	2.4	-6.2--4.5	1.7
FS7/31-20	**S-2811**	21	2.1	12.3--10.4	1.9
FS7/31-30*	**S-2812**	20	2.1	-13.5--10	3.5
	Avg	**20**	**2.2**		**2.4**
FS8/3-10	**S-2890**	7	2.3	-10.5--7.8	2.7
FS8/3-20	**S-2908**	4	2.4	-9.2--7.8	1.4
FS8/3-30	**S-2909**	3	1.9	-6.2--4.3	1.9
	Avg	**5**	**2.2**		**2.0**

C.1.3 Mass balance calculations for the Inilchek snowpit samples.

Inilchek Glacier Samples

Sample ID	Sulfur #	Top Depth (cm)	Amount of Meltwater Used (mL)	S (ppm) (NIST)	Expanded Uncertainty (95% C.I.)	Relative (%)
TS00-PIT4-01	**S-2884**	0	276	0.05	0.00085	1.84%
TS00-PIT4-02	**S-2879**	20	358	0.03	0.00014	0.47%
TS00-PIT4-03	**S-2894**	40	218	0.04	0.00027	0.69%
TS00-PIT4-04	**S-2895**	60	211	0.05	0.00028	0.59%
TS00-PIT4-05	**S-2846**	80	218	0.08	0.00044	0.52%
TS00-PIT4-06*	**S-2794**	100	233	0.17	0.00070	0.42%
TS00-PIT4-07	**S-2847**	120	218	0.13	0.00054	0.40%
	S-2847c	120	218	0.13	0.00054	0.40%
TS00-PIT4-08*	**S-2795**	140	217	0.24	0.00094	0.39%
TS00-PIT4-09	**S-2854**	160	191	0.18	0.00085	0.48%
TS00-PIT4-10	**S-2848r**	180	206	0.19	0.00066	0.35%
TS00-PIT4-11	**S-2880**	200	297	0.05	0.00019	0.41%
TS00-PIT4-12	**S-2889**	220	261	0.03	0.00033	1.01%
TS00-PIT4-13	**S-2885**	240	249	0.04	0.00084	2.24%
TS00-PIT4-14	**S-2842**	260	139	0.10	0.00051	0.51%
	S-2842c	260	139	0.10	0.00051	0.51%
TS00-PIT4-15	**S-2820**	280	180	0.08	0.00045	0.55%
TS00-PIT4-16	**S-2810r**	300	146	0.13	0.00051	0.41%
TS00-PIT4-17	**S-2843**	320	138	0.20	0.00080	0.40%
TS00-PIT4-18	**S-2796**	340	167	0.35	0.00129	0.37%
TS00-PIT4-19	**S-2855**	360	152	0.11	0.00075	0.66%
	S-2855c	360	152	0.11	0.00075	0.66%
TS00-PIT4-20	**S-2844**	380	141	0.18	0.00073	0.41%
		Avg	**205**			
FS7/31-10	**S-2856**	--	143	0.13	0.00078	0.58%
FS7/31-20	**S-2811**	--	140	0.15	0.00058	0.39%
FS7/31-30*	**S-2812**	--	137	0.15	0.00058	0.39%
		Avg	**140**			
FS8/3-10	**S-2890**	--	159	0.05	0.00035	0.75%
FS8/3-20	**S-2908**	--	108	0.04	0.00066	1.75%
FS8/3-30	**S-2909**	--	117	0.03	0.00066	2.29%
		Avg	**128**			

Inilchek Glacier Samples Continued

Sample ID	Sulfur #	S (ppb) (NIST)	Expanded Uncertainty (95% C.I.)	$\delta^{34}S$ (per mil) blank-corrected
TS00-PIT4-01	**S-2884**	46.11	0.85	4.11
TS00-PIT4-02	**S-2879**	30.91	0.14	4.35
TS00-PIT4-03	**S-2894**	38.90	0.27	5.54
TS00-PIT4-04	**S-2895**	48.23	0.28	6.74
TS00-PIT4-05	**S-2846**	84.55	0.44	6.49
TS00-PIT4-06*	**S-2794**	165.02	0.70	7.57
TS00-PIT4-07	**S-2847**	134.75	0.54	6.34
	S-2847c	134.74	0.54	6.25
TS00-PIT4-08*	**S-2795**	243.93	0.94	6.25
TS00-PIT4-09	**S-2854**	178.72	0.85	7.06
TS00-PIT4-10	**S-2848r**	187.07	0.66	6.60
TS00-PIT4-11	**S-2880**	47.12	0.19	4.10
TS00-PIT4-12	**S-2889**	33.05	0.33	5.74
TS00-PIT4-13	**S-2885**	37.64	0.84	6.22
TS00-PIT4-14	**S-2842**	98.36	0.51	6.51
	S-2842c	98.35	0.51	6.54
TS00-PIT4-15	**S-2820**	81.90	0.45	6.83
TS00-PIT4-16	**S-2810r**	125.97	0.51	7.40
TS00-PIT4-17	**S-2843**	202.75	0.80	6.51
TS00-PIT4-18	**S-2796**	350.01	1.29	5.08
TS00-PIT4-19	**S-2855**	114.46	0.75	2.68
	S-2855c	114.17	0.75	2.63
TS00-PIT4-20	**S-2844**	177.74	0.73	5.20
	Avg	**120.63**		
FS7/31-10	**S-2856**	133.72	0.78	2.79
FS7/31-20	**S-2811**	148.44	0.58	3.10
FS7/31-30*	**S-2812**	148.59	0.58	3.05
	Avg	**143.58**		
FS8/3-10	**S-2890**	47.10	0.35	2.43
FS8/3-20	**S-2908**	37.89	0.66	2.42
FS8/3-30	**S-2909**	28.70	0.66	2.32
	Avg	**37.90**		

Inilchek Glacier Samples Continued

Sample ID	Sulfur #	nss-SO_4^{2-} (ppb, µg/L) NIST	Expanded Uncertainty (95% C.I.)	Fdust (%): X	Fanthro (%): 1-X	dust-SO_4^{2-} (ppb, µg/L) NIST	anthro-SO_4^{2-} (ppb, µg/L) NIST
TS00-PIT4-01	**S-2884**	132.40	2.43	21%	79%	27.19	105.21
TS00-PIT4-02	**S-2879**	88.77	0.42	22%	78%	19.31	69.46
TS00-PIT4-03	**S-2894**	111.70	0.77	28%	72%	30.96	80.74
TS00-PIT4-04	**S-2895**	138.49	0.82	34%	66%	46.67	91.83
TS00-PIT4-05	**S-2846**	242.80	1.27	32%	68%	78.74	164.06
TS00-PIT4-06*	**S-2794**	473.87	2.00	38%	62%	179.43	294.43
TS00-PIT4-07	**S-2847**	386.93	1.54	32%	68%	122.58	264.35
	S-2847c	386.92	1.54	31%	69%	120.95	265.97
TS00-PIT4-08*	**S-2795**	700.44	2.70	31%	69%	219.00	481.44
TS00-PIT4-09	**S-2854**	513.18	2.45	35%	65%	181.20	331.98
TS00-PIT4-10	**S-2848r**	537.18	1.89	33%	67%	177.21	359.97
TS00-PIT4-11	**S-2880**	135.31	0.55	20%	80%	27.72	107.59
TS00-PIT4-12	**S-2889**	94.91	0.96	29%	71%	27.25	67.66
TS00-PIT4-13	**S-2885**	108.08	2.42	31%	69%	33.62	74.46
TS00-PIT4-14	**S-2842**	282.43	1.45	33%	67%	91.90	190.53
	S-2842c	282.40	1.45	33%	67%	92.35	190.05
TS00-PIT4-15	**S-2820**	235.18	1.29	34%	66%	80.27	154.91
TS00-PIT4-16	**S-2810r**	361.72	1.47	37%	63%	133.84	227.88
TS00-PIT4-17	**S-2843**	582.18	2.31	33%	67%	189.53	392.65
TS00-PIT4-18	**S-2796**	1005.04	3.71	25%	75%	255.23	749.81
TS00-PIT4-19	**S-2855**	328.67	2.16	13%	87%	44.09	284.59
	S-2855c	327.84	2.16	13%	87%	43.17	284.67
TS00-PIT4-20	**S-2844**	510.39	2.08	26%	74%	132.77	377.62
	Avg	**346.38**		**29%**	**71%**	**102.39**	**243.99**
FS7/31-10	**S-2856**	383.97	2.24	14%	86%	53.55	330.42
FS7/31-20	**S-2811**	426.25	1.67	15%	85%	66.03	360.22
FS7/31-30*	**S-2812**	426.66	1.68	15%	85%	65.04	361.62
	Avg	**412.29**		**15%**	**85%**	**61.54**	**350.76**
FS8/3-10	**S-2890**	135.26	1.02	12%	88%	16.40	118.86
FS8/3-20	**S-2908**	108.80	1.90	12%	88%	13.17	95.63
FS8/3-30	**S-2909**	82.41	1.89	12%	88%	9.55	72.86
	Avg	**108.82**		**12%**	**88%**	**13.04**	**95.78**

C.2.1 Major Ion Data for the Summit snowpit.

Summit, Greenland

Snowpit samples	Top Depth (m)	Na^+	K^+	Mg^{2+}	Ca^{2+}	Cl^-	NO_3^-
1.00	0.01	0.15	0.04	0.07	0.42	0.57	0.90
2.00	0.03	0.15	0.02	0.03	0.37	0.51	0.91
3.00	0.05	0.07	0.02	0.04	0.35	0.45	0.76
4.00	0.07	0.89	0.09	0.15	0.88	0.99	1.06
5.00	0.09	0.36	0.03	0.16	0.86	0.52	1.12
6.00	0.11	0.39	0.04	0.03	0.32	0.49	1.07
7.00	0.13	0.33	0.02	0.01	0.23	0.47	1.01
8.00	0.15	0.34	0.02	0.00	0.17	0.44	1.04
9.00	0.17	0.49	0.05	0.00	0.11	0.54	0.99
10.00	0.19	0.14	0.00	0.00	0.06	0.34	1.18
11.00	0.21	0.19	0.02	0.00	0.13	0.37	1.35
12.00	0.23	0.24	0.03	0.00	0.12	0.38	1.54
13.00	0.25	0.29	0.03	0.02	0.14	0.44	1.60
14.00	0.27	0.31	0.02	0.01	0.17	0.47	1.69
15.00	0.29	0.16	0.03	0.00	0.08	0.47	2.83
16.00	0.31	0.20	0.02	0.00	0.06	0.51	3.26
17.00	0.33	0.15	0.03	0.00	0.06	0.52	3.23
18.00	0.35	0.26	0.02	0.00	0.05	0.51	3.16
19.00	0.37	0.21	0.03	0.00	0.17	0.45	2.90
20.00	0.39	0.25	0.02	0.00	0.09	0.38	1.35
21.00	0.41	0.25	0.04	0.03	0.24	0.47	1.59
22.00	0.43	0.19	0.03	0.03	0.26	0.46	1.55
23.00	0.45	0.17	0.03	0.00	0.12	0.40	1.49
24.00	0.47	0.17	0.03	0.00	0.04	0.35	1.18
25.00	0.49	0.16	0.03	0.00	0.02	0.34	1.18
26.00	0.51	0.18	0.02	0.00	0.05	0.35	1.17
27.00	0.53	0.31	0.02	0.00	0.04	0.38	1.44
28.00	0.55	0.48	0.06	0.02	0.31	0.52	2.31
29.00	0.57	0.16	0.03	0.00	0.13	0.47	2.14
30.00	0.59	0.16	0.03	0.01	0.03	0.37	1.33
31.00	0.61	0.19	0.04	0.00	0.03	0.36	1.06
32.00	0.63	0.13	0.03	0.00	0.05	0.43	2.48
33.00	0.65	0.02	0.03	0.00	0.10	0.82	8.71
34.00	0.67	0.01	0.03	0.00	0.04	1.00	10.05
35.00	0.69	0.08	0.02	0.00	0.00	0.38	4.16
36.00	0.71	0.13	0.02	0.00	0.00	0.46	2.46
37.00	0.73	0.18	0.03	0.00	0.00	0.38	1.37
38.00	0.75	0.27	0.03	0.00	0.02	0.46	1.23
39.00	0.77	0.17	0.02	0.00	0.00	0.43	1.13
40.00	0.79	0.23	0.03	0.00	0.00	0.47	1.20
41.00	0.81	0.20	0.03	0.00	0.00	0.47	1.21
42.00	0.83	0.23	0.03	0.00	0.05	0.49	1.48
43.00	0.85	0.20	0.03	0.01	0.27	0.55	1.84
44.00	0.87	0.21	0.03	0.01	0.32	0.52	1.83
45.00	0.89	0.19	0.03	0.01	0.31	0.50	1.80

Summit, Greenland
Continued

Snowpit samples	Top Depth (m)	Na^+	K^+	Mg^{2+}	Ca^{2+}	Cl^-	NO_3^-
46.00	0.91	0.22	0.04	0.02	0.33	0.52	1.90
47.00	0.93	0.22	0.04	0.02	0.31	0.50	1.98
48.00	0.95	0.24	0.04	0.06	0.42	0.49	2.29
49.00	0.97	0.32	0.04	0.02	0.20	0.45	1.51
50.00	0.99	0.21	0.02	0.00	0.07	0.41	1.27
51.00	1.01	0.60	0.03	0.05	0.13	0.69	1.06
52.00	1.03	0.42	0.03	0.02	0.09	0.54	1.35
53.00	1.05	0.50	0.03	0.03	0.13	0.59	1.64
54.00	1.07	0.36	0.02	0.01	0.06	0.52	1.83
55.00	1.09	0.29	0.02	0.00	0.06	0.52	1.90
56.00	1.11	0.23	0.02	0.03	0.20	0.51	1.97
57.00	1.13	0.27	0.04	0.02	0.11	0.50	1.71
58.00	1.15	0.21	0.03	0.00	0.04	0.32	1.13
59.00	1.17	0.19	0.03	0.00	0.02	0.34	0.90
60.00	1.19	0.17	0.02	0.00	0.01	0.33	0.88
61.00	1.21	0.13	0.02	0.00	0.02	0.34	0.85
62.00	1.23	0.17	0.02	0.00	0.00	0.33	0.90
63.00	1.25	0.17	0.02	0.00	0.01	0.34	1.02
64.00	1.27	0.16	0.02	0.00	0.00	0.33	1.06
65.00	1.29	0.18	0.02	0.00	0.02	0.37	1.12
66.00	1.31	0.20	0.02	0.00	0.03	0.33	1.03
67.00	1.33	0.15	0.02	0.00	0.02	0.32	1.50
68.00	1.35	0.27	0.04	0.00	0.05	0.47	2.36
69.00	1.37	0.17	0.03	0.00	0.02	0.43	2.22
70.00	1.39	0.18	0.03	0.00	0.02	0.40	1.62
71.00	1.41	0.26	0.03	0.00	0.04	0.42	1.49
72.00	1.43	0.22	0.04	0.00	0.03	0.45	1.43
73.00	1.45	0.16	0.04	0.00	0.06	0.45	1.62
75.00	1.47	0.19	0.04	0.00	0.06	0.43	1.82
76.00	1.49	0.22	0.12	0.03	0.19	0.94	5.05
77.00	1.51	0.02	0.05	0.01	0.14	0.90	6.27
	Average	**0.23**	**0.03**	**0.01**	**0.13**	**0.48**	**1.91**
	Stdev	**0.13**	**0.01**	**0.03**	**0.17**	**0.14**	**1.55**

All concentrations are in μmoles L^{-1}.

Summit, Greenland Continued

Snowpit samples	Top Depth (m)	SO_4^{2-}	MSA
1.00	0.01	0.42	0.05
2.00	0.03	0.31	0.05
3.00	0.05	0.29	0.05
4.00	0.07	0.51	0.03
5.00	0.09	0.78	0.01
6.00	0.11	0.58	0.01
7.00	0.13	0.54	0.01
8.00	0.15	0.56	0.01
9.00	0.17	0.35	0.01
10.00	0.19	0.29	0.01
11.00	0.21	0.48	0.01
12.00	0.23	0.66	0.01
13.00	0.25	0.80	0.01
14.00	0.27	0.41	0.01
15.00	0.29	0.72	0.01
16.00	0.31	0.80	0.01
17.00	0.33	0.82	0.01
18.00	0.35	0.82	0.01
19.00	0.37	0.69	0.01
20.00	0.39	0.51	0.01
21.00	0.41	1.01	0.02
22.00	0.43	0.97	0.02
23.00	0.45	0.42	0.02
24.00	0.47	0.31	0.01
25.00	0.49	0.33	0.01
26.00	0.51	0.32	0.01
27.00	0.53	0.45	0.02
28.00	0.55	0.34	0.03
29.00	0.57	0.25	0.04
30.00	0.59	0.24	0.02
31.00	0.61	0.25	0.02
32.00	0.63	0.25	0.01
33.00	0.65	0.60	0.01
34.00	0.67	0.70	0.01
35.00	0.69	0.20	0.01
36.00	0.71	0.26	0.03
37.00	0.73	0.24	0.04
38.00	0.75	0.26	0.03
39.00	0.77	0.28	0.03
40.00	0.79	0.27	0.04
41.00	0.81	0.29	0.04
42.00	0.83	0.39	0.09
43.00	0.85	0.39	0.02
44.00	0.87	0.32	0.02
45.00	0.89	0.30	0.02

Summit, Greenland Continued

Snowpit samples	Top Depth (m)	SO_4^{2-}	MSA
46.00	0.91	0.32	0.03
47.00	0.93	0.34	0.03
48.00	0.95	0.61	0.02
49.00	0.97	0.47	0.03
50.00	0.99	0.46	0.03
51.00	1.01	1.31	0.02
52.00	1.03	0.51	0.01
53.00	1.05	0.38	0.01
54.00	1.07	0.44	0.01
55.00	1.09	0.49	0.01
56.00	1.11	0.53	0.01
57.00	1.13	0.71	0.01
58.00	1.15	0.22	0.01
59.00	1.17	0.16	0.01
60.00	1.19	0.16	0.01
61.00	1.21	0.17	0.01
62.00	1.23	0.15	0.01
63.00	1.25	0.15	0.01
64.00	1.27	0.14	0.01
65.00	1.29	0.35	0.01
66.00	1.31	0.25	0.02
67.00	1.33	0.19	0.03
68.00	1.35	0.35	0.02
69.00	1.37	0.41	0.04
70.00	1.39	0.25	0.05
71.00	1.41	0.19	0.05
72.00	1.43	0.21	0.03
73.00	1.45	0.25	0.02
75.00	1.47	0.21	0.02
76.00	1.49	0.70	0.04
77.00	1.51	0.71	0.05
	Average	**0.43**	**0.02**
	Stdev	**0.23**	**0.02**

All concentrations are in μmoles L^{-1}.

C.2.2.a Details of all actual individual measurements for the Summit snowpit using Double Spike #2.

Greenland Glacier Samples

Sample ID	Sulfur #	Mid-Point Depth (cm)	S (ppm) (UM)	S (ppm) (NIST)	Expanded Uncertainty (95% C.I.)	Relative (%)	S (ppb) (UM)	S (ppb) (NIST)	Expanded Uncertainty (95% C.I.)
S1-S5	**lost**	5	0.02	--	--	--	15.46	--	--
S6-S10	**S-2899**	15	0.02	0.02	0.00046	2.94%	15.49	15.59	0.46
S11-S15	**S-2903**	25	0.02	0.02	0.00195	10.83%	20.59	18.01	1.95
S16-S20	**S-2904**	35	0.02	0.02	0.00195	8.03%	24.35	24.30	1.95
S21-S25	**S-2913**	45	0.02	0.02	0.00146	8.61%	20.28	16.90	1.46
S26-S29, S31	**S-2914**	56	0.01	0.01	0.00145	12.08%	10.84	12.04	1.45
S32-S35	**S-2918**	66	0.01	0.02	0.00304	18.60%	14.66	16.34	3.04
S36-S40	**S-2919**	75	0.01	0.01	0.00304	51.85%	8.81	5.86	3.04
S41-S45	**S-2923**	85	0.01	0.02	0.00200	10.08%	11.33	19.89	2.00
S46-S50	**S-2924**	95	0.01	0.03	0.00201	6.44%	14.71	31.17	2.01
S51-S55	**S-2928**	105	0.02	0.02	0.00126	7.87%	20.98	16.01	1.26
S56-S60	**S-2929**	115	0.01	0.01	0.00126	12.25%	12.01	10.27	1.26
S61-S65	**S-2933**	125	0.01	0.01	0.00323	47.42%	6.37	6.80	3.23
S66-S70	**S-2934**	135	0.01	0.01	0.00141	13.06%	9.71	10.78	1.41
		Avg	**0.015**	**0.016**			**14.62**	**15.69**	

Greenland Glacier Samples
Continued

Sample ID	Sulfur #	$\delta^{34}S$ (per mil) raw	1σ	2σ	$2\sigma_m$	$\delta^{34}S$ (per mil) corrected for instrumental fractionation	1σ	2σ	$2\sigma_m$
S1-S5	**lost**	**--**	**--**	**--**	**--**	**--**	**--**	**--**	**--**
S6-S10	**S-2899**	**-0.01**	0.68	1.35	0.19	**6.63**	0.61	1.21	0.17
S11-S15	**S-2903**	**-1.72**	1.18	2.36	0.33	**8.07**	6.79	13.58	1.92
S16-S20	**S-2904**	**-0.85**	0.70	1.41	0.20	**4.22**	0.49	0.97	0.14
S21-S25	**S-2913**	**-2.35**	0.79	1.57	0.22	**6.27**	0.38	0.77	0.11
S26-S29, S31	**S-2914**	**1.26**	0.46	0.92	0.13	**6.96**	0.28	0.56	0.08
S32-S35	**S-2918**	**-3.80**	0.44	0.88	0.12	**4.79**	0.30	0.60	0.09
S36-S40	**S-2919**	**2.25**	0.63	1.25	0.18	**10.43**	0.28	0.56	0.08
S41-S45	**S-2923**	**-5.11**	0.66	1.33	0.19	**8.41**	0.16	0.33	0.05
S46-S50	**S-2924**	**-3.48**	0.59	1.17	0.17	**7.02**	0.16	0.32	0.05
S51-S55	**S-2928**	**-6.37**	0.79	1.58	0.22	**3.19**	0.38	0.76	0.11
S56-S60	**S-2929**	**-3.64**	0.92	1.85	0.26	**3.22**	0.30	0.60	0.08
S61-S65	**S-2933**	**-1.36**	0.42	0.84	0.12	**6.69**	0.43	0.86	0.12
S66-S70	**S-2934**	**2.08**	0.49	0.98	0.14	**7.27**	0.25	0.49	0.07
	Avg	**-1.78**	**0.67**	**1.35**	**0.19**	**6.40**	**0.83**	**1.66**	**0.24**
	STD (1σ)	**2.70**				**2.09**			

Greenland Glacier Samples Continued

Sample ID	Sulfur #	$\delta^{34}S$ (per mil) blank-corrected	1σ	2σ	Improvement in Precision Uncor to Cor	Voltage on 34	Voltage on 34 (@ end)
S1-S5	**lost**	**--**	**--**		**--**	**--**	**--**
S6-S10	**S-2899**	**7.83**	0.77	1.55	1.1	21-14	14
S11-S15	**S-2903**	**9.13**	0.58	1.16	0.2	42-8	8
S16-S20	**S-2904**	**4.63**	0.21	0.42	1.4	92-21	21
S21-S25	**S-2913**	**7.11**	0.46	0.93	2.0	86-40	40
S26-S29, S31	**S-2914**	**8.31**	0.91	1.81	1.7	139-52	52
S32-S35	**S-2918**	**5.57**	0.47	0.95	1.5	104-35	35
S36-S40	**S-2919**	**13.31**	2.51	5.01	2.2	91-47	47
S41-S45	**S-2923**	**9.19**	0.37	0.75	4.0	146-57	57
S46-S50	**S-2924**	**7.45**	0.19	0.38	3.7	124-66	66
S51-S55	**S-2928**	**3.60**	0.22	0.45	2.1	71-24	24
S56-S60	**S-2929**	**3.86**	0.44	0.87	3.1	51-30	30
S61-S65	**S-2933**	**8.57**	1.64	3.28	1.0	56-41	41
S66-S70	**S-2934**	**8.55**	0.82	1.64	2.0	69-44	44
	Avg	**7.47**	**0.74**	**1.48**	**2.0**		
	STD (1σ)	**2.63**					

Greenland Glacier Samples Continued

Sample ID	Sulfur #	Approximate Sample/ Blank Molar Ratio	μmoles of natural	μgrams natural	Sample/ Spike Ratio Molar Ratio	Range of Uncor Data (per mil)	Per mil Change thru Run
S1-S5	**lost**	**--**	**--**	**--**	**--**	**--**	**--**
S6-S10	**S-2899**	6.64	0.11	4	1.3	-3.3--2	1.1
S11-S15	**S-2903**	7.97	0.13	4	1.8	-5.5--1.5	4.0
S16-S20	**S-2904**	11.07	0.19	6	2.0	-3--2	1.0
S21-S25	**S-2913**	8.13	0.14	4	1.6	-6--3.7	2.3
S26-S29, S31	**S-2914**	5.68	0.10	3	2.1	-0.9-0.4	1.3
S32-S35	**S-2918**	6.30	0.11	3	2.0	-5.8--4.5	1.3
S36-S40	**S-2919**	2.98	0.05	2	1.1	-0.8-0.8	1.6
S41-S45	**S-2923**	11.00	0.19	6	4.7	-7--4.8	2.2
S46-S50	**S-2924**	17.13	0.29	9	4.7	-5.2--3.5	1.7
S51-S55	**S-2928**	9.00	0.15	5	1.7	-9.3--7	2.3
S56-S60	**S-2929**	5.78	0.10	3	1.5	-7--4	3.0
S61-S65	**S-2933**	3.85	0.07	2	2.8	-3--2	1.0
S66-S70	**S-2934**	6.06	0.10	3	2.1	-0.15-1	1.2
	Avg	**7.81**	**0.13**	**4**	**2.2**		**1.8**

C.2.2.b Details of all modified individual measurements for the Summit snowpit using Double Spike #2. (Modified using improved blank concentration and composition).

Greenland Glacier Samples

Sample ID	Sulfur #	Mid-Point Depth (cm)	S (ppm) (UM)	S (ppm) (NIST)	Expanded Uncertainty (95% C.I.)	Relative (%)	S (ppb) (UM)	S (ppb) (NIST)	Expanded Uncertainty (95% C.I.)
S1-S5	**lost**	5	0.02	--	--	--	15.46	--	--
S6-S10	**S-2899**	15	0.02	0.02	0.00046	2.94%	15.49	15.59	0.46
S11-S15	**S-2903**	25	0.02	0.02	0.00195	10.83%	20.59	18.01	1.95
S16-S20	**S-2904**	35	0.02	0.02	0.00195	8.03%	24.35	24.30	1.95
S21-S25	**S-2913**	45	0.02	0.02	0.00146	8.61%	20.28	16.90	1.46
S26-S29, S31	**S-2914**	56	0.01	0.01	0.00145	12.08%	10.84	12.04	1.45
S32-S35	**S-2918**	66	0.01	0.02	0.00304	18.60%	14.66	16.34	3.04
S36-S40	**S-2919**	75	0.01	0.01	0.00304	51.85%	8.81	5.86	3.04
S41-S45	**S-2923**	85	0.01	0.02	0.00200	10.08%	11.33	19.89	2.00
S46-S50	**S-2924**	95	0.01	0.03	0.00201	6.44%	14.71	31.17	2.01
S51-S55	**S-2928**	105	0.02	0.02	0.00126	7.87%	20.98	16.01	1.26
S56-S60	**S-2929**	115	0.01	0.01	0.00126	12.25%	12.01	10.27	1.26
S61-S65	**S-2933**	125	0.01	0.01	0.00323	47.42%	6.37	6.80	3.23
S66-S70	**S-2934**	135	0.01	0.01	0.00141	13.06%	9.71	10.78	1.41
		Avg	**0.015**	**0.016**			**14.62**	**15.69**	

Greenland Glacier Samples Continued

Sample ID	Sulfur #	$\delta^{34}S$ (per mil) raw	1σ	2σ	$2\sigma_m$	$\delta^{34}S$ (per mil) corrected for instrumental fractionation	1σ	2σ	$2\sigma_m$
S1-S5	**lost**	**--**	**--**	**--**	**--**	**--**	**--**	**--**	**--**
S6-S10	**S-2899**	**-0.01**	0.68	1.35	0.19	**6.63**	0.61	1.21	0.17
S11-S15	**S-2903**	**-1.72**	1.18	2.36	0.33	**8.07**	6.79	13.58	1.92
S16-S20	**S-2904**	**-0.85**	0.70	1.41	0.20	**4.22**	0.49	0.97	0.14
S21-S25	**S-2913**	**-2.35**	0.79	1.57	0.22	**6.27**	0.38	0.77	0.11
S26-S29, S31	**S-2914**	**1.26**	0.46	0.92	0.13	**6.96**	0.28	0.56	0.08
S32-S35	**S-2918**	**-3.80**	0.44	0.88	0.12	**4.79**	0.30	0.60	0.09
S36-S40	**S-2919**	**2.25**	0.63	1.25	0.18	**10.43**	0.28	0.56	0.08
S41-S45	**S-2923**	**-5.11**	0.66	1.33	0.19	**8.41**	0.16	0.33	0.05
S46-S50	**S-2924**	**-3.48**	0.59	1.17	0.17	**7.02**	0.16	0.32	0.05
S51-S55	**S-2928**	**-6.37**	0.79	1.58	0.22	**3.19**	0.38	0.76	0.11
S56-S60	**S-2929**	**-3.64**	0.92	1.85	0.26	**3.22**	0.30	0.60	0.08
S61-S65	**S-2933**	**-1.36**	0.42	0.84	0.12	**6.69**	0.43	0.86	0.12
S66-S70	**S-2934**	**2.08**	0.49	0.98	0.14	**7.27**	0.25	0.49	0.07
	Avg	**-1.78**	**0.67**	**1.35**	**0.19**	**6.40**	**0.83**	**1.66**	**0.24**
	STD (1σ)	**2.70**				**2.09**			

Greenland Glacier Samples
Continued

Sample ID	Sulfur #	$\delta^{34}S$ (per mil) blank-corrected	1σ	2σ	Improvement in Precision Uncor to Cor	Voltage on 34	Voltage on 34 (@ end)
S1-S5	**lost**	**--**	**--**		**--**	**--**	**--**
S6-S10	**S-2899**	**7.83**	0.41	0.83	1.1	21-14	14
S11-S15	**S-2903**	**9.13**	0.37	0.75	0.2	42-8	8
S16-S20	**S-2904**	**4.63**	0.16	0.31	1.4	92-21	21
S21-S25	**S-2913**	**7.11**	0.30	0.59	2.0	86-40	40
S26-S29, S31	**S-2914**	**8.31**	0.46	0.92	1.7	139-52	52
S32-S35	**S-2918**	**5.57**	0.27	0.55	1.5	104-35	35
S36-S40	**S-2919**	**13.31**	0.95	1.91	2.2	91-47	47
S41-S45	**S-2923**	**9.19**	0.28	0.56	4.0	146-57	57
S46-S50	**S-2924**	**7.45**	0.16	0.32	3.7	124-66	66
S51-S55	**S-2928**	**3.60**	0.15	0.30	2.1	71-24	24
S56-S60	**S-2929**	**3.86**	0.23	0.45	3.1	51-30	30
S61-S65	**S-2933**	**8.57**	0.63	1.25	1.0	56-41	41
S66-S70	**S-2934**	**8.55**	0.44	0.88	2.0	69-44	44
	Avg	**7.47**	**0.37**	**0.74**	**2.0**		**37**
	STD (1σ)	**2.63**					

Greenland Glacier Samples
Continued

Sample ID	Sulfur #	Approximate Sample/ Blank Molar Ratio	µmoles of natural	µgrams natural	Sample/ Spike Ratio Molar Ratio	Range of Uncor Data (per mil)	Per mil Change thru Run
S1-S5	**lost**	**--**	**--**	**--**	**--**	**--**	**--**
S6-S10	**S-2899**	6.6	0.11	4	1.3	-3.3--2	1.1
S11-S15	**S-2903**	8.0	0.13	4	1.8	-5.5--1.5	4.0
S16-S20	**S-2904**	11.1	0.19	6	2.0	-3--2	1.0
S21-S25	**S-2913**	8.1	0.14	4	1.6	-6--3.7	2.3
S26-S29, S31	**S-2914**	5.7	0.10	3	2.1	-0.9-0.4	1.3
S32-S35	**S-2918**	6.3	0.11	3	2.0	-5.8--4.5	1.3
S36-S40	**S-2919**	3.0	0.05	2	1.1	-0.8-0.8	1.6
S41-S45	**S-2923**	11.0	0.19	6	4.7	-7--4.8	2.2
S46-S50	**S-2924**	17.1	0.29	9	4.7	-5.2--3.5	1.7
S51-S55	**S-2928**	9.0	0.15	5	1.7	-9.3--7	2.3
S56-S60	**S-2929**	5.8	0.10	3	1.5	-7--4	3.0
S61-S65	**S-2933**	3.8	0.07	2	2.8	-3--2	1.0
S66-S70	**S-2934**	6.1	0.10	3	2.1	-0.15-1	1.2
	Avg	**7.8**	**0.132**	**4**	**2.2**		**1.8**

C.2.3 Mass balance calculations for the Summit snowpit samples.

Greenland Samples

Sample ID	Sulfur #	Mid-Point Depth (cm)	S (ppm) (NIST)	Expanded Uncertainty (95% C.I.)	Relative (%)	S (ppb) (NIST)	Expanded Uncertainty (95% C.I.)
S1-S5	**lost**	5	--	--	--	--	--
S6-S10	**S-2899**	15	0.02	0.00046	2.94%	15.59	0.46
S11-S15	**S-2903**	25	0.02	0.00195	10.83%	18.01	1.95
S16-S20	**S-2904**	35	0.02	0.00195	8.03%	24.30	1.95
S21-S25	**S-2913**	45	0.02	0.00146	8.61%	16.90	1.46
S26-S29, S31	**S-2914**	56	0.01	0.00145	12.08%	12.04	1.45
S32-S35	**S-2918**	66	0.02	0.00304	18.60%	16.34	3.04
S36-S40	**S-2919**	75	0.01	0.00304	51.85%	5.86	3.04
S41-S45	**S-2923**	85	0.02	0.00200	10.08%	19.89	2.00
S46-S50	**S-2924**	95	0.03	0.00201	6.44%	31.17	2.01
S51-S55	**S-2928**	105	0.02	0.00126	7.87%	16.01	1.26
S56-S60	**S-2929**	115	0.01	0.00126	12.25%	10.27	1.26
S61-S65	**S-2933**	125	0.01	0.00323	47.42%	6.80	3.23
S66-S70	**S-2934**	135	0.01	0.00141	13.06%	10.78	1.41
		Avg	**0.02**		**16.16%**	**15.69**	

Greenland Samples Continued

Sample ID	Sulfur #	$\delta^{34}S$ (per mil) blank-corrected	SO_4^{2-} (ppb, µg/L) NIST	Expanded Uncertainty (95% C.I.)	Na (ppb, µg/L)	UM	Mg (ppb, µg/L)	UM	Ca (ppb, µg/L)	UM	MSA (ppb, µg/L)	UM
S1-S5	**lost**	**--**										
S6-S10	**S-2899**	**7.84**	44.76	1.31	7.73		0.23		7.05		0.948	
S11-S15	**S-2903**	**9.13**	51.72	5.60	5.46		0.12		5.15		0.798	
S16-S20	**S-2904**	**4.63**	69.79	5.60	4.96		0.00		3.46		0.782	
S21-S25	**S-2913**	**7.11**	48.52	4.18	4.34		0.26		5.48		1.722	
S26-S29, S31	**S-2914**	**8.31**	34.57	4.18	6.05		0.09		4.45		2.448	
S32-S35	**S-2918**	**5.57**	46.92	8.73	1.36		0.00		1.87		0.79	
S36-S40	**S-2919**	**13.31**	16.83	8.73	4.52		0.00		0.16		3.184	
S41-S45	**S-2923**	**9.19**	57.12	5.76	4.72		0.19		7.60		3.63	
S46-S50	**S-2924**	**7.45**	89.52	5.76	5.55		0.59		10.68		2.694	
S51-S55	**S-2928**	**3.60**	45.98	3.62	9.99		0.58		3.72		1.234	
S56-S60	**S-2929**	**3.86**	29.50	3.61	4.98		0.26		2.99		0.728	
S61-S65	**S-2933**	**8.57**	19.53	9.26	3.70		0.00		0.42		0.648	
S66-S70	**S-2934**	**8.55**	30.96	4.04	4.50		0.00		1.05		3.114	
		7.47	**45.06**		**5.22**		**0.18**		**4.16**		**1.75**	

Greenland Samples Continued

Sample ID	Sulfur #	Sea Salt fss	Sea Salt [ss-SO_4^{2-}] (ppb, µg/L)	Non-sea-salt [nss-SO_4^{2-}] (ppb, µg/L)	1/Non-sea-salt [nss-SO_4^{2-}] (ppb, µg/L)	[nss-Ca+] (ppb, µg/L)
S1-S5	**lost**					
S6-S10	**S-2899**	4.3%	1.93	42.83	0.02	6.74
S11-S15	**S-2903**	2.6%	1.37	50.36	0.02	5.01
S16-S20	**S-2904**	1.8%	1.24	68.55	0.01	3.40
S21-S25	**S-2913**	2.2%	1.09	47.43	0.02	5.35
S26-S29, S31	**S-2914**	4.4%	1.51	33.05	0.03	4.26
S32-S35	**S-2918**	0.7%	0.34	46.58	0.02	1.86
S36-S40	**S-2919**	6.7%	1.13	15.70	0.06	0.15
S41-S45	**S-2923**	2.1%	1.18	55.94	0.02	7.44
S46-S50	**S-2924**	1.5%	1.39	88.13	0.01	10.51
S51-S55	**S-2928**	5.4%	2.50	43.48	0.02	3.52
S56-S60	**S-2929**	4.2%	1.24	28.25	0.04	2.86
S61-S65	**S-2933**	4.7%	0.93	18.61	0.05	0.40
S66-S70	**S-2934**	3.6%	1.12	29.83	0.03	1.01
	Avg	**3.4%**	**1.31**	**43.75**	**0.03**	**4.04**

Greenland Samples Continued

Sample ID	Sulfur #	Non-sea-salt fnss	δtot (per mil) δ34S (per mil) blank-corrected	δnss (per mil)	fmsa [R]	fD	[dust SO_4^{2-}] (ppb, µg/L)	δD
S1-S5	**lost**		**--**					
S6-S10	**S-2899**	96%	**7.83**	7.24	2.2%	2.8%	1.21	0.567
S11-S15	**S-2903**	97%	**9.13**	8.81	1.6%	1.8%	0.90	0.358
S16-S20	**S-2904**	98%	**4.63**	4.34	1.1%	0.9%	0.61	0.178
S21-S25	**S-2913**	98%	**7.11**	6.79	3.5%	2.0%	0.96	0.406
S26-S29, S31	**S-2914**	96%	**8.31**	7.73	6.9%	2.3%	0.77	0.464
S32-S35	**S-2918**	99%	**5.57**	5.46	1.7%	0.7%	0.33	0.144
S36-S40	**S-2919**	93%	**13.31**	12.75	16.9%	0.2%	0.03	0.035
S41-S45	**S-2923**	98%	**9.19**	8.94	6.1%	2.4%	1.34	0.479
S46-S50	**S-2924**	98%	**7.45**	7.24	3.0%	2.1%	1.89	0.430
S51-S55	**S-2928**	95%	**3.60**	2.60	2.8%	1.5%	0.63	0.291
S56-S60	**S-2929**	96%	**3.86**	3.11	2.5%	1.8%	0.52	0.365
S61-S65	**S-2933**	95%	**8.57**	7.95	3.4%	0.4%	0.07	0.077
S66-S70	**S-2934**	96%	**8.55**	8.08	9.5%	0.6%	0.18	0.122
		97%	**7.47**	**7.00**	**4.7%**	**1.5%**	**0.73**	

Greenland Samples Continued

Sample ID	Sulfur #	1-fd	fmb	[marine biogenic SO_4^{2-}] (ppb, μg/L)	fa	[anthro-SO_4^{2-}] (ppb, μg/L)	Total SO_4^{2-} Concentration
S1-S5	**lost**						
S6-S10	**S-2899**	0.972	24%	10.32	73%	31.30	42.83
S11-S15	**S-2903**	0.982	35%	17.77	63%	31.69	50.36
S16-S20	**S-2904**	0.991	8%	5.20	92%	62.73	68.55
S21-S25	**S-2913**	0.980	22%	10.48	76%	35.99	47.43
S26-S29, S31	**S-2914**	0.977	28%	9.18	70%	23.11	33.05
S32-S35	**S-2918**	0.993	15%	6.97	84%	39.28	46.58
S36-S40	**S-2919**	0.998	62%	9.79	38%	5.89	15.70
S41-S45	**S-2923**	0.976	35%	19.83	62%	34.77	55.94
S46-S50	**S-2924**	0.979	25%	21.88	73%	64.36	88.13
S51-S55	**S-2928**	0.985	-4%	-1.81	103%	44.65	43.48
S56-S60	**S-2929**	0.982	-1%	-0.37	99%	28.11	28.25
S61-S65	**S-2933**	0.996	31%	5.83	68%	12.70	18.61
S66-S70	**S-2934**	0.994	32%	9.51	68%	20.14	29.83
			24%	**9.58**	**74%**	**33.44**	**43.75**

References

Aizen, V. B., Aizen, E. M., Dozier, J., Melack, J. M., Sexton, D. D., and Nesterov, N. (1997a) glacial regime of the highest Tien Shan mountain, Pobeda-Khan Tengry massif. *J. Glaciol.*, v. 43, n. 145, p. 503-512.

Alexander, B., Thiemens, M. H., Farquhar, J., Kaufman, A. J., Savarino, J. and Delmas R. J. (2003) East Antarctic ice core sulfur isotope measurements over a complete glacial-interglacial cycle. *J. Geophys. Res.*, v. 108, n. D24, p. ACH 18-1 – ACH 18.7.

Alley, R. B. and Anandarkrishnan, S. (1995) Variations in melt-layer frequency in the GISP2 ice core: Implications for Holocene summer temperatures in central Greenland. *Ann. Glaciol.*, v. 21, p. 64-70.

Andreae, M. and Jaeschke, P. (1992) Exchange of Sulphur between Biosphere and Atmosphere over Temperate and Tropical Regions. In *Sulphur Cycle on the Continents: Wetlands,Terrestrial Ecosystems and Associated WaterBodies, SCOPE 48,* Howarth, R. W., Stewart, J. W. B., and Ivanov, M. V., Eds. , Wiley, Chichester, pp. 27-66.

Andreae, M. O. (1985) The Emission of Sulfur and Nitrogen to the Remote Atmosphere: Background Paper in Sulfur Emission. In *The Biogeochemical Cycling of Sulfur and Nitrogen in the Remote Atmosphere*. In Galloway, J., Charlson, R., Andreae, M. And Rodhe, J. Eds. NATO ASI Series. Reidel Publishing, Hingham, MA, p. 331-362.

Atkinson, R., Baulch, D. L., Cox, R. A., Hampson, R. F., Kerr, J. A., Rossi, M. J., and Troe, J. (1997) Evaluated kinetic and photochemical data for atmospheric chemistry: Supplement VI – IUPAC subcommittee on gas kinetic data evaluation for atmospheric chemistry. *J. Phys. Chem. Ref. Data*, v. 26, p. 1329-1499.

Barrie, L. A. (1995) Arctic aerosols: Composition, sources, and transport. In *Ice Core Studies of Global Biogeochemical Cycles*. Edited by R. J. Delmas. NATO ASI Series, Springer-Verlag, New York, NY, p. 121-138,

Barth, M., Rasch, P. J., Kiehl, J. T., Benkovitz, C. M., and Schwartz, S. E. (2000) Sulfur chemistry in the National Center for Atmospheric Research Community Climate Model: Description, Evaluation, Features and Sensitivity to aqueous Chemistry. *J. Geophys. Res.*, v. 105, p. 1387-1415.

Bates, T. S., Cline, J. D., Gammon, R. H., and Kelly, S. R. (1987) Regional and seasonal variations in the flux of oceanic dimethylsulfide to the atmosphere. *J. Geophys. Res.*, v. 92, p. 2930-2938.

Berresheim, H. (1987) Biogenic sulfur emissions from the Subantarctic and Antarctic oceans, *J. Geophys. Res.*, v. 92, p. 13,245-13,262.

Berresheim, H., Wine, P. H., and Davis, D. D. (1995) Sulfur in the Atmosphere. In *Composition, Chemistry, and Climate of the Atmosphere.* Hanwant B. Singh, Ed., Van Nostrand Reinhold.

Bory, A. J. M, Biscaye, P. E., Svensson, A., and Groussett, F. E. (2002) Seasonal variability in the origin of recent atmospheric mineral dust at North GRIP, Greenland. *Earth Planet. Sci. Lett.*, v. 196, n. 3-4, p. 123-134.

Bory, A. J. M, Biscaye, P. E., and Groussett, F. E. (2003) Two distinct seasonal Asian source regions for mineral dust deposited in greenland (NorthGRIP). *Geophys. Res. Lett.*, v. 30, n. 4, p. 16-1-16-4.

Bory, A. J. M, Biscaye, P. E., Piotrowski, A. M., and Steffensen, J. P. (2003) Regional variability of ice core dust composition and provenance in Greenland. *Geochem. Geophys. Geosys.*, Art. No. 1107.

Brimblecombe, P., Hammer, C., Rodhe, H., Ryaboshapko, A., and Boutron, C.F. (1989) Human Influence on the sulphur cycle. In *Evolution of the Global Biogeochemical Sulphur Cycle, SCOPE 39*, Brimblecombe, P. and Lein, A. Y., Eds. Wiley, Chichester, pp. 77-121.

Calhoun, J. A., Bates, T.S., and Charlson, R. J. (1991) Sulfur isotope measurements of submicrometer sulfate aerosol p[rticles over the Pacific Ocean. *Geophys. Res. Lett.*, v. 18, p. 1877-1880.

Castleman, A. W., Munkelwitz, H. R., and Manowitz, B. (1974) Isotopic studies of the sulfur component of the stratospheric aerosol layer. *Tellus*, v. 26, n. 1-2, p. 222-234.

Chambers, L. A. And Trudinger, P. A. (1979) Micorbiological fractionation of stable sulfur isotopes: A review and Critique. *J. of Geomicrob.*, v. 1, p. 249-293.

Chin, M., Rood, R. B., Lin, S.-J., Muller, J.-F., and Thompson, A. M. (2000a) Atmospheric sulfur cycle simulated in the Global Model GOCART: Model description and global properties. *J. Geophys. Res.*, v. 105, p. 24,671-24,687.

Chin, M., Savoie, D. L., Huebert, B. J., Bandy, A. R., Thornton, D. C., Bates, T. S., Quinn, P. K., Saltzman, E. S., De Bruyn, W. J. (2000b) Atmospheric sulfur cycle simulated in the Global Model GOCART: Comparison with field observations and regional budgets. *J. Geophys. Res.*, v. 105, p. 24,689-24,712.

Chin, M. and Jacob, D. J. (1996) Anthropogenic and natural contributions to tropospheric sulfate: A global model analysis. *J. Geophys. Res.*, v. 101, p. 18,691-18,699.

Christensen, J. H. (1997) The Danish Eulerian Hemispheric Model - A Three-Dimensional Air Pollution Model used for the Arctic. *Atmos. Environ.*, v. 31, p. 4169-4191.

Claquin, T., Schulz, M., Balkanski, Y. J. (1999) Modeling the mineralogy of atmospheric dust sources. *J. Geophys. Res.*, v. 104, p. 22,243-22,256.

Colin, J. L., Lim, B., Herms, E., Genet, F., Drab, E., Jafferzo, J. L., and Davidson, C. I. (1997) Air-to snow mineral transfer – crustal elements in aerosols, fresh snow and snowpits on the Greenland ice sheet. *Atmos. Envir.,* v. 31, n. 20, p. 3395-3406.

Cortecci, G. and Longinelli, A. (1970) Isotopic composition of sulfate in rain water, Pisa, Italy. *Earth Planet. Sci. Lett.*, v. 8, n. 1, p. 36-40.

Davidson, C. I., Jaffrezo, J.-L., Small, M. J., Summers, P. W., Olson, M. P., and Borys, R. D. (1993) Trajectory analysis of source regions influencing the South Greenland Ice Sheet during the Dye 3 gas and aerosol sampling program. *Atmos. Environ.*, v. 27A, n. 17/18, p. 2739-2749.

De Angelis, M., Steffensen, J. P., Legrand, M., Clausen, H., and Hammer, C. U. (1997) Primary aerosol (sea salt and soil dust) deposited in Greenland ice during the last climactic cycle: Comparison with east Antarctic records. *J. Geophys. Res.*, v. 102, n. C12, p. 26,681-26,698.

Dietz, L. A., Pachucki, C. F., and Land, G. A. (1962) Internal standard technique for precise isotope abundance measurements in thermal ionization mass spectrometry. *Anal. Chem.*, v. 34, n. 6, p. 709-710.

Dignon, J. and Hameed, S. (1989) Global emissions of nitrogen and sulfur oxides from 1860-1980. *J. Air Pollut. Control Assoc*., v. 39, n. 2, p. 180-186.

Ding, T., Valkiers, S., Kipphardt, H., De Bievre, P., Taylor, P. D. P., Gonfiantini, R., and Krouse, R. (2001) Calibrated sulfur isotope abundance ratios of three IAEA sulfur isotope reference materials and V-CDT with a reassessment of the atomic weight of sulfur. *Geochimi. Cosmochimi. Acta*, v. 65, p. 2433-2437.

Doscher, A., Gaggeler, H. W., Schotterer, U., and Schwikowski, M. (1996) A historical record of ammonium concentrations from a glacier in the Alps. *Geophys. Res. Lett.*, v. 23, p. 2741-2744.

Eugster, O., Tera, F., and Wasserburg, G. J. (1969) Isotopic Analysis of Barium in Meteorites and in Terrestrial Samples. *J. Geophys. Res.*, v. 74, n. 15, p. 3897-3908.

Faure, F. M., Mitchell, M. J., and Bartlett, R. W. (1973) Vapor pressure study of arsenic trisulfide. *High Temp. Sci.,* v. 5, p. 128-137.

Finkel, R. C., Langway Jr., C. C., and Clausen, H. B. (1986) Changes in precipitation chemistry at Dye 3, Greenland. *J. Geophys. Res.*, v. 91, n. D9, p. 9849-9855.

Fischer, H., Wagenbach, D., and Kipfstuhl, J. (1998) Sulfate and nitrate firn concentrations on the Greeland ice sheet 1. Large-scale geographical deposition changes. *J. of Geophys. Res.,* v. 103, n. D17, p. 21,927-21,934.

Goto-Azuma, K. and Koerner, R. M. (2001) Ice core studies of anthropogenic sulfate and nitrate trends in the Arctic. *J. of Geophys. Res.,* v. 106, n. D5, p. 4959-4969.

Grinenko, V. A., and Grinenko, L. N. (1974) Geochemistry of Sulphur Isotopes. Nauka, Mosocw, pp. 272.

Guidelines for Evaluating and Expressing the Uncertainty of NIST Measurement Results (1994) Taylor, B. N. and Kuyatt, C. E., NIST Technical Note 1297,US. Department of Commerce Technology Administration, National Institute of Standards and Technology.

Hall, D. K. And Martinec, J. (1985) *Remote Sensing of Ice and Snow*. London and New York: Chapman and Hall Ltd.

Hayes, J. M. (2002) Practive and principles of isotopic measurements in organic geochemistry. Ed. W. G. Meinschein. In Organic Geochemistry of Contemporaneous and Ancient Sediments (1983). Published by the Great Lakes Section of the Society of Economic Paleontologists and Mineralogist. Reedited by Alex L. Sessions, p. 1-25 (http://www.gps.caltech.edu/~als/library3.html).

Herut, B., Spiro, B., Starinsky, A., Katz, A. (1995) Sources of sulfur in rain water as indicated by isotopic $\delta^{34}S$ data and chemical composition, Israel. *Atmos. Environ.*, v. 29, p. 851-857.

Hopke, P. K., Barrie, L. A., Li, S.-M., Cheng, M. D., Li, C., and Xie, Y. L. (1995) Possible sources and preferred pathways for biogenic and non-sea-salt sulfur for the high Arctic. *J. Geophys. Res.*, v. 100, n. D8, p. 16,595-16,603.

Hynes, A. J., Wine, P. H., Semmes, D. H. (1986) Kinetics and mechanisms of OH reactions with organic sulfides. *J. Phys. Chem.*, v. 90, p. 4148-4156.

Ice Core Working Group (2003) U. S. Ice Core Science: Recommendations for the Future. A report based on the workshop: "The Future of U. S. Ice Coring Science", March 20-21, 2002, Arlington, Virginia.

IPCC (Intergovernmental Panel on Climate Change) (1995) Climate Change 1994: Radiative Forcing on Climate Change, edited by Houghton, J. T et al., Cambridge University Press: New York.

ITASE (International Trans-Antarctic Scientific Expedition) 200 Years of Past Antarctic Climate and Environmental Change - Science and Implementation Plan. Appendix B - Guide for the Collection and Analysis of ITASE Snow and Firn Samples. **www.antcrc.utas.edu.au**.

Janai, M., Rudman, P. S., Mandelbaum, A. (1978) Mass spectrometric analysis of arsenic trisulfide. *J. of Non-Crysta. Solids*, v. 27, p. 67-73.

Johnsen, S. J., Clausen, H. B., Dansgaard, W., Fuhrer, K., Gundestrup, N., Hammer, C. U., Iversen, P., Jouzel, J., Stauffer, B., and Steffensen, J. P. (1992) Irregular glacial interstadials recorded in a new Greenland ice core. *Nature*, v. 359, p. p. 311-313.

Johnson, C. M. and Beard, B. L. (1999) Correction of instrumentally produced mass fractionation during isotope analysis of Fe by thermal ionization mass spectrometry. *Intl. J. Mass Spectrometry*, v. 193, p. 87-99.

Johnson, T. M., Herbel, M. J., Bullen, T. D., Zawislanski, P. T. (1999) Selenium isotope ratios as indicators of selenium sources and oxyanion reduction. *Geochimi. Cosmochimi. Acta*, v. 63, n. 18, p. 2775-2783.

Kang, S., Mayewski, P. A., Qin, D., Yan, Y., Hou, Y., Zhang, D., Kreutz, K. J. (2002) Glaciochemical records from a Mt. Everest ice core: relationship to atmospheric circulation over Asia. *Atmos. Environ.,* v. 36, 3351-3361.

Kelly, W. R. (personal communication) Si gel was prepared by F. Tera.

Koch, D., Jacob, D., Tegen, I., Rind, D., and Chin, M. (1999) Tropospheric sulfur simulation and sulfate direct radiative forcing in the GISS GCM, *J. Geophys. Res.*, v. 104, p. 23,799-23, 823.

Kreutz, K. J. and Sholkovitz, E. R. (2000) Major element, rarer earth element, and sulfur isotopic composition of a high-elevation firn core: Sources and transport of mineral dust in central Asia. *Geochem.,Geophys., Geosys.*, v. 1, paper number 2000GC000082.

Kreutz, K. J., Aizen, V. B., Cecil, L. D., Wake, C. P. (2001) Oxygen isotopic and soluble ionic composition of precipitation recorded in a shallow firn core, Inilchek Glacier (Central Tien Shan). *J. Glaciol*., v. 47, p. 548-554.

Krouse, H. R. (1980) Sulphur isotopes in our environment. In *Handbook of Environmental Isotope Geochemistry*, Fritz, P. and J. Ch. Fontes (Eds.). Elsevier, Amsterdam, p. 435-471.

Krouse, H. R. and van Everdingen, R. O. (1983) $\delta^{34}S$ variations in vegetation and soil exposed to intense biogenic sulphur emissions near Paige Mountain, N.W.T., Canada, *Water, Air, Soil Pollut*., v. 23, p. 61-67.

Krouse, H. R., and Grinenko , V. A., (1991) Eds. Stable Isotopes: Natural and Anthropogenic Sulphur in the Environment, John Wiley & Sons: New York, v. 43.

Kuehner, E. C., Alvarez, R., Paulsen, P. J., and Murphy, T. J. (1972) Production and analysis of special high-purity acids purified by subboiling distillation. *Anal. Chem*., v. 44, n. 12, p. 2050-2056.

Lefohn, A. S., Husar, J. D., Husar, R. B. (1999) Estimating historical anthropogenic global sulfur emission patterns for the period 1850-1990. *Atmos. Environ.,* v. 33, p. 3435-3444.

Legrand, M., Hammer, C., De Angelis, M., Savarino, J., Delmas, R., Clausen, H., and Johnsen, S.J. (1997) Sulfur-Containing species (Methanesulfonate and SO_4) over the Last Climatic Cycle in the Greenland Ice Core Project (central Greenland) Ice Core. *J. Geophys. Res.*, v. 102, n. C12, p. 26,663-26,679.

Legrand, M., and Mayewski, P.A. (1997) Glaciochemistry of polar ice cores: *A Review. Rev. Geophys*., v. 35, n. 3, p.219-243.

Legrand, M. and Delmas, R. J. (1984) The ionic balance of Antarctic Snow: A 10-year detailed record. *Atmos. Environ.*, v. 18, p. 1867-1874.

Legrand, M. R., Feniet-Saigne, C., Saltzman, E. S., Germain, C., Barkov, N. I., Petrov, V. N. (1991) Ice-core record of oceanic emissions of dimethylsulfide during the Last Climate Cycle. *Nature*, v. 350, p. 144-146.

Li, S.-M. and Winchester, J. W. (1993) Particle size distribution and chemistry of late winter Arctic aerosols. *J. Geophys. Res.*, v. 95, n. D9, p. 13,897-13,908.

Li, S.-M. and Barrie, L. A. (1993) Biogenic sulfur aerosol in the Arctic troposphere: 1. Contributions to total sulfate. *J. Geophys. Res.*, v. 98, n. D11, p. 20,613-20,622.

Li, S.-M., Barrie, L. A., and Sirois, A. (1993) Biogenic sulfur aerosol in the Arctic troposphere: 2. Trends and seasonal variations. *J. Geophys. Res.*, v. 98, n. D11, p. 20,623-20,631.

Liang, J. Y. and Jacobson, M. Z. (1999) A study of sulfur dioxide oxidation pathways over a range of liquid water contents, pH values, and temperatures. *J. Geophys. Res.*, v. 104, n. D11, p. 13,749-13,769.

Lindberg, S. E., Brooks, S., Lin, J., Scott, K., Goodsite, M., Tilden, M. S., Landis, M., and Stevens, R. (2001) Dynamic oxidation of mercury in the arctic troposphere: Mercury speciation in air, deposition, and accumulation in snow from the Barrow, Alaska arctic mercury study. Abstracts of Papers of the American Chemical Society 222: 665-ENVR Part 1.

Lindberg, S. E., Brooks, S., Lin, C. J., Scott, K. J., Landis, M. S., Stevens, R. K., Goodsite, M., and Richter, A. (2002) Dynamic oxidation of gaseous mercury in the arctic troposphere at polar sunrise. *Environ. Sci. Tech*., v. 36, p. 1245-1256.

Lu, J. Y., Schroeder, W. H., Barrie, L. A., Steffen, A., Welch, H. E., Martin, K., Loclhart, L., Hunt, R. V., Boila, G., and Richter, A. (2001) Magnification of atmospheric mercury deposition to polar regions in springtime: The link to tropospheric ozone depletion chemistry. *Geophys. Res. Lett.*, v. 28, p. 3219-3222.

Mann, J. L., Long, S. E., Shuman, C. A., Kelly, W. R. (in press) Determination of mercury content in a shallow firn core from greenland by isotope dilution inductively coupled plasma mass spectrometry. *Wate, Air, Soil Pollut.*.

Mayewski, P. A., Lyons, W. B., Spencer, M. J., Twickler, Dansgaard, W., Koci, B., Davidson, C. I., and Honrath, R. E. (1986) Sulfate and nitrate concentrations from a South Greenland Ice Core. *Science*, v. 232, p. 975-977.

Mayewski, P. A., Lyons, W. B., Spencer, M. J., Twickler, M. S., Buck, C. F., and Whitlow, S. (1990) An ice core record of atmospheric response to anthropogenic sulphate and nitrate. *Nature*, v. 346, p. 554-556.

McArdle, N. C., Liss, P. S., Dennis, P. (1998) An isotopic study of atmospheric sulphur at three sites in Wales and at Mace Head, Eire. *J. Geophys. Res*., v. 103, n. D23, p. 31,079-31,094.

Mills, K. C. (1974) Thermodynamic Data for Inorganic Sulfides, Selenides, and Tellurides: Butterworths, London, p. 131-135.

Moore, L. J., Machlan, L. A., Shields, W. R., and Garner, E. L. (1974) Internal normalization techniques for high accuracy isotope dilution analyses – Applications to Molybdenum and Nickel in Standard Reference Material. *Anal. Chem.*, v. 46, p. 1082-1089.

National Academy of Science (2000) Grand Challenges in Environmental Sciences. (http://www.nap.edu/openbook/0309072549/html/l.html), p. 1-59.

Neftel, A., Beer, J., Oeschger, H., Zurcher, F., and Finkel, R. C. (1985) Sulphate and nitrate concentrations in snow from South Greenland 1895-1978. *Nature*, v. 314, p. 611-613.

Newman, L., Krouse, H.R., and Grinenko, V.A. (1991) Sulphur Isotope Variations in the Atmosphere. In *Stable Isotopes: Natural and Anthropogenic Sulphur in the Environment*, H.R. Krouse and V.A.Grinenko Eds., John Wiley and Sons Ltd. p. 440.

Nielsen, H. (1974) Isotopic composition of the major contributors to atmospheric sulfur. *Tellus*, v. 26, p. 213-221.

Nielsen, H., Pilot, J., Grinenko, L. N., Grinenko, V. A., Lein, A. Y., Smith, J. W., and Pankina, R. G. (1991) Lithospheric sources of sulphur. In *Stable Isotopes: Natural and Anthropogenic Sulphur in the Environment*, H.R. Krouse and V.A.Grinenko Eds., John Wiley and Sons Ltd. p. 133-176.

Norman, A. L., Barrie, L. A., Toom-Sauntry, D., Sirois, A., Krouse, H. R., Li, S. M., and Sharma, S. (1999) Sources of aerosol sulphate at Alert: Apportionment using stable isotopes. *J. Geophys. Res.*, v. 104, n. D9, p. 11,619-11,631.

Nriagu, J. O., and Coker, R. D. (1978) Isotopic composition of sulfur in precipitation within the Great Lakes Basin. *Tellus*, v. 30, p. 365-375.

Nriagu, J. O., Coker, R. D., and Barrie, L. A. (1991) Origin of sulphur in Canadian Arctic Haze from isotope measurements. *Nature*, v. 349, p. 142-145.

Ohizumi, T., Fukuzaki, N., Kusakabe, M. (1997) Sulfur isotopic view on the sources of sulfur in atmospheric fallout along the coast of the Sea of Japan. *Atmos. Environ.*, v. 31, p. 1339-1348.

Pashinkin, A. S., Molodyk, A. D., Belousov, V. I., Stell'chenko, S. S., Fedorov, V. A. (1974) Composition of As_2S_3 Vapor. *Inorg. Mat. Russia*, v. 10, p. 1379-1381.

Patris, N., Delmas, R. J., Legrand, M., De Angelis, M., Ferron, F. A., Stievenard, M., Jouzel, J. (2002) First sulfur isotope measurements in central Greenland ice cores along the preindustrial and industrial periods. *J. of Geophys. Res.*, v. 107, n. D11, p. ACH 6-1 – ACH 6-13.

Patris, Nicolas, Delmas, Robert J., and Jouzel, Jean (2000a) Isotopic signatures of sulfur in shallow Antarctic ice cores. *J. of Geophys. Res.*, v. 105, n. D6, p. 7071-7078.

Patris, Nicolas, Mihalopoulos, Nikolaos, Baboukas, Evangelos D., and Jouzel, Jean (2000b) Isotopic composition of sulfur in Size-resolved marine aerosols above the Atlantic Ocean. *J. Geophys. Res.*, v. 105, n. D11,p. 14,449-14,457.

Paulsen, P. J. And Kelly, W. R. (1984) Determination of sulfur as arsenic monosulfide by Isotope Dilution Thermal Mass Spectrometry. *Anal. Chem.*, v. 56, p. 708-713.

Peng, T. H., Takahashi, T., and Broecker, W. S. (1974) Surface radon measurements in the North Pacific Ocean Station Papa, *J.of Geophys. Res.,* v. 79, p. 1772-1780.

Penkett, S.A., Jones M. R., Brice, K. A., Eggleton, A. E. (1979) The importance of atmospheric ozone and hydrogen peroxide in oxidizing sulphur dioxide in cloud and rainwater. *Atmos. Environ*., v. 13, p. 123-137.

Polian, G., Lambert, G., Ardouin, B., and Jegou, A. (1986) Long-Range transport of continental radon in Subantarctic and Antarctic Areas. *Tellus*, v. 38, p. 178-189.

Pruett, L. E., Kreutz, K. J., Wadleigh, M., and Aizen, V. (2004) Assessment of sulfate sources in high-elevation asian precipitation using stable sulfur isotopes. *Environ. Sci. Technol.*, v. 38, n. 18, p. 4728-4733.

Qi, H. P. and Coplen, T. B. (2003) Evaluation of the $^{34}S/^{32}S$ ratio of Soufre de Lacq elemental sulfur isotopic reference material by continuous flow isotope-ratio mass spectrometry. *Chemical Geology*, v. 199, p. 182-187.

Raab, M. And Spiro, B. (1991) Sulfur isotopic variations during seawater evaporation with fractional crystallization. *Chemical Geology*, v. 86, p. 323-333.

Rasch, P. J., Barth, M. C., Kiehl, J. T., Schwartz, S. E., and Benkovitz, C. M. (2000) A Description of the global Ssulfur cycle and its controlling processes in the National Center for Atmospheric Research Community Climate Model, Version 3. *J. Geophys. Res.*, v. 105, p. 1367-1385.

Rees, C. E., Jenkins, W. J., and Monster, J. (1978) The isotopic composition of ocean water sulfate. *Geochimi. Cosmochimi. Acta*, v. 42, p. 377-381.

Rees, C. E. (1978) Sulphur isotope measurements using SO_2 and SF_6. *Geochimi. Cosmochimi. Acta*, v. 42, p. 383-389.

Russell, W. A., Papanastassiou, D. A., and Tombrello, T. A. (1978) Ca isotope fractionation on the Earth and other solar system materials. *Geochimi. Cosmochimi. Acta*, v. 42, p. 1075-1090.

Saltzman, E. S., Brass, G., and Price, D. (1983) The mechanism of sulfate aerosol formation: Chemical and sulfur isotopic Evidence. *Geophys. Res. Let.*, v. 10, p. 513-516.

Savarino, J., Lee, C. W. L., Thiemens, M. (2000) Laboratory oxygen isotopic study of sulfur (IV) oxidation: Origin of the mass-independent oxygen isotopic anomaly in atmospheric sulfates and sulfate mineral deposits on Earth. *J. Geophys. Res*., v. 105, n. D23, p. 29079-29088.

Schroeder, W. H., Anlauf, K. G., and Barrie, L. A. (1998) Arctic springtime depletion of mercury. *Nature*, v. 394, p. 331-332.

Seinfield, J. H. and Pandis, S. N. (1998) Atmospheric Chemistry and Physics, 1326 pp. John Wiley and Sons, New York.

Shuman, C. A., Alley, R. B., Anandakrishnan, S., White, J. W. C., Grootes, P. M., and Stearn, C. R. (1995) Temperature and accumulation at the Greenland Summit: Comparison of high-resolution isotope profiles and satellite passive microwave brightness temperature trends. *J. of Geophys. Res.*, v. 100, p. 9,165-9,177.

Shuman, C. A., Alley, R. B., Fahnestock, M. A., Bindschadler, R. A., White, J. W. C., Winterle, J., and McConnell, J. R. (1998) Temperature history and accumulation timing for the snowpack at GISP2, central Greenland. *J. of Glaciol.*, v. 44, p. 21-30.

Skulan, J., Depaolo, D. J., and Owens, T. L. (1997) Biological control of calcium isotopic abundances in the global calcium cycle. *Geochimi. Cosmochimi. Acta*, v. 61, p. 2505-2510.

Spiro, P. A., Jacob, D. J., and Logan, J. A. (1992) Global inventory of sulfur emissions with 1° X 1° resolution. *J. Geophys. Res*., v. 97, p. 6023-6036.

SRM 3154 (Sulfur Spectrometric Solution) National Institute of Standards and Technology (https://srmors.nist.gov/view_detail.cfm?srm=3154).

SRM 2724b (Sulfur in Diesel Fuel Oil) National Institute of Standards and Technology (https://srmors.nist.gov/view_cert.cfm?srm=2724B).

Steffen, A., Schroeder, W. H., Bottenheim, J., Narayan, J. and Fuentes, J. D. (2002) Atmospheric mercury concentrations: Measurements and profiles near snow and ice surfaces in the Canadian Arctic during ALERT 2000. *Atmos. Environ*., v. 36, p. 2653-2661.

Steffensen, J. P. (1997) The size and distribution of microparticles from selected segments of the Greenland Ice Core Project Ice Core Representing Different Climate Periods. *J. Geophys. Res.*, v. 102, p. 26,755-26,763.

Sun, J. M., Zhang, M. Y., and Liu, T. S. (2001) Spatial and temporal characteristics of dust storms in China and its surrounding regions, 1960-1999. *J. Geophys. Res.*, v. 106, p. 10,325-10,333.

Tanaka, N. Rye, D. M., Xiao, Y., and Lasaga, A. C. (1994) Use of stable sulfur isotope systematics for evaluating oxidation reaction pathways and in cloud-scavenging of sulfur dioxide in the atmosphere. *Geophys. Res. Lett.*, v. 21, p. 1519-1522.

Taylor, B. E., Ding, T., Halas, S., Breas, O., Robinson, B. W. (2000) Accurate Calibration of the V-CDT Scale: Proposed $\delta^{34}S$ values for Calibration and Reference Materials and Methods of Correction for SO_2-based Analyses. Report of Sulfur Isotope Working Group 8th Advisory Group Meeting on Future Trends in Stable Isotope Reference Materials and Laboratory Quality Assurance, September 18 – 22, 2000, IAEA Headquarters, Vienna Australia.

Thode, H. G., Monster, J., and Dunford, H. B. (1961) Sulfur isotope geochemistry. *Geochimi. Cosmochimi. Acta*, v. 25, p. 159-174.

Thompson, L. G., Yao, T., Mosley-Thompson, E., Davis, M. E., Henderson, K. A., and Lin, P.-N. (2000) A aigh-resolution millennial Record of the South Asian Monsoon from Himalayan Ice Cores. *Science*, v. 289, n. 5486, p. 1916- 1919.

Todt, W., Cliff, R.A., Hanser, A., and Hoffmann, A.W. (1996) Evaluation of a ^{202}Pb-^{205}Pb Double Spike for High-Precision Lead. Isotope Analysis. Earth Processes: Reading the Isotopic Code – Geophysical Monograph 95. American Geophysical Union. p. 429-437.

Toom-Sauntry, D., and Barrie, L. A. (2002) Chemical composition of snowfall in the High Arctic: 1990-1994. *Atmos. Environ.*, v. 36, p. 2683-2693.

Vaughn, B. H., White. J. W. C., Delmotte, M., trolier, M. Cattani, O., and Stievenard, M. (1998) An automated system for hydrogen isotope analysis of water. *Chemical Geology*, v. 152, n. 3-4, p. 309-319.

Wadleigh, M. A., Schwarcz, H. P., Kramer, J. R. (1996) Isotopic evidence for the origin of sulphate in coastal rain. *Tellus Series B*, v. 48, p. 44-59.

Wake, C. P., Mayewski, P. A., Spencer, M. J. (1990) A review of central Asian glaciochemical data. *Ann. Glaciol.*, v. 14, p. 301-306

Wake, C. P., Mayewski, P. A., Ping, W., Yang, Q., Jiankang, H., Zichu, X. (1992) Anthropogenic sulfate and Asian dust signals in snow from Tien Shan, northwest China. *Ann Glaciol.*, v. 16, p. 45-52.

Wake, C. P., Mayewski, P. A., Li, Z., Han, J., and Qin, D. (1994) Modern eolian dust deposition in central Asia. *Tellus*, v. 46B, p. 220-233.

Wedepohl, K. H. (ed.) (1978) Handbook of Geochemistry: Vol. II. Springer-Verlag: Heidelberg.

Zdanowicz, C. M., Zielinski, and Wake, C. P. (1998) Characteristics of modern atmospheric dust deposition in snow on the Penny Ice Cap, baffin Island, Arctic, Canada. *Tellus Series B*, v. 50, p. 506-520.